Structural Characteristics of Various Types of Helically Wound Cables in Bending

Doctoral thesis by

Sajjad Wali Khan

Submitted in Partial Fulfillment of the Requirements for the Award of the

Degree of Doctor of Philosophy

School of Civil and Building Engineering, Loughborough University, United Kingdom.

September 2013

Dedicated to My Beloved Parents

ABSTRACT

The primary aim of this research was to investigate the bending behaviour of helically wound steel cables of various types (i.e. normal spiral strands, sheathed spiral strands and locked coil cables) in the presence of friction and to propose more efficient computational models for their analysis under combined tension and bending.

The proposed model fully takes into account interwire contact forces both in the radial direction (point contact between wires in different layers) and hoop direction (line contact within the wires in the same layer). Extensive theoretical parametric studies have been undertaken on a variety of cable constructions covering a wide range of geometrical and material parameters. Explicit formulations have been developed for the smooth transition of the bending stiffness from no-slip to full slip regimes, as a function of cable curvature. Based on these formulations, it is now possible to calculate the relative displacements of the wires, as well as the tensile, bending and hoop stresses in the individual wires of the cable. Furthermore, bending stiffness of the cable is shown to decrease by a factor of 2 to 16, depending upon the friction coefficient between wires and the type of cable construction. Wherever possible, the theoretical results have been compared with experimental results from the available literature and are found in very good agreement with them.

A simple method for the determination of the bending stiffness of large diameter multi-layered cable has been developed. The simplified method is further shown to provide estimates of the bending stiffness which are very close to those calculated by the original theory, allowing hand calculations for an easier use in industry.

The proposed formulations have been extended to cater for the effects of external hydrostatic pressure on sheathed spiral strands in deep water applications. These forces are shown to have a great influence on the pattern of interwire contact forces and hence the interlayer slippage between the wires in the strand. Numerical results have been obtained and analysed for three different 127 mm diameter strands with lay angles of 12°, 18° and 24° respectively, experiencing a wide range of external hydrostatic pressures of 0 to 2,000 metres. The significant increase in normal contact

force between wires is shown to suppress the slippage of wires in the cable. However, the no-slip and full slip values of the effective bending stiffness of the cable is shown to be independent of the level of hydrostatic pressure.

A theoretical model is also proposed for estimating wire kinematics, pattern of interwire slippage, contact forces as well as the flexural rigidity of locked coil cables with outer layers made of shaped wires. In order to validate this model, numerical results are reported for two different locked coil cables. It is shown that the shaped wires in the outer layers of locked coil cables play an important role in the distribution of contact forces, slip initiation and cable unwinding.

ACKNOWLEDGMENTS

Although PhD degree is awarded to one individual, but infact there is always a support and help of many people. I would like to thank the following people for their active support and contribution during this journey.

First of all, I am extending profound thanks to Dr. Alessandro Palmeri and Dr. Mariateresa Lambardo for their encouragement, constructive criticism and friendship throughout this project. I felt extremely comfortable and enjoyed working with them through this journey. Their advice and critical reviews were extremely helpful in enhancing the quality of this research, and without their valuable support this thesis would have been very difficult to accomplish. Special mention also goes to Professor Jim Chandler, Professor Tony Thorpe and Ms Helen Newbold for their immense support during different parts of the project.

My work was financed by University of Engineering and Technology Peshawar, Khyber Pakhtunkhwa, whose support I sincerely appreciate. Without their financial support this project would have not been possible.

Cordial thanks go to Professor M Raoof, for benefiting from his earlier work on this topic and making valuable suggestion in the start of this project.

I have had a lot of good laughs with many colleagues during my studies. They provided a well needed comic relief on a very regular basis and we shared too many cherishing moments. Few of them are; Aamir, Asmat, Camilo, Fayaz, Faisal, Hamid, Irum, Saleem, Shakoor, Mambo, Riaz, Sara and Waseem. I wish them all great success in life.

A special word of thanks goes to Dr. Saleem, who helped me to write the software program for this project and also assisted me in many aspects.

Finally, I am most indebted to my parents for their love, support and prayers, which made success more enjoyable and disappointments more bearable. I would also like to extend my heartfelt love to my sisters, cousins, and extended family members for their limitless love and affections. Their continued support and love have enabled me to continue my education unhindered. At the end, it would be unfair not to mention my sweet nephew Umair, who always take my apprehensions with his lovely talks.

TABLE OF CONTENTS

LIST OF FIGURES

LIST OF TABLES

LIST OF SYMBOLS

NOTATIONS	EXPLANATION
A_{core}	Area of core
A_{gi}	Gross steel area of layer *i* used in orthotropic sheet theory
A_{ni}	Net steel area of layer *i*
A_i	Cross-sectional area of wire in layer *i*
A_n^R	Net steel area of a layer with round wires
A_n^S	Net steel area of a layer with shaped wires
A_{net}	Net steel area of the cable cross-section
b_i	Half-width of the line contact patch between two wires
c_k	Ratio of the tensile stress to the diametral stress in the cable
C_i^h, C_{ij}^p	Constants of integration for wires in layer *i*
D_i	Wire diameter in layer *i*
d	Outer diameter of the cable
d_1,d_2	Cable axial and torsional stiffness coefficients.
$d\alpha_i$	Change in lay angle in layer *i*
$d\epsilon_x$	Incremental change in wire axial strain
E	Young modulus of the material
E_{eff}	Effective Young modulus of the cable
EI	Bending stiffness/Flexural rigidity

EI_{eff}	Effective bending stiffness of the cable
EI_{core}	Bending stiffness of the core
EI_i	Bending stiffness of a wire in layer *i*
G	Shear modulus
g	Acceleration due to gravity
GJ	Cable torsional stiffness
h	Water depth, length of the cable
I	Second moment of inertia of the cable
I_{core}	Second moment of inertia of the core
I_i	Second moment of inertia of a wire in layer *i*
i	Layer number (*i* = inner layer)
k_{1i}, k_{2i}, k_{3i}, k_{4i}	Stiffness coefficients for layer *i*
M	Total bending moment on the cable
ΔM	Bending moment on the cable due to tension force in wires
N	Number of layers in the cable/strand
n_i	Number of wires in layer *i* of the cable
P	Normal distributed force in the radial direction
P_{MSi}	Line contact (hoop) force in a multi-layered strand/cable
P_{RCi}	Line contact (hoop) force in the single layer strand/cable with rigid core
r_i	Helix radius of layer *i* in multi-layered strand/cable
r_i'	Helix radius of layer *i* in multi-layered strand after deformation

Δr	Change in helix radius after deformations
T_i^{stick}	Tension force in the wire in stick state
T_i^{slip}	Tension force in the wire in slip state
T_i	Tension force in a wire in layer *i*
T	Tension force in cable/strand
t_i	Thickness of layer *i* of shaped wires in locked coil cable
X_H	Magnitude of the external hydrostatic pressure per unit length of the wire on the outermost layer
X_{MSi}	Radial contact force per unit length in layer *i* of multi-layered strand/cable
X_{RCi}	Radial contact force per unit length in layer *i* of multi-layered strand/cable
x'	Tangential displacement between two wires
α_i', α_i	Lay angles in layer *i* in deformed and undeformed states respectively
$\Delta\alpha$	Change in lay angle
β_i	Angle which locates the lines of action of line contact forces in layer *i*
δ	Relative slippage of the centres of contacting cylinders/wires under the action of a monotonically increasing tangential force
Δ_l	Tangential relative displacement between two neighbouring wires in line contact
Δ_{lmax}	Maximum tangential displacement between two wires at the onset of gross sliding (full-slip)
$\varepsilon_c, \epsilon_x'$	Cable axial strain

ϵ_x	Wire axial strain
ϵ_{11}	Compliance of the orthotropic sheet in the direction parallel to wire axes
$\epsilon_{11'}$	Compliance of the orthotropic sheet in the direction parallel to cable axis
ϵ_y'	Radial contraction of a layer in the cable's normal cross-section due to interwire contact deformations (Radial strain)
ϵ_y	The approach strain normal to ϵ_x between the centres of wires in line contact
ϵ_{22}	Normal compliance of two cylinders in line contact along wire axes
$\epsilon_{22'}$	Normal compliance of two cylinders in line contact along cable axes
ϵ_{33}	Tangential compliance of two cylinders in line contact
$\epsilon_{yC'}$	Total radial strain in the cable's normal cross-section (including rigid body component)
$\epsilon_{yR'}$	The rigid body radial strain in the cable's normal cross-section in the absence of a rigid core
ϵ_{yT}	Tensorial shear strain
γ_{xy}	Shear Strain in along wire axes
γ_{xy}'	Shear strain along cable axis
κ_c	Cable bending curvature
κ_{wr}	Wire bending curvature
μ	Coefficient of friction
υ	Poisson's ratio

ρ_c	Imposed radius of curvature
ρ_w	Water density
σ_x	Axial stress in the wire
$\sigma_{x'}$	Axial stress on the cable's normal cross-section
σ_y	Radial stress in the wire
$\sigma_{y'}$	Hoop stress in the cable's normal cross-section
τ_{xy}	Shear stress in the wire
τ	Cable rotation per unit length
φ	Polar angle of wire in cable cross-section

LIST OF ABBREVATIONS AND ACRONYMS

ABBREVATIONS	EXPLANATION
ACSR	Aluminium Conductor Steel Reinforced (Cable)
FC	Fibre Core
HDS	First Alphabets of the Surnames of Three Authors of the Paper, Hong, Der-Keureghian and Sackman (2005), J Eng Mech-ASCE 131:500-511
IWRC	Independent Wire Rope Core
MHDS	Modified HDS
OST	Orthotropic Sheet Theory
WSC	Wire Strand Core

KEYWORDS

Bending Stiffness, Bending Fatigue, Hoop Contact Force, Imposed Curvature, Interwire Slippage, Locked Coil Cable, Lay angle, Radius of Helix, Radius of Curvature, Radial Contact Force, Spiral Strand, Thin Rod Model, Semi-Continuous Model, Wire rope.

Chapter 1

Introduction

In this thesis, “wire rope” is defined as a flexible tension member consisting of several helical strands laid together either in parallel pattern or twisted around a core of other strands or synthetic or natural fibre material in different concentric layers (with individual wires in the strand forming a double helix), generally intended for supporting heavy loads. One can get a lot of strength and flexibility out of wire ropes because the separate wires balance the applied force throughout (Costello, 1997).

A “spiral strand” is likewise made of individual metallic wires wrapped helically in a series of concentric layers around the king wire. Each wire in a strand follows a simple helix. In addition to helical strands there are also parallel strands and locked coil cables, the wires in a parallel strands are laid in a parallel configuration without helical twist, resulting in a more axial stiffness and less bending/torsional stiffness, compared with helical strands. In a locked coil, shaped wires of usually z sections are used to achieve substantially higher fill factors with a proportional increase in mass for a given cross section over the basic spiral strand construction. The general term “cable” refers to both wire rope and spiral strand in this thesis.

Core is the central part of a wire rope made in accordance with the best practice and design, which itself may be a small diameter fibre or independent wire rope or wire strand of either galvanized or ungalvanized wires. Wire rope/strand cores are available either as fibre or steel cores depending on application. Their principal function is being to provide support for the strands and to maintain their correct positions under working conditions. Fibre cores are manufactured from natural fibres such as sisal, hemp, jute, and cotton or, synthetic fibres such as polypropylene while steel cores are supplied in two types:

i. Independent Wire Rope Core (IWRC) which is itself an independent wire rope.

ii. Wire Strand Core (WSC) used on smaller diameter ropes, and normally with the same construction as the outer strands.

Fibre core (FC) has the advantage that it increases the flexibility of the rope, provides resistance to rotting with synthetic cores and also lubricates wires by squeezing out the lubricants in the pores under working conditions, (McKenna, et al., 2004). This reduces internal corrosion and wear between wires. On the contrary steel core has high resistance to crushing, distortion and heat and therefore, increases breaking load for the rope. Also steel core provides better support for the strands lying on it and can better resist shock loading and stretch.

1.1 Lay of Wire Rope

The lay of a wire rope describes the manner in which the wires are laid in a strand and the way its outer strands are laid around the core in a helix, as shown in Figure 1.3, (Costello., 1997). And, the angle that a strand makes with the rope axis is called lay angle of the wire rope. There are two main types of cable lay's i.e. Ordinary/Regular lay and Lang lay. In ordinary lay rope the helix of wires in the strand is in the opposite direction to that of the strand in the rope. While in Lang's lay the helix of the wires in the strand is in the same direction as that of the strands in the rope. Regular lay rope is more stable as compared to Lang lay and can be handed easily but, due to point contact on the crown wires in the strands it has low resistance to wearing and therefore, abrasive fatigue occur quickly at these points due to high contact stresses. On the other hand in Lang's lay the surface pressure is spread over a longer length of wire of the strand which is in line contact with each other. Therefore, resistance to abrasion is more in comparison with regular laid ropes furthermore, bending of Lang's laid rope over sheaves is much easier. But, it has the disadvantage of producing high torque value under working conditions. This may untwist the rope if the ends are not fixed to rotate.

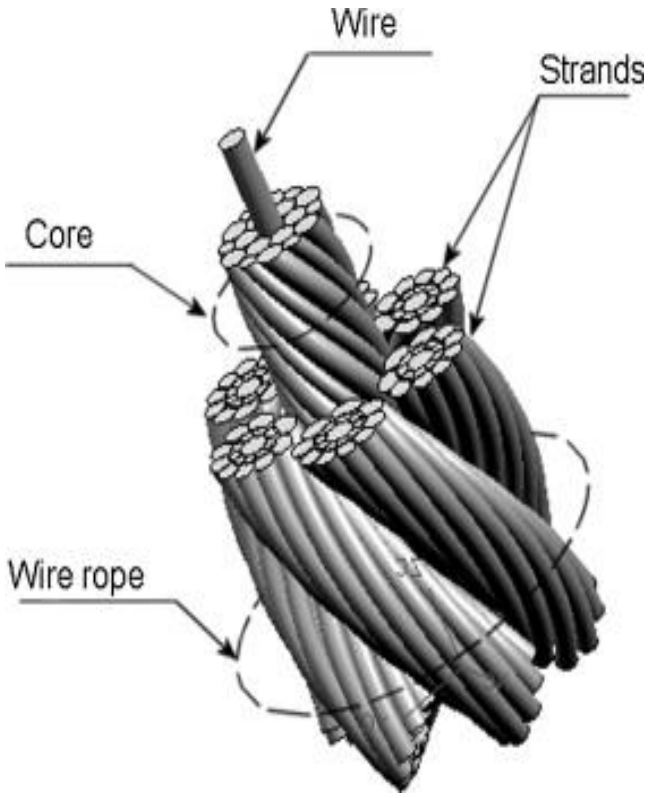

Figure 1-1: Various Components of Spiral Strand and Wire Rope.

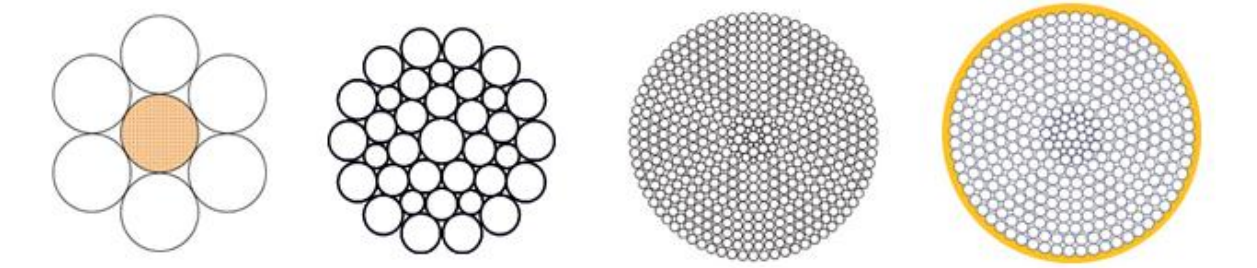

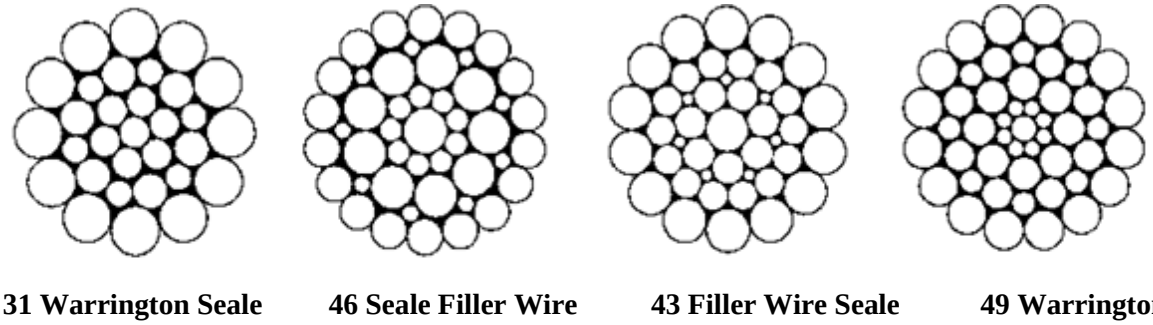

Figure 1-2: Typical Cross sectional Constructions of Spiral Strands/Wire Ropes (continued).

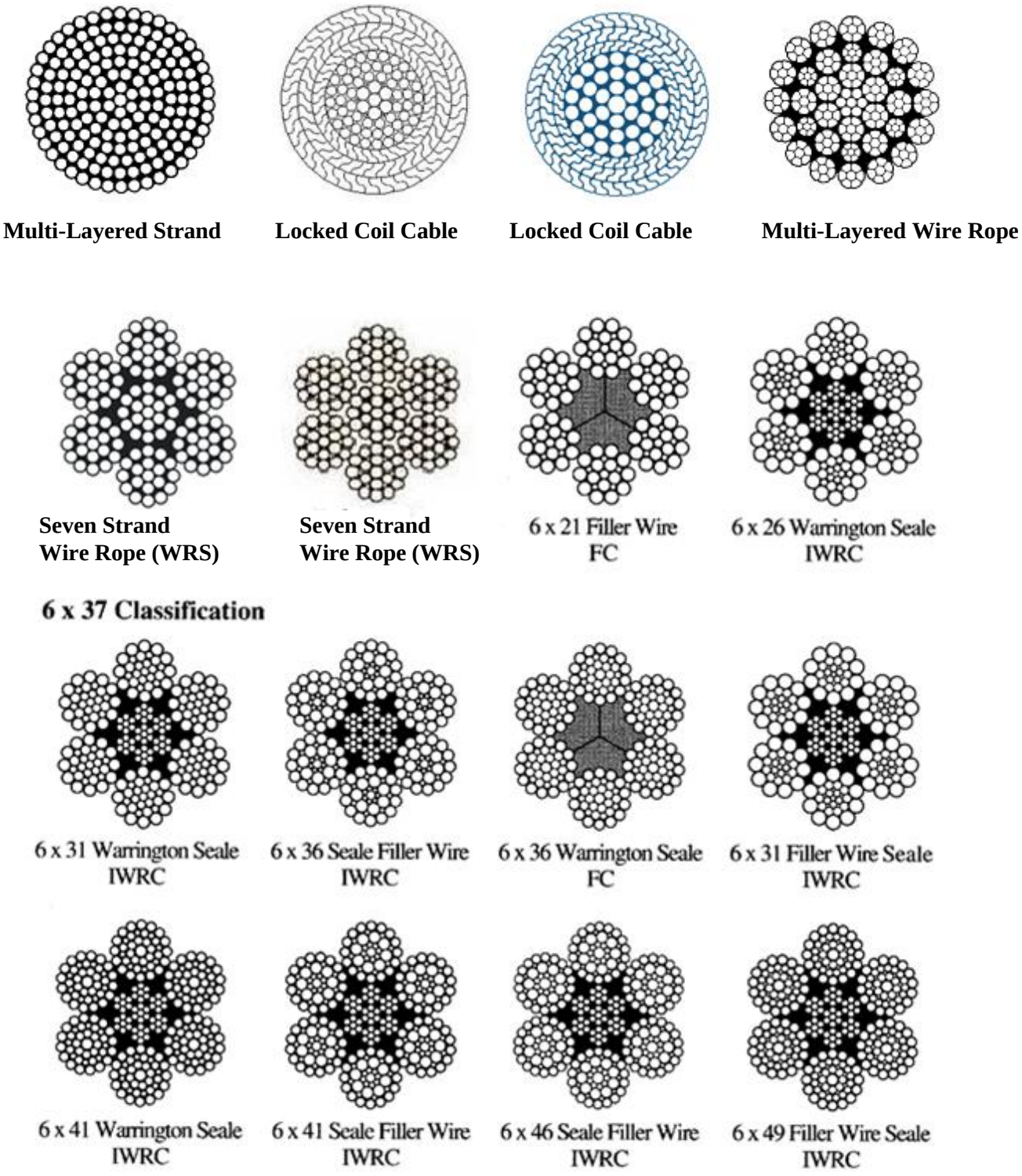

Figure 1-2: Typical Cross sectional Constructions of Spiral Strands/Wire Ropes.

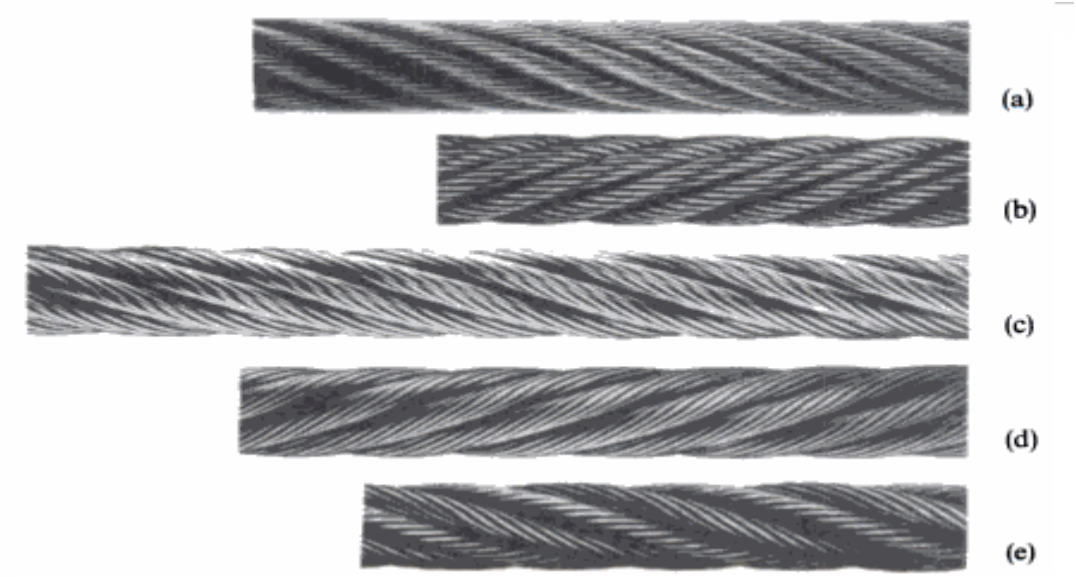

Figure 1-3: Typical Wire Rope Lays ; **(a)** Right Regular Lay; **(b)** Left Regular Lay; **(c)** Right Lang's Lay; **(d)** Left Lang's Lay; and **(e)** Right Alternative Lay Wire Ropes.

Although spiral strand and wire rope is essentially an element normally used for transmitting tensile load, but based on cable construction individual wires in a rope or strand are subjected to bending and torsional moments and bearing loads, as well as tensile forces. The overall response of a rope or strand, in terms of axial displacement/extension and rotation is the magnitude and distribution of stresses resulting from these loading. Cable ends where the tensile load is transferred to another element is of particular interest to the researchers because the mechanism of transferring load from individual wires to the gripping medium of the termination can give rise to the stress concentration that will be discussed in this thesis later. Friction between wires makes the problem more complex making stress distribution more uneven and hence the cable response to the load unpredictable. Ideally the end fitting must be capable of transferring the breaking strength of the cable without exceeding its own yield strength.

Due to high axial strength, high durability under large loads, high strength to weight ratio and relatively low cost, wire ropes and spiral strands have many important applications both in the onshore and offshore structures: which include hangers for suspension bridges, overhead transmission lines, the main cables of cable stayed bridges, lift applications (i.e. crawler & truck cranes, dragline, clamshell, shovels and

logging), stays for guyed masts, use in aircraft control systems, ship rigging or aircraft carrier catapults, applications in oil wells dragging and mining draglines, mooring system for deep sea offshore platforms and for post and pre tensioning of concrete, are few to list here.

1.2 Research Aim and Objectives

This research aims to investigate the bending behaviour of various types of helically wound steel cables (spiral strands, sheathed spiral strands and locked coil cables) under different loading conditions. During bending of such cables, slippage takes place between individual wires, which is mainly governed by interwire frictional forces acting at the contact patches between wires. The non-linearity in the mechanical behaviour of the cable will be shown to be caused by the change in the state of the wires from stick state to slip state.

To achieve the aim of the project, the research can be divided into the following distinct stages, one for each of the main objectives:

1. To critically review the available literature in order to identify possible shortcomings as well as strengths in the previously reported models and to present, both on the experimental and theoretical sides, reliable information of direct practical use.
2. To develop more efficient theoretical models, fully taking into account the effect of interwire frictional forces and contact deformations.
3. To analyse and present the results for different cables under different loading different conditions, in order to get a sound understanding of the key parameters influencing the problem.
4. To develop simple methods for bringing the theoretical solutions closer to practice.
5. To draw conclusions in comparison with the previous research and give directions for future work.

1.3 Methodology

In order to accomplish this research, a novel approach will be derived for the analysis of helically wound cables by combining the two selected non-linear models; Hong et al., (2005) and Hobbs and Raoof (1982). The first model provides explicit formulations for the smooth transition of the bending stiffness of the cable from no-slip to full-slip regime during bending, whereas the second model fully takes into account interwire frictional forces and contact deformations both in radial and hoop directions.

Based on the strain distribution on the curvature, three distinct stages will be addressed during the bending cycle of the helical cable: (a) no-slip; (b) partially slip; and (c) full-slip. In the first stage, all the wires in the cable will be shown to stick together forming a solid bar, such that the bending moment-curvature relationship is linear. Second will be the transitional stage, when some parts of the cable are sliding whereas others do not. The bending moment-curvature relationship will be shown to become non-linear in this case over a range of curvature, due to the variation of strain energy of slipped wires in the cable. In the final stage, for a critical curvature, the wires in the cable will be shown to slide everywhere in the presence of friction.

After developing a more efficient novel approach, extensive theoretical parametric studies will be carried out to determine the key parameters that govern the contact deformations during bending of the cable. In order to perform the necessary numerical calculations and to carry out the parametric studies, a computer programme has been developed in Java. This programme will be used to analyse the response of helical cables to different loading; to calculate the bending stiffness of spiral strands; and to analyse certain effects of an external hydrostatic pressure applied to sheathed spiral strands. The results will be obtained for various types of cables (spiral strand in air-condition, deep water applications and locked coil cables) covering a wide range of cable geometrical parameters, and will be compared with the experimental data in the literature.

After a sound understanding of the controlling parameters, the proposed improved theoretical solutions will be brought closer to the engineering practice, by means of simplifying them to the point where hand calculations are feasible.

1.4 Structure of the Thesis

The completed research in this thesis comprises eight main chapters which forms the structure of the thesis:

Chapter 1 gives an introduction and a general background to the wire ropes, spiral strands and locked coil cables. The main aim and objectives of the present research are also outlined here.

The literature review in **Chapter 2** highlights the shortcomings and some of the problems that the researchers have faced, attempting to analyse various aspects of helical cables. Both on the experimental and theoretical sides, reliable information of direct practical use are presented.

In **Chapter 3** an insight is given into the formulations used for predicting various structural characteristics of multi-layered helical cables. The two selected models have been analysed in detail and the ranges of their validity have been identified.

After the proposed modifications in the formulations, **Chapter 4** presents an extensive body of the numerical results obtained for a variety of spiral strand constructions subjected to different loading conditions. Effective bending stiffness of the cable is shown to be a function of the cable curvature.

The findings presented in Chapter 4 are used in **Chapter 5** to develop a simple method for the determination of the bending stiffness of multi-layered large diameter strands.

In **Chapter 6**, the model formulated in Chapter 4 has been extended to cater for the effects of external hydrostatic pressures on sheathed spiral strands in deep water applications. Numerical results are reported for three different strands of 127 mm diameter with lay angles of 12°, 18°, and 24° respectively, subjected to a range of water depths (0-2000 m).

In **Chapter 7**, a novel approach is presented for estimating the pattern of interwire contact forces and bending stiffness of locked coil cables.

Chapter 8 presents key conclusions and potential directions for future research.

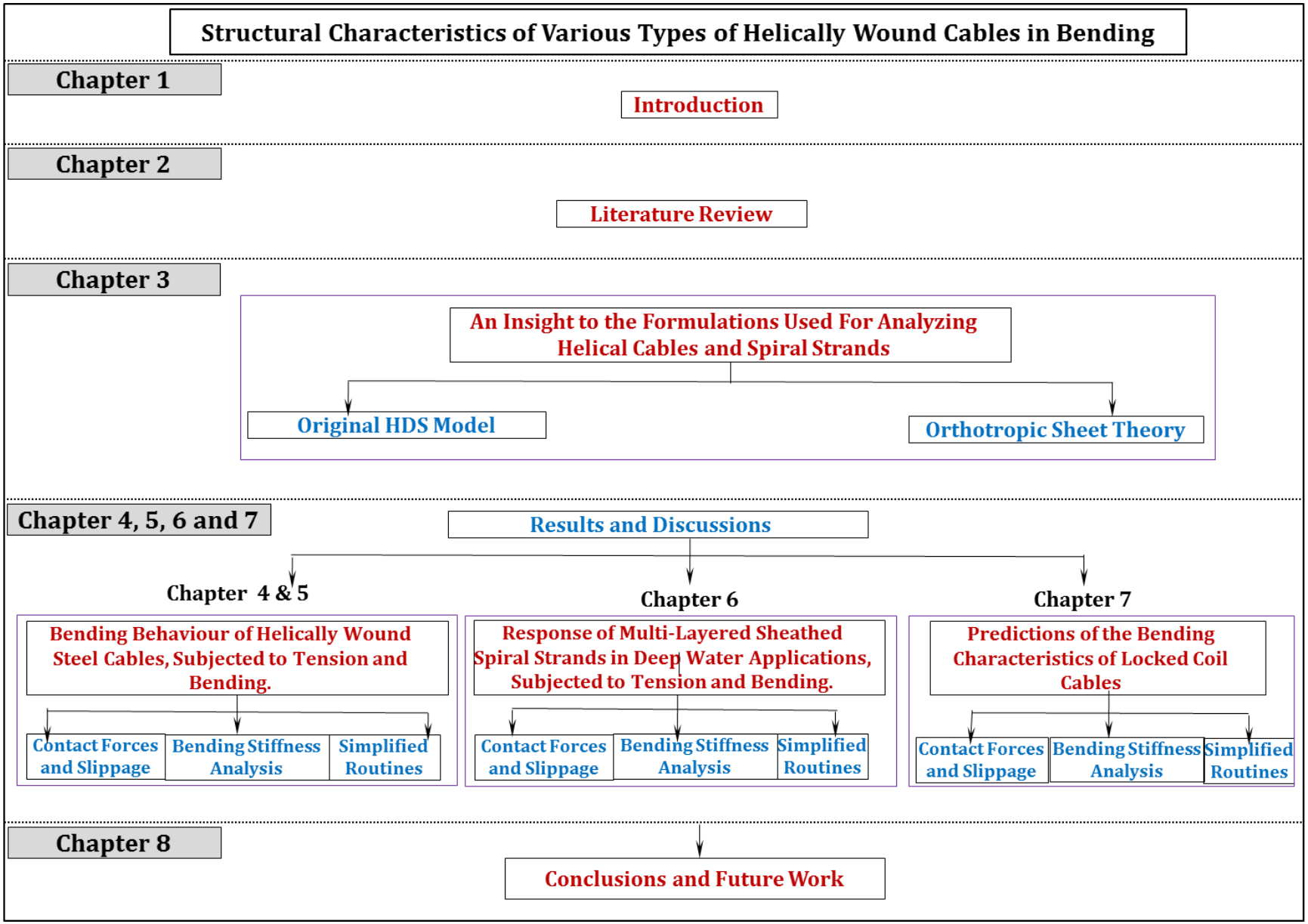
Structural Characteristics of Various Types of Helically Wound Cables in Bending
Chapter 1
Introduction
Chapter 2
Literature Review
Chapter 3
An Insight to the Formulations Used For Analyzing Helical Cables and Spiral Strands
Original HDS Model
Orthotropic Sheet Theory
Chapter 4, 5, 6 and 7
Results and Discussions
Chapter 4 & 5
Chapter 6
Chapter 7
Bending Behaviour of Helically Wound Steel Cables, Subjected to Tension and Bending.
Contact Forces and Slippage
Bending Stiffness Analysis
Simplified Routines
Response of Multi-Layered Sheathed Spiral Strands in Deep Water Applications, Subjected to Tension and Bending.
Contact Forces and Slippage
Bending Stiffness Analysis
Simplified Routines
Predictions of the Bending Characteristics of Locked Coil Cables
Contact Forces and Slippage
Bending Stiffness Analysis
Simplified Routines
Chapter 8
Conclusions and Future Work

Chapter 2

Literature Review

2.1 Introduction

A large body of available literature is critically examined in this chapter and the possible shortcomings and strengths in the previously reported models are pointed out. Several analytical models based on different hypotheses (like curved beam theory, Poisson's ratio effects, friction effects, diametral contraction and wires in pure tension) have been presented in the literature. Significant advances in the understanding of the behaviour of steel cables have been observed in the last three decades, various complex models have been developed for predicting with various degree of accuracy the mechanical response of helical strands and wire ropes under different loading conditions. Although the literature presented with these advancements in research on helical strand and wire ropes clarify the problems up to a great extent but still there are some research questions, which need to be answered. It is hoped that the research presented in this thesis will contribute to answer some of these questions.

Although cable is an element normally used for transmitting tensile load, but due to the helical nature of individual wires in a cable are subjected to bending and torsional moments and bearing loads, as well as tensile forces. The overall response of a cable, in terms of axial displacement and rotation is the magnitude and distribution of stresses resulting from these loading. Cable ends where the tensile load is transferred to another element is of particular interest to the researchers because the mechanism of transferring load from individual wires to the gripping medium of the termination can give rise to the stress concentration.

The work in this thesis is basically focused on the bending behaviour of spiral strands and the related problem of the fatigue lives of the strands under tension and bending condition. During bending of such cables, slippage takes place between individual

wires, which is mainly governed by interwire frictional forces acting at the contact patches between wires.

2.2 Contact Forces and Geometry of Cable

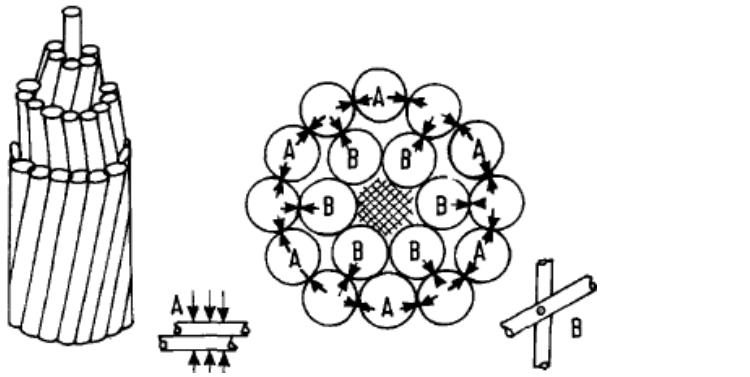

Figure 2-1: Interwire contacts in multi-layered spiral strands.

2.2.1 Contact Phenomenon

Two classes of interwire contact occur in a typical multi-layered spiral strand, as shown in Figure 2.1. The first one is the line contact within a given layer between adjacent parallel wires. The other class of interwire contact often occurs between the layers of a spiral strand, where to minimize the torque generated in the helically laid strand by an axial preload, successive layers of wires are laid in opposite directions. As a result, the wires in the two layers cross at an oblique angle, producing a point rather than a line contact. These contacts are described as 'trellis' contacts. Because they are localized, the contact stresses are much higher than on the line contacts within a layer.

These two classes of interwire contact (line and trellis), the nature of the movements on them and the associated contact stress patterns are central to an understanding of the elastic, hysteretic and fatigue properties of spiral strands. The behaviour of the strand is perhaps best understood, because the single level (cf. ropes, double level) of twist in a given wire has made it possible to develop a strong body of analytical work (supported by experimental studies). This work has concentrated on assessing contact

forces and the associated relative displacements between individual wires, taking full account of frictional effects, in large multi-layered spiral strands undergoing a wide variety of loading regimes.

2.2.2 Helix Geometry

An individual wire in the strand follows a helical path around the core, where a single lay length of the helical wire in the cable can be always unwrapped to form a right-angled triangle as shown in Figure 2.2b. Every wire in the cable has a specific value of polar angle, which describes the position of a wire in the cable cross-section. The position of an individual wire in the cable changes along the length of the cable, therefore the value of the polar angle of a wire varies from 0 to ±π, as shown in Figures 2.2a.

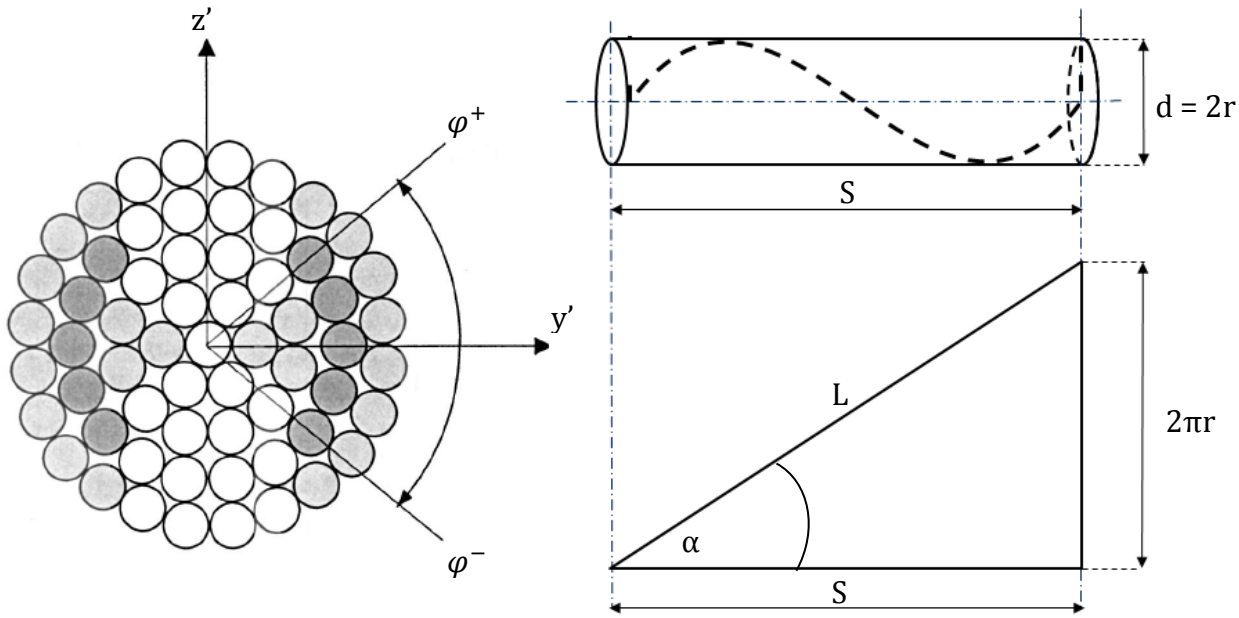

Figure 2-2: (**a**) Illustration of the polar angle in the cable cross-section; (**b**) Geometry of a wire in an arbitrary layer of the cable, where a helix may always be unwrapped to form a right-angled triangle.

In Figure 2.2b, *L* is length of the helical wire in the cable, *r* is the radius of helix, d is the outer diameter of the cable, α is the lay angle of the wire in the cable and φ is the polar

angle of a wire the cable, which describes the position of wire in the cable cross-setion.

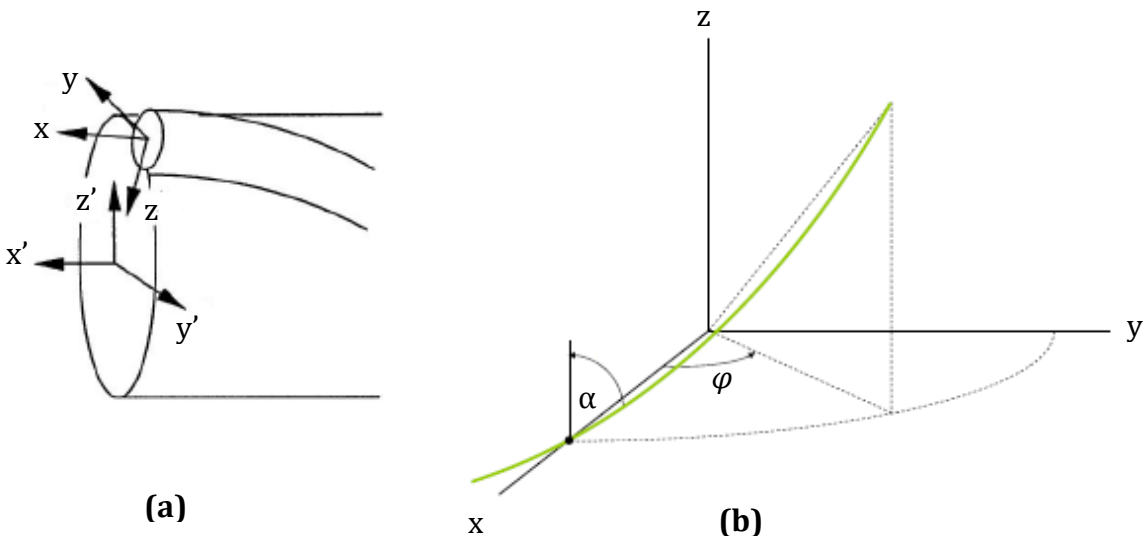

Figure 2-3: (a) Illustration of the global (cable) and local (wire) coordinates; (b) Geometry of a helical wire in the cable.

In Figure 2.3a & b the helical coordinates used in this thesis are described with the polar angle in the (x, y, z) frame. This angle rotates around the longitudinal axis of the helix and coincides with the centre line of the cable. In the current study, x, y and z represent local (wire) axes, whereas x', y' and z' are used for global (cable) axes as shown in Figure 2.3a.

The parametric function for a wire having polar angle φ, in any arbitrary layer is then given by:

$$H(\varphi) = \begin{Bmatrix} x = r\cos\varphi \\ y = r\sin\varphi \\ z = r(\cot\alpha)\varphi \end{Bmatrix} \quad 2.1$$

Once the geometry of helix and the contact forces between the wires are defined in this section, a detailed literature review has been presented in the next section. The main motivation for this study arose from the interest that due to the helical nature of a wire interwire contact forces in the hoop direction are inherent in the cable, and have a great influence on interlayer slippage and overall contact deformations.

2.3 Mechanical Models

In the last few decades, a series of attempts have been made to develop engineering models for predicting the mechanical behaviour of helically wound steel cables. These models vary in accuracy and complexity from Hruska's simple model to the complex models of Lutchansky (1969), Costello (1977, 1978, 1983, 1997), Knapp (1975, 1979, 1988), Raoof (1982, 1983, 1988, 1990, 1992), Papailiou (1997) and Hong (2005). Due to the development of computing power (FEM packages) calculation time has been reduced dramatically and this development motivates the use of FEM approach. However, a better use of FEM techniques could be made possible, if a more detailed insight is gained into the interwire contact deformations analytically. The various FEM models, however reported have been in good correlation with experimental results. As the vast majority, of available theoretical models for cables do not cater for the ever presence of interwire friction and contact deformations.

2.3.1 Purely Tensile Models

Hruska (1951) was the first researcher who made a fundamental approach at the theoretical modelling of a spiral strand. He published his first paper on the tensile forces in the wire ropes as a result of the strong desire to refute Hall's (1951) assumptions. Hall took into account only the tensile forces in the component wires of a wire rope and concluded that the axial stresses in the outer wires of a rope were greater than the stresses in the inner wires. He neglected the effect of interwire friction.

Hruska (1951) considered in his first paper the tensile forces in the wire ropes, and discussed the three important internal actions (i.e. tensile, radial and hoop forces) to be considered in the analysis of wire ropes subjected to tensile forces only. Hruska completely ignored the bending and twisting effects of helical wires in his analysis. Hruska totally disagreed with Hall's (1951) results, and found that for axial load the core wires were more stressed than the outer wires. He also developed a formula for calculating the tensile stresses in each individual layer of a wire rope and concluded that tensile stresses in each layer is directly proportional to the square of the cosine of the lay angle for that particular layer. Hruska neglected the effect of slight changes in

lay angle and helix radii after the application of axial load. Hruska was also the first one who mentioned the importance of interwire friction in the wire rope, and argued that a broken wire will be able to take full share of its load within a distance of few lay lengths.

In his second paper, Hruska (1952) tried to establish a relationship between radial and tensile forces in a layer of wire strand, ignoring once again the effect of slight changes in lay angle and strand diameter. The findings of this study were that the radial forces increased inward for each layer of rope construction and were therefore reached a maximum for core wires.

Hruska (1953) then analysed the effects of the tangential forces in the wire ropes. In this paper Hruska showed the way to calculate internal moments and torques in the wire rope which were specifically generated by hoop forces in the wires due to inline contact with each other within the same layer of wire strand. Hruska however did not provide any experimental evidence.

2.3.2 Thin Rod, Discrete Rod, Helical Rod or Curved Rod Models

Owada (1952) proposed a method for estimating the axial and torsional stiffnesses of a simple strand by employing Kirchoff's equations of equilibrium for smooth thin rods. In his model the contact deformations between adjacent wires and the core were taken into account when calculating changes of wire helix radius and core deformations. His model was supported by some limited experimental data.

Leissa (1959) extended Hruska's approach to find contact stresses in wire ropes. He used the Hertzian contact stress theory to calculate the normal contact stresses in the rope. His analysis was based on the maximum shear theory and the maximum normal stress theory applied to the point at critical regions of contact between the core and outer wires. In order to make the analysis simple Leissa restricted his investigations to seven wire strand subjected to axial tensile load only. Although Leissa completely ignored the effect of interwire frictional forces and contact deformations, but his work

gave an insight to the complex study of contact stresses in the wire ropes. This inspired other researchers to deal with this problem.

Chi (1971) prolonged Hruska's method for the analysis of stresses in the wire ropes. Chi took into account the effect of diametric contraction of strand when loads were applied. Hruska didn't cater for diametric contraction in his model and supposed that the diameter of the strand is the same before and after the application of load and also neglected the effect of end rotations and deformations. In order to deal satisfactorily with diametric contraction, Chi suggested a formula for finding the axial strains in all the wires of a strand catering for the effect of reduced cross sectional area of the wires.

Chi (1972) analysed in another paper multi wire strands subjected to tensile force only and for the combination of tension and torsion both. Based on his analysis, Chi proposed a design procedure for a wire rope of three layers including core wires, without providing any experimental data to support his theory.

Durelli et al., (1972) gave some fragile coating to the strand wires and mounted electrical resistance strain gauges on the wire surface in directions parallel to the wire axis and measured the direct strains in various helical wires of a seven wire strand. The strand was subjected to axial, bending or torsional loading with either both ends free to rotate or both ends fixed. Although the data was very dispersed but, the response of the strand was yet in agreement with the theory that they developed. Strains in some wires were however, not linearly proportional to load. Authors also concluded that the average longitudinal strain in the core was more than the longitudinal strain in the helical wires which confirmed Hruska's findings. In addition to this, it was observed that repeated load didn't change appreciably the non linear behaviour of wires nor the uneven distribution of load between wires.

Machida and Durelli (1973) proposed certain linear expressions for the determination of tension and bending plus twisting moments in helical wires assuming that deformations are small enough to neglect the change in helix angle under load. The core was assumed to act as a simple rigid bar subjected to axial and torsional loads. Interwire contact deformations and Poisson's effect on individual wires due to axial

strain were neglected. While normal contact force between wires was taken into account. In addition to this, circular cross sections were used both for helical and core wires to determine stresses in them. Elementary theories of bending and torsion were applied to determine stresses in helical wires and core. Although the equations given were initially used for seven wire strand only with small deformations but similar linear equations could be developed for a multi wire strand or strands with large deformations. Also, measurements on oversize epoxy model showed good correlation with the theory concluded that axial load had no effect on the effective torsional rigidity of the strand. Durelli and Machida (1973) observed that it was difficult to measure axial strain in the small wires. In order to overcome this problem, the authors tested some oversize plastic models of strands in tension, torsion and bending. It was found that in addition to electrical resistance strain gauges and brittle lacquer, Huggenberger gauges and rosette strain gauge could easily attach to the surface of oversize models. In spite of some discrepancies and uneven load sharing between identical wires the results were found in good correlation compared with theoretical values.

Costello and Phillips (1973) studied the contact stresses in twisted wire cable and took a more fundamental approach than the previous modelling approaches for the analysis of wire ropes. They considered individual wires of the strand as thin rod cylinders, subjected to bending, twisting, contact and axial loads. For every separated thin rod six geometrically non-linear equations were developed and then solved for bending and twisting of the thin rod subjected to axial load. A single layer strand was considered and the frictional force between the wires was neglected. It was further assumed that the wires were just touching each other in the unloaded state and, that the core was compressible so that, the radial force exerted by core on the wire could be neglected. A simple procedure was then developed for determining the contact stresses in twisted wire ropes. Catering for the change in helix angle due to loading the authors found that the bearing load between the wires was increased with increasing axial load up to some extent and then started decreasing until the wires of the cable were straightened i.e. at helix angle 0.

Costello and Phillips (1974) derived some new expressions for the contact stresses in helically wrapped wire cables that were mainly dependent on the contact angle between the two adjacent wires in the cable. Phillips and Costello (1977b) extended their previous work to determine the dynamic behaviour of axially loaded twisted wire cables. Using Laplace transformations, equations of motion were linearized for a single lay twisted wire rope, catering for both, the axial and twisting moments in the cable element for some specific boundary conditions.

Costello (1977) investigated the problem of large deflections in helical springs, subjected to bending only. The spring was considered as a thin wire and likewise, Costello previous work solution was sought out for the differential equations of equilibrium once again neglecting the friction force between the wires.

Costello and Sinha (1977a) presented a frictionless theory for the determination of the static behaviour of a wire rope. The authors treated wire rope in the same way as wires were treated in the strand in previous papers. The bending, torsional and axial response of the strand was determined, and then incorporated all these in the equilibrium equations for a wire rope neglecting the effect of ever present frictional force. In another paper Costello and Miller (1979) proposed a theory for predicting the static response of regular and Lang lay wire rope. Investigating a variety of wire ropes, it was concluded that Lang lay rope had practically no torsional stiffness under tension and lay just unwrapped itself, when torsion was applied. Regular lay in contrast, tended to stiffen as load increased therefore, it was suggested that Lang lay rope should not be used in the case when the ends of the rope are free to rotate.

Costello (1978) summarized the long history of wire rope properties and its applications, which make them useful structural elements. In his paper, he briefly discussed various theoretical models developed until 1978, based on various simplifying assumptions. It was pointed out that the available literature employed frictionless helical rod approach, and the future work should include the effect of friction between wires.

Phillips, Miller and Costello (1979) for the first time considered contact stresses at the crossover points between wires of a rope. Results were shown for a rope of 1x19

constructions. It was found that the contact force was small enough in comparison with tensile force applied to the rope, but could be significantly increased with increasing tension in the wires and could get larger value than the tensile stresses in the wires.

Costello (1990) presented theoretical formulations for analysing in detail wire rope based on Kirchhoff's equations for the equilibrium of thin rods. The equations for a simple strand were linearized and applied to stranded wire ropes with IWRC. Forces and deformations on the cable were related through non-dimensional stiffness coefficients. The effect of interwire frictional forces was reported to have very small effect in wire ropes. He stated that in the case of pure tension either no sliding between the wires took place or only a very small level of sliding occurred. In the case of bending, tensile stresses in wire due to bending were found to be small enough to produce significant frictional effects.

Huang (1978) examined the response of an elastic seven-wire strand with a central core wire subjected to tensile and torsional loads. The significance of this work was that it took into account the Poisson's effects on helical wires. Before the application of loads core and helical wires were assumed just to touch each other. It was observed that when a tensile load is applied to the strand, the core and strand wires came closer to each other resulted compressive stresses between core and helical wires. An opposing pressure was observed to develop between the wires that were in line contact with each other caused by the contact pressure which, caused wire slippage in the outer layers of the strand. Furthermore, it was found that the slippage of wires in outer layer is a function of the magnitude of contact pressure between wires and the magnitude of axial tensile load carried by outer wires. Analysis were carried out for the extension of the strand with a separation of outer helical wires and extension of the strand without separation of outer wires assuming two types of end conditions namely: fixed-fixed and fixed free to rotate. Recently, W.G Jiang (2005) discussed Huang's model and pointed that by neglecting contact deformation in most of the previous discrete models including Huang's (1978) might lead to incorrect conclusion and that the extension of the strand could never cause a separation between helical wires in line contact, even if the core and surrounding wires are made of the same

materials, which confirmed Hobbs and Raoof (1982) homogeneous strand model of lateral contact mode.

Knapp (1979) derived a new stiffness matrix for armoured cables taking into account tension and torsion only. Due to the construction of spiral strand configuration, which consisted of different layers of different materials having totally different structural properties, Knapp treated the cable as a composite element in his analysis. Knapp assumed that helical wire diameter remained constant during interwire contact pressure but, at the same time he catered for the compressibility of central core wires. Based on these assumptions the author first developed geometrically non-linear equations for internal deformations i.e. axial displacement and rotation, which were then linearized to develop linear stiffness matrices both for tension and torsion in the cable. Experimental results were in good agreement with analytical values for geometrically compatible wire strands therefore, the author concluded that the predicted theory is applicable only for geometrically compatible wire strands and cables.

Utting and Jones (1985) reported test results conducted on a different type of seven wire spiral strand. The test procedure was described in detail for obtaining the experimental results for a seven wire strand. The test results were compared with Machida and Durelli (1973) theoretical predictions, which neglect interwire friction forces, Poisson's ratio effects, and wire flattening due to contact forces, and were found to agree reasonably well. Furthermore, it was found that the load sharing between nominally identical wires were unequal particularly in the regions near to the end grips, which may have considerable effect in the axial fatigue studies. The problem of end termination was resolved later for future tests and it was suggested that each wire should be bent through 360° before socketing

Utting and Jones (1987a) carried out another set of experiments on straight single steel strands subjected to axial loads with various end restraints. The strand extension, torque, rotation, tension and bending moment were measured. The strand lay angle was ranged from 9.2° to 17°, with core and helical wires diameters of 3.94 and 3.73mm respectively. A mathematical model was developed to investigate the change in helix angle under axial load, due to Poisson's ratio effects in the wires, wire

flattening effect due to contact pressure and the effect of friction force between the core and helical wires. In a companion article Utting and Jones (1987b) compared the test results with previously published analytical work of Machida and Durelli (1973) and his own theoretical results. The strand extension for free end was observed 70% more than that in the fixed end conditions. Furthermore, strand extension was found to be larger for small helix angles in fixed end test conditions while rotations were greater for strands having small helix angles in free end tests. Uneven load sharing was observed between identical wires for surface strains and the unevenness of this loading remained unchanged under repeated loading. According to the computed results of this study in comparison with previous analytical work Poisson's ratio effect, friction between wires and wire flattening at the contact surfaces increased elongation of cable up to 2.3% only with no effect on rotations. In addition slip between core and helical wires was not observed in the strand for the strand length tested.

Utting and Jones (1988) further extended their previous work and carried out tests on multi-layer strands of nineteen wires that had a core and helical wire diameters of 3.66 and 3.33 mm respectively. Tests were conducted for different end conditions e.g. fully fixed, partially restrained and totally free ends against torsion. The rate of elongation and strand rotation were found maximum for free end conditions and vice versa. The test values occurred for free end test largely deviated from theoretically predicted values for increasing axial load. However, the theoretical determined deformation of individual wires showed a more uniform distribution of load for fixed end conditions, which did not exist in reality and therefore, the deformation of a particular wire may be much greater than that predicted by existing theories. It was also observed that the change in the rate of bending moment varied with strand load such that increasing strand load tended to decrease the tensile stresses in the wire crown with less torsional restraints. Finally the results were compared with the experimental results of Velinsky et al., (1984), as well as their own test data (Utting and Jones, 1987a and 1987b). The main point, based on this comparison was that the theoretical predictions of the overall response of a seven wire strand were more accurate than those for a nineteen wire strand.

Kumar and Cochran (1987) applied Costello's (1983) theory in conjunction with the assumption of small change and developed closed-form solutions for various elastic deformation characteristics of a more complex wire rope model with a metallic core, subjected to external tensile and torsional loads. A simple design procedure was established for non-rotating cables that were found quite well in predicting the rope stiffness against axial displacement and rotation of the rope. In addition, effects of the layout of layers, number of wires in each layer and the direction and magnitude of lay angles, on these deformations were also investigated. The effect of interwire frictional forces was ignored once again.

Kumar and Cochran (1990) developed closed form solutions capable of predicting static deformations of the twisted wire ropes with fibrous cores subjected to axial and torsional loads. The wires in the same layer were assumed to touch each other in line contact before the load was applied. The rope was analysed for two different cases: namely, when both ends are fixed against rotation, and when one end is free to rotate keeping other fixed. The importance of the number of helical wires was signified for both the cases and that when both the ends of the cable were fixed against rotation the steel Poisson's ratio was found to have negligible effect on cable axial stiffness. In addition it was found that the lay angle of the wires has a strong effect on the axial stiffness of the cable. Finally numerical results were compared with the corresponding numerical results of Costello and Phillips (1976).

Jolicoeur and Cardou (1991) numerically compared many of the previous mathematical models, which in turn were compared again with the experimental results of Utting and Jones (1987a, 1987b), McConell and Zemke (1982) and Knapp (1979). It was observed that the results of all models were quite accurate as long as axial stiffness of the cable was concerned. The degree of agreement between theoretical and experimental results was noted to vary, when the coupling coefficients were calculated. Also, it was discovered that all the models yielded comparable results as for as global stiffness of the cable was concerned, but they were not equivalent when it came to find local effects such as interwire or interlayer pressure and non-linear behaviour. To address these cases more advanced model should be used, such as orthotropic sheet model of Hobbs and Raoof (1982).

Ramsey (1990) proposed a thin rod model for the analysis of steel cables experiencing extension and twist, taking into account both interwire frictional forces between the adjacent wires in the same layer, as well as between wires in the adjoining layers. It was stated that these forces existed only in the form of couples which oppose changes of the wire lay angles.

Lee (1991) developed a mathematical model based on vector geometry to investigate the geometrical properties of rope helices. A computer programme was derived from the mathematical model for calculating the geometrical parameters of double and triple helical wires in the strands and ropes. The bending of strands and ropes over a sheave or around a drum was investigated. It was found that the wire curvature and torsion functions could be related to the bending stress in addition, it was discovered that the properties of these functions and their implications for bending and twisting stresses were dependent on the lay of the strand and wire rope. It was stated that the geometrical analysis presented in this paper could be applied to any rope with axisymmetric strands.

Jiang (1995) gave some general formulations for the non linear and linear analysis of wire ropes, neglecting the effect of frictional forces between wires. In these formulations wires, strands and wire ropes were considered as a kind of identical structure, only with different values of stiffness and deformation constants. It was stated that the general formulations developed could be used for the analysis of wire ropes consisting of various complex cross sections as well as simple wire strands. It was further stated that in this way various strand and wire rope problems could be attacked with one general formulation. Jiang's work was later discussed by Jolicoeur (1996), who pointed out some typing errors and a sign error in the formulation. Sathikh et al (1996) discussed the lack of symmetry in the stiffness matrix. It was proposed that in order to make the solution theoretically sound and consistent, the stiffness matrix should always be symmetrical.

Sathikh et al., (1996) presented a symmetric linear elastic model for helical wire strand using discrete thin rod theory. The problem of asymmetry common to the majority of discrete models was solved. Analyses were carried out for seven wire strand with rigid core, having only core to wire contact, neglecting interwire contact

forces. The wire tension, torsion and bending was considered in the analysis. The predictions based on this approach were compared with those of other thin rod models and experimental results available on a variety of seven wire strand, and was found to provide reasonable results. The model was based on Ramsey (1988 and 1990) - Wempner (1973) theory of generalized strains. Although this model identified the origin of the lack of symmetry in the stiffness matrix of earlier models, it is still a discrete model, and discrete model has always shown less favourable results than a semi continuous model particularly, when the number of wire in the spiral strand increases to say, more than nineteen.

Kumar et al., (1997) extended Costello and Phillips, theory of wire rope and obtained analytical closed-form expressions for critical line contact stresses in a single seven wire strand cable with fibrous core. It was observed that lay angle has a strong effect on the life span of a cable and using very large lay angles, e.g. 45°, would essentially promote a longer life span for a cable. In addition it was found that for wire ropes whose main function is dissipating vibrational energy, then, lay angle as large as 30° cause much larger contact stresses and hence, frictional hysteresis. However, as for as the knowledge of the present author is concerned, cables with lay angles of 30° and above are not used in practice. The practical lay angles being used are generally within the range of $11° \leq \alpha \leq 24°$.

Sathikh et al., (2000) proposed a more generalized discrete thin rod model to study the pre-slip behaviour of a seven wire strand. The helical wires were assumed to be in contact with the core under Coulomb stick friction and the effect of rolling of wires on core was neglected. The main purpose of this study was to improve the characterization of the strand behaviour in free bending over other available discrete models. Numerical comparison of various discrete models was made, and it was stated that the discrete models of Knapp (1988), Lutchansky (1969), Lanteigne (1985), LeClair and Costello (1988) were only the special cases of the present general model. As discussed earlier, such discrete models could only produce reasonable results for a wire strand up to say nineteen wires. This is because for a large number of wires, discrepancies in results increase by considering the equilibrium of individual

wires in the cable. Advanced models, like orthotropic sheet model should be used for the analyses of multilayer helical strands of more than, say nineteen wires.

Elata et al., (2004) proposed a new model for simulating the mechanical behaviour of a wire rope with an independent wire rope core subjected to axial load as well as axial torque. Unlike previous discrete models, this model fully took into account the double helix configuration of individual wire in the wire rope that was based on the kinematics of individual wires within the rope. Two different cases were considered namely: open sieves that had very low friction, and closed sieves that had infinite friction between adjacent wires. The axial stress predicted at the wire level for both the cases was considerably different. The rope stiffness matrix coefficients were compared with the experimental data collected, which were found in reasonable agreement. It was suggested that the model could be used to predict failure, fatigue and fretting at the wire level that could be used for designing rope cross sections with the properties of rotation resistant and uniform load distribution. Bending and torsion stiffness of the individual wires were completely neglected in the analysis.

Yen and Chen (2006) developed a theoretical model for predicting the behaviour of axially loaded complex wire ropes. The model was based on the frictionless theory of Costello and others i.e. considering wire rope as an assembly of helical wires and in addition to this Love's theory of thin rod was also applied. The results obtained for the relation of axial stress and strain by the presented theory were found less stiff than the results determined by Costello's model. It was shown in the results that approximately linear relations existed between load and axial strain for zero rotational strain of the wire rope. This modified theoretical approach was used in the analysis 6x7 wire rope with an independent wire rope core, completely ignoring the effect of intewire frictional forces. Some comparisons to other research results were provided with no experimental data in support.

In another paper Ghoreishi et al., (2007b) presented several closed form formulations to predict the behaviour of fibrous structures, made of six helical strands wrapped helically around a straight core. The helical strands were assumed as Kirchhofs-Love beams, by neglecting the effects of bending moments and shear forces. In addition to this, the friction effects and lateral contraction of the core was also neglected due to

the static load assumption and small lay angles. The model results were compared with an existing model of Leech that was found in reasonable agreement, except a notable difference for the torsional stiffness of the rope. The model was initially developed for metallic cables, which was then modified for synthetic wire ropes. It was stated that for the next higher level of the model, results from the previous level were used as input data and, by using this approach from lowest to higher the axial stiffness matrix of the rope was developed. Finally, test results on both fibre ropes with 25 tons and 205 tons rupture load, were reported to obtain experimentally the values of the rope stiffness matrix. A very close agreement was claimed to find between the model and experimental data at the low level of the input material characteristics.

Kenta et al., (2007) investigated the mechanical behaviour of multi order helical structures in electrical cables and developed an analytical model for calculating the stress in second order helical structures fully taking into account frictional forces between wires. Stresses in every individual wire were calculated first and then by summing them up the overall response of the cable to bending was determined. It was found that the internal stress and number of slipping wires were the key properties for the life estimation of the cable. Furthermore, it was stated that the behaviour of the wires were not only affected by applied loading but also by the pressure from clamping jacket, insulation materials and other components, that resulted frictional force on the surface. The theoretical results from the model were compared with experimental data to estimate the unknown pressures developed from jacket and insulation materials. The transition from stick state to full slipping state was achieved by fully considering the effects of interwire frictional forces.

Usabiaga and Pagalday (2008) developed a new theoretical procedure for modelling of wire ropes having wire strand core and subjected to tensile and torsional loading. The proposed theory was based on Love's (1944), general thin rod theory with beam assumption by taking into account the double helix configuration of individual wires in the rope. It was further assumed that the friction between wires is high enough to prevent the slippage between the wires in the strands, which does not seem to be a practical assumption and the strand stiffness largely varies with relative slippage of

wires. It was stated that the wire contraction due to Poisson's ratio had no significant effect on the overall stiffness of the rope. Based on Love's curvature a simple procedure was developed for computing bending stresses for double helical wires. The predicted results from this model were compared with the previous analytical models of Costello, Ghoreishi et al. (2007a) and Ashkenazi et al. (2003) as well as experimental results reported by Utting and Jones (1987), which were found in reasonable agreement with some disagreements for local stress and torsional stiffness values of the strand.

Ivan (2011) proposed a discrete mathematical model for calculating analytically the transverse contraction of the wire strand through Poison's ratio and local contact deformations. It is shown that for small lay angles (less than 15) Poison's ratio effect were more dominant over the effect of interwire contact. For lay angles beyond 25, the impact of interwire contact (i.e wire flattening) effect dominates the Poison's ratio effect.

2.3.3 Semi-Continuous Models

All the models discussed in the previous section are known as discrete models, as the compatibility equations are developed for every individual wire of the strand and then solved to find the internal actions. Semi-Continuous model approach is totally different, as in this case a strand consisting of a core and N layers of helical wires is mathematically represented by N concentric orthotropic cylinders, whose mechanical properties are averaged to form a continuum which matches the behaviour of their corresponding layer of wires. Since the properties of the strand are averaged in semi continuous models, the accuracy tends to increase with the number of wires in the strand. The other major advantage of semi continuous model is that the problem of interwire contact is sufficiently simplified to be mathematically tractable. Since there are a lot of uncertainties in calculating the interwire line contact stresses on a nominal basis due to irregularities in the fit of the wires, semi continuous models have also provided very good results to address the problem of statically indeterminate contact stresses between the wires of a spiral strand. Hobbs and Raoof (1982) were the first who developed the concept of orthotropic sheet theory known as the first semi-

continuous model which was then described in detail by Raoof (1983) and later on, extended by Raoof and his associates over almost three decades.

Currently, there are three types of semi continuous model approaches used for the analysis of wire ropes. The first was developed by Hobbs and Raoof (1982), and is known as orthotropic sheet model. It is postulated that each layer of wires in the strand has enough wires for the properties to be averaged so that, the layer can be treated as cylindrical orthotropic sheets, which is assumed to be thin and in plane stress state. The elastic properties of the sheet are then derived as a function of the external load perturbation, with reference to the principal axes parallel and perpendicular to the wires, using mechanical contact theories and assuming Coulomb's friction between wires. Then Hearmon (1961) formulation can be used to transform the elastic properties of the sheet to values parallel and perpendicular to strand axis. The compatibility equations are initially developed for a strand with its ends fixed against rotation, it is assumed that the wires in each layer are just touching each other in line contact in the unstressed configuration. As the theory is developed for strands with large number of wires say, more than 19 therefore, it is further assumed that the wire cross sections in a normal section of the strand will be treated as ellipses. It is postulated that in multi layered strand the diametric contraction of individual layers due the Poisson's ratio effects in wire material is quite uniform over cable cross section and therefore Poisson's ratio does not affect the contact stress between individual wires in different layers. It is further assumed that twisting and bending moments of individual wires are negligible and that plane sections remain plane during strand deformations away from clamping points. For a counter laid construction, the elastic stiffness in the radial direction across the trellis crossing of cylinders (wires) is quite smaller than in the hoop direction across line contact between cylinders (wires).

Another semi-continuous model was developed by Blouin and Cardou (1989) that was later followed by Jolicoeur and Cardou (1994, 1996). This model shares some similarities with the model of Raoof and Hobbs (1982) but the two models rely on entirely different theoretical grounds and are different in the evaluation of strand stiffness and slip effects. Also in orthotropic sheet model the cylinders are considered

thin with negligible thickness of wires and the problem is two dimensional, while in this model the thickness of cylinders is considered that makes the problem tridimensinal. Both approaches however, are based on continuum mechanics and the elasticity of anisotropic material. The model was initially developed for ACSRs cables, which was then extended to other types of helical strands and wire ropes. Like orthotropic sheet model of Raoof, this model also replaces each layer of wires with a cylinder of orthotropic material. Stress-strain equations are derived for such a cylinder experiencing axisymmetric loading: axial force, twisting moment and uniform radial external and internal pressure forces. These equations were then generalized to a system of N co-axial cylinders with an isotropic core. The model was further extended by Joulicour and Cardou (1994) and some general analytical solutions were obtained for describing the behaviour of a system of co-axial orthotropic cylinders under tensile bending and torsion loads considering two types of boundary conditions at the interface between two cylinders: no slip and no friction. For simplification, it was further assumed that cylinders were cylindrically anisotropic, and the stresses and strains along the axis of the cylinder were constant. Lutchansky's (1969) stress functions were used to form a system of two partial differential equations in terms of radial and tangential coordinates that were then solved analytically for stresses and displacements of one orthotropic cylinder. The two cases of no-slip and no friction, with respect to other cylinder were estimated by obtaining numerical results for a simple application. It was stated that under no slip case a positive radial stress appeared to develop at the interface between the cylinders, which should be counterbalanced either by axial pre-stressing force or by bonding between the cylinders in order to prevent separation. It was further postulated that under no end effects, no coupling between bending and tension-torsion was observed that lead to the conclusion that a cylinder subjected to bending would not elongate or rotate and vice versa. In addition it was stated that the bending moment caused a curvature in a plane perpendicular to the axis of the applied moment with no deviation observed. In order that the cylinder appropriately represents a layer of wires in the strand, Joulicour and Cardou (1996) developed a procedure for determining the elastic properties of the orthotropic cylinder.

Jolicoeur (1997) compared the two semi-continuous model approaches of Hobbs and Raoof (1982) and Jolicoeur and Cardou (1996). The similarities and differences in many important points were mentioned. After obtaining numerical results for a seven wire strand and a multi layered ACSR conductor cable, it was stated that both models produced same stiffness results for tension and torsion, when same values of orthotropic material properties were used. However, the torsional stiffness values obtained from Jolicoeur and Cardou (1996) model were higher than those predicted by orthotropic sheet model of Hobbs and Raoof (1982). It was claimed that Jolicoeur and Cardou model was more sensitive to bending stiffness of the cable in comparison with orthotropic sheet model and therefore could be used to accurately predict the important variations between maximum and minimum bending stiffness. It was further claimed that with a slight modification to orthotropic sheet model of Hobbs and Raoof reproduced very good results even for seven wire strands and ACSR conductor cables.

Davies (2000) presented a detailed comparative analysis between the original orthotropic sheet theoretical model of Raoof and Hobbs (RH), and a slightly modified version of the RH model ($RH_{2)}$, featuring the modifications proposed by Jolicoeur as well as including the proposed assumptions of original orthotropic sheet theory. After conducting an extensive series of theoretical parametric studies on a variety of spiral strand constructions, covering a wide range of wire and cable diameters and lay angles, it was stated that in spite of oversights in formulations by Jolicoeur, no practically significant difference in the results of RH model was found with those of RH_2 model. Furthermore, Jolicoeur's analyses were restricted to seven wire strands and one multi-layered strand, with a very narrow range of lay angles, which limited his findings. It would have been more helpful if the models had been compared by conducting a comprehensive analysis using larger diameter multi-layered spiral strands with varying lay angles, which is the key controlling geometrical parameter as long as strand stiffness is concerned (Raoof, 1997). The coupling coefficient A_3 was found the main difference between the results from the two (RH and RH_2) models and this difference was somewhat more pronounced for the no slip case, especially when the lay angle increased from 12° to 24°, however was not significant for the full slip layer stiffness coefficients. It was further stated that in Jolicoeur's model the ever

present curvature of the strand in the hoop direction was not taken into account for both the stiffness calculations and the calculation of c_k, which in some cases lead to positive values of this parameter, which is not the practical case for the axially preloaded spiral strand.

Ghoreishi et al., (2007a) developed a new non linear elastic continuum model for the analysis of axial stiffness of multi layered fibrous ropes with a large number of twisted components, subjected to static monotonic axial load. The material has been assumed to behave linearly by neglecting the effects of inter-fibre frictional forces. It is further assumed that due to small lay angles (less than 15°), there is no overall diametral contraction in the rope. Unlike previous semi-continuous model approaches the model does not consider multi-layered geometry as an assembly of layers, but rather treats it as a continuum formed by a set of coaxial helixes, with the same number of turns per unit length of the cable. It is further observed that due to the lack of consistency in various simplifying hypothesis, the stiffness matrix of all the previous models deviate slightly from symmetry. Finally, the authors compared the results of their model with models of Leech, Hobbs and Raoof, which were found in close agreement with them. However, a significant difference was observed with respect to the torsional stiffness of the rope.

2.3.4 Finite Element Models

Finite element analysis (FEA) is basically a computer model of a material or design that is loaded and analysed for specific load conditions that could be used for the design of new structure or reinforcement of the existing structure. The mechanism of FEA is that the whole structure is divided into small elements forming a mesh such that the continuity of displacements between the elements is enforced. The elements are connected at specific points called nodes. The mesh is then programmed to contain the material and structural properties, which can predict the response of a structure to certain loading conditions. Generally, two types of analysis are used in FEA namely: 2-D modelling and 3-D modelling. The 2-D modelling analysis is usually simpler, faster but less accurate compared with those of 3-D modelling. The accuracy of model increases with a decrease in the size of elements in the mesh and increasing

number of nodes. Linear systems usually do not take into account the plastic deformations while non-linear systems fully take into account plastic deformations of the material and can be used for testing a material all the way to testing node (Nicholas, 1988).

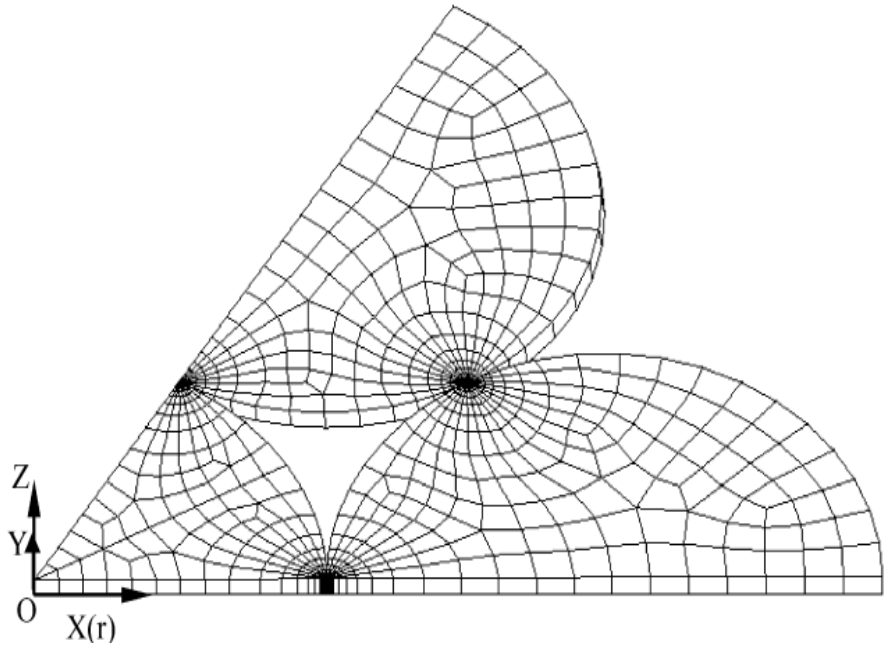

Figure 2-4: Finite Element Mesh after Jiang et al., (2008).

Chiang (1996) proposed some finite element methods and statistical design of experiments to explore the characteristics of simple stranded wire ropes subjected to axial loading. The effect of six design factors (radius of core wires, radius of helical wires, helix angle, strand's length, contact condition between core and helical wires and boundary conditions) was studied on the axial stiffness and axial stress rises at the ends of the cable as well as at middle cross section. Conclusion to this paper included the comparison of the results from both statistical predictive model and finite element analysis, which were found to be in good correlation for both axial stiffness and axial stress. Furthermore, it was stated that although the method presented is for 1x7 simple stranded cable, but it could be used for the analysis of more complex cross sections.

Jiang et al., (1999) developed an accurate general strand model using finite element method (FEM), which took full advantage of the helical symmetry features of a strand.

It was stated that the model is capable of taking into account the non-linear effects of tension, torsion, bending, shear, friction, contact as well as the effect of local plastic yielding, which were quite difficult to address theoretically. The model was successfully used to predict the global response of the straight wire rope strand and the stress distribution within the wires under axial loading conditions. Accurate boundary conditions were established during the implementation of the finite element analysis. The finite element analysis results of the model were compared with the analytical theory of Costello and experimental results of Utting and Jones, which were found to show an excellent agreement with them. Jiang and Henshall (2000) addressed the problem of extension and torsion in helical springs subjected to axial loads, and developed an accurate finite element model for predicting the behaviour of helical springs. It was observed that for small helical angle and the ratio of wire radius to coil radius, finite element analysis results agreed very well with the analytical models predictions for tension and torsion springs. While the disagreement between FEM results and analytical models was found to increase with the increase in helical angle and the ratio of wire radius to coil radius that was thought to be due to neglecting higher order terms in the series expansion.

Saevik and Bruasth (2005) proposed a finite element model and an algorithm for predicting the behaviour of complex umbilical cross sections, subjected to tension, torsion, internal and external pressure as well as external contact forces. The effects of material non linearities, hoop contact between wires and wires, gap formation and curvature change were taken into account. It was stated that the model could estimate the stresses and displacements of individual structural elements/wires as well as the overall response of the cable. Simulation results for a value of 100 Mpa axial tensions were presented and tested with both previously published data and new experiments. A very close agreement was found between the test and simulations results, when applying this value of axial tension. The effects caused by gap formation between the wires and other structural elements were managed by a surface stiffness penalty parameter applied to the contact elements. It was suggested that the model is very good especially for the range of umbilical cross sections used in the experiments, which might be lead towards more optimized design procedures for umbilicals in future.

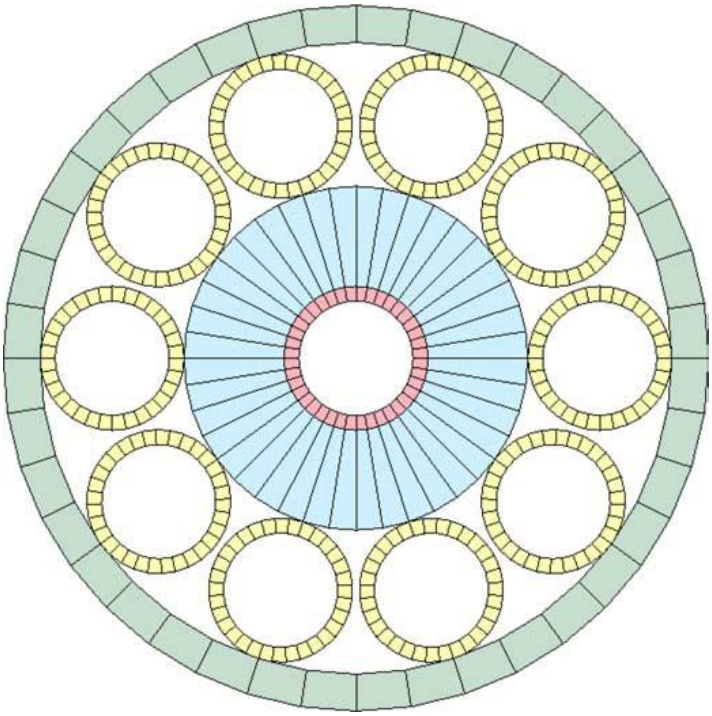

Figure 2-5: Typical Finite Element Model of an Umbilical Cross-Section after Saevik and Bruasth (2005)

Jiang et al., (2008) presented a simple finite element model to predict more accurately the behaviour of a simple strand, made from only one layer of circular wires helically wrapped around a circular straight core, subjected to axial tensile load only. It was observed that contact could take simultaneously between the core and helical wires, and between adjacent neighbouring helical wires, which form a statically indeterminate contact problem. Analysis for cyclic axial load was performed taking into account the effect of frictional forces between helical wires. It was shown numerically that the assumption of an elliptical cross section of a helical wire in a plane perpendicular to the strand symmetric axis was quite accurate compared with the exact shape of the wire, when lay angle was less than 20°. The contact stresses in radial direction were found higher than those in hoop direction by about 19%. The problem of statically indeterminate contact between the wires in a spiral strand has already been discussed by Raoof and his associates in some more details and analytical formulas for determining contact stresses both in radial and hoop directions have been presented.

Zhu and Meguid (2007) reported a finite element model to quantify the dynamic behavior and flexural damping of slacking wire cables. The cable was fixed at one end and vibrated at the other and the shapes of the vibrating cable were captured by high speed digital camera. These images were then analysed by using photogrammetry to determine the flexural damping coefficient of slacking wire cable. It is stated that a high flexural damping is observed to occur when there was no tension force applied to the cable. Further, the cable was also analysed using the non-linear curved beam element and Rayleigh damping. The results from the finite element model were found in good correlations with the experimental measurements.

Erdonmez and Imrak (2011) proposed a three dimensional modelling approach and finite element analysis for the double helix of a wire rope subjected to axial loads. The proposed model fully accounted for frictional and plastic behaviour of the wire strand. Taking into account of the wires real helical geometry, wire by wire based results were obtained by using the proposed modelling and analysis method under various loading conditions. For a simple straight strand, numerical results were obtained for both frictionless elastic and frictional elastic–plastic analyses. It was stated that wire contraction due to Poisson's ratio effect has a very little role over the whole model analysis. The results from the FE model were compared with the analytical model of Costello (1990) and available test results of Utting and Jones (1987), and were found in good agreement.

Judge et al., (2012) developed a 3D elasto-plastic finite element models for multi-layer large diameter cables with complicated geometry and contact conditions. The authors stated that the developed models can not only predict the global responses of the cable, but also capable of predicting the highly non-linear local effects in the wires. The key geometrical parameters identified for governing these properties were: lay angle, the number layer in the cable, the number of wires in the layer, lay length, and the diameters and locations of wires in specific layer. The authors also stated that the quality of the cable end terminations has a paramount for the cable to achieve its designed loading capacity.

2.4 Axial and Torsional Stiffness Characteristics of Cables

Costello and Phillips (1976) considered the elongation of the wire strand in the compatibility equations and found that, the stiffness of the cable was high when its ends were fixed against rotation and therefore the authors concluded that the type of end conditions plays an important role in the cable stiffness (except for those having initial helix angle near to ninety degrees). Furthermore, for fixed-end cables, change in axial load didn't affect the stiffness of the cable, on the other hand for those cables whose ends were free to rotate, the stiffness was observed to increase sharply with increasing axial load. However, the supposed values of axial strain for the analysis of the strand were very large and not applicable practically. The authors used value of axial strain .02 and above which does not exist in reality and 0.008 is thought to be maximum strain observed in the cable.

Costello and Sinha (1977b) started from Costello's previous assumptions reported elsewhere (Costello, 1977), and investigated the torsional stiffness of a single layer wire cable. It was observed that the torsional stiffness of the cable was not remarkably affected by the axial load or twisting moment applied at the ends of the cable.

Hobbs and Raoof (1982) showed the torsional and axial stiffness's of a wire rope as a function of the applied torque and axial load perturbations that varied between full slip and no slip limits. The degradation of the axial and torsional stiffness was associated with the development of interwire slip (Hobbs and Raoof, 1986). A simple relationship between the no slip and full slip limits was presented graphically, full slip limit was found to be a function of lay angle only. Raoof and Hobbs (1988a) extended their previous work (Hobbs and Raoof, 1982) and presented some experimental results on the torsional characteristics of the axially preloaded large spiral strands. Contact forces and the associated relative displacements between the wires were carefully assessed, taking fully into account interwire frictional forces with the ends of the wire rope fixed against rotation. The experimental results were found in great conformity with theoretical predictions for torsional stiffness of the cable, using the same value of the co-efficient of friction. The strand axial stiffness was found to be a

non-linear function of the applied load perturbations, due to interwire frictional effects.

Raoof and Hobbs (1989) investigated the response of a multi-layer strand to an externally applied torque for a mean axial load. The full slip histories on the interwire contact patches, from micro slips on the periphery at low loads to onset of gross slip at higher loads were predicted, taking fully into account the interwire frictional forces. The torsional stiffness was found to be a function of the applied torque and mean axial load. The torsion modulli for the two limits (no slip and full slip) were observed to be independent of the interwire friction coefficient. The theory also predicts the torsional energy dissipation quotient under continued cyclic loading, with experimental verification discussed in detail elsewhere by Raoof and Hobbs (1988b).

Raoof (1990e) developed simple design formulations for predicting various structural characteristics of both the spiral strands and multi-strand ropes, which can be adopted for engineering design applications. Using orthotropic sheet theory, these formulations were derived after a series of extensive parametric studies on a variety of spiral strands, having different wire diameters, lay angles and cable diameters. Reliable estimates were obtained for the no slip and full slip limits to the axial modulli of the spiral strands and related maximum level of logarithmic decrement under sustained axial uniform repeated loading, and their corresponding load range/mean ratio. The numerical results from the formulae were compared with experimental results on a spiral strand of 127 mm outer diameter, and a close agreement was found between the numerical and experimental results. The upper and lower bounds to the axial stiffness of multi strand rope were predicted by an extended version of orthotropic sheet theory. A very encouraging agreement was found between the theoretical full slip stiffness prediction and experimental results on a newly manufactured 40 mm outside diameter multi strand rope, which was found to be independent of the life history and level of bedding in of the wire rope. The no slip prediction was however, found to be dependent on the wire ropes with a stabilized pattern of interwire contact, which normally develops after thousands times repeated axial loading phases. The no slip prediction, for a newly manufactured strand was observed to provide a very helpful upper bound to the experimental data.

Tabatabai et al., (1995) published a series of full-scale axial fatigue tests on stay cables with epoxy coated, as well as uncoated, seven-wire strands conducted by Construction Technology Laboratories. Test specimens of various lengths varying from 4.6 m to 14.6 m were tested for different anchorage systems. It was found that for a load range of 36% to 45% of the ultimate breaking load, most cables experience wire fracture during 2 million-cycle. It was further stated that the percentage of broken wires after two million cycles range from 0% to 27%, whereas in some tests failure occurred at the corroded areas of the strand.

Conducting another series of extensive parametric studies on a wide range of spiral strand constructions, Raoof (1992d) provided some simple formulations for estimating various kinematical characteristics of the spiral strands, and specifically for wire axial strains and stresses, slippage over the line contact patches in each layer and rotations over trellis points of interlayer contact. Simple routines were also provided for estimating axial and free bending stiffnesses of a preloaded spiral strand that varied between two limits of no slip and full slip, depending on the magnitude of the applied axial load or free bending perturbations. In addition strand lateral contraction under axial load from first principles could be easily predicted. It was stated that the formulations presented could be used as a simple tool for calculating the associated relative interwire/interlayer displacements within the strand, which is used as an input data to the interwire fretting fatigue experiments.

Raoof and Kraincanic (1995a) reported the results from an extensive series of theoretical parametric studies based on orthotropic sheet theory, for multi-layer strands. The results covered a wide range of cable and wire diameters and lay angles. A simple method was proposed for predicting reliable estimates of the 2x2 stiffness matrix, relating to the axial/torsional coupling of large diameter and axially preloaded spiral strands. Simple routines were developed for obtaining the no slip and full slip limits to the stiffness coefficients. The proposed formulations were simple enough to do calculations by hand, using a pocket calculator, which are quite useful for practicing engineers.

Using the orthotropic sheet model, Raoof and Kraincanic (1995b) presented some theoretical results for predicting the behaviour of the constituent helical strands of a

large diameter wire rope, taking fully into account frictional forces between helical wires. It was stated that the model provided a very simple means for predicting the no slip and full slip limits to the effective axial stiffness of the wire rope. The model results were compared with experimental data reported elsewhere, that were found in reasonable agreement.

Kraincanic and Hobbs (1998) studied the axial stiffness and torsional effects in a 76 mm wire rope based on orthotropic sheet approach. Experimental results were obtained for 7 m long specimen, whose ends were fixed against rotation and subjected to axial loads ranging up to 1.4 MN. The no-slip and full slip axial stiffness of the cable was determined from the considerations of the frictional phenomena whereas; the no-slip torsional stiffness of the rope is shown to greatly depend on the axial load. Over all, the theoretical model and experimental data were in good agreement for a large rope reported here.

Raoof and Davies (2003) developed two slightly different models for the determination of the axial stiffness of large diameter wire rope both with IWRC or fibre core. In their work, they used Hruska's simple parameter to estimate the overall axial stiffness of the cable. The lay angles (both of the wires in the strand and of strand in the rope) were found to be the controlling parameter in the axial stiffness of the wire rope. A slight increase in lay angle is found to decrease axial stiffness of the cable. Similarly, the cross-sectional areas of the individual wires also play an important role in the axial stiffness. The available experimental data for three different wire rope constructions have been found to provide encouraging support for the theoretical predictions of their model.

2.5 Hysteretic Characteristics of Helical Cables

For many engineering applications where structural cables are subjected to aero-hydrodynamic actions, e.g. wind gust, ocean waves or traffic load, the amount of energy dissipation exhibited by the cable is of key importance. The nonlinear properties of the cables are mostly caused by internal damping in the cable. In modern bridges, the major sources of damping in the deck system of earlier designs has been greatly reduced due to the bridge deck being integrated with the main load bearing

members and the extensive use of welding. Therefore, cable used as hangers in suspension bridges and cable stayed bridges, can form a much larger part of the total damping in the recent structures.

Hobbs and Raoof (1984) developed a new method for predicting the axial hysteresis in the spiral strand. It was stated that the method could predict the significant variations in the hysteresis with pre load as well as load range for any type of spiral strand construction. The theoretical predictions of full slip stiffness for a number of spiral strands were compared with the experimental results reported elsewhere founding an encouraging agreement. The level of energy dissipation found was quite low than the results reported by Roberts and Severn (1968).

The authors mentioned that under random loading conditions, the level of axial and torsional hysteresis of a spiral strand could significantly increase. A notable reduction in the energy dissipation was observed with the increasing working life of a spiral strand, with a high value found for newly manufactured strand. Therefore, it was suggested that the hysteresis measurements on such a newly manufactured strand could be misleading for long-term applications. In addition, it was concluded that the energy dissipation in spiral strand could be easily increased, with a small increase in the lay angle of the strand, which will slightly decrease the stiffness of the spiral strand. The variation in the damping, by modification of friction coefficient was shown theoretically. Damping was observed to reduce for certain load ranges by increasing coefficient of friction, However it was suggested that the peak values of damping are independent of the degree of bedding in and friction coefficient.

Raoof (1990a) discussed the hysteretic behaviour of a newly manufactured spiral strand and an old and fully bedded in helical strand. It was shown theoretically that the damping characteristics of newly manufactured strand could vary in a very complex fashion, due the nature of the internal structure of the spiral strand. According to Raoof, the gradual nature of interwire/interlayer fretting, helical strands required a long time to bed in before their internal structure becomes reasonably stabilised. It was stated that the hysteretic measurements for such strands and ropes might be misleading however, the full slip axial and tosional stiffnesses are independent of the degree of bedding in.

Raoof and Huang (1991) proposed an analytical model for obtaining an upper bound to single layer strand damping under repeated bending for constant radius of curvature. Unlike traditional Coulomb rigid-plastic model, this theory provided an alternative interwire/interlayer friction formulation that fully catered for no slip to full slip friction transition over the individual contact patches. Results for two types of cable constructions were presented i.e. the cable in which the helical outer wires only touched the core wires and the cable whose outer wires just touched each other in line contact with no contact to the core wires. Results for both types of cable construction showed that the Coulomb rigid-plastic model tends to grossly overestimate cable damping for large radii of curvature. However, for small radii of curvature, full slip interwire movements predominates over the entire length of the cable and predictions of Coulomb's rigid plastic model were found similar to the proposed model of Raoof and Huang (1991) model. The analysis results also indicated that cable damping may be increased by increasing number of wire or decreasing the helix angle (within certain ranges) and hence for very large radii of curvature and cable axial strains, increasing helix angle caused an increase in cable damping, which may only be predicted using no slip to full slip interwire/interlayer friction model.

Using orthotropic sheet model, Raoof and Davies (2006) conducted an extensive series of parametric studies on a variety of spiral strand constructions and developed simple hand based formulations for predicting the maximum values of the axial and torsional energy dissipation in an old, axially preloaded multi layered strands, subjected to steady repeated loading. The reported results were suggested to be of great value to the design of hydrodynamic stabilities of cable supported bridges, offshore platforms and overhead transmission lines. It was shown that the axial specific loss of a strand could be easily increased by slight increases in the lay angle, which will essentially cause some reduction in the strand axial stiffness. Also for a given spiral strand construction, increasing maximum axial specific loss, by increasing lay angle resulted a reduction in the maximum level of torsional specific loss. It was pointed that modification to the coefficient of friction μ could also increase frictional damping, but the coefficient of friction was found difficult to modify, hard to predict and harder to control. In addition axial and torsional specific losses for a fully bedded in strands were found two or three times as large as those predicted by orthotropic

sheet theory and therefore, the presented simple formulations for old spiral strands gave a lower limit to the maximum specific loss for random loading conditions. Furthermore, increasing mean axial strain of the strand also caused a very slight increase in the torsional specific loss for a given spiral strand construction, which was believed to be of no practical significance.

Rawlins (2009) presented an analytical model for estimating internal damping of overhead electrical transmission conductors in flexure. It was stated that fatigue of cable occurred at the location of supporting towers due to vibration wave created by wind action, where the reflection of these waves caused concentrated localized flexure of the conductor. The relative movements caused by flexure between wires of the cable were constrained by friction between the wires. Although the frictional forces between the wires in overhead transmission line conductors were found enough to prevent gross sliding, under normal conditions but instead a micro slip at the edges of contacts was observed that caused frictional dissipation. In addition, shear strains were developed at the contact patches by frictional forces that caused material damping. The model results were found in reasonable agreement with available data on inherent-damping for a limited range of axial load.

Impollonia et al., (2009) proposed a model for the dynamic characterization of stay cables with viscous rotational dampers at the ends. Their model cast a significant light on the effectiveness, as well as the limitations of the rotational viscous dampers mounted at the two ends of a taut cable. Complex modal analysis was carried out and a numerical procedure for time-step integration was applied. Furthermore, a comparison with reference to intermediate dampers was reported with the limitations and advantages of the proposed mechanism being highlighted. It was stated that the vibrations in the short length stay cables could be significantly reduced by means of such viscous dampers that cause damage to the cable. The model was applied to a cable exposed to wind action.

2.6 **Bending of Steel Cables**

Lutchansky (1969) studied the behaviour of armoured cables bent over sheaves and proposed a simple mathematical model for determining the axial stresses induced in

helically wound armour wires of the cable. Distributed shear stiffness was assumed for the interaction of outer layer wires and the core, which depends on the material properties of the core and wires diameter, while the core itself was assumed to suffer no shear distortion. Using the proposed model, simple estimation of the axial stress concentration at the end terminations or apparatus housing was obtained. Expressions for the stresses in the free field were also obtained for the two limits of interactions, i.e. frictionless slip and infinite interaction shear stiffness. It was found that beamlike extreme fibre stresses were produced for an infinite interaction case as well as the case, when infinitely long lay lengths thin wires were running parallel to cable axis. Lutchansky did not provide any experimental data in support of his model, rather than he only quoted tentative values for the shear stiffness coefficient. In addition, the model is unable to predict interwire slippage, which is very important in the analysis of interwire fretting process near the terminations. The model of Lutchansky was extended by Raoof and Hobbs (1984), Raoof (1990b), to allow predicting interwire slippage occurrence in the cable.

Raoof and Hobbs (1984) addressed the problem of bending of spiral strands and armoured cables and offered simple means of determining the strand behaviour near the clamp as well as in the free field. Special emphasis was given to the situation where pulleys and other restraints were not provided. Unlike Lutchansky's model this model was capable of predicting the variations of the secant shear stiffness between the wires from no-slip to full slip regimes and beyond. No interwire/interlayer slippage was observed at the clamping positions and therefore, it was stated that interlayer stiffness is independent of the imposed radius of curvature for a given mean axial load. The no slip shear stiffness values of the model for multi layered steel strands were very high than those selected by Lutchansky in his study for large diameter under water cable systems. However, it was stated that the variation of shear stiffness over the full practical range of the cable axial loads was not very significant. The interesting conclusion to this paper was that the first wire fracture near end terminations occurred near the neutral axis rather than extreme fibres, which verified as well as theoretically explained the experimental observation of Hobbs and Ghavami (1982) in bending fatigue tests on a 39 mm outer diameter wire

strand. The proposed model is also capable of exploring fully interwire movements and fretting in multi layered strands.

Vinogradov and Atatekin (1986) investigated the friction losses due to wire twist in single layer bent cable. The slippage due to twisting of wires was assumed to be the main source of internal friction. Based on this assumption it was observed that slippage between wires started near the clamp and then propagated along the cable with the increase in load. Furthermore, it was stated that load deflection characteristics of the cable were linear when no slippage between the wires occurred and become non linear for some critical load when the wires of the cable slipped. It was found that the post slippage characteristics of cable were strongly dependent on helix angle. Two types of hysteretic loops were analyzed in this paper: local, associated with wires cross sections and global, associated with the point of load application. The local hysteretic loop was found to be symmetrical and closed but, a very different correspondence in terms of load twisting curves for the wires cross sections were observed between simple bending and cyclic bending. The boundaries of slipping wire segment were found to vary between two extremes in a symmetrical way. Also, it was shown in the numerical analysis that the total friction losses in a cable depend on helix angle and tightness of the wires; as long as these two parameters were increased the losses in the cable were also increased.

LeClair and Costello (1988) proposed a theory for determining the axial and bending response of a single layer spiral strand, taking into account the effect of frictional forces between the wires. It was assumed that the axial load was large enough to maintain the contact between the outer helical wires and the central king wire, when the strand was bent. Like Costello's previous work solution was sought out for bending of cable by satisfying six non linear equations of equilibrium for individual wires in the cable. Two cases for the curvature and twist were investigated and the tensile forces in outer wires for both the cases were found very small in comparison with the usual tensile loads in the axially loaded cable. In addition to this the maximum tensile stresses in outside wires were found to occur at the crossing points of neutral axis, which confirmed the experimental observation of Hobbs and Ghavami (1982) as well as the theoretical findings of Raoof and Hobbs (1984). It was further

stated that the tensile forces due to bending were very small, when compared with tensile loads in the strand and could be therefore, neglected in stress determination.

Raoof (1992c) addressed the problem free bending fatigue life estimation of axially preloaded spiral strands with its ends clamped. The possible shortcomings in the existing modelling approaches were pointed and a new parameter was proposed to overcome these limitations and make an accurate estimate of the free bending fatigue life of axially preloaded spiral strands. It was stated that the model is capable of predicting the considerable reductions in free bending fatigue life of sheathed spiral strand subjected to high level of hydrostatic pressures, which was completely ignored by designers in past. It was further stated that interwire/interlayer fretting was the main mechanism that caused wire fractures under cyclic loading. Also in the light of experimental observations it was once again indentified that the location of first wire fracture occurred in the vicinity of neutral axis near the socket. Finally, the new model was found in close agreement with available experimental data on fatigue on some substantial spiral strands.

Nabijou and Hobbs (1994) studied the frictional behaviour of wire ropes bent over sheaves, with 6x36, 28 mm and 35 mm diameters, IWRC and fibre core, subjected to heavy load. It was observed that the coefficient of friction falls with increasing tension in the rope and decreasing sheave diameter. It was further stated that the nature of the rope didn't considerably affect the pulley coefficient of friction, when subjected to higher bending stiffness with IWRC. The value of the coefficient of friction for a bright rope was found higher than the galvanized rope. The surface contaminants were found to play an important role in the frictional behaviour of the wire rope such that the sand could be used to enhance the friction but at the cost of accelerated damage. Finally, it was shown that two apparently identical sheaves manufactured by different manufacturers showed different frictional performance, therefore the data provided by two different organizations should be handled carefully.

Papailiou (1997) proposed a very interesting theoretical model for axially preloaded spiral strands undergoing non-plane section bending. According to his model, the interlayer slippage starts near the neutral axis, with the predictions of strand bending stiffness exhibiting a smooth transition from a no-slip (maximum) to a full-slip

(minimum) state. The propoed model catered for interwire slippage and friction during bending of the cable. His model quantified the non-linear behaviour of the cable bending stiffness with varying cable curvatures. The theoretical results obtained from this model were compared with test results obtained from an innovative measurement setup “cable scanner”. It is stated that cable scanner method detects the displacement and the curvature of the conductor axis without touching the conductor surface. The effect of line contact forces between the wires in the same layer is however, ignored in this model.

Giglio and Manes (2003) reported some test results on free bending fatigue of a metallic wire rope used for aircraft rescue hoists. It is observed that the swinging of the rope end caused bending near end termination, leading to wire fracture due to the resultant fatigue stress. It is further stated, that the bending angle of the rope played an important role in the fatigue life estimation of the rope. For angles from 40° to 60° a progressive failure has been observed for the external wires in contact with the sheaves. For increasing bending angle, a progressive separation of fractured wires and strands was found due to internal breakage. It is argued that by conservative extrapolation, an angle of less than 28° should not cause severe damage to the rope. Finally, it was concluded that the breakage of inner strands not only happened but, at high angles, involved most of the inner rope.

Raoof and Davies (2004) studied the bending behaviour of the spiral strand and presented a novel experimental method for obtaining reliable measurements of the effective bending stiffness of axially preloaded spiral strands. It was stated that beyond certain limit of lateral deflection/span ratio, plane sections didn’t remain plane and interlayer slippage occurred, starting from the outer layer and spreading towards the centre of the strand, which was in turn dependent on the magnitude of axial load and imposed radius of curvature. The method was claimed to relatively inexpensive and very simple to use in practice, even for very large outside diameter spiral strands. Using the proposed method effective bending stiffness values of a 164 mm outside diameter spiral strand were obtained for axial load up to 3MN that was supported by a detailed theoretical analysis. A significant difference for the bending stiffness measurements was found between experimental and predicted values for the

first and final runs, which were believed to be due to the gradual nature of bedding in of the strand.

Hong et al., (2005) extended the earlier model of Papailiou (1997) and proposed a mechanical model. The oversight in Papailiou's conjecture that the bending stiffness of the cable would approach a minimum value independent of the cable tension force and coefficient of friction has been correctly pointed out. Hong's model correctly predicts that the bending stiffness of the cable for large curvatures approaches a constant value depending on the tension force in the cable and coefficient of friction between the wires. Unlike Papailiou's model the assumptions and approximations made in the derivation are explicitly stated and numerically validated for Jessamine conductor cable. The derivation properly account for variation of the differential angular extent of wires in different layers. The formulations are also extended to cables having varying lay angles, which commonly occur in practice. The derivation provides a new and clear description and better understanding of the kinematic behaviour of the cable as wire slippage propagates with increasing curvature. In their model they examined in detail the bending behaviour of helically wound steel cables and proposed a mechanical model that takes into account the slippage of wires under friction and increasing imposed curvature of the cable. Wire slippage has been shown to start near neutral axis expanding symmetrically towards the extreme fibre positions, causing a decrease in the effective bending stiffness of the cable. However the effect of line contact forces in the hoop direction has been ignored this model.

2.7 Conclusions

A large body of available literature on wire ropes and spiral strands has been examined, and an attempt has been made to highlight some of the gaps in previously reported models. This literature survey indicates the lack of experimental data in the field, which may be due to the high cost of testing and hardships in measuring deformations of small individual wires. It is also noted that most of the earlier researchers ignored the effect of interwire friction and contact deformations in their analysis. After the pioneering effort of Hruska, various other authors proposed different models of varying complexities and accuracy, to predict the response of wire

ropes and spiral strands to various loading conditions. Lutchansky, Knapp, LeClair, Costello, Phillips, Durelli, Machida, Velinsky, Satikh, Kumar, Ramsey, Chun, Kenta and Ghoureshi are a few to list here.

All the models presented by these authors are discrete models and they do not include interwire contact deformations in their analysis, which is very important in strand modelling. Kenta and Elata included interwire friction and double helix configuration in their analysis. Costello and his associates studied reasonably in depth the static response of spiral strands and wire ropes under various loading (tensile, bending and torsional) conditions. But the main problem with Costello's work was that he neglected the effect of interwire frictions and limited his research to single layered small spiral strands. Therefore, all the discrete models which neglect the effect of interwire friction and contact deformations can only predict accurately the behaviour of small single layered spiral strands and when the number of wires in the strand increases the accuracy of these models decreases and may lead to wrong conclusions.

In order to overcome this problem, Hobbs and Raoof developed a very different homogenization approach by considering each layer of wires mathematically equivalent to an orthotropic cylinder, whose mechanical properties are averaged to match the behaviour of its corresponding layer of wires, known as orthotropic sheet model. The problem of contact is sufficiently simplified to be easily dealt with mathematically. Unlike the discrete model approach the accuracy of this model increases as the number of wires in the spiral strand increases, because the properties of the strand are averaged over a greater number of wires. Another semi-continuous model has been developed by Jolicoeur and Cardou that shares some similarities with the orthotropic sheet model, but essentially relies on entirely different grounds and evaluates the spiral strands stiffness and slip effect in a different way. However, both of these semi-continuous approaches provided superior results in comparison with discrete models for large diameter multi-layered spiral strands. Ghoreishi et al recently developed a non-linear elastic continuum model after following the semi-continuous model approach of Hobbs and Raoof, and recognized that homogenization approach is very good approximation for the analysis of multi-layered fibrous or metallic wire ropes.

The work in this thesis is focussed on the bending behaviour and the related formulations of the interwire contact problem in multi-layered strands, and the non-linear behaviour of the cable to large deflections which is presented in detail in the next chapter.

Chapter 3

An Insight to the Formulations Used For Analysing the Helical Cables and Spiral Strands.

3.1 Introduction

In this chapter a substantial effort has been made to assess the magnitudes of contact forces and their associated displacements between wires, fully taking into account the interwire friction. From the technical and scientific literature, it appears that these aspects are practically important when analysing helical cables in bending, a common engineering situation. Typical examples include: suspension and cable-stayed bridges, tall guyed towers to power transmission lines and flexible electrical conductors. Fatigue failures caused by aero or hydrodynamic loading in such structures near end terminations are very common. The interaction between the wires in a rope is extremely difficult to determine accurately by either theory or experiments, as in addition to other parameters it depends upon the manufacturing process and also the response varies with time. Among other parameters, the interaction between the individual wires of a cable depends on the magnitude of the axial or torsional load perturbations and applied moment. For sufficiently small perturbations, the wires are stuck together due to frictional forces but large perturbations mobilize the wires and cause slippage. Similarly, increasing bending near the clamp will also lead to interwire slippage in the due course.

In the last few decades a series of attempts have been made to develop engineering models for predicting accurately the mechanical behaviour of helically wound steel cables, which vary in accuracy and complexity. In design analysis, cables are traditionally assumed to carry tensile loads only; therefore, there is very little information available to investigate the bending behaviour of cables. In this chapter an insight is given to basic formulations of the two models used for analysing the bending behaviour of helically wrapped steel cables. These two models are: Hong et al., (2005) and orthotropic sheet theory of Hobbs and Raoof (1982). The reason for selecting

these two models is that the first model provides explicit formulations for the transition of bending stiffness from no-slip to full slip for spiral strands, whereas the second model fully takes into account interwire frictional forces and contact deformations both in radial and hoop directions. The work in this thesis is basically focused on the bending behaviour of cables and the related problem of the fatigue lives of the cable under tension and bending condition. Therefore, based on these formulations, it is now possible to describe the cable sag at specific tension force and cable curvature along its axis. The relative displacement of the wires, the tensile, hoop and the bending stresses in the individual wires of the cable can be determined. Finally, no theory can be used with confidence without appropriate experimental support which reveals the real limitations of idealizations adopted during the development of the mathematical model. For this purpose, the results from both the models have been compared with the experimental observations of Raoof, 1992 (a &b).

3.2 **Hong's Model**

Hong et al., (2005) reported a mechanical model to describe the behaviour of helically wound steel cables subjected to tension and bending forces. The effective bending stiffness of the cable is shown to vary between two extremes, corresponding to no-slip and full-slip cases. Initially, when all the wires are in stick state, the cable behaves as a solid bar and therefore bending stiffness of the cable is maximum. Under increasing bending curvature, effective bending stiffness of the cable decreases, and eventually reaches a constant value in the case of full slip. The final stiffness corresponds to essentially fully slipped state of the cable with all its wires slipping in the presence of friction. All the wires in slip state behave as an independent helical springs bending about their own axis. The final value of the bending stiffness of the cable after slippage depends on the coefficient of friction between the wires and the type of cable construction and is independent of the tension force in the wires.

3.2.1 Improvements Made to Papailiou's Model.

Hong et al., (2005) model is based on the earlier model of Papailiou (1997), with some significant enhancements:

- Unlike Papailiou's model, the assumptions and approximations made in the derivation are explicitly stated and numerically validated for Jessamine conductor cable.
- The oversight in Papailiou's conjecture that the bending stiffness of the cable would approach a minimum value independent of the coefficient of friction has been correctly pointed out.
- The derivation properly accounts for the variation of the differential angular extent of wires in different layers. The formulations are also extended to cables having varying lay angles, which commonly occur in practice.
- The derivation provides a new and clear description and better understanding of the kinematic behaviour of the cable as wire slippage propagates with increasing curvature.

The full derivation of the formulation is given in the paper by, Hong et al., (2005) and will be not repeated here but, the key features are reported here for the sake of completeness. Before going into more detail, the basic assumptions made in the derivation of this model are:

1. All wires are made of the same material and all the contact surfaces have the same coefficient of friction.
2. Interwire frictional forces between wires in the same layer are neglected, and it is assumed that contact only occurs between wires in the two adjacent layers, with negligible torsional stiffness. Furthermore, the wires are unable to carry any compressive force.
3. The strain in each wire is continuous along its length.
4. In the fully stick state, when the centreline of the cable is subjected to an axial strain of ε_c, all the wires in the cable must necessarily be in tension and the cable behaves according to Bernoulli Euler Navier (BEN) beam theory.

5. In partially slip state, the portion of the cable that remains in the stick state continuous to behave according to the BEN beam theory. Whereas, the tension and bending of the cable is limited to the cases where the centreline of the cable always remains in stick state with respect to the innermost layer with its axial strain being ε_c.
6. Finally, the wire axial strains due to the tension force only, after the slippage remains equal to ε_c not only for wires in stick state, but also for wires in the slip state. In other words, due to variable bending strain in different wires, all the wires in the cable experience different strains, but the strain due to tension force in the wires remain the same both for wires in stick and slip state.

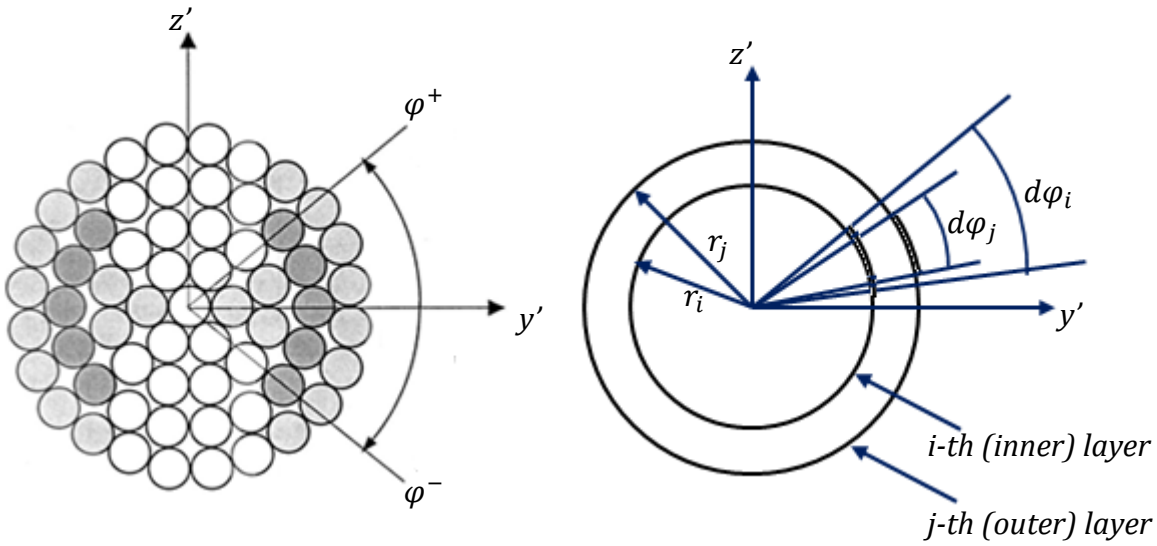

Figure 3-1: Illustration of polar angle φ, and the postulated behaviour of wire slippage with φ after Hong et al., (2005). Wires in stick (unshaded) and slip (shaded) regions.

3.2.2 Normal and Friction Forces Acting on Wire

To develop expressions for the frictional forces acting on the wire, the complex geometry of helically wound wire cable has to be carefully examined. To define the geometry of the cable, the layers are numbered from inside out, i= 1,….N, where layer 1 is the innermost layer wounded around the core (which is composed either of a single straight wire or an assembly of a number of equal lay wires i.e. equal lay core) and N denotes the outermost layer. Also n_i denotes the number of wires in the ith layer, r_i denotes the radial distance/helix radius from the centre of the cable to the

centre of the wire in the *i*th layer of the cable and φ is the polar angle of wires on cable cross section as shown in Figure 3.1.

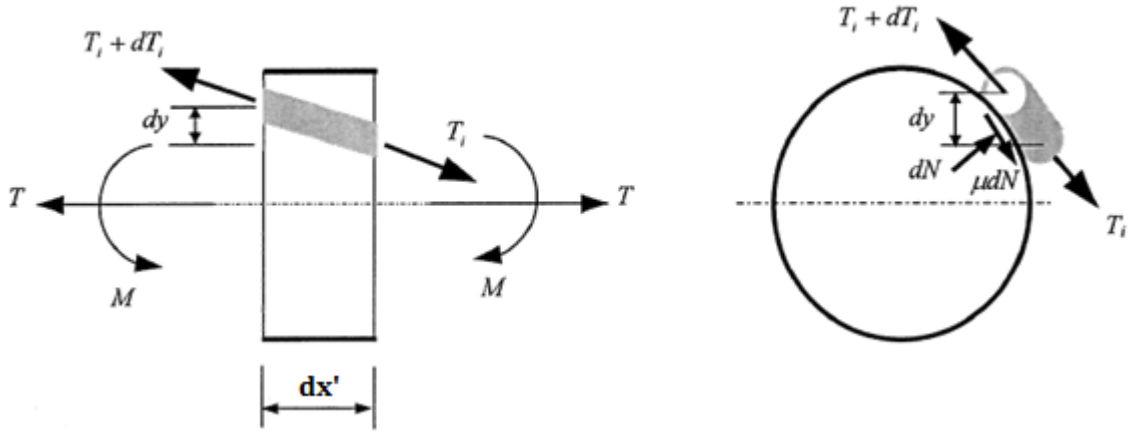

(a) (b)

Figure 3-2: Forces acting on differential wire element after Hong et al., (2005).

Figure 3.2a shows the differential segment of the cable under axial tension T and bending moment M. When the cable is subjected to an imposed curvature, a differential force arises because of the difference dy between the vertical distances of the two ends of the wire element from the centreline of the cable. This differential tension force dT_i tends to slide the wire along its axis. Normal forces are used to describe the conditions for slip and stick states of each wire. The normal force develops at the interface between two neighbouring wires in different layers gives rise to the friction force. In stick state, the unbalanced force in the wire is balanced by friction force acting on the wire as shown in Figure 3.2b. When dT_i exceeds the maximum friction force generated at the contact patches between the wires, the wire is mobilized, and slides along its axis. Once the wire starts slippage, forces acting on the wire redistribute and slippage continuous until equilibrium is reached.

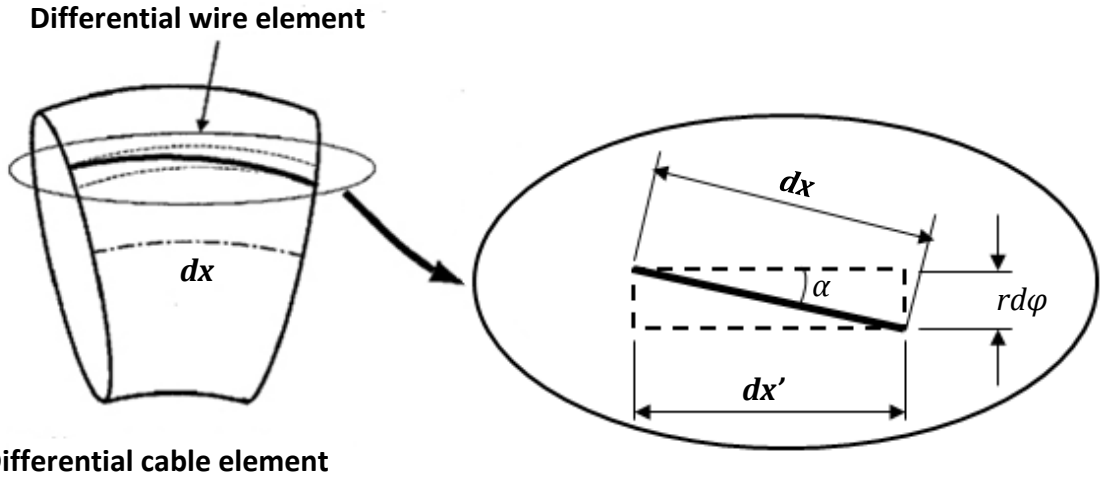

Figure 3-3: Differential wire element in deformed cable after Hong et al., (2005).

First a differential element of wire in the outermost layer is considered and the normal distributed force P acting in the radial direction on the wire element is obtained as:

$$P = \kappa_{wr} T_N \tag{3.1}$$

where κ_{wr} is the curvature of wire in radial direction and is given by, $\kappa_{wr} = \frac{\sin^2 \alpha_N}{r_N}$, with α_N and r_N being the lay angle and radial distance of outermost layer N respectively, and the radial distance r_i for any arbitrary layer *i*, can be calculated as:

$$r_i = {}^{n_i D_i \cos \alpha_i}/_{2\pi} \tag{3.2}$$

where D_i and n_i are the diameter and number of wires in the *i*th layer of the cable respectively. Multiplying Eq. (3.1) by the arc length of the wire element as shown in Figure 3.3, $dx = \frac{r_N d\varphi}{\sin \alpha_N}$, the total normal force acting on the wire element is obtained as:

$$dN_N = T_N \sin \alpha_N \, d\varphi \tag{3.3}$$

Eq. (3.3) is valid as long as wire is under tension, if wire is not under tension, no normal force acts on the wire. For large values of curvature, wires on the concave side of the cable are compressed and essentially take no tension force.

Now if we consider a wire in an ith inner layer, $1 \leq i < N$, such a wire is subjected to normal forces on both its inner and outer surfaces. The normal force on the outer surface of wire is the accumulation of all the normal forces resulting from tensions in the wires of layers $i+1$ to N. The normal forces acting on the outer surface of the wire are ruled by:

$$dN_{i,outer} = \sum_{j=i+1}^{N} T_j \sin\alpha_j \frac{r_i n_j \tan\alpha_j}{r_j n_i \tan\alpha_i} d\varphi \tag{3.4}$$

where, $(r_i n_j \tan\alpha_j \,/\, r_j n_i \tan\alpha_i)$ is the variation of forces transferred from one layer to the other due to variation of lay angles and wire diameters from one layer to other. In special case when the lay angles and wire diameters are invariant, this term becomes unity and the expressions simplifies accordingly.

The normal contact force acting on the inner surface of wire in the *i*th layer is the sum of Eq. (3.4) plus the contribution from the tension force in the wire itself.

$$dN_{i,inner} = \left(T_i \sin\alpha_i + \sum_{j=i+1}^{N} T_i \sin\alpha_j \frac{r_i n_j \tan\alpha_j}{r_j n_i \tan\alpha_i} \right) d\varphi \tag{3.5}$$

where, n_i and $n_i$denote the number of wires in layer *i* and *j=i+1.*

3.2.3 Stick and Slip Tension in the Wire

In the fully stick state, if the centreline of the cable is subjected to an axial strain of ε_c and an imposed curvature κ_c, the longitudinal strain in the wire along the axis of the cable is calculated as follows:

$$\varepsilon_{xi}^{stick} = \varepsilon_c + \kappa_c r_i \sin\varphi \tag{3.6}$$

Where φ is the polar angle of an individual wire which shows its position in the cable cross section. The value of polar angle varies from 0 to ±π, for the wires of any arbitrary layer *i* of the cable as shown in Figure 3.1.

Eq. (3.6) is the axial strain along the cable axis that make an angle α_i with the wire axis, in order to transform the strain tensor into the axial direction of the wire, the axial strain of the wire is determined. The axial strain of the wire along its own axis is then given by:

$$\varepsilon_i^{stick} = \cos^2 \alpha_i \, (\varepsilon_c + \kappa_c r_i \sin \varphi) \tag{3.7}$$

After getting wire axial strain, the tension force in the wires is then obtained by multiplying this with the Young modulus and cross-sectional area of the wire:

$$T_i^{stick} = EA_i \cos^2 \alpha_i \, (\varepsilon_c + \kappa_c r_i \sin \varphi) \tag{3.8}$$

The second term inside parenthesis on the right hand side of Eq. (3.8) is the contribution from imposed bending curvature of the cable. For wires on the concave ($\varphi < 0$) side of the cable this term becomes negative and experience less tension, whereas wires on the convex side of the cable wires are more stressed. Similarly in case, if the cable is straight (i.e. $\kappa_c = 0$) this term becomes zero.

Now if the wire is subjected to imposed curvature, there is an unbalanced tension force acting on the wire. For a differential wire segment in the ith layer, the unbalanced tension force in the stick state is obtained by differentiating Eq. (3.8) with respect to φ:

$$dT_i^{stick} = EA_i \kappa_c r_i \cos^2 \alpha_i \cos \varphi \tag{3.9}$$

This unbalanced force in the wire must be in equilibrium with friction force generated at the contact patches of the wire. Slippage begins, when the unbalanced force in the wire segment exceeds the maximum friction generated at the wire surfaces. Once the wire slips, the forces in the wire re-distribute until equilibrium is achieved. Therefore, the condition of a differential wire segment in the outermost layer of the cable to be in the slip state is given as:

$$dT_N^{slip} = \mu T_N^{slip} \sin \alpha_N \, d\varphi \tag{3.10}$$

In Eq. (3.10), μ is the friction coefficient between wires with α_N being lay angle of wires in the outermost layer. The solution to this first order differential equation is then given as:

$$T_N^{slip} = C_N^h \exp(\mu\varphi_N \sin\alpha_N) \tag{3.11}$$

where C_N^h is the constant of integration and can be obtained by satisfying a boundary condition. From assumption 6, by putting the value of zero polar angle in Eq. (3.11), $T_N^{slip}(0) = EA_N\varepsilon_c \cos^2\alpha_N$ and thus $C_N^h = EA_N\varepsilon_c \cos^2\alpha_N$.

Next, considering a wire in an inner layer i, such that the normal forces are acting on both inner and outer surfaces of the wire:

$$dT_i^{slip} = \left(\mu T_i^{slip} \sin\alpha_i + 2\mu \sum_{j=i+1}^{N} T_j^{slip} \sin\alpha_j \frac{r_i n_j \tan\alpha_j}{r_j n_i \tan\alpha_i}\right) d\varphi \tag{3.12}$$

It is clear in the above equation that the solution can be proceed further by solving it for the wire forces from outer to inner layers. Thus it is assumed that the solutions for the forces in the outer slipped wire are available. The solution for this first order differential equation consists of two parts: homogeneous (first part) and particular (second part).

$$T_i^{slip} = T_i^h + T_i^p \tag{3.13}$$

The solution of the homogeneous part is then given as:

$$T_i^h = C_i^h \exp(\mu\varphi \sin\alpha_i), \quad 1 \le i < N \tag{3.14}$$

where the integration constant for this solution C_i^h is obtained again by satisfying boundary condition at $\varphi = 0$. The solution for the particular part of the equation is

$$T_i^p = \sum_{j=i+1}^{N} C_{ij}^p \exp\left(\mu\varphi \sin\alpha_j\right), \quad 1 \le i < N \tag{3.15}$$

where the constants C_{ij}^{p} is determined by satisfying the differential Eq. (3.12). As mentioned earlier, by considering the *i*th layer, we assume the solutions for all the outer layers are available. The slip tension force in the inner ith layer is then given by:

$$T_i^{slip} = C_i^h \exp(\mu\varphi \sin\alpha_i) + \sum_{j=i+1}^{N} C_{ij}^{p} \exp\left(\mu\varphi \sin\alpha_j\right), 1 < i \leq N \qquad (3.16)$$

Note that the constant of integration for the particular part is zero for the outermost layer i.e. $C_{Nj}^{p} = 0$ as is clear from Eq. (3.11) whereas for the inner layers the constant C_{ij}^{p} is obtained by satisfying Eq. (3.12). Using Eq. (3.15) and (3.16) in conjunction with Eq. (3.12), summing the homogeneous and particular solutions after some algebra and equating the terms on the two sides, one gets:

$$C_{ij}^{p} = \frac{2\sin\alpha_j \frac{r_i n_j \tan\alpha_j}{r_j n_i \tan\alpha_i} C_i^h + \sum_{k=i+1}^{j-1} \sin\alpha_j \frac{r_i n_k \tan\alpha_k}{r_k n_i \tan\alpha_i} C_{kj}^{p}}{\sin\alpha_j - \sin\alpha_i}$$

$$1 \leq i < j \leq N \qquad (3.17)$$

In the above expression, the second term in the numerator drops out when the penultimate layer, $i = N - 1$, is considered. The constant of integration for the homogeneous part in Eq. (3.14) is then obtained by satisfying the boundary conditions $\varphi = 0, T_i^{slip}(0) = T_i^h(0) + T_i^p(0) = C_i^h + \sum_{j=i+1}^{N} C_{ij}^{p} = EA_i\varepsilon_c \cos^2\alpha_i$ therefore,

$$C_i^h = EA_i\varepsilon_c \cos^2\alpha_i - \sum_{j=i+1}^{N} C_{ij}^{p} \quad 1 \leq i < N \qquad (3.18)$$

The above solution is applicable only when, the lay angle of the two layers are not the same otherwise the corresponding constant in Eq. (3.17) becomes infinite. Thus for the cable with same lay angles the homogeneous solution remains the same as in Eq. (3.14) but, the particular solution then takes the form

$$T_i^{p} = \exp(\mu\varphi \sin\alpha_i) + \sum_{j=i+1}^{N} C_{ij}^{p}\varphi \quad 1 \leq i < N \qquad (3.19)$$

Using this form of particular solution, one gets

$$C_{ij}^{p} = 2\mu \, sin\, \alpha \sum_{k=i+1}^{N} \frac{r_i n_k}{r_k n_i} C_k^h \quad 1 \le i < j = N \tag{3.20}$$

$$C_i^h = EA_i \varepsilon_c \cos^2 \alpha \tag{3.21}$$

3.2.4 State of a Wire

Using the formulation summarised in the previous subsection, forces in all the wires of the cable can be determined that are either in stick or slip state.

The state of a wire in the ith layer is obtained by setting unbalanced tension force equal to the maximum friction force

$$EA_i \kappa_c r_i \cos^2 \alpha_i \cos \varphi = \mu \left(T_i^{stick} \sin \alpha_i + 2 \sum_{j=i+1}^{N} T_i^{slip} \sin \alpha_j \frac{r_i n_j \tan \alpha_j}{r_j n_i \tan \alpha_i} \right) \tag{3.22}$$

For a given layer, the unbalanced tension force is maximum at neutral axis i.e. $\varphi = 0, \pm\pi$ and this decreases with increasing $|\varphi|$ such that it becomes zero at $\varphi = \pm\frac{\pi}{2}$. Therefore, slippage in each layer begins at neutral axis and propagates almost symmetrically into the lower and upper halves of the cable with increasing $\pm\varphi$. According to the assumption (2) in subsection 3.2.1, for large values of imposing curvature, the entire lower half of the cable on the concave side of the bending is in slip state. The reason for this is that increasing bending curvature of the cable causes negative bending stress in the wires on the concave side of the cable, according to Eq. (3.8). Therefore, for sufficiently large values of imposed curvature the all the wires on the concave side of the cable are compressed and considered in slip state.

3.2.5 Resultant Tension Force on Cable

In order to calculate the corresponding resultant tension force in the cable, the forces in all wires are added together, after projecting them along the cable axis. The tension force T_i in the individual wire depends on the state of the wire and it may be either T_i^{stick}, T_i^{slip} or zero. The resultant tension force on the cable is then obtained by:

$$T = \sum_{all\ wires} T_i \cos \alpha_i \tag{3.23}$$

In Eq. (3.23) T is the resultant tension force on the cable. During bending the wires in the cable experience different tension force depending on its location in the cable cross section as well as the state of the wire.

The bending moment in the cable cross-section caused by the tension force in individual wires is given by:

$$\Delta M = \sum_{all\ wires} T_i\, r_i \cos \alpha_i \sin \varphi \tag{3.24}$$

The above equation clearly shows that as the polar angle of a wire in the layer increases bending moment increases and vice versa. Similarly, tension force in individual wires also changes with polar angle, for wires on convex side it increases, concave side it decreases whereas for wires on neutral axis it does not change. The resultant bending moment in the cable is the above (i.e. Eq. 3.24) plus the bending moment of each individual wire, including those having zero axial force, and the core.

$$M = \left(\sum_{all\ wires} EI_i + EI_{core} \right) \kappa_c + \sum_{all\ wires} T_i\, r_i \cos \alpha_i \sin \varphi \tag{3.25}$$

where, $I_i = \pi d_i^4/64$ is the moment of inertia of each wire in layer i and $I_c =$ moment of inertia of the core.

The resultant tension force and bending moment are the non-linear function of ε_c and κ_c after the initiation of wire slippage, whose application shows that the behaviour of the cable under constant tension and increasing imposed curvature is similar to the behaviour of elastic plastic material.

3.3 Orthotropic Sheet Theory

The orthotropic sheet model was initially developed by Hobbs and Raoof (1982) for the analysis of multi-layered spiral strands with counter-laid layers. The theory is based on the main assumption that the gaps between the wires under zero external

load are small enough to be neglected. According to this approach a strand consisting of a core and *N* layers of helical wires is mathematically represented by *N* concentric orthotropic cylinders, whose mechanical properties are averaged as a continuum to match the behaviour of their corresponding layer of wires. Since the properties of the strand are averaged, the accuracy of the model increases with increasing the number of wires in the strand. The elastic properties of the sheets, whose principal axes run parallel and perpendicular to the individual wire axes, are determined as a function of the external load perturbation. Using Hearmon (1961) formulations, the elastic properties are transformed to values parallel and perpendicular to the strand axis. It is postulated that for a counter-laid construction, the stiffnesses in hoop direction are much greater than the ones in the radial direction. The core of the strand is assumed to resist the rigid body movement which would occur in its absence due to change in the lay angle. This causes wires to assume a closer packing formation.

List of the basic assumptions that underly orthotropic sheet theory is as follows:

1. In the unloaded condition the wires within the layer are just touching each other.
2. During deformation, twisting and bending of individual wires is negligible and thus wires carry only pure tension.
3. Centre line of wire forms a helix both before and after deformation.
4. When considering a large number of wires in a layer, > 19, and small lay-angles, < 30, the cross-section of a wire can be reasonably approached as an ellipse.
5. The influence of the transverse contraction is negligible for the derivation of the wire slippage in the presence of a rigid core.
6. The helical strands are approached as being straight.
7. The strand tensile load is uniform over the whole strand cross-section because the lay-angles in different layers are very similar.

The notations used for strain tensor compliances are given are as follows:

$$\begin{bmatrix} \epsilon_x \\ \epsilon_y \\ \gamma_{xy} \end{bmatrix} = \begin{bmatrix} \epsilon_{11} & \epsilon_{12} & 0 \\ \epsilon_{21} & \epsilon_{22} & 0 \\ 0 & 0 & \epsilon_{33} \end{bmatrix} \begin{bmatrix} \sigma_x \\ \sigma_y \\ \tau_{xy} \end{bmatrix} \tag{3.26}$$

Where ϵ_x and ϵ_y are the direct strains parallel and perpendicular to the wire axis respectively; γ_{xy} is the shear strain; σ_x and $\sigma_y$are the are the axial and radial stresses in the wires respectively; and τ_{xy} is the shear stress.

Note that X, Y and XY represent the directions parallel, perpendicular and tangential (shear) along the axis of the wire respectively as shown in Figure 3.4. Furthermore, the notations with x, y and xy represent local (wire) deformations, whereas notations with x', y' and xy' are used for global (cable) strains (axial, radial and shear strains) respectively.

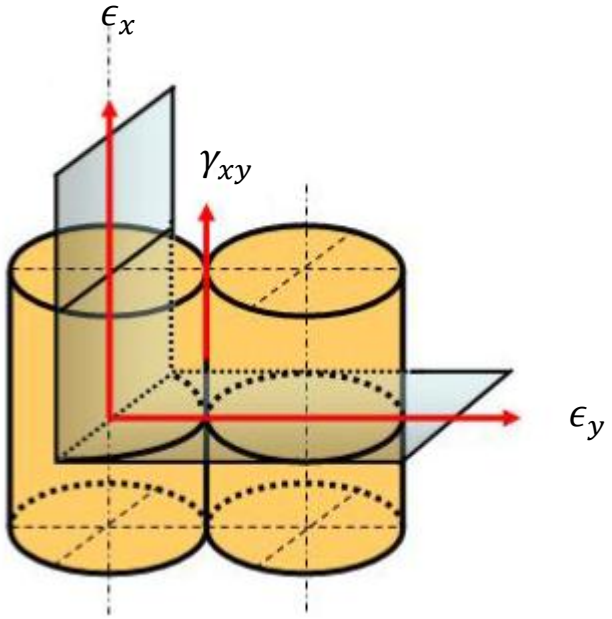

Figure 3-4: Symmetry planes of the orthotropic tensor of a wire layer after Erik (2011).

3.3.1 Calculation of Strand Layer Deformations

The model uses a set of compatibility equations to establish the kinematics of the cylinder. Using these compatibility equations the cylinder local (wire) strains are obtained from the global (cable) strains.

For a given axial strain (global) of the cable ε_c, an expression for the axial strain in individual wire has been derived from experimental data after Raoof (1988) for the (local) wires strains:

$$\frac{\epsilon_x}{\varepsilon_c} = (1 - 0.146\alpha_i + 0.706{\alpha_i}^2 - 5.097{\alpha_i}^3) \tag{3.27}$$

where ε_c is the strand axial strain with α_i being the lay angle of wire in layer i expressed in radians. Eq. (3.27) can be used to estimate the axial strain in a wire due to tension force only. When the cable is subjected to combine tension and bending; the combine axial strain of the wire can be estimated by replacing $\cos^2 \alpha_i$ in Eq. (3.7) by polynomial given in Eq. (3.27). The difference between calculations based on the Eq. (3.7) and Eq. (3.27) is given in Chapter 4, Figure 4.1.

The two dimensional element rotated at an angle $\Delta\alpha_i = \alpha_i - \alpha_i'$ after the application of load as shown in Figure 3.5a, where α_i is the lay angle of *i*th layer in the undeformed state, α_i' is the lay angle of *i*th layer after deformation.

From Figure 3.5a for an un-deformed cable:

$$\cos \alpha_i = \frac{x_i}{l_i} \tag{3.28}$$

where x_i is the length of the wire along the cable axis and l_i is the length of the wire along its own axis. The same relation for deformed lay angle is then given as:

$$\cos {\alpha_i}' = \frac{{x_i}'}{{l_i}'} = \frac{x_i(1 + \varepsilon_c)}{l_i(1 + \epsilon_x)} \tag{3.29}$$

Dividing Eq. (3.29) by (3.28), the deformed lay angle of the wire can be determined as:

$$\alpha_i' = \cos^{-1}\left[\cos \alpha_i \left(\frac{1 + \varepsilon_c}{1 + \epsilon_x}\right)\right] \tag{3.30}$$

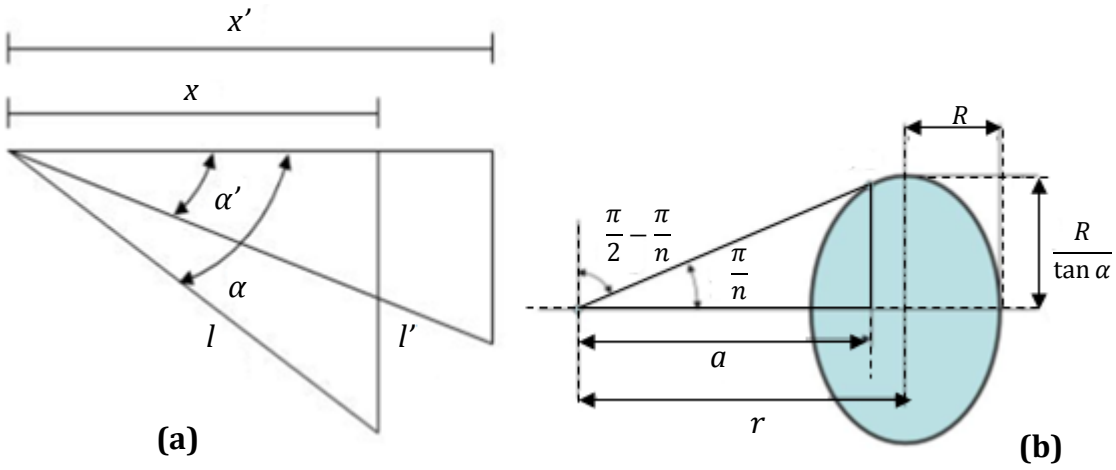

Figure 3-5: (a) Helix geometry before and after cable deformation (b) Description of helix radius in cross-section of an elliptical wire normal to cable axis after Hobbs and Raoof (1982).

Following Phillips and Costello (1973) the helix radius for a layer of wires before deformation is given as:

$$r_i = \frac{D_i}{2}\sqrt{\left(1 + \frac{\tan^2\left(\frac{\pi}{2} - \frac{\pi}{n_i}\right)}{cos^2\alpha_i}\right)} \tag{3.31}$$

where D_i is the wire diameter and n_i is the number of wires in *i*th layer. For the loaded configuration Eq. (3.31) becomes:

$$r_i{}' = \frac{D_i}{2}\sqrt{\left(1 + \frac{\tan^2\left(\frac{\pi}{2} - \frac{\pi}{n_i}\right)}{cos^2\alpha_i{}'}\right)} \tag{3.32}$$

Or alternately,

$$r_i{}' = r_i\left(1 + \epsilon_{yR'}\right) \tag{3.33}$$

where $\epsilon_{yR'}$ is the radial strain in the cable cross-section due to the change in helix radius. From Eqs (3.31) and (3.33):

$$\epsilon_{yR'} = \left(\sqrt{\left[\frac{\cos^2 \alpha_i \left(\cos^2 \alpha_i' + \tan^2 \left(\frac{\pi}{2} - \frac{\pi}{n_i} \right) \right)}{\cos^2 \alpha_i' \left(\cos^2 \alpha_i + \tan^2 \left(\frac{\pi}{2} - \frac{\pi}{n_i} \right) \right)} \right]} \right) - 1 \tag{3.34}$$

where α_i is the lay angle of *i*th layer in the undeformed state, α_i' is the lay angle of *i*th layer after deformation.

The strand axial strain ε_c results a change in lay angle α_i' accompanied with a change in helix radius r'. Thus the total diametral strain $\epsilon_{yC'}$, in the cable cross-section is calculated as:

$$\epsilon_{yC'} = (1 + \varepsilon_c) \frac{\tan \alpha_i'}{\tan \alpha_i} - 1 \tag{3.35}$$

where ε_c is the cable axial strain.

Since the strain $\epsilon_{yR'}$ is caused as a result of rigid body movements, it does not contribute to line-contact forces and deformations, and therefore it has been subtracted from $\epsilon_{yC'}$ to find net diametral strain $\epsilon_{y'}$. Using Eqs. (3.34) and (3.35), the contraction in the cable cross-section $\epsilon_{y'}$ due to the interwire deformations is then calculated as:

$$\epsilon_{y'} = \epsilon_{yC'} - \epsilon_{yR'} \tag{3.36}$$

As shown in Figure 3.6, the wires in the corresponding layer experience a slight decrease in their axial strain due to change in lay angle (i.e. diametral strain), which may be found by setting axial strain equal to zero.

$$\Delta\epsilon_x = \left(\cos \alpha_i \sqrt{1 + \left(1 + \epsilon_{yC}'\right)^2 \tan^2 \alpha_i} \right) - 1 \tag{3.37}$$

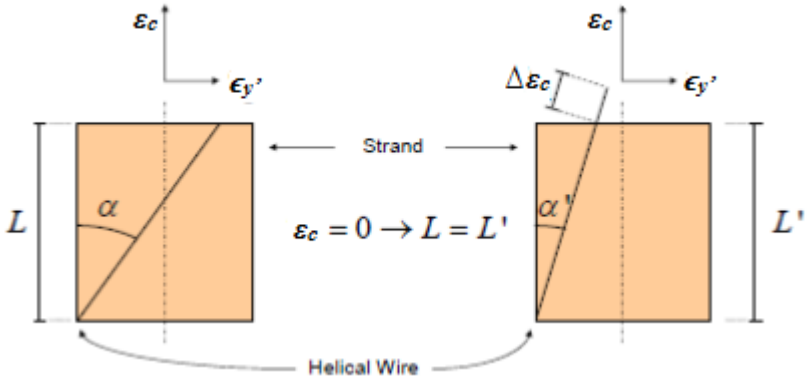

Figure 3-6: Illustration of $\Delta\epsilon_x$ as a result of strand tensile strain $\varepsilon_c = 0$.

Using global strains of the strand, the hoop strain in the wire is obtained by:

$$\epsilon_y = -\frac{\varepsilon_c + \epsilon'_y}{2}\cos 2\,\alpha'_i + \frac{\varepsilon_c + \epsilon'_y}{2} \tag{3.38}$$

The tensorial shear strain in the layer is then given by:

$$\gamma_{xyT} = \frac{1}{2(1+\epsilon_y)}[\tan\alpha_i(1+\epsilon_x - \Delta\epsilon_x - \tan\alpha'_i)] \tag{3.39}$$

In the above ϵ_x and ϵ_y are the wire strains along the axis, parallel and perpendicular to the wire axis respectively.

For a given cable axial strain ε_c, these eight non-linear equations [Eq. (3.27), (3.30), (3.34)-(3.39)] are solved simultaneously for the eight unknowns ($\epsilon_x, \alpha'_i, \epsilon'_{yR}, \epsilon'_{yC}, \epsilon'_y, \Delta\epsilon_x, \epsilon_y$ and γ_{xyT}). These equations are solved by treating ϵ_x as the primary unknown, using the same order as they are presented above.

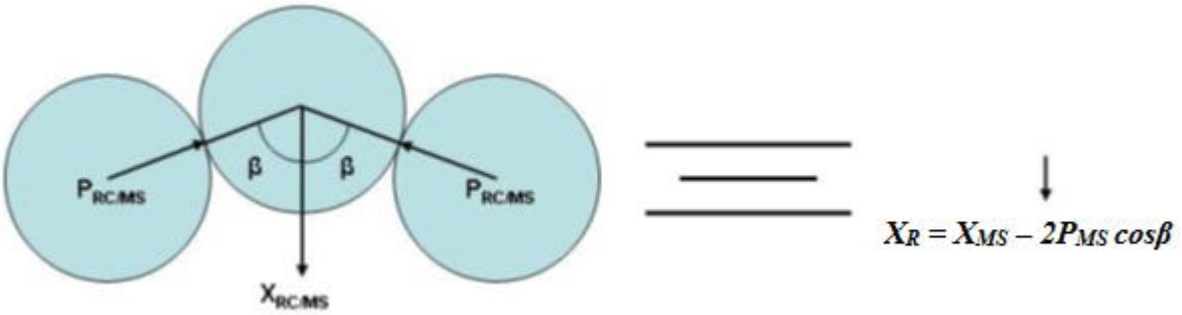

Figure 3-7: Resultant radial load transfer from an outer layer to adjacent inner layer.

3.3.2 Radial and Circumferential (Hoop) Contact Forces in the Strand

There are two types of contact forces acting in a multi-layered spiral strand. The first one is the line contact force within a given layer between adjacent parallel wires. The other type of interwire contact force occurs in the successive layer of wires which, are laid usually in opposite directions. The radial force exerted on any layer is due to the tension in the wire itself plus the clenching effects of outer layers (Hobbs and Raoof, 1982). The effect of the radial force grows inwards, starting with the outermost layer.

The radial force X_{RC_i}acting as a body force in the wires in *i*th layer, assuming that the wire axial strain ϵ_x is known can be given by (Hobbs and Raoof, 1982):

$$X_{RC_i} = \frac{EA_i\epsilon_x \sin^2\alpha_i}{r_i} \tag{3.40}$$

where $A_i = \frac{\pi {D_i}^2}{4\cos\alpha_i}$ is the cross-sectional area of a wire in *i*th layer with its diameter D_i.

Two types of line contact force between two wires in hoop direction (P_{RC_i} and P_{MS_i}) are introduced for each wire layer. Thus P_{RC_i} is the tangential line contact force generated due to the tension force in the wire itself, whereas P_{MS_i} is line contact force in the layer when in addition to P_{RC_i}, the effect of all outer layers are also taken into account. As part of the radial force transferred from previous layers goes to line contact force.

For each wire layer i, it is possible to determine the normal line contact force P_{RC_i}, between the wires. The equation for normal contact forces are derived with the assumption that a rigid core is present and there are no other forces acting upon the layer. Resulting forces in one layer acting upon the next one thus still need to be taken into account and are denoted as P_{MSi} and X_{MSi}. The force equilibrium describing the whole strand is a statically indeterminate problem. The resulting radial contact force X_{Ri} can finally be determined and the next layer can be evaluated.

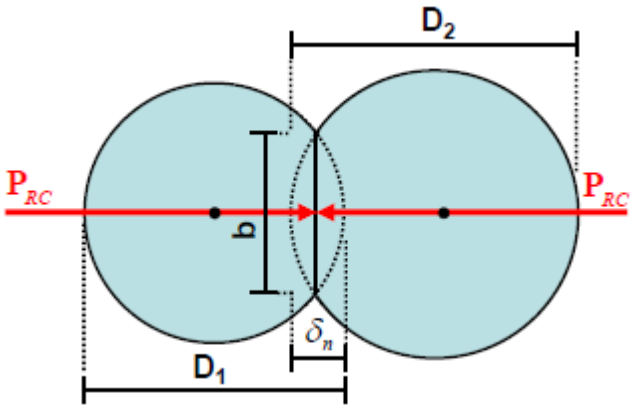

Figure 3-8: Cross-section of two wires in line-contact showing the diametral deflection δ_n as a result of the line-contact force P_{RCi} after Erik (2011).

The line contact force P_{RC_i}between two adjacent wires in *i*th layer subjected to diametral strain ϵ_{yi} that results from strand axial strain ε_c, is given by Hobbs and Raoof (1982) as:

$$\epsilon_{yi} D_i = \frac{4P_{RC_i}(1-\upsilon^2)}{\pi E}\left(\frac{1}{3} + \ln\frac{D_i}{b_i}\right) \tag{3.41}$$

where the subscript *RC* refers to the rigid core being present, υ is the Poisson's ratio, E is the Young modulus of the material, ϵ_{yi} is the diametral strain in the hoop direction in *i*th layer and b_i is the width of the rectangular contact area in the *i*th layer as shown in Figure 3.8 and is given by:

$$b_i = 0.8\left(\sqrt{\left(\frac{P_{RC_i} D_i (1-\upsilon^2)}{E}\right)}\right) \tag{3.42}$$

Using Eqs. (3.41) and (3.42) it is chosen to make a guestimate of line contact width b_i that depends on the wire diameter. Using this guestimate, line contact force is then calculated. With the knowledge that the contact width is a small fraction of the wire diameter, Erik (2011) suggested that if $b_i = \frac{D_i}{100}$ is chosen as first guestimate, only few iteration are needed to find the final values of line contact force P_{RC_i}.

From Figure 3.7 the resultant radial load transfer from an outer layer $j = i + 1$ to the neighbouring inner layer i is calculated as:

$$X_{R_j} = X_{MS_j} - 2P_{MS_j}\cos\beta_j \tag{3.43}$$

In the above equation, the subscript *MS* refers to multi-layered strand, where X_{MS_i} is the total radial (radial force transferred from outer layers plus contribution from the tension force in the wire itself) body force in multi-layered strand, given by equation (3.45), $P_{MS_i}$is the line contact hoop force between two adjacent wires when all the outer layers are taken into account for the statically indeterminate problem, given by Eq. (3.46), and β_i is the angle between the line of action between these two forces as shown in Figure 3.7 and is given by Eq. (3.44)

$$\cos\beta_i = \frac{1}{\sin^2\alpha_i}\left\{\sqrt{1+\frac{\tan^2\left(\frac{\pi}{2}-\frac{\pi}{n_i}\right)}{cos^2\alpha_i}}-\left(\tan^2\left(\frac{\pi}{2}-\frac{\pi}{n_i}\right)\right)\right. \times \left.\sqrt{\left(1+\frac{1}{cot^2\alpha_i\cos^2\left(\frac{\pi}{2}-\frac{\pi}{n_i}\right)\left(cos^2\alpha_i+\tan^2\left(\frac{\pi}{2}-\frac{\pi}{n_i}\right)\right)}\right)+cot^4\alpha_i}\right\} \tag{3.44}$$

where α_i is the lay angle and n_i is the number of wires in *i*th layer.

Then the total radial body force X_{MS_i} experienced by each wire in the inner layer of a multi-layered strand can be calculated as:

$$X_{MS_i} = \frac{EA_i\epsilon_x \sin^2\alpha_i}{r_i} + X_{R_j}\frac{n_j \cos\alpha_i}{n_i \cos\alpha_j} \tag{3.45}$$

First part on the right hand of Eq. (3.45) is the radial force generated due tension force in wire whereas the second part is the contribution of radial force from the outer layars.

The line contact force P_{MS_i} can be then determined with the force ratio within the layer *i*:

$$P_{MS_i} = \frac{P_{RC_i}X_{MS_i}}{X_{RC_i}} \tag{3.46}$$

It is worth mentioning that not only does each wire layer i have a certain P_{RCi}/ X_{RCi} ratio, the ratio also changes for different strand tensile strains ε_c. It is, therefore, necessary to calculate the P_{RCi} and X_{RCi} forces for each tensile strain perturbation for each layer and use their ratio to determine the multi-strand line contact force P_{MSi}: The process is then repeated, moving to another layer each time, until the whole strand has been analysed.

3.3.3 Compliances of Orthotropic Sheet Theory

In the orthotropic sheet approach, the wires in each layer of a strand are considered as prestressed cylindrical sheets. The properties of the orthotropic sheets in the principal directions (parallel and perpendicular to the wire axes) of orthotropy are estimated from contact stress theory. Using Hearmon's (1961) notations the strains and stresses in the strand along the principal directions 1, 2 and 6 (parallel, perpendicular and tangential to the wire axes) are given by:

$$\epsilon'_x = \varepsilon_c = \epsilon_{11'}\sigma_{x'} + \epsilon_{12'}\sigma_{y'} + \epsilon_{13'}\gamma_{xy'}$$

$$\epsilon_{y'} = \epsilon_{21'}\sigma_{x'} + \epsilon_{22'}\sigma_{y'} + \epsilon_{23'}\gamma_{xy'}$$

$$\gamma_{xy'} = \epsilon_{21'}\sigma_{x'} + \epsilon_{22'}\sigma_{y'} + \epsilon_{23'}\tau_{xy'} \tag{3.47(a-c)}$$

The axes of wire makes an angle α to the strand axis therefore, the corresponding compliances in the principal directions relating to strand axes can be found by rotation of axes by an angle α. Assuming $\cos\alpha_i = m$ and $\sin\alpha_i = n$ the compliances of the strand in the principal directions are given as:

$$\epsilon_{11'} = m^4\epsilon_{11} + 2m^2n^2\epsilon_{12} + n^4\epsilon_{22} + m^2n^2\epsilon_{33}$$

$$\epsilon_{12'} = m^2n^2\epsilon_{11} + (m^4 + n^4)\epsilon_{12} + m^2n^2\epsilon_{22} - m^2n^2\epsilon_{33}$$

$$\epsilon_{13'} = -2m^3n\epsilon_{11} + 2mn(m^2 - n^2)\epsilon_{12} + 2mn^3\epsilon_{22} - mn(m^2 - n^2)\epsilon_{33}$$

$$\epsilon_{22'} = n^4\epsilon_{11} + 2m^2n^2\epsilon_{12} + m^4\epsilon_{22} + m^2n^2\epsilon_{33}$$

$$\epsilon_{23'} = -2mn^3\epsilon_{11} - 2mn(m^2 - n^2)\epsilon_{12} + 2m^3n\epsilon_{22} - mn(m^2 - n^2)\epsilon_{33}$$

$$\epsilon_{33'} = 4m^2n^2\epsilon_{11} - 8m^2n^2\epsilon_{12} + 4m^2n^2\epsilon_{22} + (m^2 - n^2)^2\epsilon_{33} \qquad (3.48\ a - f)$$

The gross area A_{gi} for each shell i is approximated by approaching each wire as a square with sides equal to the diameter D_i of the wire. In order to conserve the effective axial stiffness of a wire layer, the area ratio needs to be taken into account by determining a Young's Modulus E_{net} compliant with this stiffness. The stiffness per unit length of a wire layer i in the direction of orthotropy is thus equal to $E_{gi}A_{net}$. The compliance of the sheet in the direction parallel to wire axes, ϵ_{11} is expressed as the ratio between the sheet area and the wire cross-sectional area:

$$\frac{E_{net}}{E} = \frac{A_{net}}{A_{gross}} = \frac{\pi}{4} \qquad (3.49)$$

$$\epsilon_{11} = \frac{1}{E_{net}} = \frac{4}{\pi E} \qquad (3.50)$$

where, E is the actual Young modulus of the material and $E_{net}$is the effective Young modulus of the material after the application of load.

Similarly the coupling compliance $\epsilon_{12} = \epsilon_{21}$ in the presence of axial load in the wires is then:

$$\epsilon_{12} = -\frac{\upsilon}{E_{net}} = -\frac{4\upsilon}{\pi E} \tag{3.51}$$

where υ is the Poisson's ratio of the wire material. The negative sign indicates that the cross-section of the strand shrinks in the presence of axial load.

Following Hobbs and Raoof (1982), for individual wires in line contact their normal compliances ϵ_{22} are given as:

$$\epsilon_{22} = \frac{1}{E}\left(0.11 + 0.59 \ln \frac{E D_i}{P_{MSi}}\right) \tag{3.52}$$

In the above D_i is the diameter of wires in ith layer whereas P_{MSi} is the line contact force per unit length in the ith layer of multi-layered strand.

The tangential compliance ϵ_{33} is also given by Hobbs and Raoof (1982), as:

$$\epsilon_{33} = \frac{\epsilon_{22}}{1-\upsilon}\left(\sqrt{\left(1 - \frac{\Delta_l}{2\Delta_{lmax}}\right)}\right) \tag{3.53}$$

where Δ_l is the tangential displacement between the centre-lines of the wires, with Δ_{lmax} being the maximum value at the onset of gross sliding (full-slip). Whereas, $2\Delta_{lmax}$ is the implitude of the sliding corresponding to uniform cyclic loading, with reversed tangential displacements taking place. This limiting displacement is obtained as:

$$\Delta_{lmax} = \frac{3}{4}\frac{\mu P_{MSi}}{1-\upsilon}\epsilon_{22} \tag{3.54}$$

where, the above equation is valid for $\Delta_l \leq 2\Delta_{lmax}$, with ϵ_{33} becoming infinite at the limit. For larger values of Δ_l, ϵ_{33} can be taken as infinitely large corresponding to the case of full-slip, whereas for no-slip case $\Delta_l = 0$.

3.3.4 Effective Young Modulus of the Layer

To derive an expression for the effective Young's modulus of a cable E_{eff}, the shear strain is assumed to be zero ($\gamma_{xy} = 0$). Following Hobbs and Raoof (1982) it is stated

that the ratio of the stresses in the axial direction to the stresses in the circumferential direction is equal for both local (wire) and global (cable) co-ordinate system of the layer i.e.

$$\frac{\sigma_{y'}}{\sigma_{x'}} = \frac{\sigma_y}{\sigma_x} = c_k \tag{3.55}$$

This condition applies both to no-slip and full-slip conditions.

Eqs (47a-c) can be solved to yield the relation for strand tensile strain and stress respectively.

$$\frac{\sigma_{x'}}{\varepsilon_c} = \left(\epsilon_{11'} + \epsilon_{12'} c_k - \frac{\epsilon_{13'}}{\epsilon_{33'}} (\epsilon_{13'} + \epsilon_{23'} c_k) \right)^{-1} \tag{3.56}$$

The non-dimensional stiffness coefficient for each layer of the strand is then expressed as:

$$k_{1i} = \frac{4}{\pi E} \left(\frac{\sigma_{x'}}{\varepsilon_c} \right) \tag{3.57}$$

and,

$$d_1 = A_{net,i} k_{11,i} + A_{core} \tag{3.58}$$

where, d_1 represents the constitutive constant (mm^2) for the axial direction of the strand.

The effective Young modulus is then given by Hobbs and Raoof (1982) as follows:

$$E_{eff} = \frac{E d_1}{A_{net,i}} \tag{3.59}$$

Similarly to derive an expression for torsional stiffness it is assumed that pure torsion exists in a layer of the cable (i.e. $\varepsilon_c = \epsilon_{y'} = 0$. From Eqs. 3.47(a-c), the tangential shear flexibility is obtained as:

$$\frac{\tau_{xy'}}{\gamma_{xy'}} = \epsilon_{33'} + \frac{2\epsilon_{12'}\epsilon_{13'}\epsilon_{23'} - \epsilon_{22'}{\epsilon_{13'}}^2 - \epsilon_{11'}{\epsilon_{13'}}^2}{\epsilon_{11'}\epsilon_{22'}{\epsilon_{12'}}^2} \tag{3.60}$$

The non-dimensional shear stiffness coefficient for each layer of the strand is then expressed as:

$$k_{4i} = \frac{4}{\pi E}\left(\frac{\tau_{xy'}}{\gamma_{xy'}}\right) \tag{3.61}$$

$$d_4 = A_{net,i}{r_i}^2 k_{4,i} \tag{3.62}$$

The effective shear modulus is then obtained by:

$$G_{eff} = \frac{d_4 E}{A_{net,i}{r_i}^2} \tag{3.63}$$

With the above formulations, it is now possible to determine the forces that are at play within a strand.

3.4 Conclusion

This chapter presents two alternative analytical formulations for calculating wire kinematics, pattern of interwire frictional forces and bending stiffness of the cable subjected to tension and bending. The first model (Hong et al, 2005) presents explicit formulations for the smooth transition of the flexural rigidity from no-slip to full-slip regimes of the cable as a function of bending curvature, neglecting the effect of line contact forces in the same layer. The second model (OST) fully takes into account interwire friction both in radial and hoop directions as well as contact deformations. Since the line contact forces have a great influence on the pattern of wire slippage and contact deformations. Therefore, using contact mechanics of the OST, the Hong et al, 2005 (HDS) model has been modified and enhanced to include the effect of interwire line contact forces within the same layer. The combination of the two models results in an improved and enhanced (MHDS) model for analysing large diameter multi-layered cables. The proposed modification and implementation of newly developed model will be the subject of the next chapter, where results have been presented for a variety of cable constructions.

Chapter 4

Bending Behaviour of Helically Wound Steel Cables, Subjected to Tension and Bending.

4.1 Introduction

Chapter 3 presents a detailed analysis of the mathematical formulations and their limitations of the two selected non-linear theoretical models used in this study. The aim of this chapter is to investigate the mechanical behavior of helically wound steel cables under tension and bending, using the new modified model. During bending of such cables, slippage takes place between individual wires, which is mainly governed by interwire frictional forces acting at the contact patches between wires. As a result of this slippage, the effective bending stiffness of the cable cross section varies between two extremes. These two extremes are: no slip (i.e. when all the wires are stuck together and act as a solid bar) and full slip (i.e. when all the wires in the cable act independently and bend about their own axis). As long as the unbalanced forces on the cable cross-section are smaller than the friction forces, all the wires in the cable behave as a solid rod and its response is almost linear. When the cross-sectional forces overcome the interwire/interlayer friction, sliding occurs between the layers and the structural response becomes non-linear.

The motivation for this study arose from the interest that interwire normal hoop contact forces have a significant effect on the values of interlayer radial contact forces over the trellis contact patches and hence the interlayer slippage for the given value of mean axial strain and imposed curvature. As in the case of multi-layered large diameter spiral strands the radial load transfer from one layer to another is found to decrease tremendously, when line contact hoop forces were taken into account. Cardou and Cloutier (1989) have shown that wires breakages at the trellis contact patches between wires of two different layers are about ten times more than wires of the same layer, in line contact with each other. Keeping in mind their significant influence on interwire contact deformations, the effect of the line contact forces has

been taken into account. Explicit formulations describing the variation of the bending stiffness of a helical cable as a function of cable curvature, friction coefficient and interwire/interlayer contact forces from the no-slip to the full-slip stiffness have been developed.

The study in this chapter also throws some light on the validity of the traditional assumption of a constant effective bending stiffness for predicting the minimum radii of curvature, at the fixed terminations to spiral strand; and whether it provides accurate predictions to be used as an input into the subsequent design calculations against restrained bending fatigue. Although the small curvature assumption of the cable may be valid in the parts away from termination, but the possible development of a large curvature at the bearings and end terminations cannot be ignored nor avoided. Related to this, the term restrained bending fatigue refers here to those cases where spiral strand fatigue failures occur in the vicinity of partially or fully restrained terminations caused by hydrodynamic or aerodynamic cyclic loading. Based on the new insights gained here into the internal cable deformation mechanisms, the present study provides a foundation for solving conductor fatigue problems, which depends on bending stiffness of the cable as a function of friction, cable curvature and tensile force on the cable, including the displacement behaviour of the wires in the cable construction.

Building upon an extensive theoretical parametric studies, using a corrected and subsequently extended version of Hong et al., (2005) model, it has been established that beyond a certain level of imposing curvature, the assumption of constant effective bending stiffness is unreasonable. Depending on the level of mean axial load of the cable, increasing bending near the end termination will lead to interwire/interlayer slippage. As a result, the flexural stiffness of the cable reduces by a factor of 2 to 16, depending upon the co-efficient of friction between the wires and the type of cable construction. For the present purposes, much attention is devoted to the interwire/interlayer contact forces and the associated slippage between the wire under frictional interaction. The effective bending stiffness of the cable is shown to be amplitude dependent, changing significantly as a function of changes in the cable curvature.

The effect of different geometrical parameters is also demonstrated, e.g. a slight increase in lay angle leads to decrease clench forces in the radial direction with a notable increase in normal contact forces in hoop direction. Thus increasing lay angle delays the initiation of wire slippage in the outer layers, but due to less radial load transfer into the inner layers slippage penetrates quickly into the inner layers of the strand. Similarly, the interlayer slippage is found to start at alarmingly small values of imposed curvature for large diameter multi-layered strands. This is because the unbalanced force on a wire is directly proportional to the radial distance of the wire from the centre of the strand. It is noticed that the ratio of the strand to wire diameter (d/D) also plays an important role in the pattern of interwire slippage and contact deformations, with larger wire diameters showing a slight delay in the initiation of wire slippage in the cable. The theoretical results obtained from this model are found in good correlation with the full scale test results reported by Raoof (1992) for 39 and 41 mm diameter strands with rather different lay angles. Regarding the magnitude of the bending stiffness of the strand, the no slip and full slip bending stiffness test results for a 164 mm diameter strand have been compared with theoretical predictions, showing a good agreement with. It is then concluded that the fatigue design curves based on a constant effective bending stiffness could be misleading.

4.2 Background

Costello and Butson (1982) proposed a theoretical model for predicting the static response of wire ropes subjected to tension, torsion and bending. It was assumed that under axial loading condition there was no contact between the core and outer wires. The maximum tensile stress was shown to occur in the core wire, which receives the largest axial and bending strain. LeClair (1989) reported a model for predicting the upper bound of the relative movements between the wires in bending. The wires were assumed to slip under frictional forces in the bent cable over a sheave for a seven wire strand.

Raoof (1989, 1990 and 1992) has shown in a series of publications that for the case of cross laid, large diameter spiral strands fretting between the outermost and penultimate layer is the prime initiator of fatigue cracks leading to wire breakages in

the vicinity of neutral axis as opposed to the extreme fire positions. Although outer wire strain measurements show that maximum strain occurs at the extreme fibre position (in bending terms).

Raoof and Hobbs (1984) and Raoof (1990a) explained analytically the unexpected experimental observations of Hobbs and Ghavami (1982) that the first wire fractures invariably occurred at the neutral axis (in terms of bending) rather than at the extreme fibre position. Raoof (1990b) has proposed a theoretical model for estimating axial fatigue life of multi-layered spiral strands undergoing uniform axial repeated loading. Raoof and Huang (1992) have shown that even with infinite shear stiffness between the layers of an axially preloaded spiral strand, interwire slippage within the wires in line contact can take place throughout the strand. This causes some reductions in the effective bending stiffness of the strand.

Raoof and Davies (2005) showed that the effective fixed end of the spiral strands undergoing cyclic bending is not located on the face of the socket but within the socket at some distance away (approximately 1.5 diameters) from the face of the socket. It has been suggested that for calculating the effective bending stiffness of the strand, plane section bending may reasonably assume for spiral strands with mean axial strains $\varepsilon_c \leq 0.0025$ and outside diameter $d \leq 40$ mm such that the ratios of the estimated minimum radii of curvature at the fixed end of the strand ρ, to the strand outside diameter d, is greater than 630. For a strand under free bending the radius of curvature is greatest at the fixed end and reduced very rapidly as one moves away from the point of restraint.

In correlation with Raoof's experimental results, Papailiou (1997) proposed a very interesting model for axially preloaded spiral strands undergoing non-plane section bending. According to his model, the interlayer slippage starts near neutral axis, with the predictions of strand bending stiffness exhibiting a smooth transition from no-slip (maximum) to full-slip (minimum) state. Kraincanic and Kebadze (2001) proposed analytical formulations for the determination of the bending stiffness of a helical layer in unbonded flexible pipes. After certain levels of bending curvature, the non-linearity of the layer caused by slippage of individual helical wires between the layers were fully taken into account. Hong *et al*. (2005) examined in detail the bending behaviour

of helically wound steel cables and proposed a mechanical model that takes into account the slippage of wires under friction and increasing the imposed curvature of the cable. Wire slippage has been shown to start near the neutral axis expanding symmetrically towards the extreme fire positions, causing a decrease in the effective bending stiffness of the cable. However, the effect of line contact forces in the hoop direction has been ignored in this model.

4.3 Theory

As part of the present research, two aspects of Hong et al*.'s* original model have been improved. Firstly, the present work fully caters for the ever presence of line contact hoop forces in various layers as predicted by the orthotropic sheet theory of Raoof (1982). These forces have a very significant influence on the values of the radial load transfer over the trellis contact patches and hence interlayer slippage, as shown in Figs 4.4 (a-f). Secondly, the influence of geometrical non-linearities on the estimates of the axial strains in the individual helical wires in various layers has been considered. This gains importance for sufficiently large values of the lay angle within the manufacturing range of $11° \leq \alpha_i \leq 24°$ as shown in Figure 4.2. Although Hong's model provided a base for estimating the reductions in the effective bending stiffness of the strand in the free field to increasing values of curvature, when interwire/interlayer slippage takes place, but failed to cater fully for interwire contact deformations.

In this thesis, the original Hong's model will be referred to as HDS model hereafter, (from the surnames of the three authors, Hong, Der-Kiureghian and Sackman), whereas after the proposed modifications, the new model developed in this chapter will be referred as to MHDS (i.e. modified HDS) model.

4.3.1 Tension in a Wire

Two types of tension forces are introduced namely: stick tension and slip tension corresponding to the state of the wire. It is now possible to calculate the ordinary bending strain plus tensile strain in all the wires of a multi-layered cable.

When the strand is subjected to an axial strain ε_c, and bending curvature k_c then, using Hong et al., (2005) model the strain in individual wire along the cable axis can be calculated after rearranging Eq (3.6):

$$\epsilon_{xi}^{stick} = \varepsilon_c \left(1 + \frac{k_c r_i \sin\varphi}{\varepsilon_c}\right) \tag{4.1}$$

where r_i is the helix radius of wire in ith layer and is given by Eq. (3.31).

In conjunction with Hobbs and Raoof (1982), after proper tensorial transformation the axial strain of the wire along its own axis is then given:

$$\epsilon_{xi}^{stick} = \epsilon_x \left(1 + \frac{k_c r_i \sin\varphi}{\varepsilon_c}\right) \tag{4.2}$$

where ϵ_x is the axial strain in the wire in straight configuration ($\kappa_c = 0$) and can be calculated using Eq.(3.27).

Equation (4.2) gives the exact wire strain (axial+bending) in fully stick state, where the wire is supposed to have a bent helix configuration in the deformed cable. In Eq. (4.3), the first contribution in the right hand side is the axial strain due to the tension force on the wire, whereas the second contribution is due to the bending of the cable. This second part in Eq. (4.2) depends on the polar angle $\pm\varphi$, in the cable cross-section of the cable. For negative polar angle ($\varphi < 0$), this term becomes negative and thus the wires on concave side experience less tension and vice versa for the wires on the convex side. If there is no bending i.e. $k_c = 0$, the second part on the right hand side of Eq. (4.2) vanishes. The positive curvature is assumed to cause maximum stress at the extreme fibre position in bending term. Thus, frictional forces on wires in different layers increase or decrease rapidly under increasing curvature.

In the fully stick state, tension force in the wire is obtained by multiplying axial strain in the wire with the Young modulus and cross-sectional area of the wire Hong *et al,* (2005):

$$T_i^{stick} = EA_i\epsilon_x\left(1 + \frac{k_c r_i \sin\varphi}{\varepsilon_c}\right) \tag{4.3}$$

where E is the Young modulus of the material, and $A_i = \frac{\pi D_i^2}{4\cos\alpha_i}$ is the cross-sectional area of individual wire, $\varphi =$ polar angle of the wire describes the position of wire in cable cross-section, r_i is the helix radius of the wire layer i, ϵ_x is the axial strain of the wire in straight configuration calculated by Eq. (3.27), and ε_c is the axial strain along the centreline of the cable.

According to Hong et al, (2005), a differential force arises on the wire, when the cable is subjected to bending. For a differential wire segment in the ith layer, the unbalanced tension force in the stick state is obtained by differentiating Eq. (4.3) with respect to φ_i, which then replaces Eq. (3.9) in original HDS model.

$$dT_i^{stick} = \frac{EA_i\epsilon_x k_c r_i \cos\varphi}{\varepsilon_c} \tag{4.4}$$

This unbalanced force in the wire must be in equilibrium with friction force generated at the contact patches of the wire. Slippage begins, when the unbalanced force in the wire segment exceeds the maximum friction generated at the wire surfaces. Once the wire slips, the forces in the wire re-distribute until equilibrium is achieved. Therefore, the condition of a differential wire segment in the outermost layer of the cable to be in the slip state is given by Eq. (3.10).

And the constant of integration and can be obtained the same way by satisfying a boundary condition, by putting the value of polar angle zero.

Next, considering a wire in an inner layer i, such that the normal forces are acting on both inner and outer surfaces of the wire.

$$dT_i^{slip} = \left(\mu T_i^{slip}\sin\alpha_i + 2\mu X_{R_j}\frac{r_j}{\sin\alpha_j}\frac{\tan\alpha_j n_j}{\tan\alpha_i n_i}\right)d\varphi \tag{4.5}$$

The solution for this first order differential equation is given as (which replaces Eq. (3.16):

$$T_i^{slip} = C_i \exp(\mu\varphi \sin\alpha_i) - \frac{2X_{R_j} r_j}{\sin\alpha_j \sin\alpha_i} \frac{\tan\alpha_j n_j}{\tan\alpha_i n_i} \tag{4.6}$$

where, the integration constant for this solution C_i is obtained again by satisfying boundary condition at $\varphi_i = 0$ and solving for C_i, we get

$$C_i = EA_i\varepsilon_c \cos^2\alpha_i + \frac{2X_{Rj} r_j}{\sin\alpha_j \sin\alpha_i} \frac{\tan\alpha_j n_j}{\tan\alpha_i n_i} \tag{4.7}$$

where n_i and n_j are the number of wires in layer i and $j = i + 1$ respectively, and X_{R_j} is the radial load transfer from the outer layer, where the effect of all outer layers has been taken into account in case of multi-layered cable Hobbs and Raoof (1982).

Note that in the above equation account has been made for different lay angles in different layers of the cable. This analysis provides the forces in all wires in tension that are either in stick state or slip state.

4.3.2 Contact Forces and State of Wire

It is important to mention here that the magnitude of unbalanced force is negligible for small curvatures, but increases exponentially as bending increases. Now, if the unbalanced force in the wire exceeds the maximum friction force generated at the contact patches between the wires interlayer slippage starts. Also, as the polar angle φ varies along the axis of a given wire, there is a curvature range, where parts of the same wire have slipped while others have not. The state of any individual wire for given value of polar angle in the cable cross section can be determined by:

$$\begin{aligned} &EA_i k_c r_i \cos\varphi \,(1 - 0.146\alpha_i + 0.706{\alpha_i}^2 - 5.097{\alpha_i}^3) \\ &= \mu\left(T_i^{slip} \sin\alpha_i + 2X_{Ri} \frac{r_j}{\sin\alpha_j} \frac{\tan\alpha_j n_j}{\tan\alpha_i n_i}\right) \end{aligned} \tag{4.8}$$

It is clear from the above equation that slippage in any layer begins near the neutral axis ($\varphi = 0$) and propagates almost symmetrically to the upper and lower halves of the cable ($\pm\varphi$ increasing).

4.3.3 Calculation of the Theoretical Bending Stiffness

As described earlier, effective bending stiffness of the cable depends on interlayer/interwire slippage, as wire starts slippage according to Eq.(4.8), the effective bending stiffness of the cable decreases until all the wires in the cable are slipped. The bending moment in the specific support cross-section is proportional to the cable curvature of the cross-sectional area at that position. The resultant bending moment in a cable cross-section can be calculated under a given imposed curvature k_c, Hong et al. (2005):

$$M = \left(\sum_{all\ wires} EI_i + EI_{core} \right) k_c + \sum_{all\ wires} T_i r_i \cos\alpha_i \sin\varphi \tag{4.9}$$

In the above k_c is the strand curvature, T_i is the tension force in individual wire in layer i, r_i is the helix radius in layer i, α_i is the lay angle with φ being the polar angle of a wire in layer i, represents its position in the cross-section of the strand. Whereas $I_i = \pi d_i^4/64$ is the moment of inertia of each wire in the ith layer and I_{core} is the moment of inertia of the core.

Note that the first term inside parenthesis on the right-hand side of the Eq. (4.9) accounts for the bending stiffness of each individual wire, including those having zero axial force, and the core. The second term represents the contribution to the bending moment due to the tension force in each of the wires.

Finally, the bending stiffness of the cable is determined from the slope of the moment versus curvature curve. The resultant bending moment of the cable is a non-linear function of cable axial stain and curvature.

In the final MHDS model in this chapter, Eq. (3.9) in HDS model is replaced by Eq. (4.4) taking into account the geometrical non-linearities and Poisson's ratio effect on the estimates of tension force in the wires. The difference between two models for this

effect is demonstrated in Figures 4.1. Similarly, Eq. (3.12) is replaced by Eq. (4.5) in MHDS model after catering for the effect of line contact force between the wires in the same layer. Furthermore, slip tension force in the wires depends on the contact force and the friction coefficient between the wires. The influence of line contact forces on the estimates of radial load transfer is presented in Figures 4.3 (a-f). Finally, the equilibrium equation for a wire is changed accordingly in MHDS model, Eq. (4.8) replaces Eq. (3.22), demonstrated in Figures 4.4 (a-f).

4.4 Experimental Observations

There are various experimental techniques, as discussed by Malinovsky (1993), available for the determination of a cable's effective bending stiffness. It is noted that large scale experimental data is always very expensive and time consuming to acquire, and the results are usually of restricted application in the absence of adequate theoretical interpretation. It is further, noted that even for the same diameter and loading, different cable constructions are found to have different characteristics. Malinovsky (1993) used two different methods for the determination of the bending stiffness using a 34 mm outside diameter fibre-core wire rope. These two methods were; the frequency method, and the method of static bending, and the bending stiffness was found to be 3000 and 534 Nm^2 respectively. The difference between the experimental results is very significant; with the value of the bending stiffness determined by frequency method being 5.6 times greater than as determined by using the method of static bending. The problem with the experimental determination of the effective bending stiffness using different methods is mainly due to the experimental conditions and depends on the level of imposed curvature.

Works by Costello and his associates were also supported by some limited experimental data obtained from static tests on two types of wire ropes. Phillips and Costello (1985) reported test results for the effective Young modulus of a wire rope with IWRC. Velinsky (1985b) reported test results for a fibre-core wire rope, to measure the axial stiffness and radial contraction of a single specimen under static monotonic loading. However, the correlation between test data and theory were found encouraging. Utting and Jones (1987a, and b) reported a variety of test data on

seven wire strands subjected to an axial load with various end restraints, in order to measure the strand extension, rotation, torque and bending moment. Later on in another paper Utting and Jones (1988) reported similar test results for nineteen wire strand. On comparing the test results with the theoretical model of Machida and Durelli (1973) it was stated that axial strain measurements on helical wire surfaces revealed unequal load sharing between identical helical wires. This phenomenon was particularly observed in the region close to end terminations, which is considered to have severe implications in fatigue studies. Strzemieki and Hobbs (1988) carried out static and dynamic tests on a number of spiral strands and wire ropes which were subjected to cyclic axial or bending load perturbations. It was shown that the effective axial stiffness of the cable change from no-slip to full-slip limit as a function of variations in the range/mean ratio of the axial load.

Recently, Wood and Frank (2009) investigated experimentally bending fatigue performance of grouted stay cables and reported the results from twelve bending fatigue tests. In line with previous results of Raoof, they stated that the risk of bending fatigue damage was low at the tension rings, along the free length of the stays, whereas, fretting of adjacent wires within a strand was the dominant cause of bending fatigue damage in the tested specimens. It is further stated that the damage tended to increase at the end terminations and other locations where concentrated loads were applied to the specimens.

The majority of theories developed based on these experimental results have previously assumed either plane-section bending or in many cases have totally ignored the ever-present interwire friction, assuming that the individual helical wires act as simple helical springs. It is particularly noteworthy that for large diameter multi-layered spiral strands, the difference between the two limits of bending stiffness, corresponding to zero and infinite interlayer friction is unacceptably large. This can be given approximately by the square of the strand/wire diameter ratio. There was, therefore, a pressing need to develop reasonably more accurate methods for estimating the bending stiffness of particularly large-diameter spiral strands.

Very often, experiments have been carried out on small diameter strands, consisting of only six or seven wires with a single layer. In the present case, the previously

reported experimental results of a series of free bending tests on 39 and 41 mm diameter strands have been compared with theoretical predictions. For 39 mm strand, the deflected shapes of the strand were obtained for mean axial loads of 0.205, 0.41 and 0.61 MN. Similarly, experimentally determined bending stiffness for a 164 mm outside diameter spiral strand has been compared with the bending stiffness predictions based on the recently proposed new method by the present author.

4.4.1 Test Specimen and Equipment

Full details of the large scale experiments are reported elsewhere (Raoof, 1992a), and will be not repeated here, but a few of the most relevant observations will be repeated here for completeness. The free bending tests of Raoof (1983) were carried out on a 7.9m long axially pre-loaded 39 and 41 mm spiral strands with the construction details given in table (4.1a) and (4.1b). Two different 7.9 m long galvanized specimens of both the strands with axial loads of 0.215, 0.41 and 0.615 MN for 39 mm and 0.22, 0.44 and 0.66 MN for 41 mm strand were used respectively. These correspond to 16.7%, 33.3% and 50% of the ultimate load for 39 mm strand and 15.9%, 31.7% and 47.8% of the ultimate load for the 41 mm strand. Both were terminated with zinc-poured sockets to BS463: 1958 except for an elongated jaw. The 39 mm specimen had seen 15 years' service as part of a 170 m long guy, and hence its characteristics were thought to closely resemble those of other strands in long-term applications. The random external loads over a period of years cause significant interwire abrasion and compaction which is not easy to simulate under laboratory conditions. The 41 mm strand was newly manufactured with some noticeable gaps in its outer layer. Sixty 20 mm Tokyo Sokki wire on polyester base electrical resistance strain gauges were placed in two different locations on the individual outer wires of both 39 and 41 mm outside diameter strand specimens. One set of the gauges, were placed close to the mouth of the socket while the other were deployed at some distance two meters away, in the free field on a similar section. In a series of experiments conducted by Raoof, the test set-up enabled Raoof to obtain certain test data regarding the Poffenberger-Swart to differential displacements in the vicinity of the socket.

The limitations for these experiments were that the behaviour of practical sockets was highly complex, and it was not easy to accurately determine the degree of end fixity on individual wires, which were collectively (as a bunch) imbedded in the relatively soft zinc matrix. Furthermore, the exact location of the cable interface was unknown, occurring at some distance inside the conical housing from the face of the socket. Raoof and Davies (2005) later showed that actual fix end to the cable occur at a distance around 1.5 times the diameter of the cable from the face of the socket. For an axially preloaded spiral strands, the end of the cable are supposed to be ideally fixed at the face of the socket. Also, the main thrust of these experiments was on torsional and bending measurements of the above two strands under various steady mean axial loads. Therefore, the equipment used was unsuitable for axial hysteresis measurements of the cable.

As a result of these tests, Raoof (1992a) has shown experimentally that axially pre-loaded spiral strands undergo plane-section bending only for sufficiently small levels of lateral deflections. Beyond a certain level of lateral deflection interlayer slippage takes place starting from outer layer and spreading towards the centre of the strands, depending on the level of axial tension and imposed curvature. Thus the theoretical predictions for the proposed model have been compared with the large scale experimental data for 39 and 41 mm outside diameter strands. The plotted test data points in Fig. (4.4a & 4.4b) verify the validity of the proposed modified theory. Guided by the test results presented in Fig.4.4a & b and theoretical predictions for different strand constructions, it is concluded that the lay angle in different layers of the strand plays an important role in the bending behaviour of the strand. Increasing lay angle delays the initiation of wire slippage in outer layers, but the slippage penetrates more rapidly towards the centre of the strand, as radial load transfer for large angles is much less compared to small lay angles.

Table 4-1a: Construction Details for the 39 mm Outside Diameter Spiral Strand.

Layer No	Number of Wires n_w	Lay Direction	Wire Diameter D(mm)	Lay Angle (degrees)	Helix Radius r(mm)	Net Steel Area A_n(mm^2)	Gross Steel Area A_g (mm^2)
1	30	RH	3.54	17.74	17.73	310.010	394.717
2	24	LH	3.54	16.45	14.1	246.297	313.595
3	18	LH	3.54	15.93	10.57	184.236	234.577
4	12	RH	3.54	14.9	7.04	122.217	155.611
5	7	RH	3.54	15.42	4.19	71.469	90.997
King	1	-	5.05	-	-	-	20.030
			A_{core} = 20 mm^2		A_{net} = 954 mm^2		

Table 4.1b: Construction Details for the 41mm Outside Diameter Spiral Strand

Layer No	Number of Wires n_w	Lay Direction	Wire Diameter D (mm)	Lay Angle (degrees)	Helix Radius r (mm)	Net Steel Area A_n (mm^2)	Gross Steel Area A_g (mm^2)
1	24	RH	4.57	12.45	17.93	403.151	513.308
2	18	LH	4.57	11.96	13.45	301.805	384.270
3	12	RH	4.57	11.25	8.99	200.692	255.529
	6	RH	3.43	7	-	-	54.210
Core	6	RH	3.43	7.7	-	-	32.694
	6	RH	3.38	4	-	-	53.444
	1	-	3.38	-	-	-	8.973
			A_{core} = 150 mm^2		A_{net} = 1054.9 mm^2		

Table 4.1c: Construction Details for the 127 mm Outside Diameter Spiral Strand, (α = 12°).

Layer No	Number of Wires n_w	Lay Direction	Wire Diameter D(mm)	Lay Angle (degrees)	Helix Radius r(mm)	Net Steel Area $A_n(mm^2)$	Gross Steel Area $A_g(mm^2)$
1	56	RH	6.6	12	60.17	1958.67	2493.86
2	50	LH	6.6	12	53.73	1748.81	2226.66
3	44	LH	6.6	12	47.29	1538.96	1959.46
4	38	RH	6.6	12	40.85	1329.10	1692.26
5	32	LH	6.5	12	33.89	1085.58	1382.20
6	26	RH	6.5	12	27.56	882.03	1123.04
7	20	LH	6.5	12	21.23	678.49	863.88
8	14	RH	6.6	12	15.15	489.67	623.46
	7	-	4	8.57	-	85.05	-
Core	7	-	5.2	8.03	-	144.33	-
	7	-	5.2	4.92	-	147.02	-
	1	-	7.1	-	-	39.59	-
A_{core} = 415.99 mm^2				A_{net} = 10127 mm^2			

Table 4.1d: Construction Details for the 127 mm Outside Diameter Spiral Strand, (α = 18°).

Layer No	Number of Wires n_w	Lay Direction	Wire Diameter D(mm)	Lay Angle (degrees)	Helix Radius r(mm)	Net Steel Area $A_n(mm^2)$	Gross Steel Area $A_g(mm^2)$
1	54	RH	6.55	18.01	59.22	1913.31	2436.10
2	48	LH	6.55	18.01	52.64	1700.72	2165.42
3	42	LH	6.55	18.01	46.07	1488.13	1894.74
4	36	RH	6.55	18.01	39.5	1275.54	1624.07
5	31	LH	6.55	18.01	34.02	1098.38	1398.50
6	25	RH	6.55	18.01	27.46	885.79	1127.82
7	19	LH	6.55	18.01	20.9	673.20	857.15
8	14	RH	6.3	18.01	14.85	458.90	584.29
	7	-	3.9	13.07	-	77.29	-
Core	7	-	5.1	12.2	-	133.53	-
	7	-	5.25	7.62	-	142.55	-
	1	-	7	-	-	38.48	-
A_{core} = 391.85 mm^2				A_{net} = 9779.4 mm^2			

Table 4.1e: Construction Details for the 127 mm Outside Diameter Spiral Strand, (α = 24°).

Layer	Number of Wires n_w	Lay Direction	Wire Diameter D(mm)	Lay Angle (degrees)	Helix Radius r(mm)	Net Steel Area $A_n(mm^2)$	Gross Steel Area $A_g(mm^2)$
1	54	RH	6.4	24	60.23	1901.57	2421.16
2	48	LH	6.4	24	53.54	1690.29	2152.14
3	42	LH	6.5	24	47.58	1525.58	1942.43
4	36	RH	6.5	24	40.79	1307.64	1664.94
5	30	LH	6.6	24	34.53	1123.49	1430.47
6	24	RH	6.6	24	27.64	898.79	1144.38
7	18	LH	6.8	24	21.38	715.57	911.09
8	14	RH	6.1	24	14.94	447.87	570.24
	7	-	3.9	17.89	-	72.07	-
Core	7	-	5.1	16.75	-	125.56	-
	7	-	5.25	10.58	-	143.94	-
	1	-	7	-	-	38.48	-
A_{core} = 380 mm^2				A_{net} = 9990.7 mm^2			

Table 4.1f: Construction Details for 164 mm Outside Diameter Spiral Strand, (α = 18°).

Layer	Number of Wires n_w	Lay Direction	Wire Diameter D(mm)	Lay Angle (degrees)	Helix Radius r(mm)	Net Steel Area $A_n(mm^2)$	Gross Steel Area $A_g(mm^2)$
1	72	RH	6.5	18.01	78.34	2512.276	3198.73
2	66	LH	6.5	18.01	71.81	2302.920	2932.17
3	60	RH	6.5	18.01	65.29	2093.564	2665.61
4	54	LH	6.5	18.01	58.77	1884.207	2399.05
5	48	RH	6.5	18.01	52.24	1674.851	2132.49
6	42	LH	6.5	18.01	45.72	1465.495	1865.93
7	36	RH	6.6	18.01	39.8	1295.086	1648.95
8	30	LH	6.6	18.01	33.18	1079.238	1374.13
9	24	RH	6.6	18.01	26.56	863.391	1099.3
10	18	LH	6.6	18.01	19.95	647.543	824.477
	14		6	17.99	-	340.575	-
	7	-	3.7	12.98	-	69.641	-
Core	7	-	4.85	12.15	-	120.824	-
	7	-	4.95	7.53	-	131.254	-
	1	-	6.7	-	-	35.257	-
A_{core} = 697.55 mm^2				A_{net} = 20140.8 mm^2			

4.5 Results and Discussion

Tables 4.1 (a & b) give the construction details of 39 and 41 mm (outside) diameter strands used in the large scale experiments reported by Raoof (1992 a &b) whereas Tables 4.1 (c-f) give the construction details of three different 127 mm (outside) diameter strands with lay angles of 12°, 18° and 24°, with nominally similar values for the other geometrical parameters. The first two multi-layered axially preloaded spiral strands have different lay angles of around 17 and 11 degrees respectively with approximately same outer diameters. For the 164 mm diameter strand with lay angle of 18°, experimentally determined values of the effective bending stiffness are reported in this Chapter, taken from Raoof and Davies (2005).

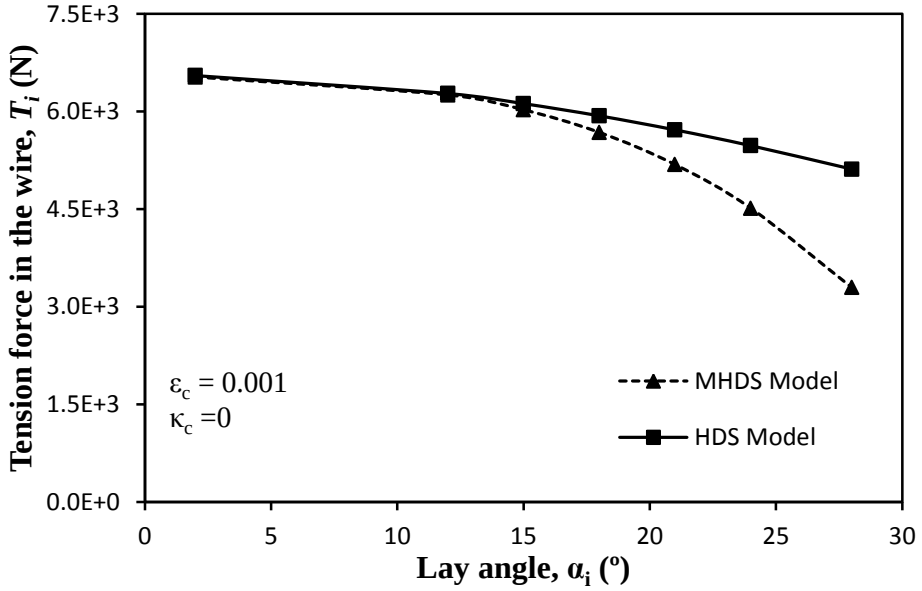

Figure 4-1: Tension force versus lay angle measurements in individual wire of 127 mm diameter strand using HDS and MHDS models.

Figure 4.1 shows the influence of geometrical nonlinearities on the axial strains in the individual helical wires in various layers. Since the curvature is zero therefore, all the wires in the cable are equally stretched. The difference between the two models particularly gains importance for sufficiently large values of the lay angle(s) within the manufacturing range of ($11° \leq \alpha_i \leq 24°$). Here, *MHDS* model based on the previously reported orthotropic sheet model, not only takes the effects of geometrical

nonlinearities on the axial wire strains but also the important reductions in cable diameter due to both interwire normal contact deformations and the Poison's ratio effect of steel. For lay angles beyond 15°, the significant difference between the two models has shown in the Figure 4.1. For lay angle of 28°, the difference between the two models exceeds 1820 N for a single wire, which when sum up for all the 268 wires of the cable becomes 487 KN. Furthermore, material non-linearities due to the presence of friction between wires and non-linear nature of the elastic contact problem is also considered in this work.

The associated tension force in individual wires based on HDS and MHDS models is presented in Figures 4.2 (a-c), for three same diameter strands with different lay angles of 12°, 18° and 24° respectively. The results in Figures 4.2 (a-c) clearly demonstrate the difference in the estimates of tension force in individual wires for the two models increases with increasing lay angles. These values have been obtained for the case, when the bending curvature is zero and all the wires in the cable are equally stretched. For lay angle of 24° for example, tension force in a wire for an axial strain of 0.006, is 13540, 16424 N for HDS and MHDS models respectively. This shows a percentage difference of 21.3 % for the selected axial strain of ε_c = 0.006 for a single wire in the cable.

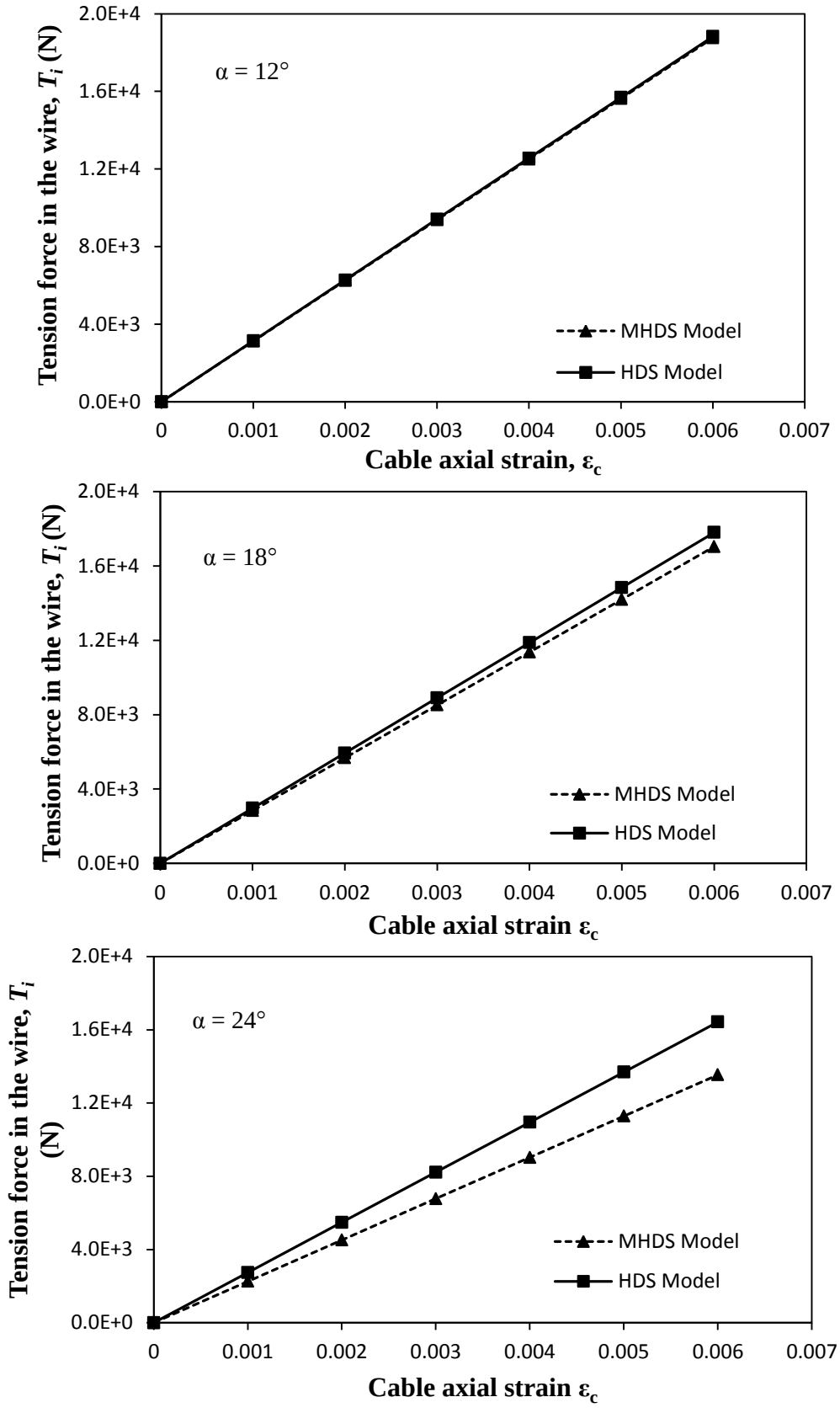

Figure 4-2: (a-c): Theoretical predictions of tension force in the wire of three same diameter strands with varying lay angles of: (a) 12°; (b) 18°; and (c) 24° respectively.

Figures 4.3 (a-f) present comparisons between the theoretical values of radial contact forces per unit length for all the layers of the above six different strand constructions for HDS and MHDS models respectively. These are the values obtained for the case when the wire strains due to tension force in the wires are much greater than the wire strains due to bending. Keeping in view the helical nature of the individual wires in axially pre-loaded spiral strands, the radial contact forces are minimum at the interface between outermost and penultimate layer and increase towards the centre of the strand as shown in Fig. 4.3 (a-f). Unlike HDS model, the proposed MHDS model fully takes into account normal contact forces both in the hoop and radial directions, following orthotropic sheet theory formulations. The crucial effect of including line contact hoop forces on the estimates of interlayer friction results in reducing the bending stiffness with increasing curvature is clearly demonstrated.

This difference in radial load transfer at the trellis contact patches for the two models is shown to increase tremendously for inner layers as well as for an increasing axial strain of the strand. And thus in the case of MHDS model, interlayer/interwire slippage in the inner layers is observed to occur at relatively small values of imposed curvature for multi-layered strands. A slight increase in lay angle leads to decrease clench forces in the radial direction with a notable increase in normal contact forces in hoop direction. The effect of lay angle on the estimates of radial contact forces is demonstrated in Figures 4.3 (c-e) for the three same outer diameter strands with different lay angles of 12°, 18° and 24° respectively.

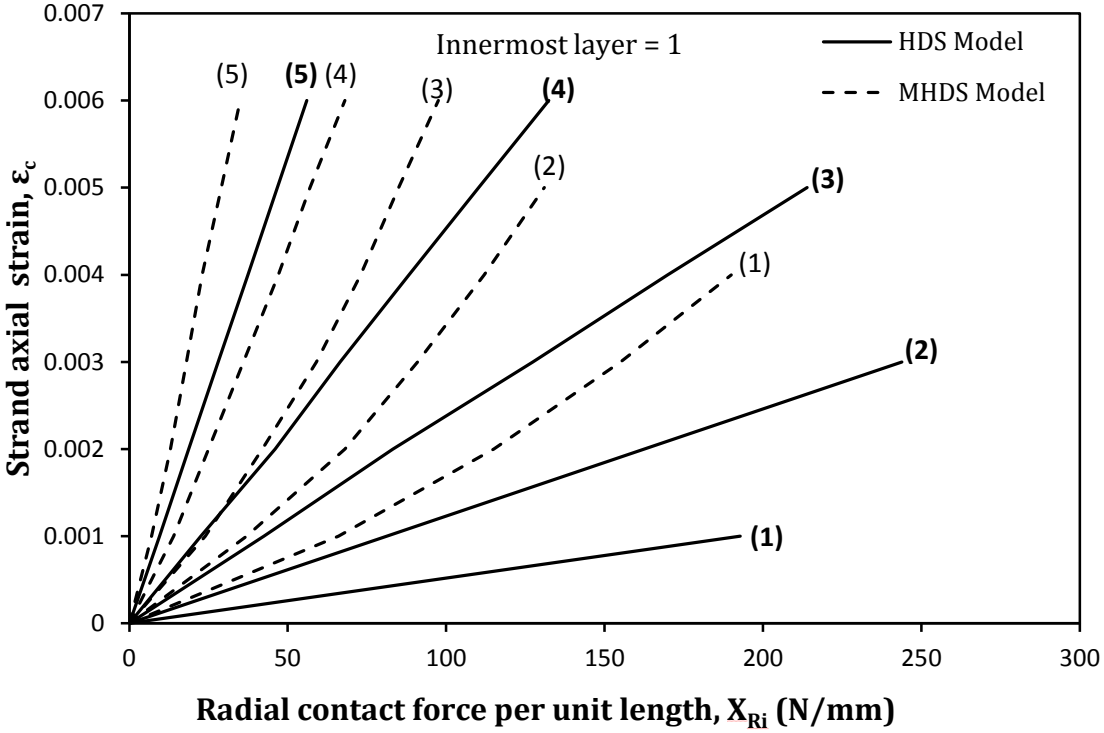

Figure 4-3a: Comparison of X_{Ri} versus ε_c plots, for the MHDS and HDS models, for all the layers of 39 mm outside diameter strand.

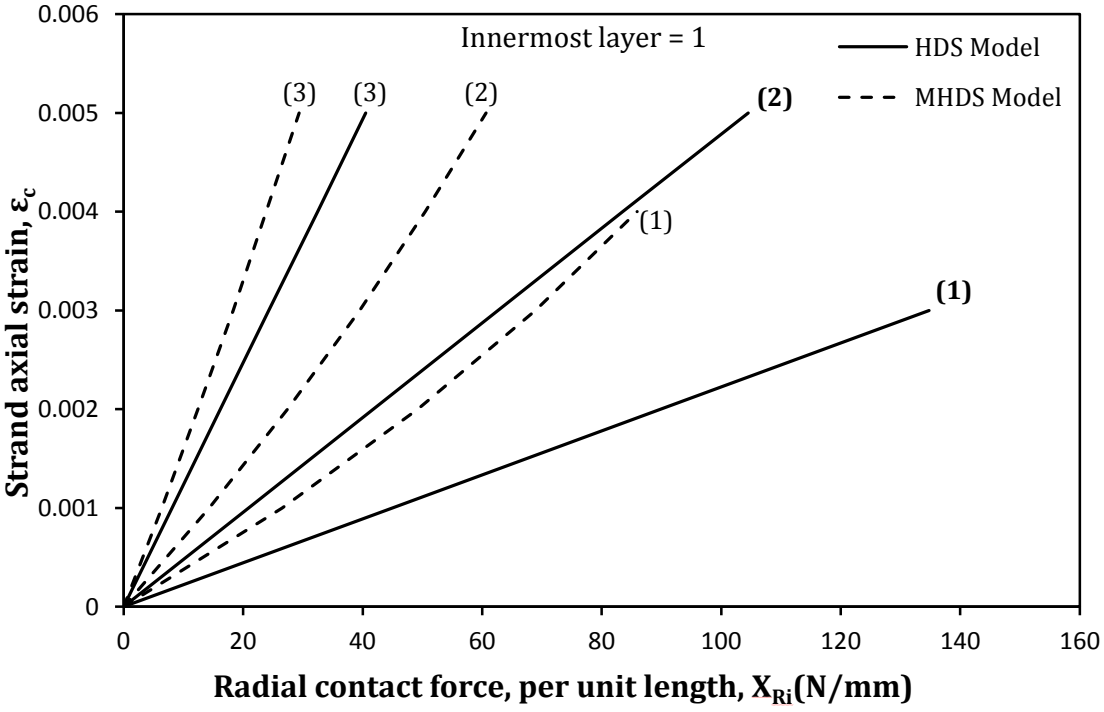

Figure 4.3b-Comparison of X_{Ri} versus ε_c plots, for the MHDS and HDS models, for all the layers of 41 mm outside diameter strand.

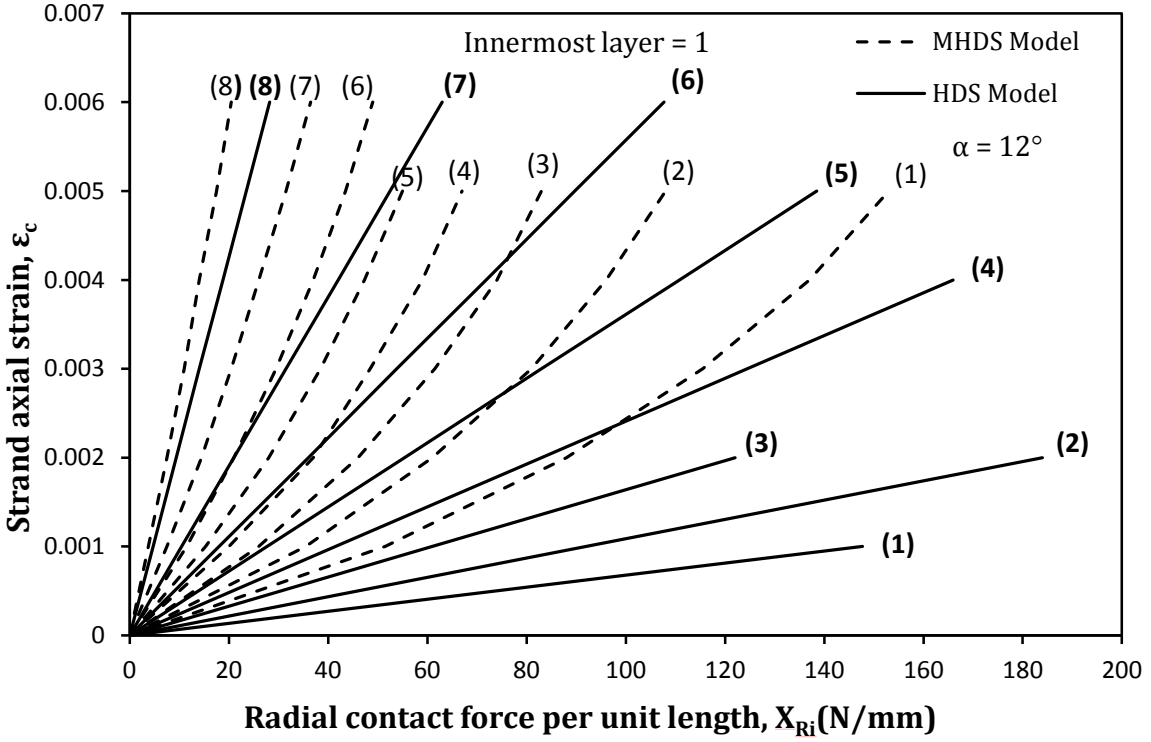

Figure 4.3c-Comparison of X_{Ri} versus ε_c plots, for the MHDS and HDS models, for all the layers of 127 mm (α = 12°) outside diameter strand.

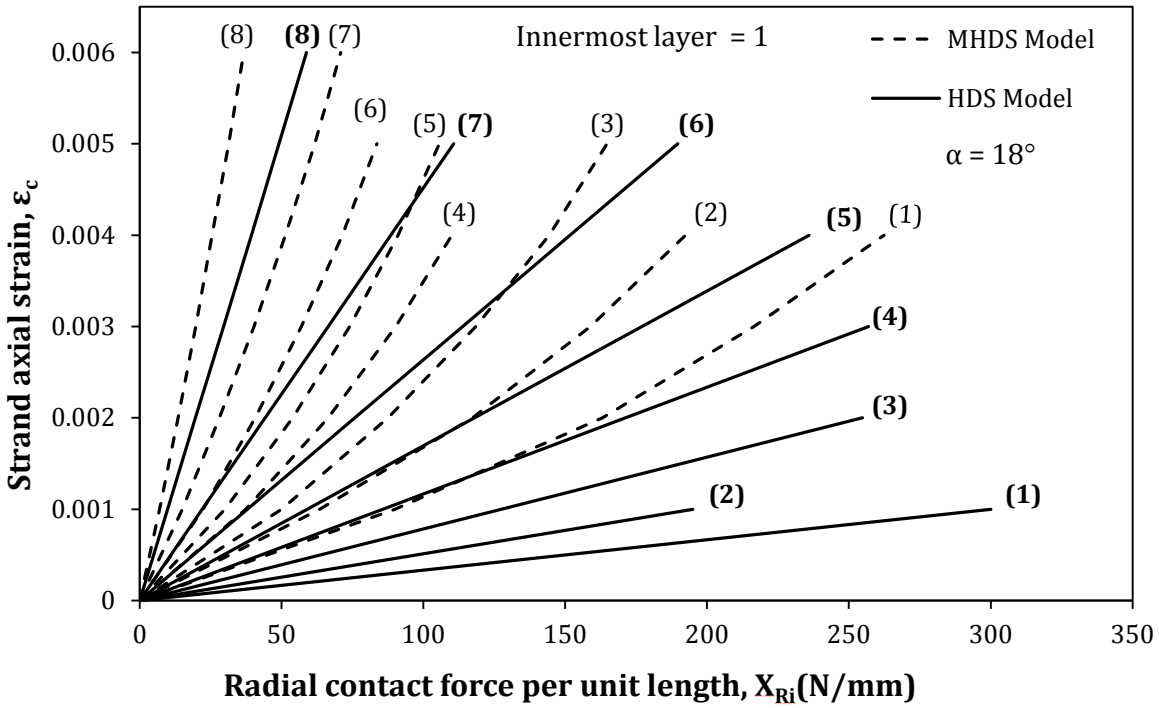

Figure 4.3d-Comparison of X_{Ri} versus ε_c plots, for the MHDS and HDS models, for all the layers of 127 mm (α = 18°) outside diameter strand.

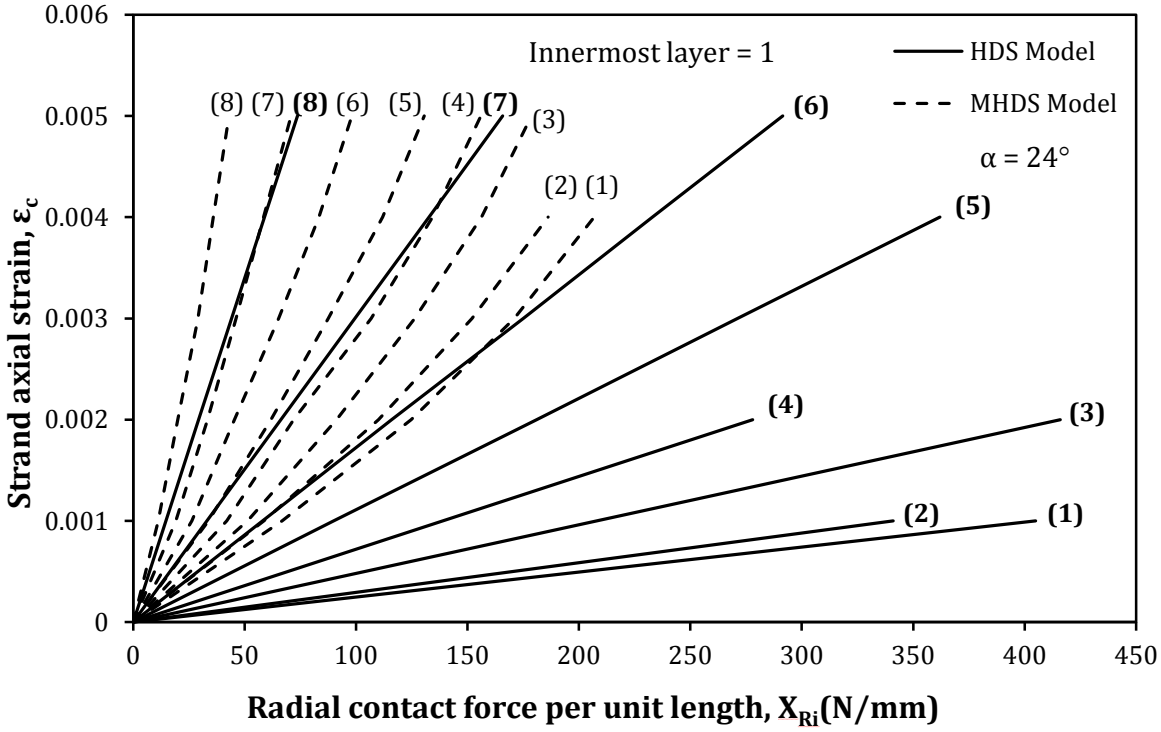

Figure 4.3e-Comparison of X_{Ri} versus ε_c plots, for the MHDS and HDS models, for all the layers of 127 mm (α = 24°) outside diameter strand.

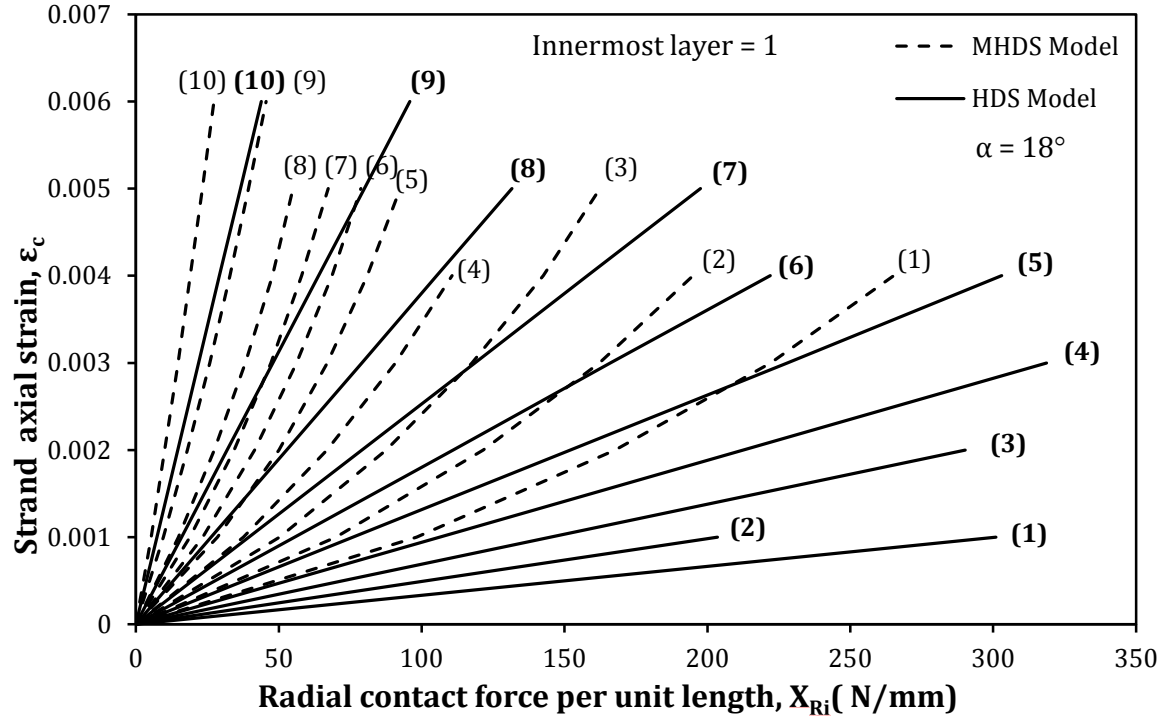

Figure 4.3f-Comparison of X_{Ri} versus ε_c plots, for the MHDS and HDS models, for all the layers of 164 mm (α = 18°) outside diameter strand.

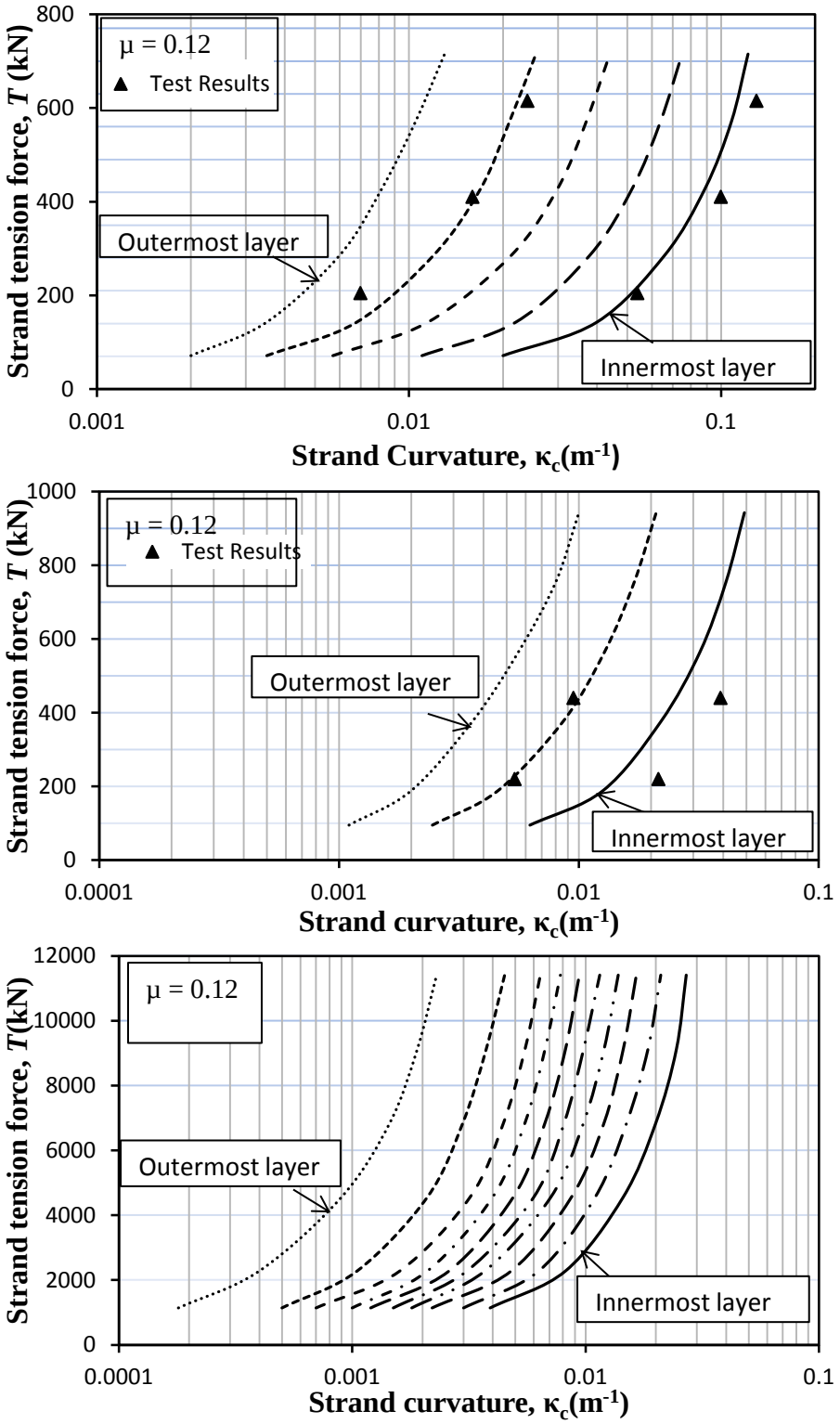

Figure 4-4 (a-c): Experimental support for the predictions of the MHDS model in the case of two different cable constructions: (a) 39 mm; (b) 41 mm diameter strands; and (c) theoretical predictions of interwire slippage at neutral axis for164 mm strand.

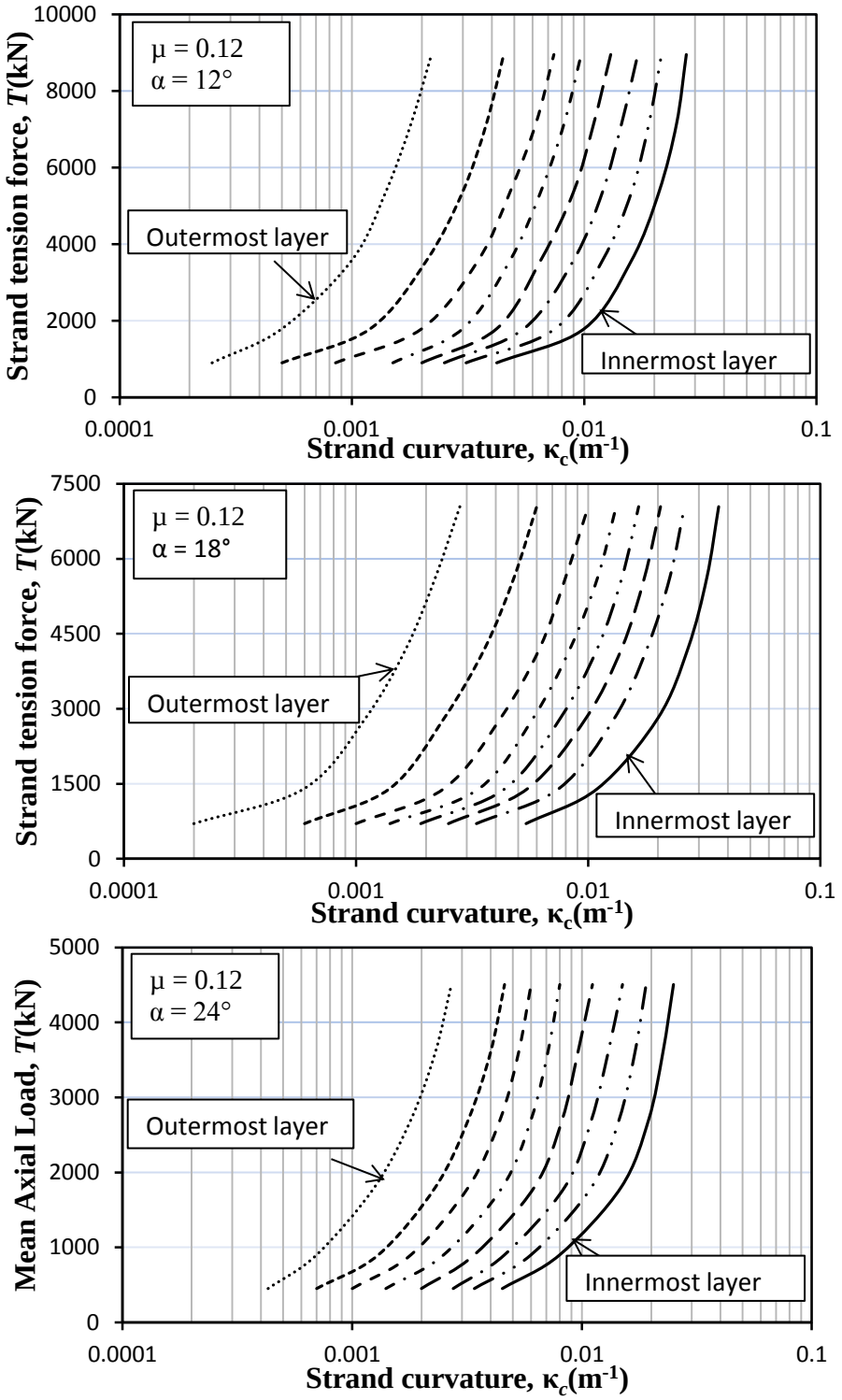

Figs 4.4 (d-f) Values of critical curvature for various layers of three different cable constructions of: (d) 127 (α =12°); (e) 127 (α =18°); and (f) 127 (α =24°) mm diameter strands at which interlayer slippage initiated near neutral axis for different strand tension forces.

The plots based on the MHDS model, in Figures 4.4 (a-f) show the critical curvatures at which interwire slippage initiated at the so called neutral axis throughout the strand for all the layers of different strand constructions given in tables 4.4 (a-f) respectively. The results in Figures 4.4a and 4.4b present the encouraging large scale experimental support for the predictions of the MHDS model for the two 39 and 41 mm spiral strands covering a wide range of cable mean axial strains $0.0015 \leq \varepsilon_c \leq 0.044$ and $0.00115 \leq \varepsilon_c \leq 0.0023$, respectively. These correspond to mean axial loads equal to 16.7%, 33.3% and 50% of their ultimate loads for 39 mm, as well as 15.9% 31.7% and 47.7% for the 41 mm strand. Each pair of triangle horizontally inline is obtained for the above selected cable axial strains for both the cables. The two horizontally inline triangular points show the values of curvature at which interwire slippage in the outermost layer begins near neutral axis and extreme fibre position respectively. Therefore,the first triangular point is the curvature at which interwire slippage begins at neutral axis of the cable, whereas the second point shows the curvature at which wire near extreme fibre position in the outermost layer slips for the selected axial strain.

Increasing lay angle delays the initiation of wire slippage in the outer layers but due to less radial load transfer into the inner layers slippage penetrates quickly into the inner layers of the strand. Hence, the resulting predictions of reductions in bending stiffness with increasing curvature, with the errors for the two models increasing substantially with modest increases in lay angle, α_i ,within the current manufacturing range of $11° \leq \alpha_i \leq 24°$. Similarly, increasing strand diameter caused wire slippage to occur at small values of curvature, as the unbalanced force on wire increases with increasing radial distance from the centre of the strand.

Figures 4.5 (a-c) present the boundaries between stick and slip regions versus curvature on the cross section of three same diameter spiral strands with different lay angles of 12°, 18° and 24° respectively. For the cable mean axial strain $\varepsilon_c = 0.003$, the mean axial loads for these three cables are 5560, 4708 and 3560 kN respectively. Here, interlayer slippage in any layer begins in the vicinity $\varphi = 0$ and propagates with $|\varphi|$ increasing. For the *i*th layer, the boundary between the no-slip and full-slip states is denoted by φ^+ and φ^- for the upper and lower halves of the cross section,

respectively. In the case of the 127 mm (α = 12°) cable, for example, as the strand curvature increases, wires in the outermost layer start slipping (near the neutral axis) at around κ_c = 0.0014 m^{-1}. Slippage in the penultimate layer starts at around κ_c = 0.0038 m^{-1} and in the remaining six inner layers slippages start at κ_c =0.0063 m^{-1}, κ_c = 0.0082 m^{-1}, κ_c = 0.01 m^{-1}, κ_c = 0.014 m^{-1}, κ_c = 0.021 m^{-1} and κ_c = 0.03 m^{-1} respectively.

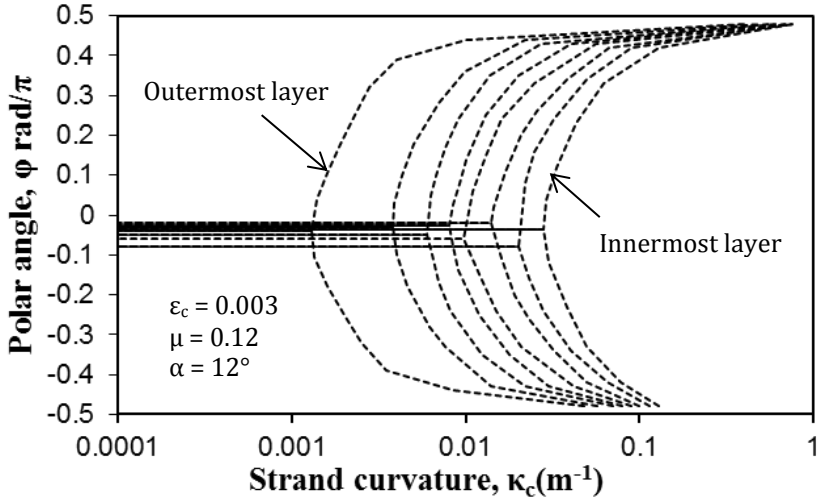

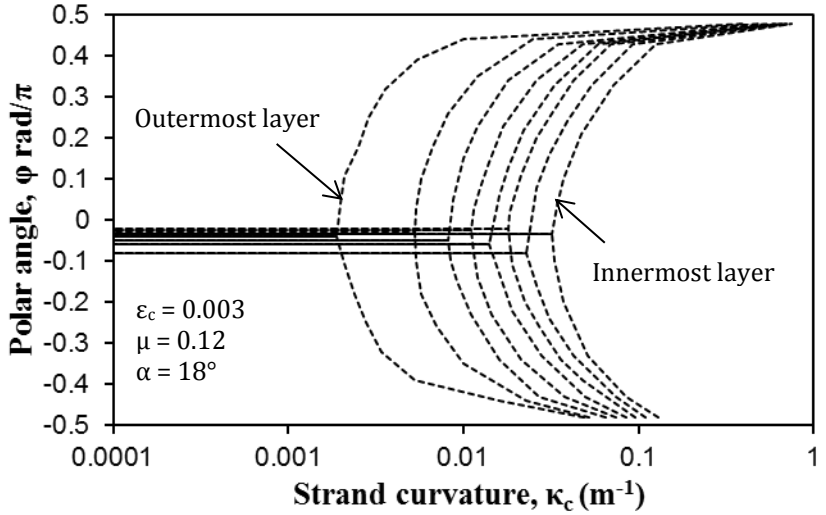

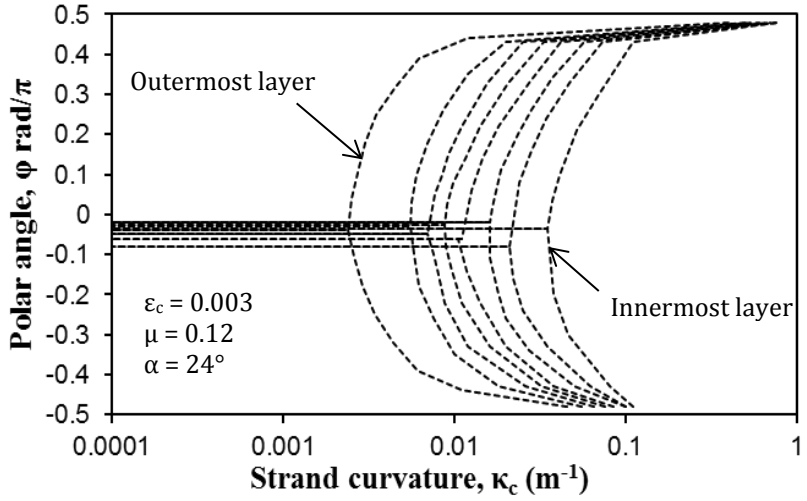

Figure 4-5(a-c): Boundaries between stick and slip regions vs curvature, on cross section of three 127 mm dia strands with lay angles of: (a) 12°; (b) 18°; and (c) 24°

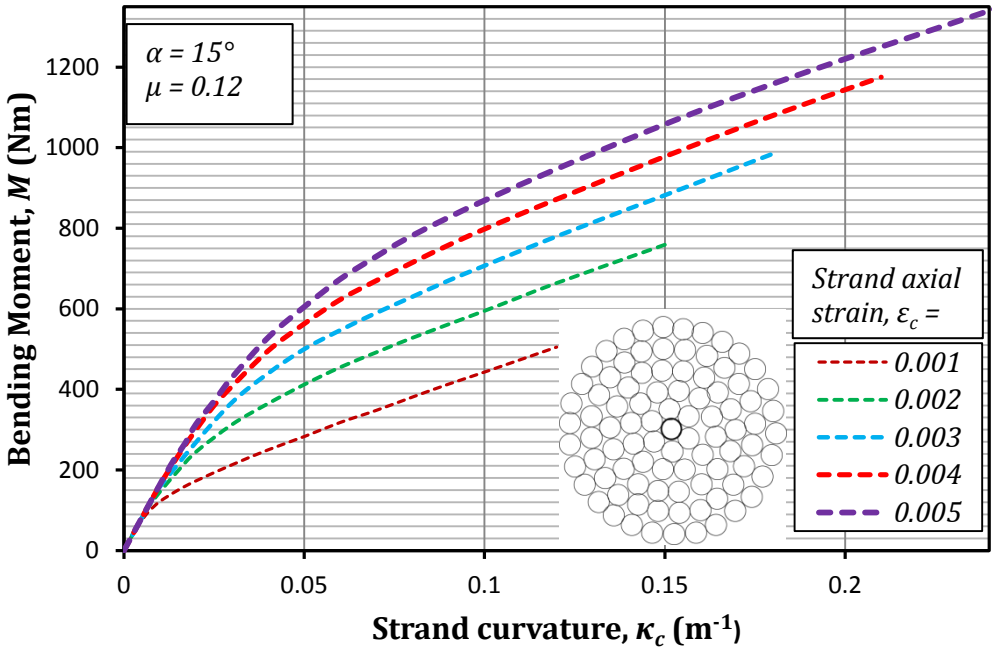

Figure 4-6a: Moment versus curvature plots for 39mm diameter strand for selected axial strains.

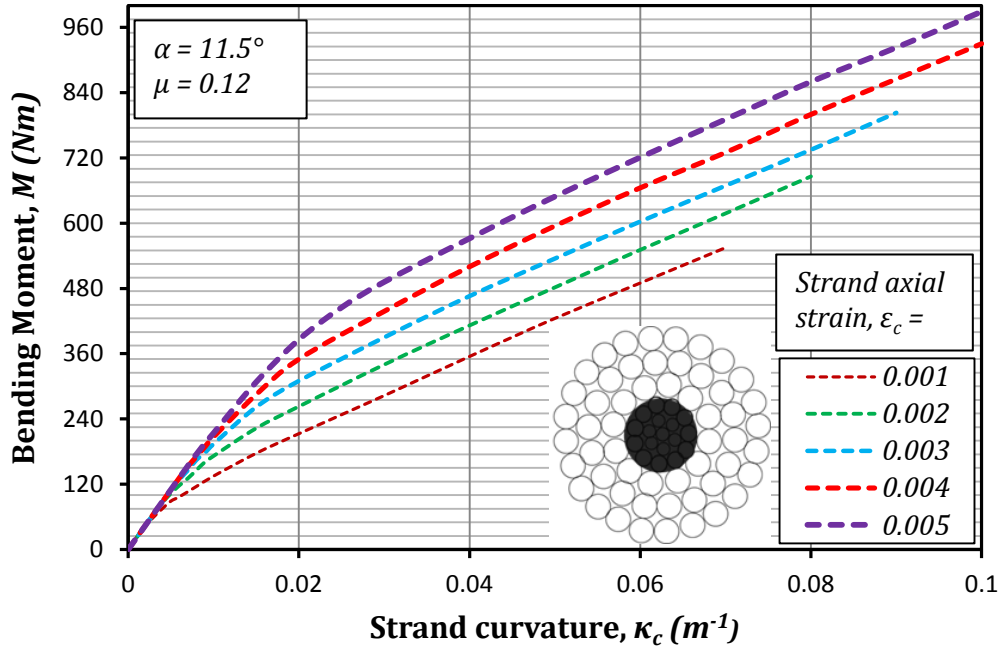

Figure 4-6b: Moment versus curvature plots for 41mm diameter strand for selected axial strains.

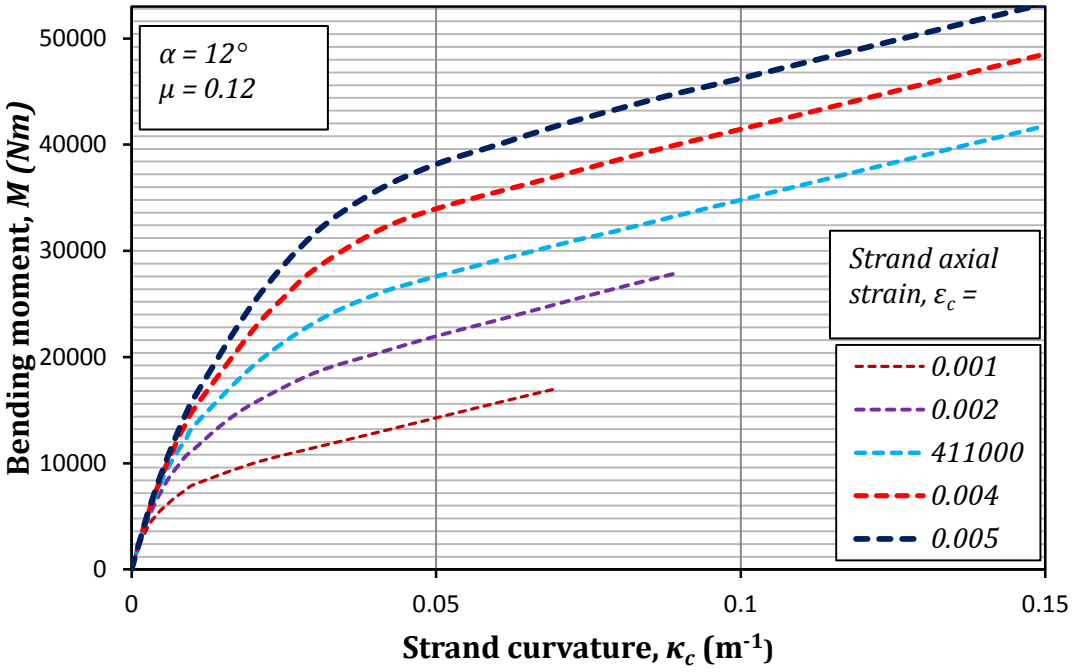

Figure 4-6c: Moment versus curvature plots for 127 mm (α = 12°) diameter strand for selected axial strains.

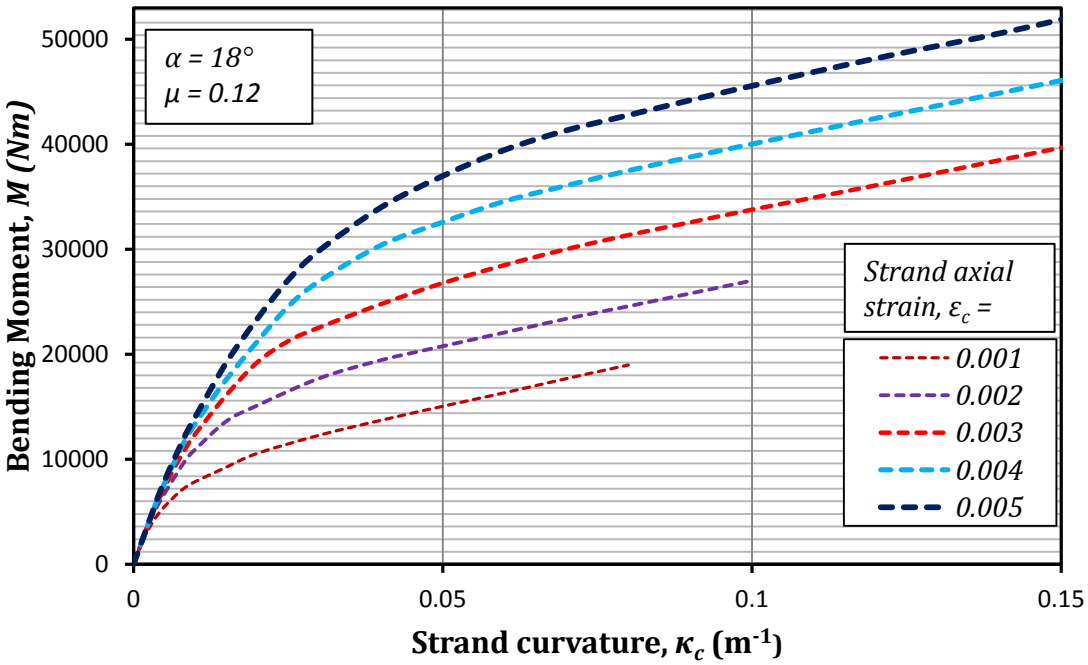

Figure 4-6d: Moment versus curvature plots for 127 mm (α = 18°) diameter strand for selected axial strains.

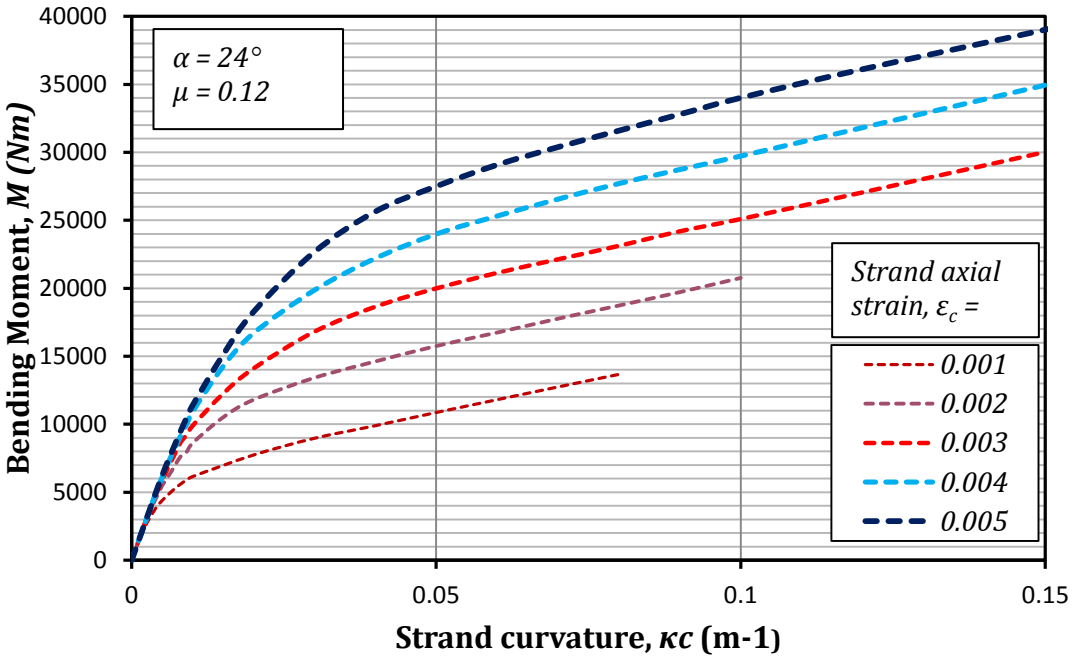

Figure 4-6e: Moment versus curvature plots for 127 mm (α = 24°) diameter strand for selected axial strains.

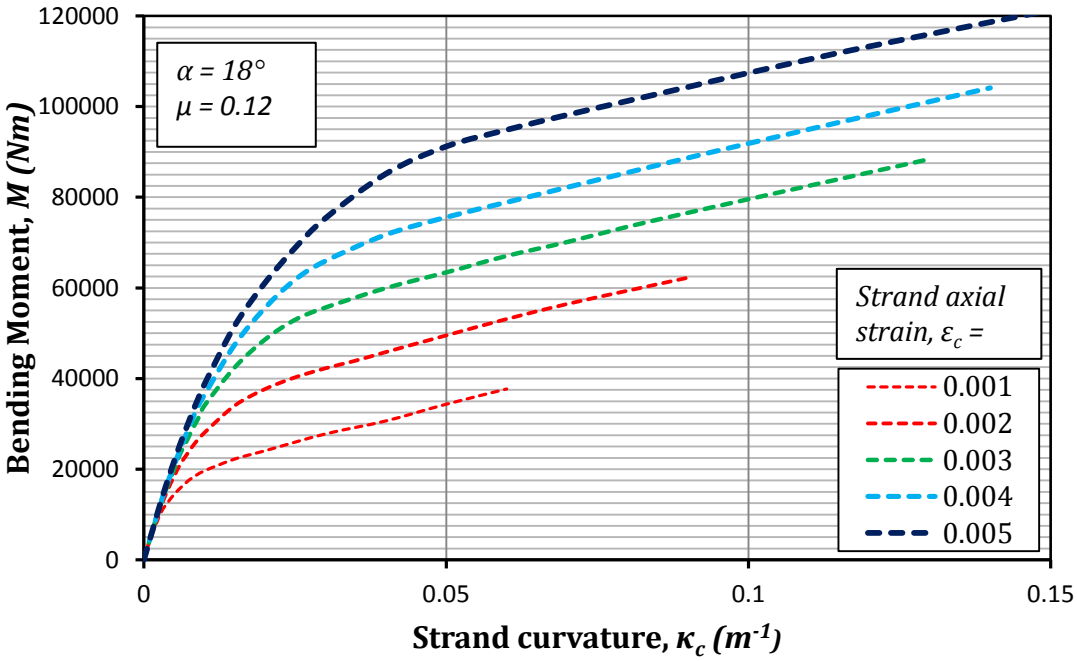

Figure 4-6f: Moment versus curvature plots for 164 mm (α = 12°) diameter strand for selected axial strains.

Figures 4.6 (a-f) show the moment versus curvature plots for the above six different strand constructions, using the proposed modified model, MHDS. It is shown that initially, the bending moment of the cable is linearly proportional to the imposed curvature, when all the wires in the cable are stuck together. After the initiation of the wire slippage, bending moment becomes a non-linear function of the strand curvature. However as shown, when all the wires slip, the bending moment of the cable gets a constant trend for a given axial strain, as slip tension force T_i^{slip}, is independent of the imposed curvature. After applying a small curvature increment, the strain energy of the stick wires is changed while the strain energy of the slipped wire remained constant. The non-linearity in the bending moment is caused by the change in the state of the wires from stick state to slip state.

Based on the strain distribution on the curvature, three distinct stages are created during the bending cycle of the helical cable: (a) no-slip; (b) partially slip; and (c) full-slip. In the first stage, all the wires in the cable are stuck together and the stiffness of the cable is at its maximum with the bending moment-curvature relationship linear. Second is the transitional stage, when some parts of the cable are sliding whereas others do not. The bending stiffness of the cable gradually decreases in this case over a range of curvature. When the curvature reaches a critical value such that the wire in the cable slide everywhere, this corresponds to the third stage. At this final stage the stiffness of the cable drops to a minimum constant value depending on the assumed coefficient of friction. It is worth to mention that the state of the wires at the neutral axis does not have a significant effect on the bending moment values of the cable whereas the state of the wires at the extreme fibre position greatly affects the overall bending moment of the strand. The results also highlight the limitations of assuming a uniform state of axial strain in all wires.

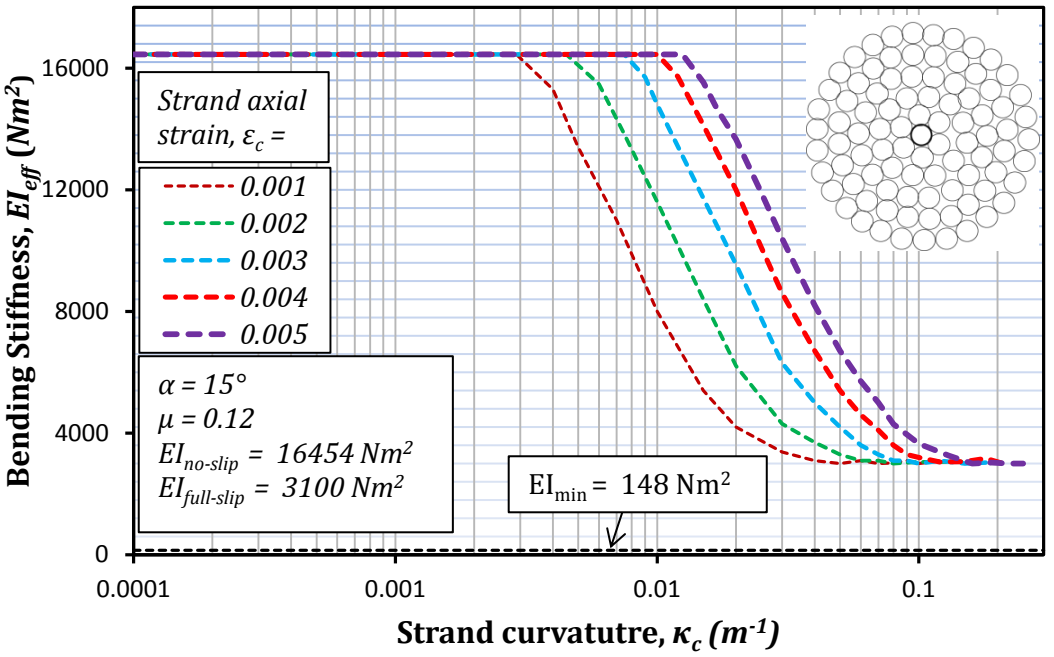

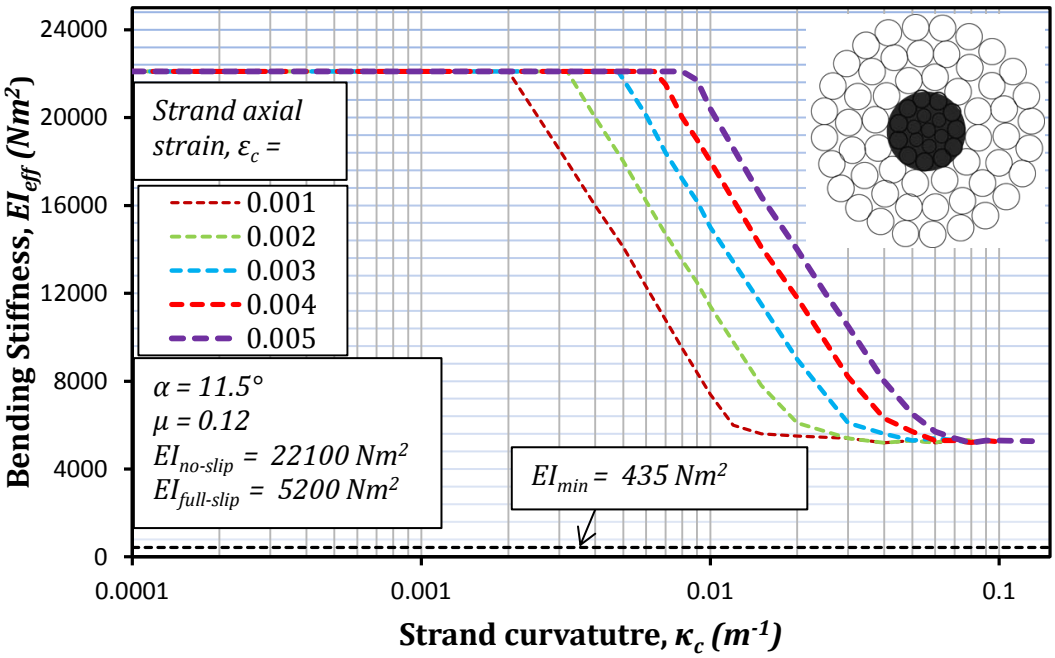

Figure 4-7(a & b): Plots of EI_{eff} versus strand curvature, covering $0.001 \leq \varepsilon_c \leq 0.005$, for two different cable constructions: (a) 39; and (b) 41 mm diameter spiral strands.

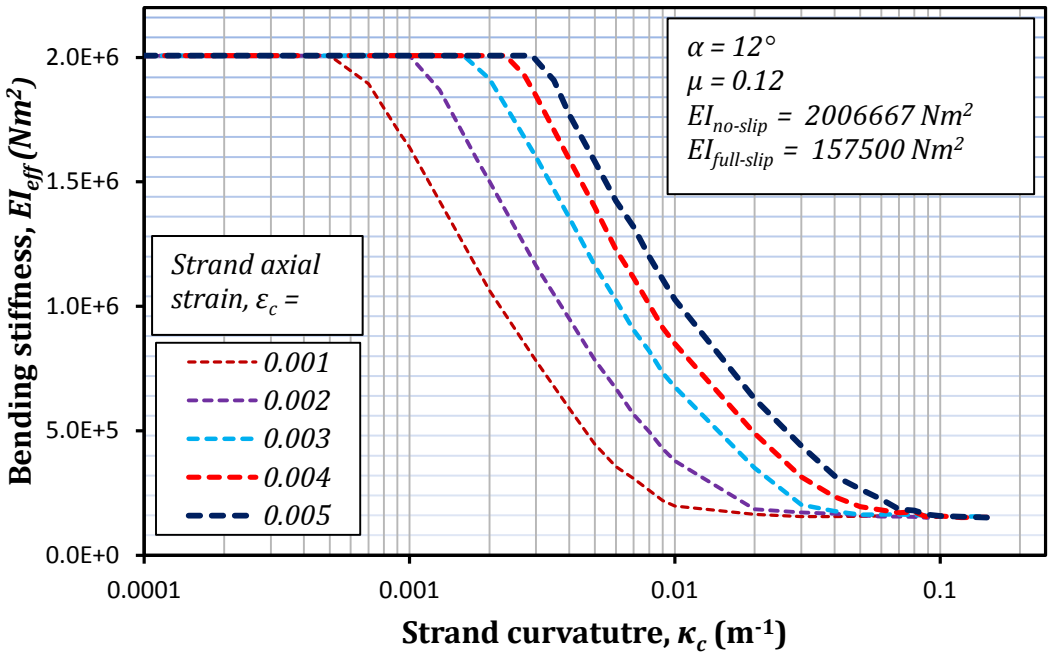

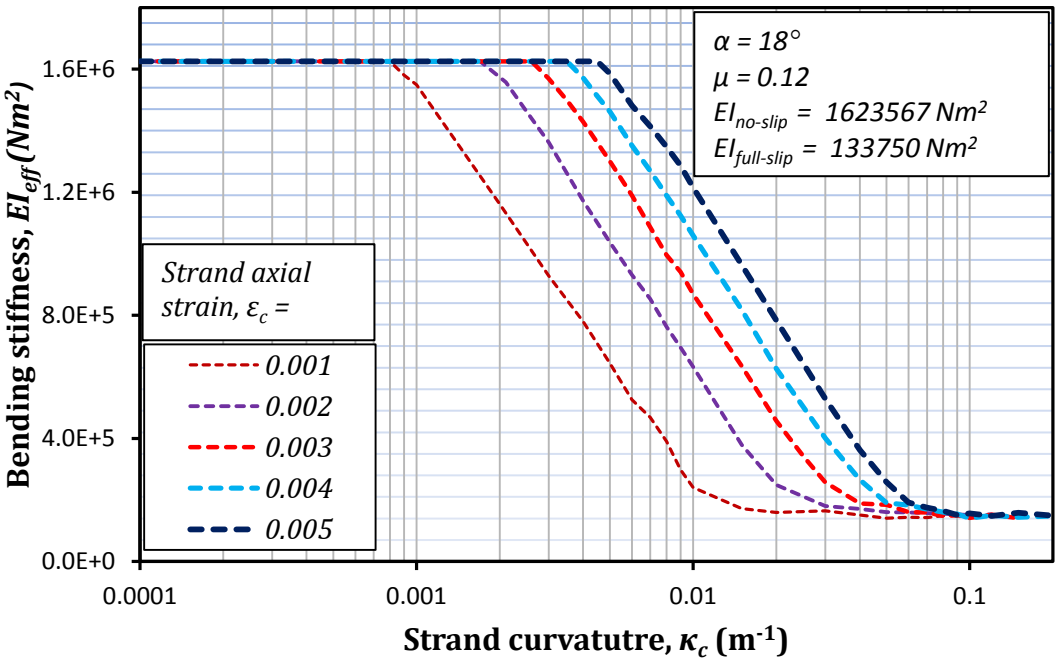

Figures 4.7 (c & **d)** Plots of EI_{eff} versus strand curvature, covering $0.001 \leq \varepsilon_c \leq 0.005$, for two 127 mm diameter different cable constructions: (c) lay angle 12°; and (d) lay angle 18° respectively.

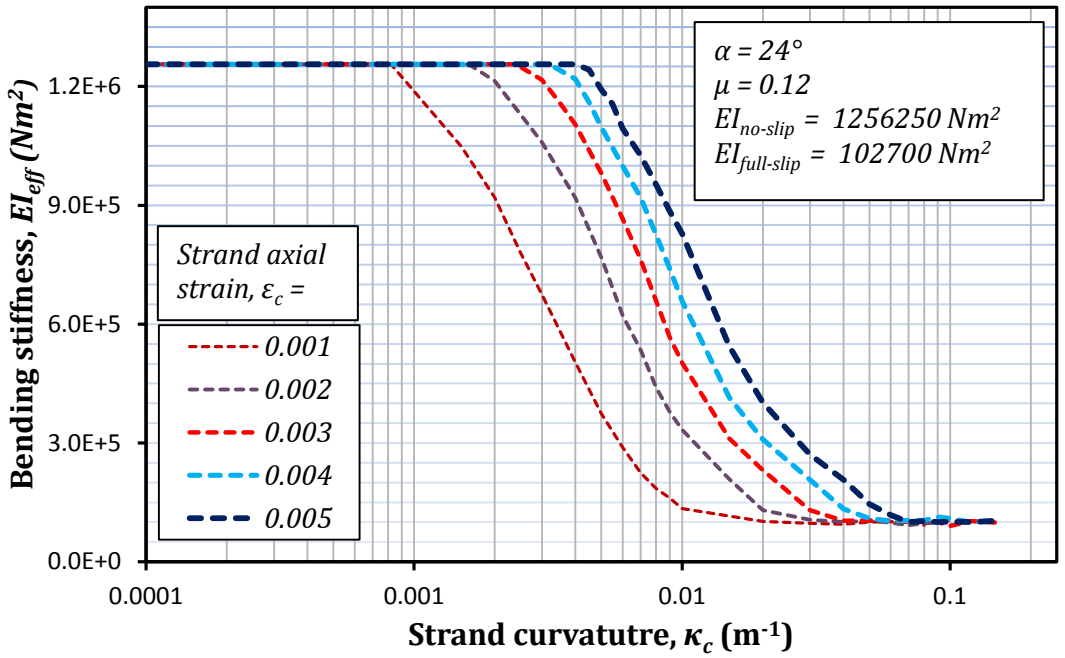

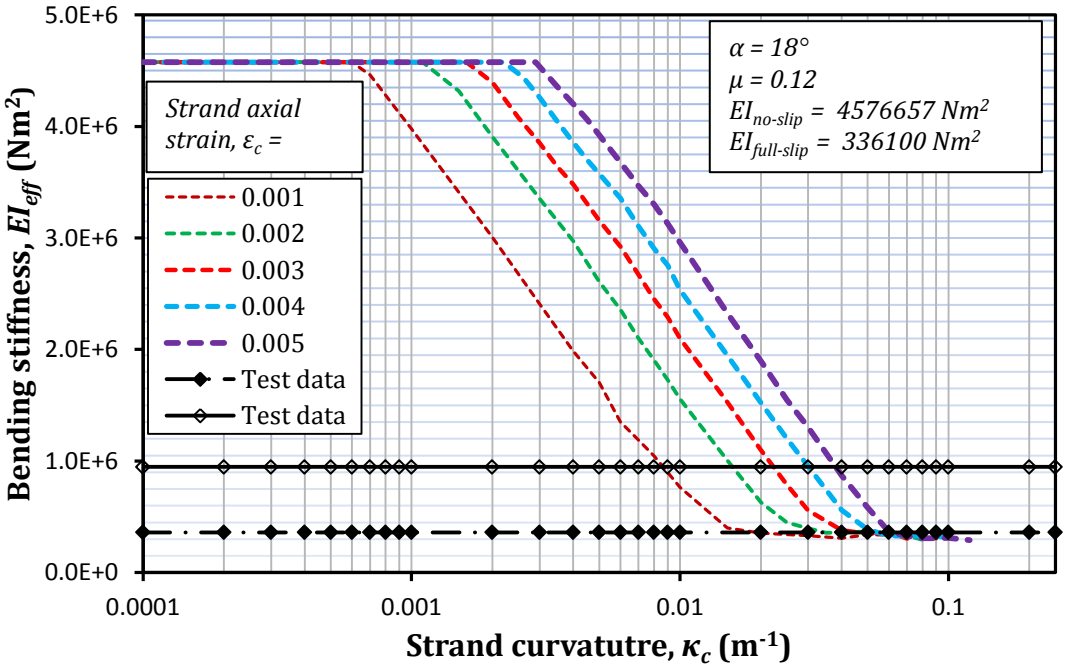

Figures 4.7 (e & **f)** Plots of EI_{eff} versus strand curvature, covering $0.001 \leq \varepsilon_c \leq 0.005$, for two different cable constructions: (e) 127 (α = 24°); and (f) 164 (α = 18°) mm diameter spiral strands.

Based on MHDS model, Figures 4.7 (a-f) show the reductions in the magnitude of bending stiffness of the strands as a function of cable curvature for different axially preloaded strands. This covers the practical range ($0.001 \leq \varepsilon_c \leq 0.005$) of strand axial strains. Initially, the bending stiffness of the strand is constant at EI_{max}, when all the wires are sticking together. As the wires slip, the bending stiffness of the strand decreases and eventually approaches a constant value, depending on the assumed coefficient of friction and the type of cable construction. This constant value always remains above the absolute minimum value EI_{min}, corresponding to the case of zero coefficient of friction. In the later case of zero friction, all the wires in the strand bending about their own neutral axis, as a collection of individual helical springs. It is found that the difference between two extreme stiffness values for any cable depends on the coefficient of friction between the wires and the type of cable construction, but is independent of the tension force in the cable. Increasing strand tension only delays the initiation of interlayer slippage, resulting bending stiffness to remain constant under large values of imposed curvature. After the initiation of interlayer slippage, the flexural stiffness of the strand drops to same constant value for different load perturbations.

The numerical results obtained for different cable constructions confirmed that the full slip bending stiffness value increases with increasing the value of friction coefficient between the wires. Strand outer diameter is shown to play an important role on interlayer contact deformations and slippage pattern. It is readily seen that for the larger strand diameters EI_{max} remain constant for very small values of strand curvature. The reason for this is that the unbalanced force on wires in the outer layer of large diameter cable increases tremendously, due to increasing radial distance from the centre of the strand. For a selected axial strain of $\varepsilon_c = 0.001$, the bending stiffness for the two strands of 39 and 127 mm diameter strands with approximately same lay angles, EI_{max} remain constant under the imposed curvature values of 0.0029 and 0.0008 (m^{-1}) respectively. In other words, the wires in the outer layer of 39 mm strand slipped at a curvature value almost three times larger than that for 127 mm strand, which is almost equal to the ratio of the outer diameter (127/39) of the two strands.

Lay angle of wires in different layers of the strand not only play an important role in the pattern of wire slippage and other contact deformations, but the value of EI_{max} notably decreases with increasing lay angle. The results for the three same diameter strands with different lay angles of 12°, 18° and 24°, have EI_{max} values of 2006667, 1625090 and 1256250 Nm^2 respectively.

As regards the magnitude of the bending stiffness, Figure 4.4f gives the comparison of the theoretical predictions and experimentally determined values of the bending stiffness for 164 mm outside diameter cable. The experimental values of the bending stiffness of the cable were obtained for both the first (♦) and final (◊) loading runs respectively, as reported by Raoof and Davies (2005). It is claimed that the values of different material parameters (coefficient friction, modulus of elasticity, Poisson's ratio etc.) were similar as assumed in this study. As mentioned earlier, the difference between two extreme bending stiffness values is unacceptably large. Comparing the experimentally obtained full slip bending stiffness value for the final loading run shows a difference by a factor of 13, with experimentally determined value being thirteen times less than the no slip bending stiffness value. The theoretical full slip value for 164 mm diameter cable is $E_{full\text{-}slip}$ = 356700 Nm^2, whereas the experimentally determined value is $E_{full\text{-}slip}$ = 361100 Nm^2. The results in Figure 4.4f shows very encouraging support for the predictions of the MHDS model for a multi-layered large diameter cable of 164 mm.

Table 4-2a: Values of imposed curvature for MHDS model at which interlayer/interwire slippage initiated at the neutral axis of the strand for all the layers of 39 mm outside diameter spiral strand.

Mean Axial Strain ε_c	Layer Number														
	1			2			3			4			5		
	Curvature, $\kappa_c(m^{-1})$	Rad: of curvature, ρ (m)	ρ/d	Curvature, $\kappa_c(m^{-1})$	Rad: of curvature, ρ (m)	ρ/d	Curvature, $\kappa_c(m^{-1})$	Rad: of curvature, ρ (m)	ρ/d	Curvature, $\kappa_c(m^{-1})$	Rad: of curvature, ρ (m)	ρ/d	Curvature, $\kappa_c(m^{-1})$	Rad: of curvature, ρ (m)	ρ/d
0.0005	0.0015	666.67	17094	0.0035	285.71	7326	0.006	166.67	4274	0.011	90.91	2331	0.02	50.00	1282
0.001	0.003	333.33	8547	0.007	142.86	3663	0.012	83.33	2137	0.022	45.45	1166	0.04	25.00	641
0.002	0.0045	222.22	5698	0.013	76.92	1972	0.023	43.48	1115	0.043	23.26	596	0.078	12.82	329
0.003	0.007	142.86	3663	0.019	52.63	1350	0.034	29.41	754	0.06	16.67	427	0.11	9.09	233
0.004	0.009	111.11	2849	0.025	40.00	1026	0.045	22.22	570	0.085	11.76	302	0.13	7.69	197
0.005	0.011	90.91	2331	0.032	31.25	801	0.053	18.87	484	0.1	10.00	256	0.16	6.25	160

Table 4.2a: Values of imposed curvature for MHDS model at which interlayer/interwire slippage initiated at the neutral axis of the strand for all the layers of 41 mm outside diameter spiral strand.

Mean Axial Strain	Layer Number								
	1			2			3		
	Curvature, $\kappa_c(m^{-1})$	Rad: of curvature, ρ (m)	ρ/d	Curvature, $\kappa_c(m^{-1})$	Rad: of curvature, ρ (m)	ρ/d	Curvature, $\kappa_c(m^{-1})$	Rad: of curvature, ρ (m)	ρ/d
0.0005	0.0008	1250.00	30488	0.0025	400	9756.10	0.0065	153.85	3752
0.001	0.0015	666.67	16260	0.005	200	4878.05	0.013	76.92	1876
0.002	0.0031	322.58	7867.8	0.0098	102.04	2488.80	0.023	43.48	1060
0.003	0.0046	217.39	5302.2	0.014	71.43	1742.16	0.034	29.41	717.4
0.004	0.0061	163.93	3998.4	0.019	52.63	1283.70	0.043	23.26	567.2
0.005	0.0076	131.58	3209.2	0.024	41.67	1016.26	0.053	18.87	460.2

Table 4.2b: Values of imposed curvature for MHDS model at which interlayer/interwire slippage initiated at the neutral axis of the strand for all the layers of 127 mm outside diameter spiral strand with lay angle, $\alpha = 12°$.

Mean Axial Strain ε_c	Layer No											
	1			2			3			4		
	Curvature, κ_c (m^{-1})	Rad: of curvature, ρ (m)	ρ/d	Curvature, κ_c (m^{-1})	Rad: of curvature, ρ (m)	ρ/d	Curvature, κ_c (m^{-1})	Rad: of curvature, ρ (m)	ρ/d	Curvature, κ_c (m^{-1})	Rad: of curvature, ρ (m)	ρ/d
0.0005	0.00027	3703.70	29163	0.0006	1666.67	13123	0.001	1000.00	7874	0.0016	625.00	4921
0.001	0.00043	2325.58	18312	0.0013	769.23	6057	0.0021	476.19	3750	0.0031	322.58	2540
0.002	0.0009	1111.11	8749	0.0024	416.67	3281	0.0041	243.90	1920	0.0056	178.57	1406
0.003	0.0013	769.23	6057	0.0038	263.16	2072	0.0061	163.93	1291	0.0081	123.46	972
0.004	0.002	500.00	3937	0.0048	208.33	1640	0.0075	133.33	1050	0.011	90.91	716
0.005	0.0025	400.00	3150	0.006	166.67	1312	0.01	100.00	787	0.0145	68.97	543
	5			6			7			8		
	Curvature, κ_c (m^{-1})	Rad: of curvature, ρ (m)	ρ/d	Curvature, κ_c (m^{-1})	Rad: of curvature, ρ (m)	ρ/d	Curvature, κ_c (m^{-1})	Rad: of curvature, ρ (m)	ρ/d	Curvature, κ_c (m^{-1})	Rad: of curvature, ρ (m)	ρ/d
	0.0028	357.14	2812	0.0035	285.71	2250	0.004	250.00	1969	0.006	166.67	1312
	0.0056	178.57	1406	0.007	142.86	1125	0.0082	121.95	960	0.012	83.33	656
	0.0078	128.21	1009	0.012	83.33	656.2	0.015	66.67	525	0.023	43.48	342
	0.0092	108.70	855.9	0.015	66.67	524.9	0.02	50.00	394	0.03	33.33	262
	0.014	71.43	562.4	0.019	52.63	414.4	0.024	41.67	328	0.036	27.78	219
	0.018	55.56	437.4	0.023	43.48	342.3	0.029	34.48	272	0.041	24.39	192

Table 4.2c: Values of imposed curvature for MHDS model at which interlayer/interwire slippage initiated at the neutral axis of the strand for all the layers of 127 mm outside diameter spiral strand with lay angle, α = 18°.

Mean Axial Strain ε_c	Layer No											
	1			2			3			4		
	Curvature, κ_c (m^{-1})	Rad: of curvature, ρ (m)	ρ/d	Curvature, κ_c (m^{-1})	Rad: of curvature, ρ (m)	ρ/d	Curvature, κ_c (m^{-1})	Rad: of curvature, ρ (m)	ρ/d	Curvature, κ_c (m^{-1})	Rad: of curvature, ρ (m)	ρ/d
0.0005	0.00032	3125.00	24606	0.001	1000.00	7874	0.0015	666.67	5249	0.002	500.00	3937
0.001	0.00065	1538.46	12114	0.002	500.00	3937	0.003	333.33	2625	0.004	250.00	1969
0.002	0.0013	769.23	6056.9	0.0036	277.78	2187	0.0059	169.49	1335	0.0077	129.87	1023
0.003	0.002	500.00	3937	0.0054	185.19	1458	0.0084	119.05	937.4	0.011	90.91	715.8
0.004	0.0026	384.62	3028.5	0.0071	140.85	1109	0.011	90.91	715.8	0.0145	68.97	543
0.005	0.0032	312.50	2460.6	0.0092	108.70	855.9	0.014	71.43	562.4	0.019	52.63	414.4
	5			6			7			8		
	Curvature, κ_c (m^{-1})	Rad: of curvature, ρ (m)	ρ/d	Curvature, κ_c (m^{-1})	Rad: of curvature, ρ (m)	ρ/d	Curvature, κ_c (m^{-1})	Rad: of curvature, ρ (m)	ρ/d	Curvature, κ_c (m^{-1})	Rad: of curvature, ρ (m)	ρ/d
	0.0025	400.00	3149.6	0.0035	285.71	2250	0.0046	217.39	1712	0.007	142.86	1125
	0.0052	192.31	1514.2	0.007	142.86	1125	0.0093	107.53	846.7	0.014	71.43	562.4
	0.0098	102.04	803.47	0.013	76.92	605.7	0.018	55.56	437.4	0.026	38.46	302.8
	0.014	71.43	562.43	0.018	55.56	437.4	0.025	40.00	315	0.035	28.57	225
	0.018	55.56	437.45	0.022	45.45	357.9	0.029	34.48	271.5	0.039	25.64	201.9
	0.023	43.48	342.35	0.027	37.04	291.6	0.034	29.41	231.6	0.046	21.74	171.2

Table 4.2d: Values of imposed curvature for MHDS model at which interlayer/interwire slippage initiated at the neutral axis of the strand for all the layers of 127 mm outside diameter spiral strand with lay angle, α = 24°.

Mean Axial Strain ε_c	Layer No											
	1			2			3			4		
	Curvature, κ_c (m^{-1})	Rad: of curvature, ρ (m)	ρ/d	Curvature, κ_c (m^{-1})	Rad: of curvature, ρ (m)	ρ/d	Curvature, κ_c (m^{-1})	Rad: of curvature, ρ (m)	ρ/d	Curvature, κ_c (m^{-1})	Rad: of curvature, ρ (m)	ρ/d
0.0005	0.00041	2439.02	19205	0.001	1000.00	7874	0.0015	666.67	5249	0.0024	416.67	3281
0.001	0.00082	1219.51	9602	0.002	500.00	3937	0.003	333.33	2625	0.0038	263.16	2072
0.002	0.0017	588.24	4632	0.0039	256.41	2019	0.0053	188.68	1486	0.0065	153.85	1211
0.003	0.0024	416.67	3281	0.0055	181.82	1432	0.0073	136.99	1079	0.0089	112.36	885
0.004	0.0034	294.12	2316	0.0071	140.85	1109	0.0095	105.26	829	0.011	90.91	716
0.005	0.0042	238.10	1875	0.0086	116.28	915.6	0.011	90.91	716	0.0135	74.07	583
	5			6			7			8		
	Curvature, κ_c (m^{-1})	Rad: of curvature, ρ (m)	ρ/d	Curvature, κ_c (m^{-1})	Rad: of curvature, ρ (m)	ρ/d	Curvature, κ_c (m^{-1})	Rad: of curvature, ρ (m)	ρ/d	Curvature, κ_c (m^{-1})	Rad: of curvature, ρ (m)	ρ/d
	0.0028	357.14	2812	0.0032	312.50	2461	0.004	250.00	1969	0.007	142.86	1125
	0.0045	222.22	1750	0.005	200.00	1575	0.007	142.86	1125	0.012	83.33	656
	0.0076	131.58	1036	0.012	83.33	656.2	0.016	62.50	492	0.023	43.48	342
	0.011	90.91	715.8	0.017	58.82	463.2	0.021	47.62	375	0.029	34.48	272
	0.014	71.43	562.4	0.021	47.62	375	0.026	38.46	303	0.035	28.57	225
	0.017	58.82	463.2	0.025	40.00	315	0.03	33.33	262	0.04	25.00	197

Table 4.2e: Values of imposed curvature for MHDS model at which interlayer/interwire slippage initiated at the neutral axis of the strand for all the layers of 164 mm outside diameter spiral strand with lay angle, α = 18°.

Mean Axial Strain ε_c	Layer No														
	1			2			3			4			5		
	Curvature, κ_c (m^{-1})	Rad: of curvature, ρ (m)	ρ/d	Curvature, κ_c (m^{-1})	Rad: of curvature, ρ (m)	ρ/d	Curvature, κ_c (m^{-1})	Rad: of curvature, ρ (m)	ρ/d	Curvature, κ_c (m^{-1})	Rad: of curvature, ρ (m)	ρ/d	Curvature, κ_c (m^{-1})	Rad: of curvature, ρ (m)	ρ/d
0.0005	0.0003	3333.33	20325	0.0005	2000.00	12195	0.0007	1428.57	8711	0.0012	833.33	5081	0.0015	666.67	4065
0.001	0.00006	16666.67	1E+05	0.0013	769.23	4690	0.0016	625.00	3811	0.0026	384.62	2345	0.0032	312.50	1905
0.002	0.0011	909.09	5543	0.0025	400.00	2439	0.0032	312.50	1905	0.0051	196.08	1196	0.0061	163.93	1000
0.003	0.0017	588.24	3587	0.0038	263.16	1605	0.0048	208.33	1270	0.0075	133.33	813	0.0094	106.38	649
0.004	0.0023	434.78	2651	0.005	200.00	1220	0.0064	156.25	953	0.0095	105.26	642	0.013	76.92	469
0.005	0.0029	344.83	2103	0.0062	161.29	983.5	0.008	125.00	762	0.012	83.33	508	0.0155	64.52	393
	6			7			8			9			10		
	Curvature, κ_c (m^{-1})	Rad: of curvature, ρ (m)	ρ/d	Curvature, κ_c (m^{-1})	Rad: of curvature, ρ (m)	ρ/d	Curvature, κ_c (m^{-1})	Rad: of curvature, ρ (m)	ρ/d	Curvature, κ_c (m^{-1})	Rad: of curvature, ρ (m)	ρ/d	Curvature, κ_c (m^{-1})	Rad: of curvature, ρ (m)	ρ/d
	0.0019	526.32	3209	0.0023	434.78	2651	0.003	333.33	2033	0.004	250.00	1524	0.005	200.00	1220
	0.004	250.00	1524	0.005	200.00	1220	0.0062	161.29	983	0.008	125.00	762	0.012	83.33	508
	0.008	125.00	762.2	0.01	100.00	609.8	0.012	83.33	508	0.015	66.67	407	0.02	50.00	305
	0.012	83.33	508.1	0.015	66.67	406.5	0.018	55.56	339	0.022	45.45	277	0.029	34.48	210
	0.015	66.67	406.5	0.02	50.00	304.9	0.025	40.00	244	0.03	33.33	203	0.039	25.64	156
	0.02	50.00	304.9	0.024	41.67	254.1	0.03	33.33	203	0.036	27.78	169	0.048	20.83	127

Tables 4.2 (a-f) offer the values of the critical curvature at which interlayer slippage starts at the neutral axis in different layers of the above six strands. The results in these tables cover a wide range of cable axial strains, $0.001 \leq \varepsilon_c \leq 0.005$.

4.6 Conclusions

The earlier model reported by Hong has been modified and the effect of ever present line contact forces between the wires in the same layer has been included in the formulations. After the proposed modifications, a large set of numerical data have been obtained for a variety of spiral strand constructions covering a wide range of geometrical parameters. Based on those results, effective bending stiffness of the cable is shown to be a function of bending curvature, interlayer friction coefficients and interlayer normal contact forces. It is further shown that the bending stiffness of a cable drop down by a factor of 2-16 depending on the assumed value of coefficient of friction and the type of cable construction. The results for different cables confirmed that the full slip bending stiffness value of the cable increases as the value of the friction coefficient between the wires increases, whereas EI_{max} decreases, as lay angle increases. The transition of bending stiffness from no slip to full slip value is shown as a function of the imposed cable curvature. Regarding the magnitude of the effective bending stiffness of the cable theoretical results for a large diameter cable of 164 mm were compared with test data. Similarly, regarding contact deformations and slippage, the theoretical results of the model have been compared with the previously available experimental results for two different cable constructions of 39 and 41 mm diameters respectively. In both cases, a very good correlation is found between test data and theoretical predictions. Finally, it is found possible to develop a simple method for predicting the effective bending stiffness of any strand construction under any given curvature, which will be the subject of the next chapter.

Chapter 5

Simple Method for the Determination of the Bending Stiffness of Large Diameter Multi-Layered Spiral Strands.

5.1 Introduction

This chapter focuses on the development of a simple dimensionless parameter for the determination of the effective bending stiffness of a cable. In Chapter 4, a very accurate theoretical model for calculating the bending moment-curvature relationship of large diameter multi-layered spiral strands has been developed. But the potential problem is that it consists of very lengthy mathematical formulations and involves certain iterative procedures. With this in mind, it is desirable to have a simple yet reliable method to accurately predict the effective bending stiffness of the cable under varying cable curvatures. The reliability of any restrained bending design procedure is based on a reasonably accurate estimation of the minimum critical radii of curvature at the fixed end(s). Such values of curvature and the corresponding bending stiffness are then used as an input into the fatigue design model.

Having gained a sound understanding of the controlling parameters, it is now possible to develop and describe a simplified method for calculating the effective bending stiffness of the strand under varying cable curvatures. The practical implications of assuming a constant effective bending stiffness for calculating the deflected shape of the cable has already been addressed in the previous chapter. It is however, a point of concern that the steel cable design and manufacture, is the area where still the rule of thumb reigns supreme with the past commercial experience being largely limited to the performance of cables with small diameters. Although cable manufacturers are now able to manufacture helically wound steel cables with diameters well in excess of 100 mm. In order to use such large diameter cables with confidence, reliable performance data for large diameter constructions under realistic conditions must be obtained.

For the free bending of long steel cables subjected to an approximately steady mean axial load, it has been shown in Chapter 4 that the effective bending stiffness of the cable vary greatly between two extremes. The theoretical results from Chapter 4 will be used in the following to develop a straightforward yet accurate method for estimating the bending stiffness of the strand. Thus the proposed method is backed by a large body of numerical results obtained for a variety of realistic multi-layered large diameter (e.g. 100mm) spiral strands, bending in the absence of sheaves or other formers, so that the radius of curvature of the strand is not predetermined.

Therefore, a dimensionless new parameter has been determined for design against such rather common and often very costly fatigue failures. Using this newly proposed parameter, it is now possible to determine the effective bending stiffness of the strand under any given cable curvature, for any cable construction subjected to any load perturbations. The proposed formulations are very simple in nature for direct engineering applications and the effective bending stiffnesses of the cable can be determined easily, even with a pocket calculator.

5.2 Background to the Simple Methods Developed

Different attempts have been made to simplify with acceptable accuracy the complex mathematical formulations used for the analysis of cables. Hruska (1951) proposed a simple formula for calculating the effective axial stiffness of the cable. Cable axial stiffness was shown to be a weighted function of the lay angles of the wires in the strand. In another publication Hruska (1952) tried to establish a relationship between radial and tensile forces in a layer of wire strand. The findings of this study were that the radial forces increased inward for each layer of helical cables and are therefore reached a maximum for core wires.

Strzemiecki and Hobbs (1988) extended Hruska's approach and proposed a general form of Hruska's formulations for estimating the full-slip axial stiffness of a wire rope. Raoof and Davies (2003) extended further the work of Strzemiecki and Hobbs (1988) and develop simple formulations for calculating the no-slip and full-slip axial stiffnesses of wire ropes either with IWRC or fibre cores.

Lanteingne (1985) proposed a simple means for the estimation of the degradation of the flexural rigidity of the cable under gradual increases in the cable curvature. In his model, he used Hruska's (1952) formula to obtain the estimates of radial contact force at trellis contact patches i.e. line contact forces between the wires in the same layer were ignored. Later, Raoof (1994) showed that for small radii of curvature, interlayer slippage occur on the contact patches, and plane sections do not remain plane during the bending cycle. An attempt has been made to predict no-slip and full slip values of the bending stiffness as a function of increasing cable curvature. It is argued that the magnitude of interlayer slippage between wires at extreme fibre position considerably lags behind those near to the neutral axis. There are also attempts in the literature to extrapolate test results on small scale model strands to predict the properties of large diameter cables (Chien, LeCair and Costello, 1988). A similar attempt has been made by Yeung and Walton (1985) to simplify and make economically acceptable axial fatigue tests, for large diameter cables used in the offshore platforms. Hong et al, (2005) proposed a theoretical model which was not only capable of calculating the no-slip and full slip bending stiffness values but the smooth transition between these two extremes is shown to be a function of the strand radii of curvature. However, the effect of interwire contact forces between the wires in the same layer was ignored in this model. Hong's model was subsequently modified and extended to cater for the ever present line contact forces in the same layer. The salient features of which have already been reported in Chapter 4: the proposed formulations are found to predict with a fairly good degree of accuracy, the mechanical characteristics of helical cables.

5.3 Theoretical Parametric Studies

In order to simplify the formulations proposed in Chapter 4, theoretical parametric studies were carried out on a variety of structural strands with their construction details given in Tables 4.1 (a-f). These geometric parameters cover a wide range of lay angles, number of wires, number of layers and wire and strand diameters. Using the original formulations proposed in Chapter 4, interwire contact deformations in terms of the parameters describing overall strand deformations, moment-curvature plots were obtained for each of the six different strand constructions. It is shown that the helical cables exhibit large non-linearities during bending because of the wire slippage

under frictional forces. The plots for the smooth transition of the bending stiffnesses of the strands from no-slip to full slip were produced from the slope of the deflection curves. Based on the results from these extensive theoretical parametric studies, it has been shown that the effective bending stiffness of the strand mainly depend on the axial load perturbations and the imposed curvature. Thus, a new parameter has been developed composed of radius of curvature times the axial strain of the strand divided by the strand outer diameter, $\boldsymbol{\rho_c \varepsilon_c / d}$. Using this parameter it is now possible to estimate the effective flexural stiffness of the cable subjected to any bending curvature.

5.3.1 Range of Parameters Used

In the present analysis, the following values of the various material parameters are used: Young Modulus for Steel E_{steel} = 200 kN/mm^2, Coefficient of friction μ = 0.12, Poisson's Ratio υ = 0.28. The full range of various strand geometrical parameters used in the present analysis is given below in Table 5.1. Whereas the full construction details of various structural strands are given in Chapter 4, Tables 4.1 (a-f).

Table 5-1: Full range of various geometrical strand parameters used in the present analysis.

Parameters	Range of Parameters
Strand diameter, d (mm)	$41 \leq d \leq 164$
Number of layers, N	$3 \leq N \leq 10$
Number of wires in each layer, n_i	$12 \leq n_i \leq 74$
Total number of wires in the strand, N_T	$19 \leq N_T \leq 522$
Lay angle, α_i, (degrees)	$11 \leq \alpha_i \leq 25$
Wire diameter, D (mm)	$3.54 \leq D \leq 6.55$

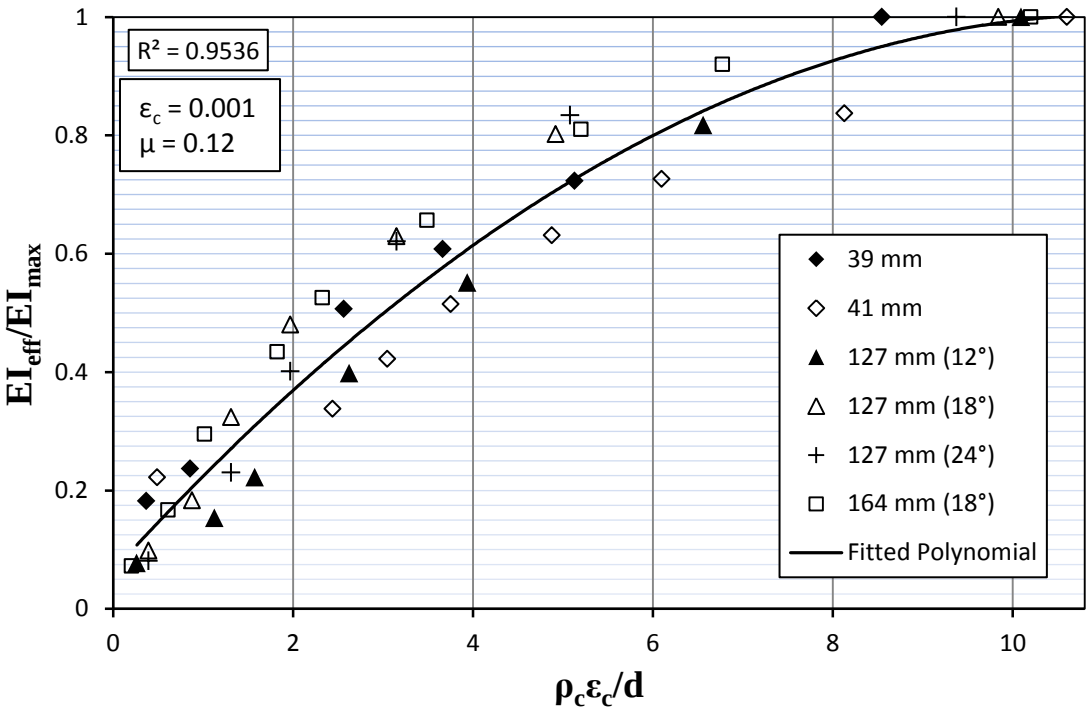

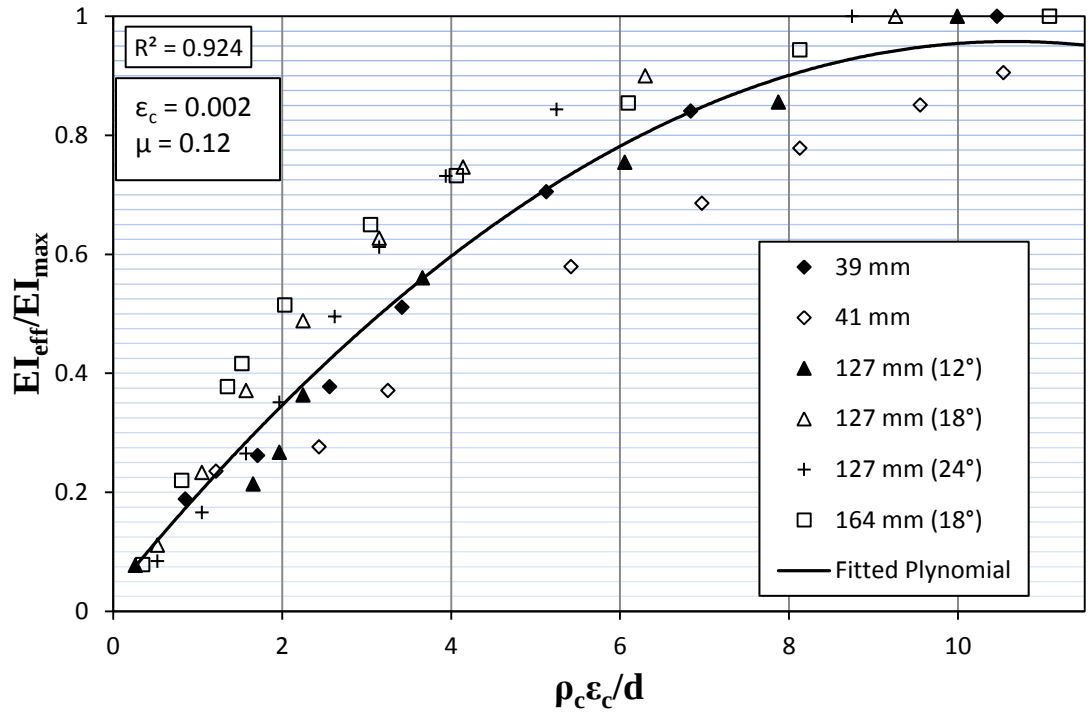

Figure 5-1 (a & b): Simple design curves based on the theoretical parametric studies, using the MHDS model with mean axial strains of; (a) 0.001; (b) 0.002 respectively.

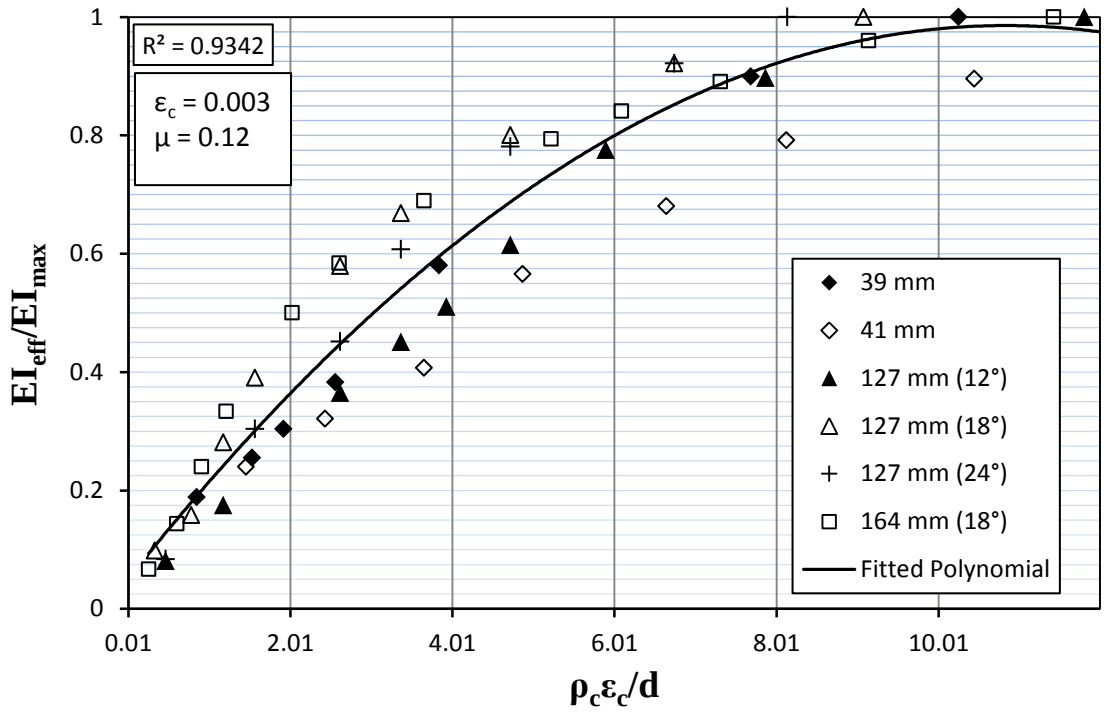

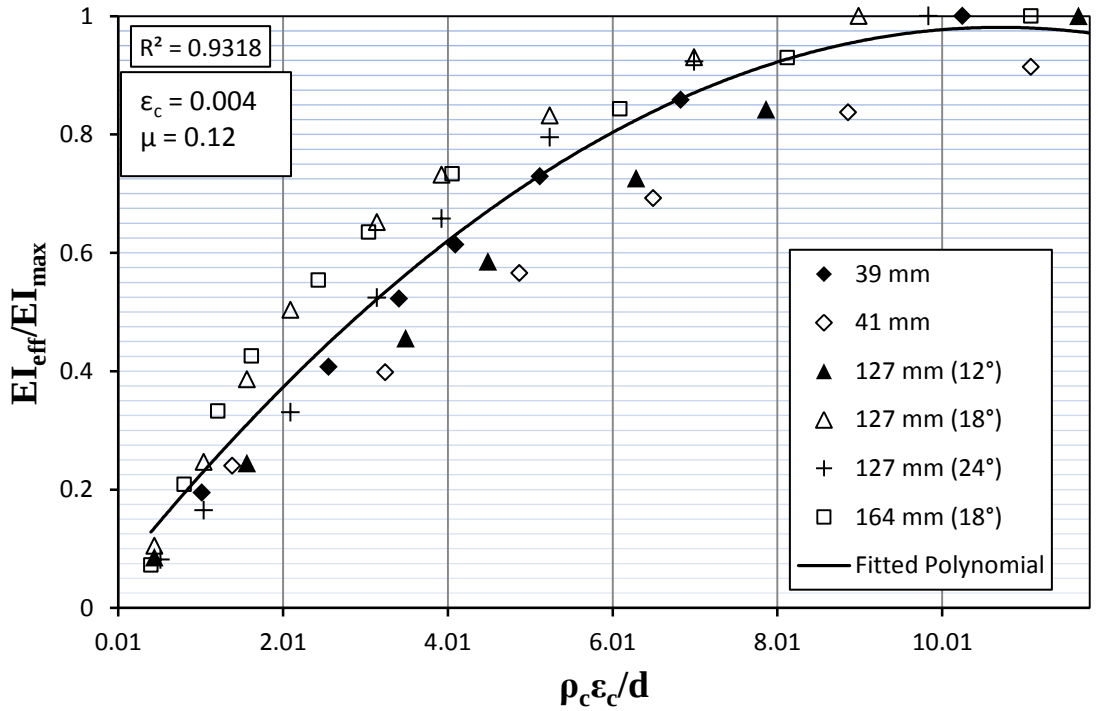

Figures 5.1 (c & d) Simple design curves based on the theoretical parametric studies, using the MHDS model with mean axial strains of; (c) 0.003; (d) 0.004 respectively.

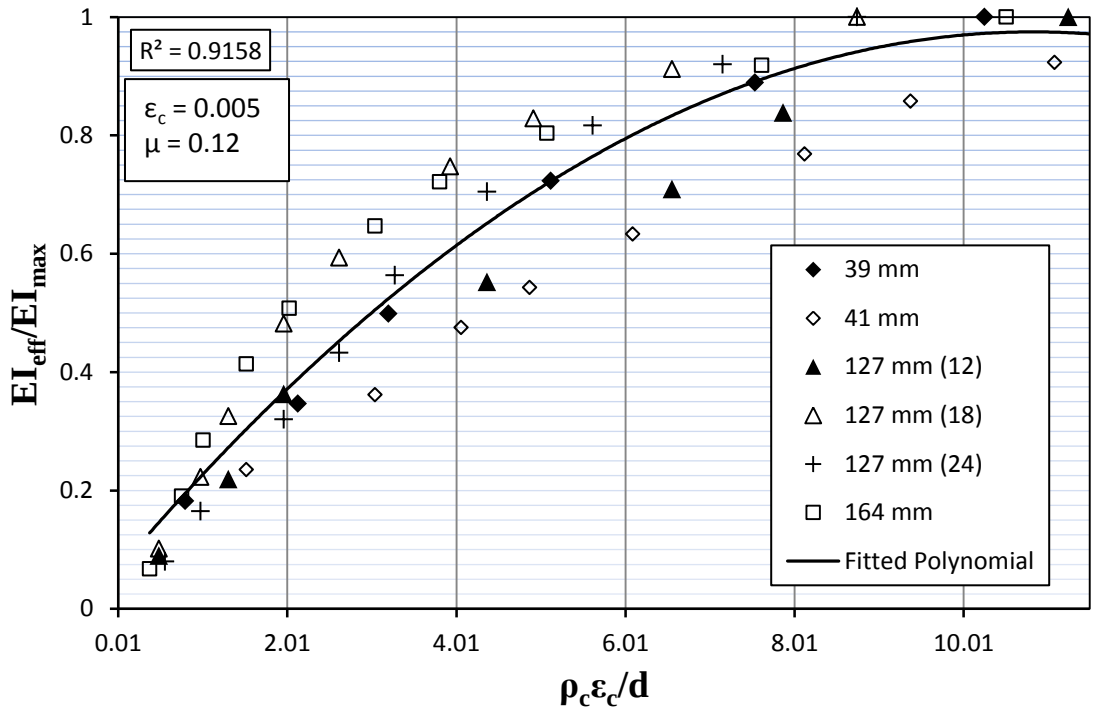

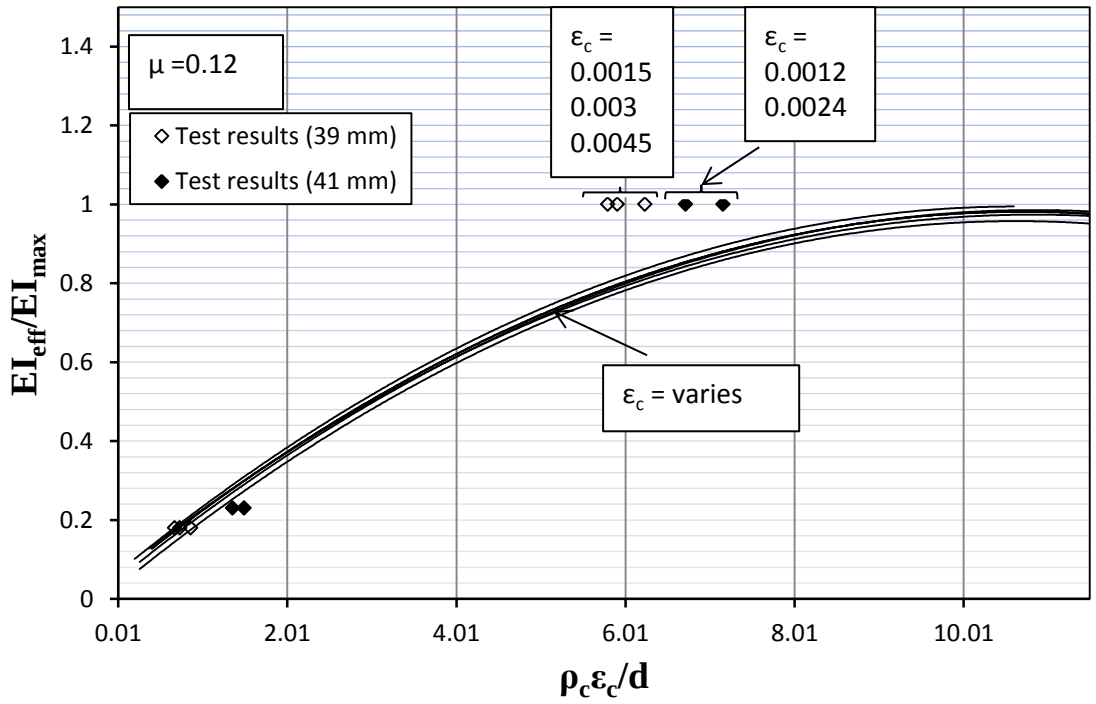

Figures 5.1 (e & f) Simple design curves based on the theoretical parametric studies, using the MHDS model with mean axial strains of; (e) 0.005; (f) ε_c varies.

5.4 Results

Figures 5.1 (a-e) present the plots of $\rho_c\varepsilon_c/d$ versus EI_{eff}/EI_{max} for all the six strand constructions, using MHDS model with axial strains of 0.001, 0.002, 0.003, 0.004 and 0.005 respectively. These plots have been obtained for a number of structural strands with their construction details presented in Tables 4.1 (a-f). The bending stiffness of the cable is shown to be a non-linear function of the newly proposed dimensionless parameter. Thus the reasonable estimate of the newly proposed parameter is sufficient for obtaining fairly accurate estimates of the effective flexural stiffness of the cable. The range of geometrical parameters used in this study is shown in Table 5.1. For modest curvature, when the wires in cable have not slipped yet, there is an upper bound limit of the new parameter given for these plots (i.e. 10). Beyond this value the simple method given in this chapter is not applicable, and if the value of the proposed parameter is greater than 10, the flexure rigidity of the cable will be at its maximum i.e. EI_{max}. These plots have been obtained for the selected friction coefficient, Poison's ratio and modulus of elasticity values of 0.12, 0.28 and 200 kN/mm^2 respectively.

It is also worth mentioning here that the values of this parameter are approximately same for different loading perturbations. This is because the radius of curvature decreases with increasing tension force in the strand. As predicted by the theory, increasing tension force in the cable delays the initiation of wire slippage, and hence imposed radius of curvature decreases, as a result the two parameters (ε_c and ρ_c) balances the effect of each other. All the figures for different mean axial loads show good correlations between the available more involved theory results and the fitted curves. The correlation coefficient R^2 for all the above plots is above 0.9 which is a measure of the accuracy of the curve. The closer is the value gets to 1 the closer are the data points around the fitted curve and therefore, more accurate is the curve. Microsoft excel has built in function for the correlation coefficient, therefore, in Figures 5.1 (a-e) the values of the correlation coefficients are calculated automatically by Microsoft excel for the given curves.

Finally, in Figure 5.1f a unified single plot of $\rho_c\varepsilon_c/d$ versus EI_{eff}/EI_{max}, irrespective of the specific cable construction, imposed curvature and mean axial strain has been

obtained. It covers all possible cases in practice and the correlations between the test data and the unified plot in Figure 5.1f, suggests the plot to be accurate and reliable. The slight discrepancy between test data and theoretical predictions for the innermost layer is due to reason that; theoretical plots are obtained from the critical curvature values at which wires on the neutral axis starts slippage; whereas, the test results show the curvature values at which wires on extreme fibre position slide in the outermost layer. The pattern of wire slippage is already discussed in quite detail as shown in Figure 3.1.

Since the contact forces accumulate inward and, are larger for wires in the inner layers. Therefore, interlayer slippage initially starts between outermost and penultimate layers near the so called neutral axis and gradually moves towards the centre of the strand. In other words, a wire in an inner layer will slip only if all outer wires in its sector have slipped. On the other hand, unbalanced force acting on a wire is maximum at the neutral axis (*i.e.* $\varphi = 0, \pm\pi$) and is observed to be minimum for wire on extreme fibre positions $\left(i.e.\varphi = \pm\frac{\pi}{2}\right)$. Therefore, for large cable curvature, it is possible for the innermost layer to experience some form of interlayer slippage in the vicinity of neutral axis prior to the occurrence of slippage between outermost layers around the extreme fibre positions. In Figure 3.1, the unshaded wires are in stick state whereas shaded wires are shown to be slipped according to the pattern explained above.

5.5 Simple Formulations

Using the results presented in the previous section, a very simple method for calculating the bending stiffness of the cable can be developed by simply fitting various non-linear curves through the data. In Figures 5.1 (a-e) the newly proposed simple dimensionless parameter $\boldsymbol{X = \rho_c \varepsilon_c / d}$, can be simply calculated by multiplying the cable radius of curvature by given cable axial strain divided by cable outer diameter. Once this parameter is calculated, the effective bending stiffness of the cable may be found using the second order polynomial of the general form.

$$\frac{EI_{eff}}{EI_{max}} = AX^2 + BX + C \tag{5.1}$$

where, the constant coefficients A-C are given in Table 5.2 and correspond to the situations when the cables are subjected to different values of mean axial strains ranging $0.001 \leq \varepsilon_c \leq 0.005$. The fitted polynomials for Figures 5.1 (a-f) show that individual numerical results are almost independent of the level of mean axial load on the cable.

Table 5-2: Values of the constant coefficients A-C in equation (5.1) for all the fitted curves in Figures 5.1 (a-f), along with correlation coefficients R^2.

Reference	A	B	C	R^2
Fig 5.2a	-0.0074	0.1671	0.0646	0.9536
Fig 5.2b	-0.0080	0.1744	0.0304	0.9250
Fig 5.2c	-0.0079	0.1715	0.0509	0.9352
Fig 5.2d	-0.0080	0.1721	0.0595	0.9318
Fig 5.2e	-0.0077	0.1679	0.0654	0.9158

Table 5-3 (a &b): Numerical results and calculation routines of the simple method for 39 and 41 mm outer diameter cables.

Strand axial strain, ε_c	Lay angle α_i (°)	Strand diameter, d_i (m)	Strand curvature, κ_c (m^{-1})	Rad: of curvature ($\rho_c = 1/\kappa_c$) (m)	$\rho_c\varepsilon_c/d$	Effective bending stiffness, EI_{eff} (Nm^2)	EI_{eff}/EI_{max}
0.001	15.99	0.039	0.003	333.33	8.55	16454	1
0.001	15.99	0.039	0.005	200.00	5.13	11900	0.723
0.001	15.99	0.039	0.007	142.86	3.66	10000	0.608
0.001	15.99	0.039	0.01	100.00	2.56	8333.333	0.506
0.001	15.99	0.039	0.03	33.33	0.85	3900	0.237
0.001	15.99	0.039	0.07	14.29	0.37	3000	0.182

Strand axial strain, ε_c	Lay angle α_i (°)	Strand diameter, d_i (m)	Strand curvature, κ_c (m^{-1})	Rad: of curvature ($\rho_c = 1/\kappa_c$) (m)	$\rho_c\varepsilon_c/d$	Effective bending stiffness, EI_{eff} (Nm^2)	EI_{eff}/EI_{max}
0.001	12	0.041	0.0023	434.78	10.60	22500	1
0.001	12	0.041	0.003	333.33	8.13	18842	0.837
0.001	12	0.041	0.004	250.00	6.10	16346	0.726
0.001	12	0.041	0.005	200.00	4.88	14200	0.631
0.001	12	0.041	0.0065	153.85	3.75	11587	0.515
0.001	12	0.041	0.008	125.00	3.05	9500	0.422
0.001	12	0.041	0.01	100.00	2.44	7600	0.338
0.001	12	0.041	0.04	25.00	0.61	5000	0.222

Tables 5-3 (c-e): Numerical results and calculation routines of the simple method for three 127 mm outer diameter cables with lay angles: (a) 12°; (b) 18°; (c) 24°.

Strand axial strain, ε_c	Lay angle α_i (°)	Strand diameter, d_i (m)	Strand curvature, κ_c (m^{-1})	Rad: of curvature ($\rho_c = 1/\kappa_c$) (m)	$\rho_c\varepsilon_c/d$	Effective bending stiffness, EI_{eff} (Nm^2)	EI_{eff}/EI_{max}
0.001	12	0.127	0.00078	1282.05	10.09	2006666	1
0.001	12	0.127	0.0013	769.23	6.06	1640000	0.817
0.001	12	0.127	0.003	333.33	2.62	799000	0.398
0.001	12	0.127	0.005	200.00	1.57	446000	0.222
0.001	12	0.127	0.007	142.86	1.12	308000	0.153
0.001	12	0.127	0.035	28.57	0.22	154800	0.077
Strand axial strain, ε_c	**Lay angle α_i (°)**	**Strand diameter, d_i (m)**	**Strand curvature, κ_c (m^{-1})**	**Rad: of curvature ($\rho_c = 1/\kappa_c$) (m)**	**$\rho_c\varepsilon_c/d$**	**Effective bending stiffness, EI_{eff} (Nm^2)**	**EI_{eff}/EI_{max}**
0.001	18	0.127	0.00085	1176.47	9.26	1625090	1
0.001	18	0.127	0.0015	666.67	5.25	1303423	0.802
0.001	18	0.127	0.0025	400.00	3.15	1023452	0.630
0.001	18	0.127	0.004	250.00	1.97	780000	0.480
0.001	18	0.127	0.006	166.67	1.31	526000	0.324
0.001	18	0.127	0.009	111.11	0.87	298000	0.183
0.001	18	0.127	0.027	37.04	0.29	129600	0.080
Strand axial strain, ε_c	**Lay angle α_i (°)**	**Strand diameter, d_i (m)**	**Strand curvature, κ_c (m^{-1})**	**Rad: of curvature ($\rho_c = 1/\kappa_c$) (m)**	**$\rho_c\varepsilon_c/d$**	**Effective bending stiffness, EI_{eff} (Nm^2)**	**EI_{eff}/EI_{max}**
0.001	24	0.127	0.00092	1086.96	8.56	1256250	1
0.001	24	0.127	0.0015	666.67	5.25	1048000	0.834
0.001	24	0.127	0.0025	400.00	3.15	780000	0.621
0.001	24	0.127	0.004	250.00	1.97	504000	0.401
0.001	24	0.127	0.006	166.67	1.31	289000	0.230
0.001	24	0.127	0.024	41.67	0.33	101600	0.081

Tables 5-3f: Numerical results and calculation routines of the simple method for 164 mm outer diameter cable.

Strand axial strain, ε_c	Lay angle α_i (°)	Strand diameter, d_i (m)	Strand curvature, κ_c (m^{-1})	Rad: of curvature ($\rho_c = 1/\kappa_c$) (m)	$\rho_c\varepsilon_c/d$	Effective bending stiffness, EI_{eff} (Nm^2)	EI_{eff}/EI_{max}
0.001	18	0.164	0.0006	1666.67	10.16	4576667	1
0.001	18	0.164	0.0009	1111.11	6.78	4120000	0.900
0.001	18	0.164	0.0012	833.33	5.22	3707100	0.810
0.001	18	0.164	0.0018	555.56	3.39	3005000	0.657
0.001	18	0.164	0.0026	384.62	2.35	2406000	0.526
0.001	18	0.164	0.0033	303.03	1.85	1988000	0.434
0.001	18	0.164	0.006	166.67	1.02	1350000	0.295
0.001	18	0.164	0.01	100.00	0.61	765000	0.167
0.001	18	0.164	0.03	33.33	0.20	331500	0.072

5.6 **Discussion**

Tables 5.3 (a-f) present a summary of the calculation routines of the final estimates of the bending stiffnesses, based on the original formulations of the MHDS model, for each of the six different cable constructions. For a given strand geometry, the interaction between the wires is found to be a function of the axial strain and the imposed curvatures. Although, the data in these tables are obtained for the cable axial strain of $\varepsilon_c = 0.001$ for all the cables, but the value of the newly proposed parameter is found to be insensitive to cable axial strain values. This is because for increasing axial strains the radius of curvature decreases and its effect is neutralized. Even for a given cable axial strain, the data for the three same diameter strands with different lay angles of 12°, 18° and 24° show slight scatter. The upper bound value of the proposed parameter for these three different cables are for example 10.06, 9.26 and 8.56 respectively.

Numerical results based on MHDS model in Chapter 4, has been used in relation to the effective flexural stiffness of the cable for different cable constructions. As predicted by the theory, it is demonstrated that the bending stiffness of the cable mainly depends on the interwire contact forces and imposed curvature. In order to develop a simple method, one needs to perform a rigorous analysis of all the material and geometrical parameters that affect the overall bending behaviour of the cable. Therefore, a new parameter composed of two geometrical parameters (radius of curvature and cable diameter) and a mechanical parameter (axial strain) has thus been developed.

Comparing Figures 5.1 (a-e) it is found that theoretical data is less scattered around the fitted curves, when 41 mm diameter strand with IWRC core was removed. The data is found even more closer to the fitted curves when 127 mm strand with lay angle of 24° was not considered. Cables with moderate lay angles (15-18°) are noted to best fit in the curves, whereas the cables having lay angles less than 12° were found to give lower bending stiffness values. In contrast to this, cables with lay angles greater than 18° give higher bending stiffness values than as predicted by the simple method. Thus it is concluded that the overall scatter of the data from the fitted curves depend on the magnitude of lay angle and the ratio of the strand to core diameter. For example in the

case of 41 mm outer diameter cable with an IWRC core of 13.5 mm, the scatter is maximum. This is because not only the ratio of cable to core diameter is maximum for it but also the average lay angles of wires in all the three layers of the cable is small (i.e. 12°).

5.7 Numerical Example

To further explain the use of the simple method developed in this chapter, a numerical example is presented here. A 39 mm outside diameter spiral strand with geometrical details given in table 4.2a, subjected to a mean axial strain of $\boldsymbol{\varepsilon_c}$ = 0.001 is chosen as an example for the numerical example. With $EI_{max} = 16454\ Nm^2$ (as calculated by the MHDS model) is the maximum bending stiffness of the strand. For a given value of imposed curvature**,** say $\boldsymbol{\kappa_c}$ = 0.01 calculate the radius of curvature, ($\boldsymbol{\rho_c}$ =1/0.01= 100 m), with d =39 mm, being the outside diameter of the strand, gives the value of the newly proposed parameter, $\frac{\boldsymbol{\rho_c \varepsilon_c}}{\boldsymbol{d}} = \boldsymbol{X = 2.56}$**.** Read the value of effective bending stiffness of the strand from the simple curve in Fig 5.2a for this value or put this value in the second order polynomial equation. This gives the value of 7315 Nm^2, whereas the exact value of the bending stiffness calculated by original formulations is 7750 Nm^2. Due to the other sources of uncertainties affecting the problem, this discrepancy can be deemed as acceptable for design purposes.

5.8 Conclusion

As discussed earlier, a simple method has been proposed by means of which the effective bending stiffness of large diameter multi-layered cables may be estimated under any loading condition and applied bending. The proposed method is based on a large body of the numerical results obtained from MHDS model applied to a variety of cable constructions. The newly proposed parameter can be expressed as the ratio of the axial strain to two times bending strain of the cable. This study clearly demonstrates that using the simple formulations, nominally very close values of the bending stiffness are obtained when compared to the original formulations of MHDS model.

Chapter 6

Response of Multi-Layered Sheathed Spiral Strands in Deep Water Applications, Subjected to Combine Tension and Bending.

6.1 Introduction

Due to high axial strength, high durability under large loads, high strength to weight ratio and relatively low cost, wire ropes and spiral strands have many important applications both in the onshore and offshore structures. In recent times, wire ropes and spiral strands have been used in a variety of deep water applications such as mooring system for deep sea offshore platforms, floating platforms, towing of underwater vehicles and mobile drilling units etc. It is observed that in the majority of the mooring systems, due to corrosion the life of the cable is less than the installation, unless properly protected. In order to protect the large diameter spiral strands from corrosion in marine applications the strands are encased in impermeable protective polythene sheaths with the gaps between the wires filled with lubricants. This has been proved useful to stop corrosion and enhance the lives of cables significantly. In the last two decades, considerable interest has been shown in the mechanical characteristics of sheathed spiral strands and wire ropes for the use in under-water applications. In majority of the cases, cable is subjected to cyclic bending and fluctuating tension. As a result, high contact stresses and longitudinal sliding at points of contact with sheaves and winch drums occur.

The purpose of the present chapter is to extend the previously reported MHDS model, to cater for the effects of external hydrostatic pressure on sheathed spiral strands, which greatly influence the pattern of contact forces between wires in the strand. There has been a significant increase in the size of steel cable being used, particularly in the offshore industry. The suspended weight of steel mooring components is becoming a challenge as well, as floating exploration and production facilities are moving into increasing water depth raising the issue of perceived limits for steel

cables. Since the rope has to support much of its own weight, as the water depth increases, and only a small proportion of the tension in the rope may be usefully employed to run the rig to its station. Raoof (1990c) has shown theoretically that high external hydrostatic pressures significantly influence the patterns of interwire contact forces in sheathed spiral strands. Under such external pressures, the contact forces caused by the hydrostatic water pressure become more significant compared with contact forces inside the cable by the tension force in the cable. The significant increase in normal contact forces between wires suppressed the slippage of wires in the cable. Under such conditions, interwire fretting actions are accompanied with high levels of localized heating. Consequently, the fatigue life of the cable is becoming a more challenging issue, particularly in the vicinity of end terminations, where abrupt changes in curvature are found to occur. The substantial increases in the stresses at the contact patches is therefore found to lead significant reductions in the axial and restrained bending fatigue life of the cable in long term applications.

To address this problem, an extension of the previously reported MHDS model (fully catering for interwire contact forces in the strand from external hydrostatic pressures) has been presented for predicting flexural stiffness of the strands subjected to different water depths. The proposed theory is believed to be useful in giving an insight into the manner in which the effect of hydrostatic pressure from outside is determined moving towards the centre of the strand, in connection with clench forces due to the tension force in the strand. In deep water applications, the cables are assumed to be subjected to uniform external pressures. Using the proposed theory, numerical results have been obtained for three different 127 mm strands with lay angles of 12°, 18° and 24° experiencing a wide range of external hydrostatic pressures of 0 to 2000 m. It is important to mention here that the formulations presented in this chapter are applicable only to the cables with an impermeable polythene sheaths provided to seal the exterior of the cable from outside. It is then reasonable to assume that such plastic sheaths cause full hydrostatic pressure to act as a contact force in the outer layer of the cable. In the absence of such sheaths, it is possible that water enters into the cable and water pressure gets all around the wires and consequently no significant contact forces due to external pressure will develop.

Gecha (1989) presented results of the stresses, strains and displacements, for both theoretical and experimental studies carried out on sheathed spiral strands. Interwire frictional force was neglected in his formulations; however, the radial compressibility of the cable and Poisson's effect had been taken into account. Raoof (1990c) gave an insight into the effects of high external hydrostatic pressure on axial/torsional stiffnesses, hysteresis and fatigue behaviour of multi-layered sheathed spiral strands. Raoof and Kraincanic (1994) proposed a simple method for estimating the 2x2 no-slip and full-slip stiffness matrices for large diameter sheathed spiral strands.

6.2 Effect of Hydrostatic Pressure on the Cable

The salient features of the proposed MHDS model have been already reported in considerable detail in chapter 4, and will be not repeated here. Using the orthotropic sheet theoretical model, the estimates of interwire contact forces in the axially pre-loaded sheathed spiral strands have been obtained for various water depths. The externally applied hydrostatic pressure to sealed spiral strand has a significant effect on the pattern of interwire/interlayer contact forces. Thus in the case of deep water applications, X_{MSi} and X_{RCi} for outermost layer, N (and hence, P_{MSi} and P_{RCi}) are no longer the same. The radial and circumferential forces in various layers of the sheathed spiral strand, with the load transfer between layers included, can be calculated as:

$$X_{MS_N} = X_{RC_N} + X_{H_P} \tag{6.1}$$

The above equation defines the magnitude of the radial force in the outermost, N layer of the strand, with X_{RC_N} the radial force due to tension force in the wire, and X_{H_P} being the magnitude of the external hydrostatic pressure per unit length of the wires and is given by Raoof (1990d):

$$X_{H_P} = \frac{\pi d \rho_w g h}{n_N \cos \alpha_N} \tag{6.2}$$

In Eq. (6.2), d is the outer diameter of the strand, h is the depth of water, ρ_w is the water density, n_N is the number of wires in the outermost layer, g is the gravitational acceleration and α_N is the lay angle of wires in the outermost layer. With the effect hydrostatic pressure taken into account, the radial force in any arbitrary inner layer

can be calculated by the previously summarized method in chapter 3 (i.e. Eq. 3.43). Similarly, the normal forces in the hoop direction can also be estimated exactly the same way as explained in chapter 3, using Eq. (3.46).

The procedure for the calculation of interwire/interlayer contact forces is applicable to fully bedded-in spiral strands in which the individual wires are closely packed and the contact between the wires in the same layer is fully developed. Ideally, for newly manufactured strands (in the absence of external pressure), the assumption of no gaps between the wires in the individual layers, is not entirely true, and certain gaps exist between the wires in the same layer and the line contact forces are only partially developed. In marine applications, the external hydrostatic pressure brings the wires closer together and full contacts between the wires in the same layers are developed.

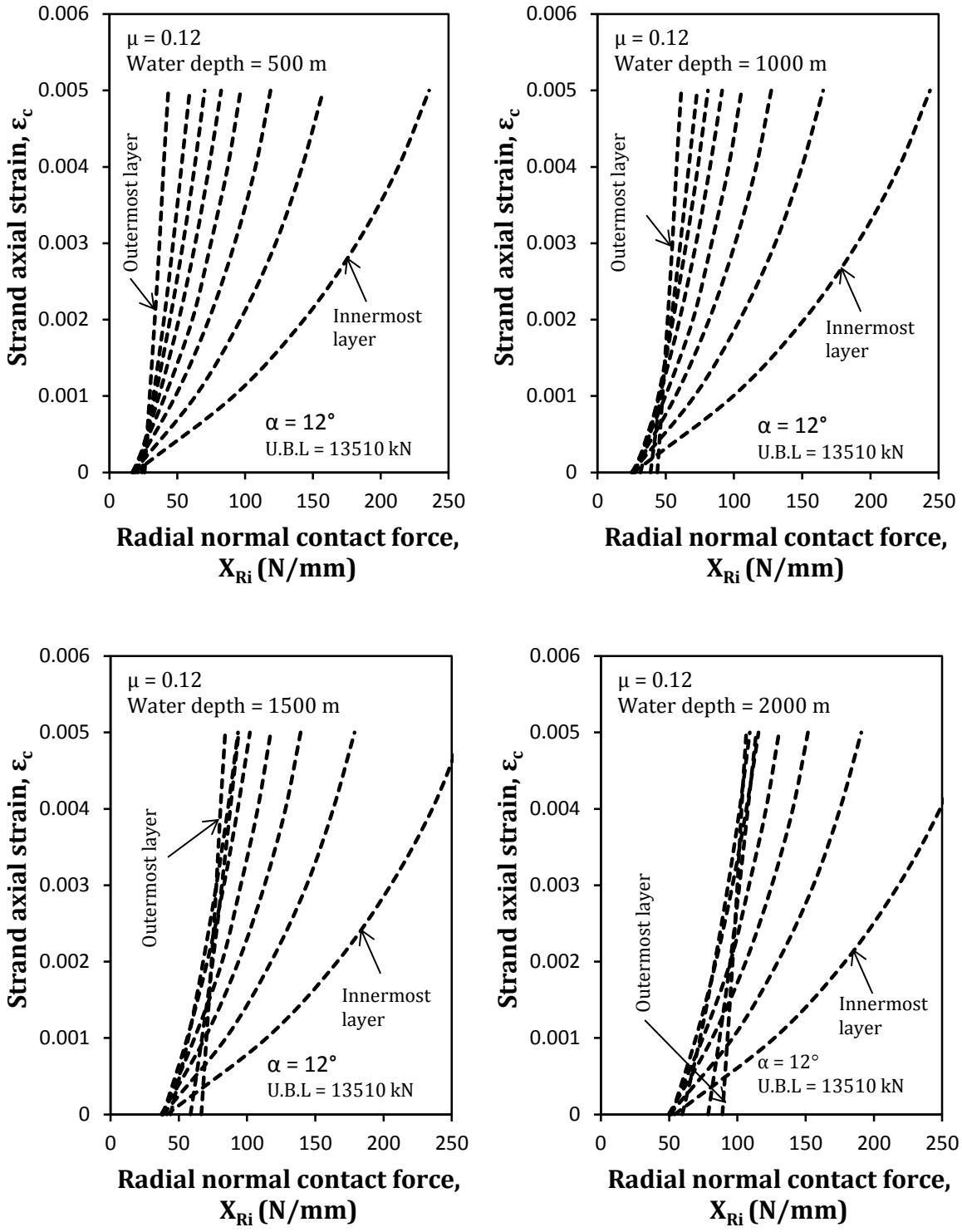

Figure 6-1 (a-d): Theoretical predictions of the interlayer radial contact forces at the interface of different layers of 127 mm outside diameter spiral strand, with lay angle, (α = 12°) for various water depth of (a) 500 m; (b) 1000 m; (c) 1500 m; and (d) 2000 m respectively.

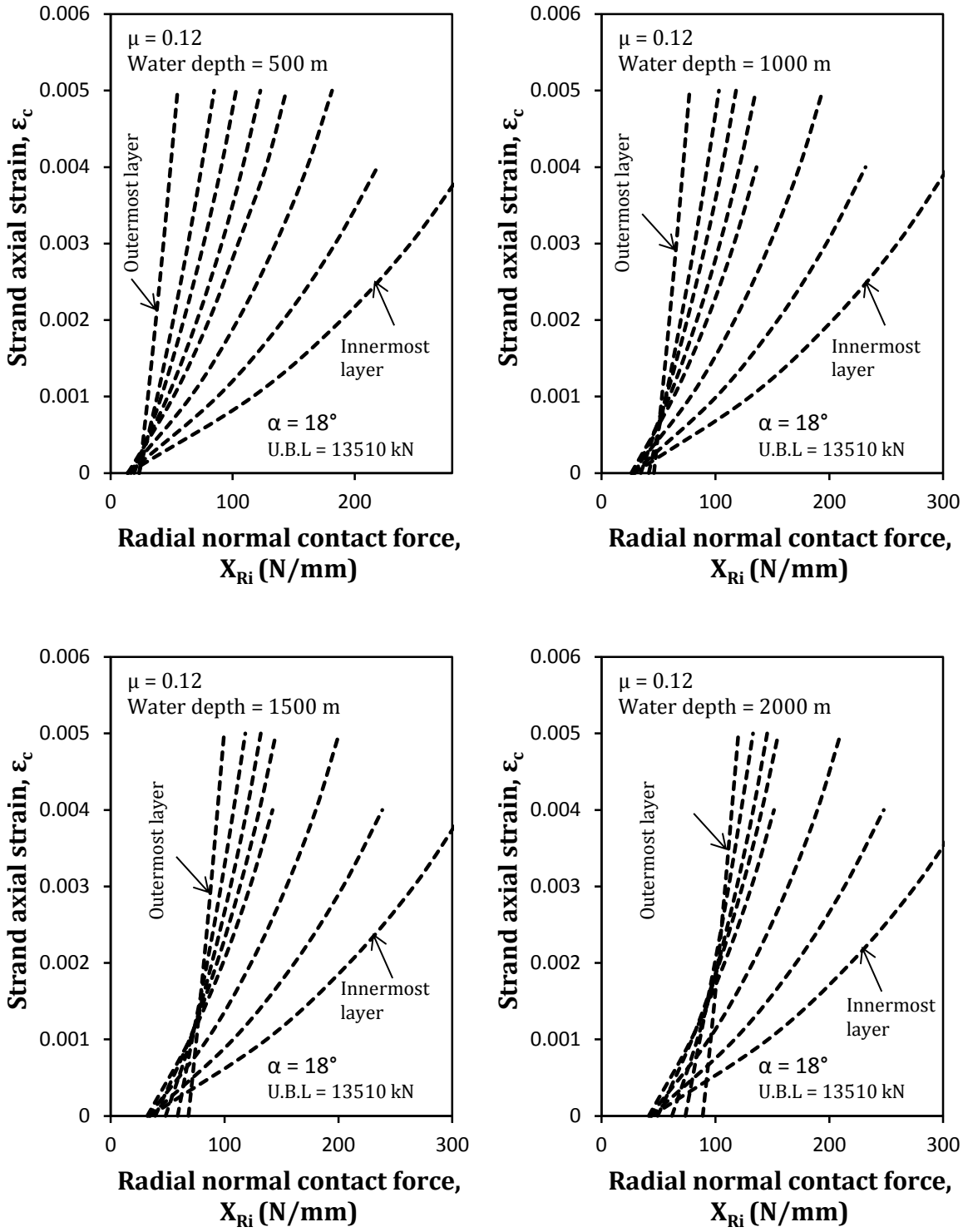

Figures 6.1 (e-h) - Theoretical predictions of the interlayer radial contact forces at the interface of different layers of 127 mm outside diameter spiral strand, with lay angle, (α = 18°) for various water depth of (e) 500 m; (f) 1000 m; (g) 1500 m; and (h) 2000 m respectively.

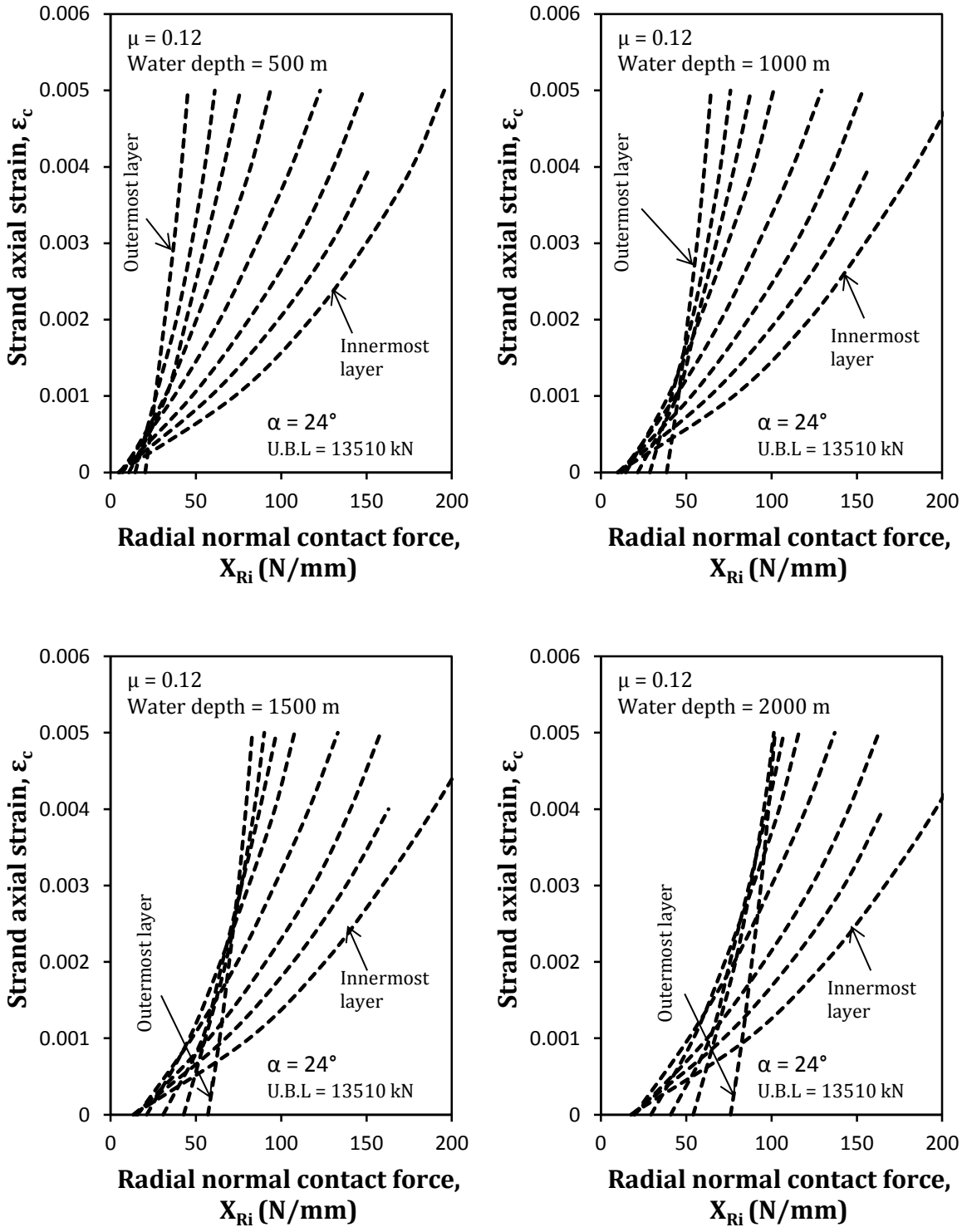

Figures 6.1 (*i-l*) - Theoretical predictions of the interlayer radial contact forces at the interface of different layers of 127 mm outside diameter spiral strand, with lay angle,(α = 24°) for the various water depth of (i) 500 m; (j) 1000 m; (k) 1500 m; and (l) 2000 m respectively.

6.3 **Results**

Figures 6.1 (a-d), (e-h) and (*i-l*) show the plots for normal contact forces at the interface of wires between different layers of three 127 mm outside diameter strands with lay angles of 12°, 18° and 24° respectively. The construction details of these three strands are already given in Tables 4.1 (c-e), but in the present case, an impermeable polythene sheaths are provided around them. For each strand, four plots are obtained for water depths of 500, 1000, 1500 and 2000 m respectively. It can be readily seen in the figures, that under high water depths the effect of hydrostatic pressure becomes more significant in comparison to axial load in the cable. For high levels of hydrostatic pressure, it is shown in these figures that interlayer contact forces is higher in magnitude compared with the radial contact forces inside the strand caused by the mean axial load. At zero cable axial strain, interwire contact forces are highest in the outer layer and lowest in the inner layers. As the tension force on the cable increases, the interlayer radial contact force grows in magnitude. Thus for higher levels of axial force, interlayer contact forces in inner layers increase at a higher rate than the outer ones, and for sufficiently large values of tension force, the outer layers have the lowest contact force compared with all other layers in the strand.

Lay angle of wires in the strand is found once again to play an important role in the distribution of interwire/interlayer contact forces. For large values of lay angle, the maximum fraction of the external hydrostatic pressure is taken by interwire line contact force and a very small fraction is transferred as radial contact force to the innermost layer. Another observation is that, increasing cable tension, for a given level of external hydrostatic pressure, brings the predictions of (radial + hoop) contact forces closer together for outer and penultimate layers. As in the case of 0 m water depth (i.e. corresponding to in air-condition) large lay angles are found to have higher values of (radial + hoop) contact force for the outermost and penultimate layers, decreasing tremendously moving towards the centre of the strand. For example for a given water depth of 1000 m, the contact force for the outermost layer of the three strands are 87, 91 and 89 N/mm for 12°, 18° and 24° respectively. The reason for this is that contact forces between wires due to the tension force, increases with increasing lay angle, but the contact forces due to hydrostatic pressure on the outer layer of the

cable, decreases with increasing lay angle. This indicates that when hydrostatic pressure is included in the analysis, the lay angle ceases to be the only first order parameter influencing the contact forces between the wires. The external pressure on these sealed strands is readily seen to suppress the slippage of wires in the strand by increasing the frictional forces. Based on these contact force distributions, the transition of bending stiffness from no-slip to full-slip are calculated as a function of imposed curvature, for various water depths. The theoretical plots in Figures (a-*l*) demonstrate that the significant increase in contact force accompanied with slippage in the outer layers can lead to decrease the fatigue life of the cable. This may have a significant bearing on the estimated operational life span of the structures used in deep water applications, which is widely ignored by the designer in the literature. The ultimate breaking load (U.B.L) for all the above three strands is 13510 kN.

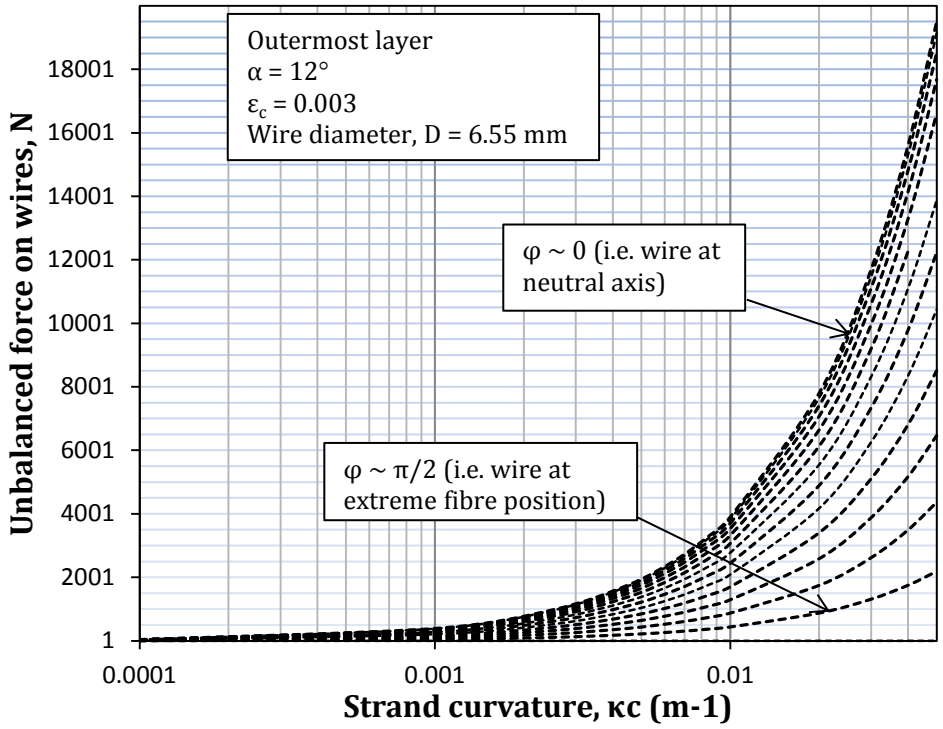

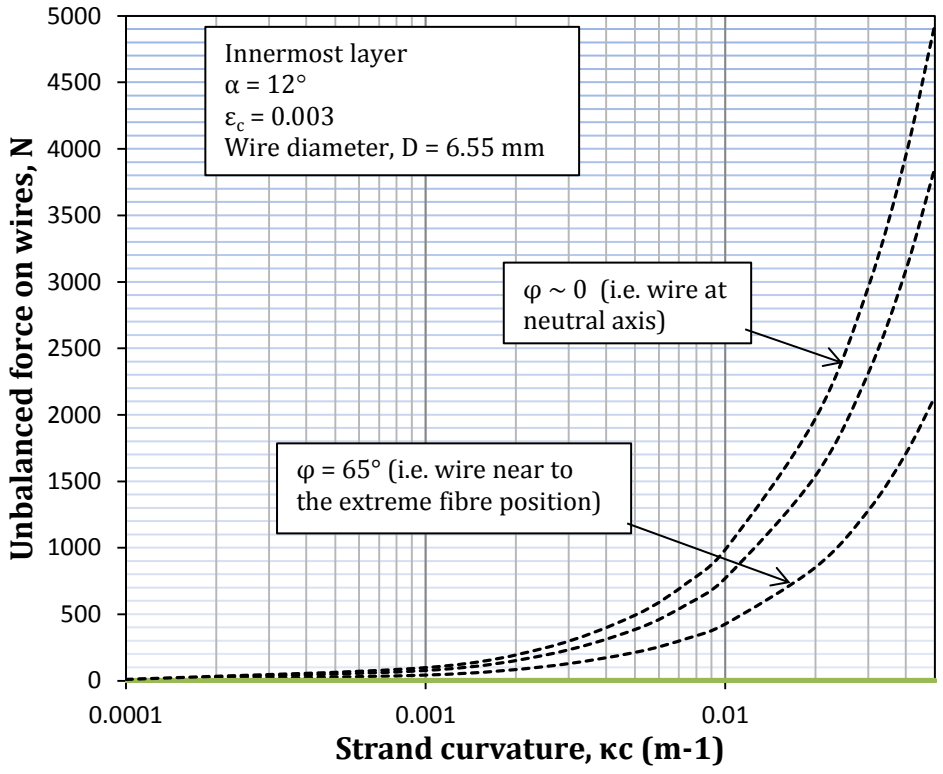

Figure 6-2 (a & b): Unbalanced forces on wires in 127 mm outside diameter strand (α = 12°) in the (a) outermost layer; (b) innermost layer respectively.

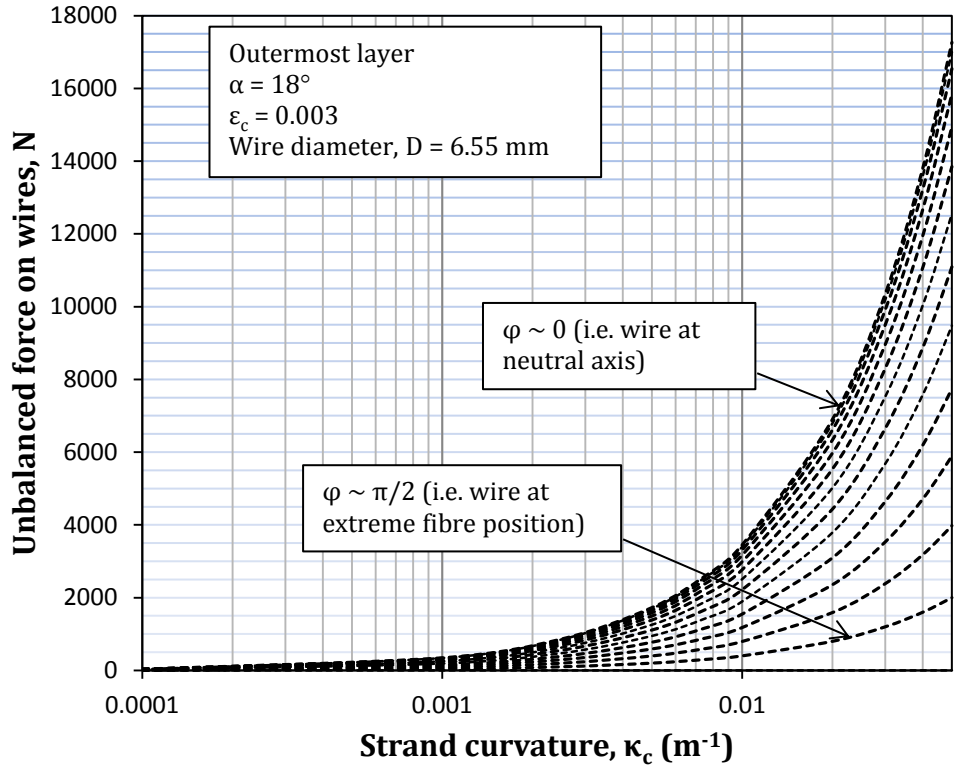

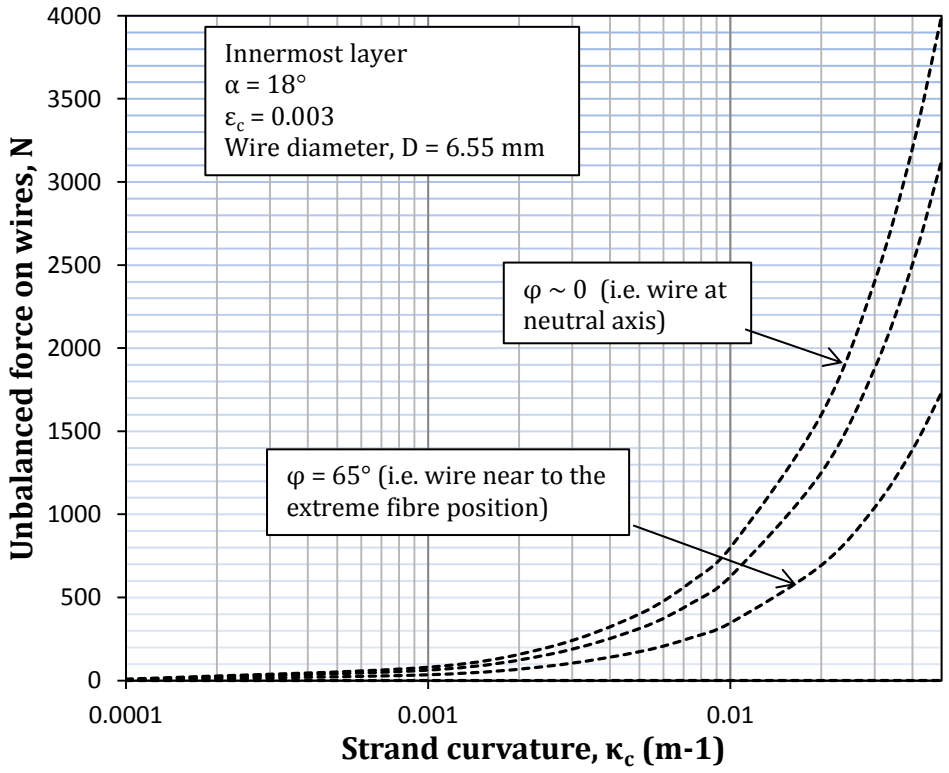

Figure 6.2 (c & d): Unbalanced forces on wires in 127 mm outside diameter strand (α = 18°) in the (c) outermost layer; (d) innermost layer respectively.

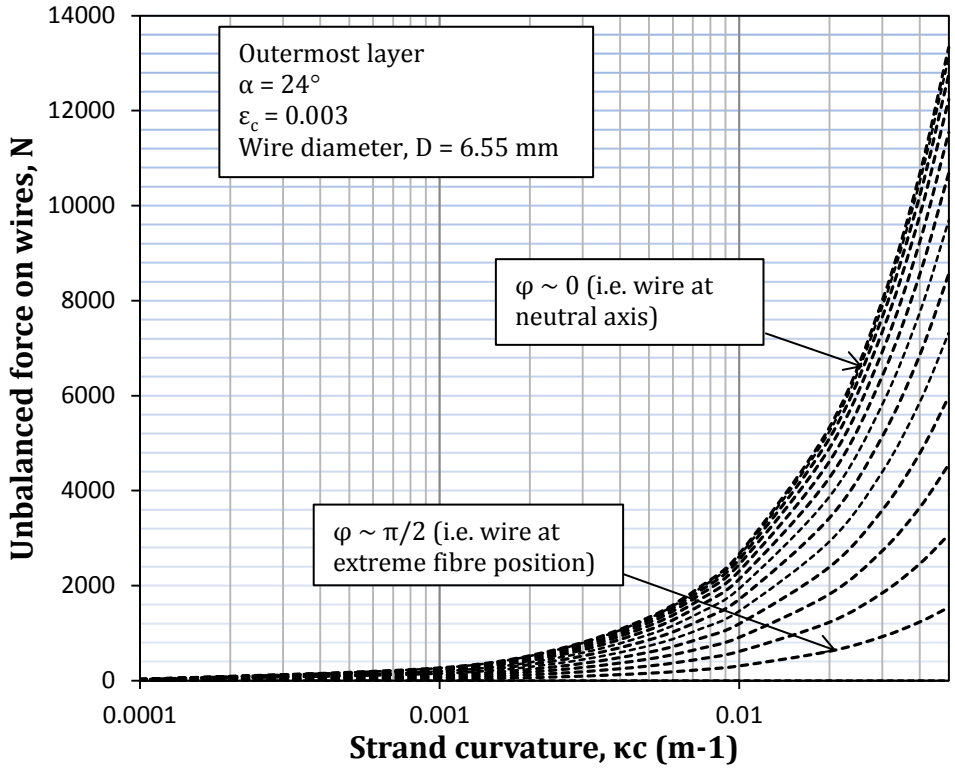

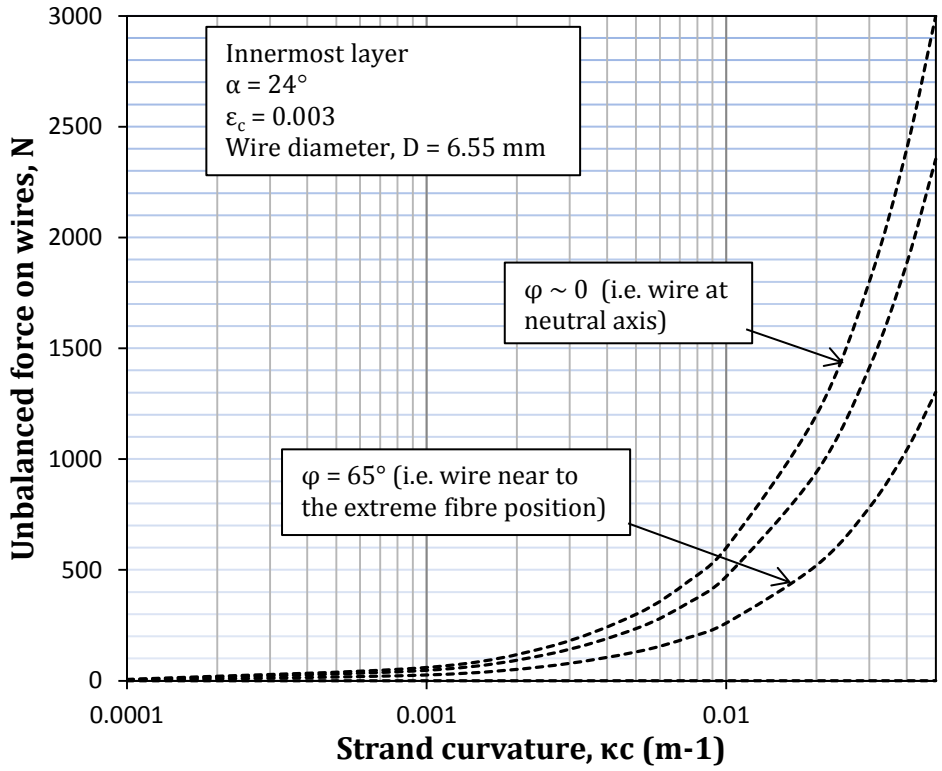

Figure 6.2 (e & f): Unbalanced forces on wires in 127 mm outside diameter strand (α = 24°) in the (e) outermost layer; (f) innermost layer respectively.

Figures 6.2 (a & b), (c & d) and (e & f) show the unbalanced forces in wires that belong to the outermost and innermost layers of the three 127 mm outside diameter strands, having lay angles of 12°, 18° and 24° respectively. The results in these figures show that the unbalanced force is negligible at small values of strand curvature but grows exponentially after certain limits of imposed curvatures. This is because it only depends on the distance from the neutral axis d_y, and therefore the plots of unbalanced forces show a symmetry about flexural axis. Results in the Figures 6.2 (a-f) suggest that the unbalanced force on wires near the neutral axis are significantly large compared with those near the extreme fibre position. Therefore, wires on the neutral axis experience maximum slippage causing first wire fractures to occur at the neutral axis as observed by Raoof (1992 a & b) in his experiments. It is worth to mention here that in the present case of sheathed spiral strands, only interwire contact forces are changed by external hydrostatic pressure whereas the magnitude of unbalanced forces remain unchanged as in air conditions.

A wire of the same diameter on the neutral axis is found to experience an unbalanced force, 270 times greater than that at the extreme fibre position. For example, in the case of 127 mm diameter strand with lay angle 12°, the unbalanced force on a wire at the neutral axis (i.e. $\varphi = 0$) and near the extreme fibre position (i.e. $\varphi = 88°$) is 74 N, 20,000 N respectively. Similarly, the results in these figures also show that unbalanced force on a wire decreases as the lay angle of the wire in the layer increases. A wire of the same diameter on neutral axis is shown to experience an unbalanced force of 19561 N, 17475 N and 13333 N, for lay angles of 12°, 18° and 24° respectively for a selected imposing curvature of 0.05 m^{-1}.

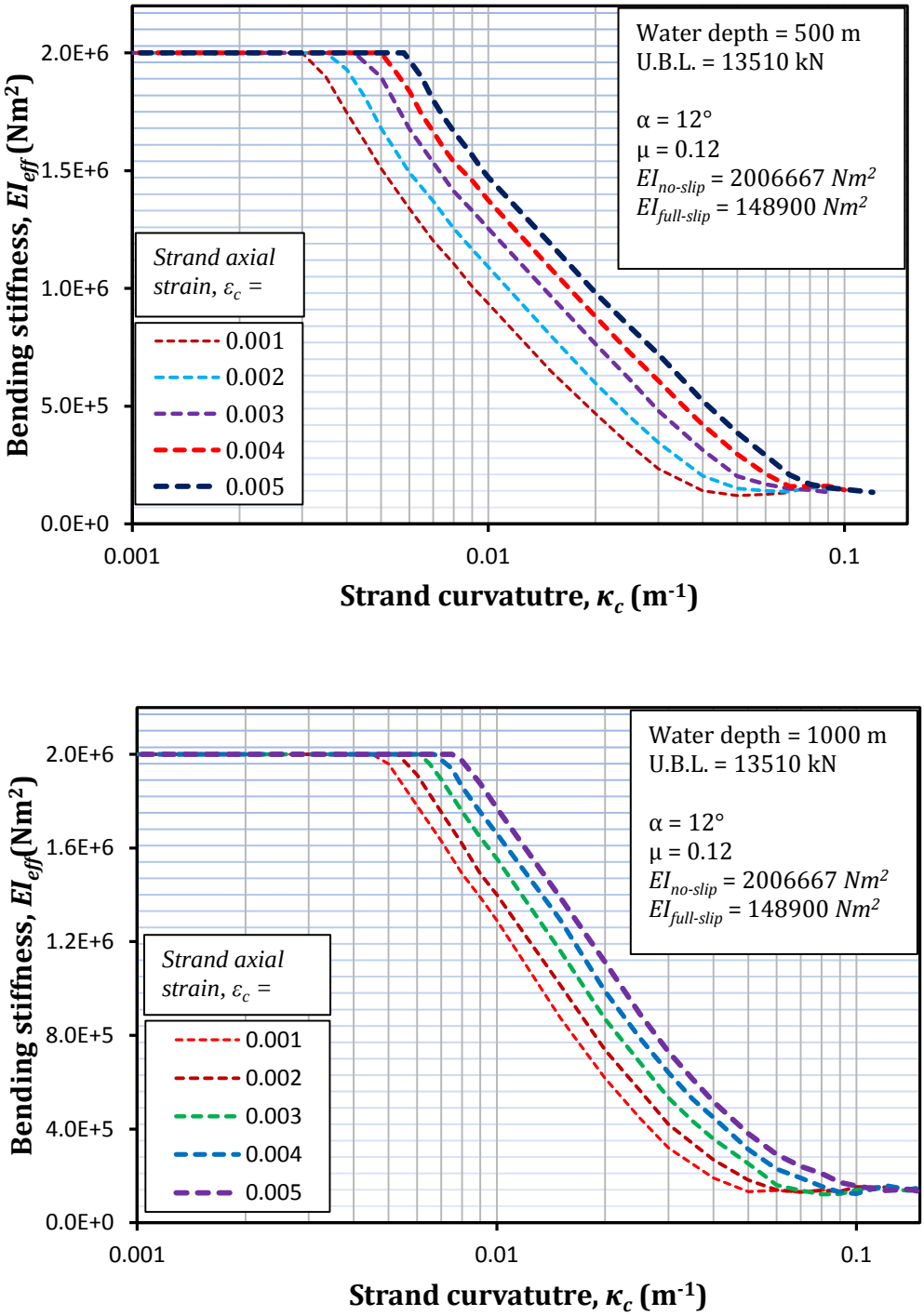

Figure 6-3 (a & b): Theoretical predictions of the variations in the flexural rigidity as a function of the bending curvature, for a 127 mm (α = 12°) outside diameter sheathed spiral strand subjected to an external hydrostatic pressure equivalent to water depth of (a) 500 m; and (b) 1000 m.

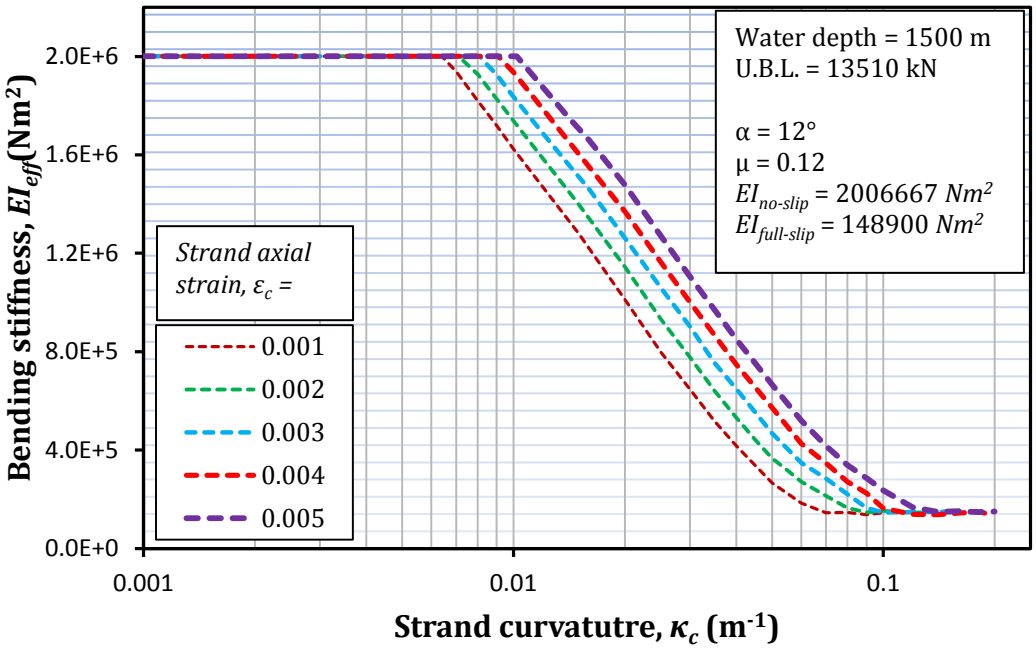

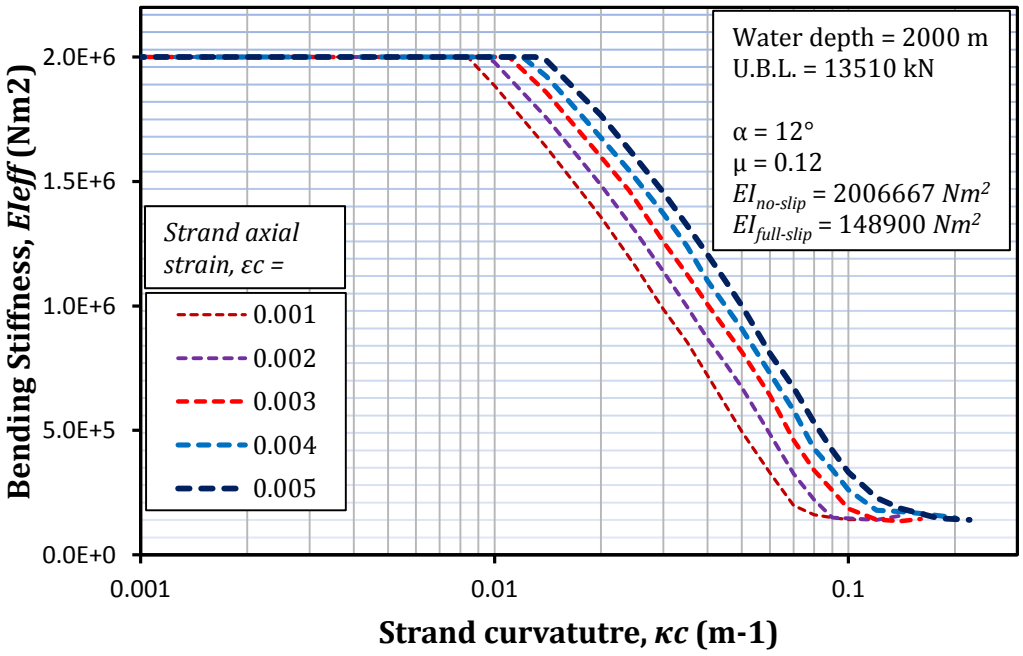

Figures 6.3 (c &d)- theoretical predictions of the variations in the flexural rigidity as a function of the bending curvature, for a 127 mm (α = 12°) outside diameter sheathed spiral strand subjected to an external hydrostatic pressure equivalent to water depth of (c) 1500 m; and (d) 2000 m.

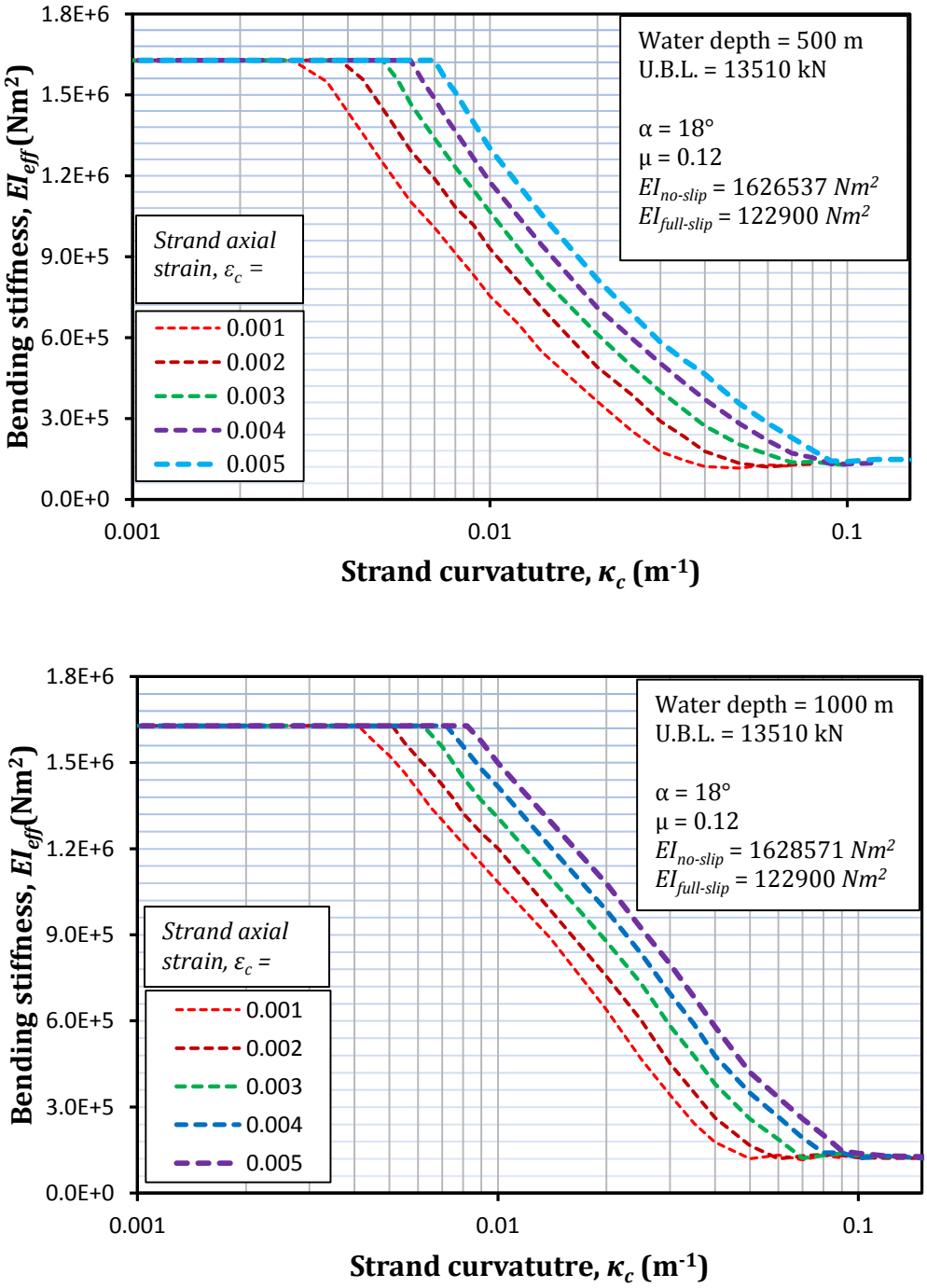

Figures 6.3 (e & f)- theoretical predictions of the variations in the flexural rigidity as a function of the bending curvature, for a 127 mm (α = 18°) outside diameter sheathed spiral strand subjected to an external hydrostatic pressure equivalent to water depth of (e) 500 m; and (f) 1000 m.

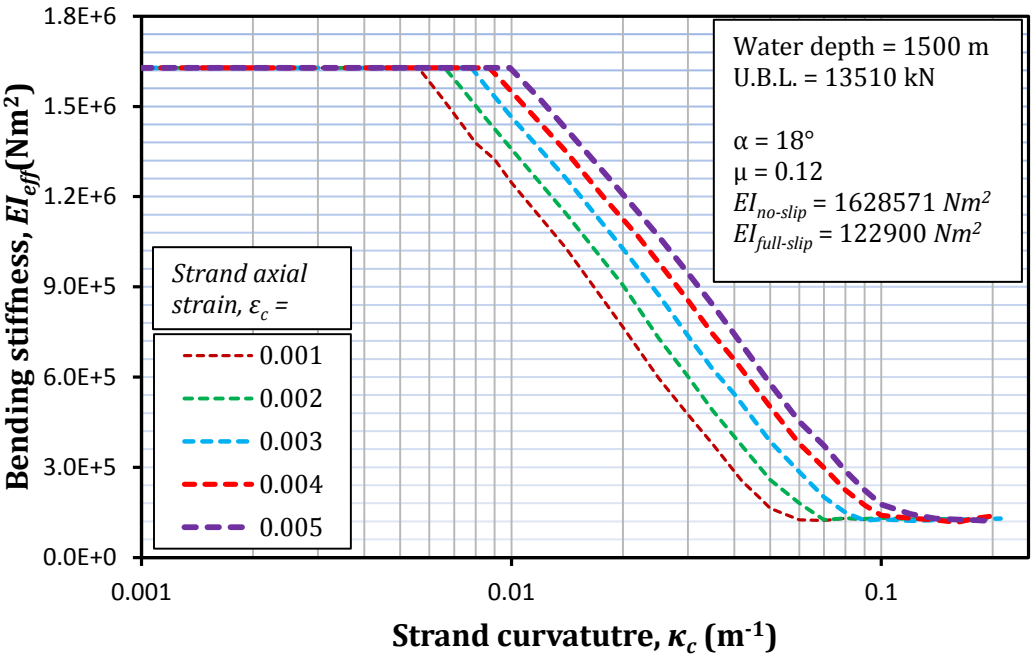

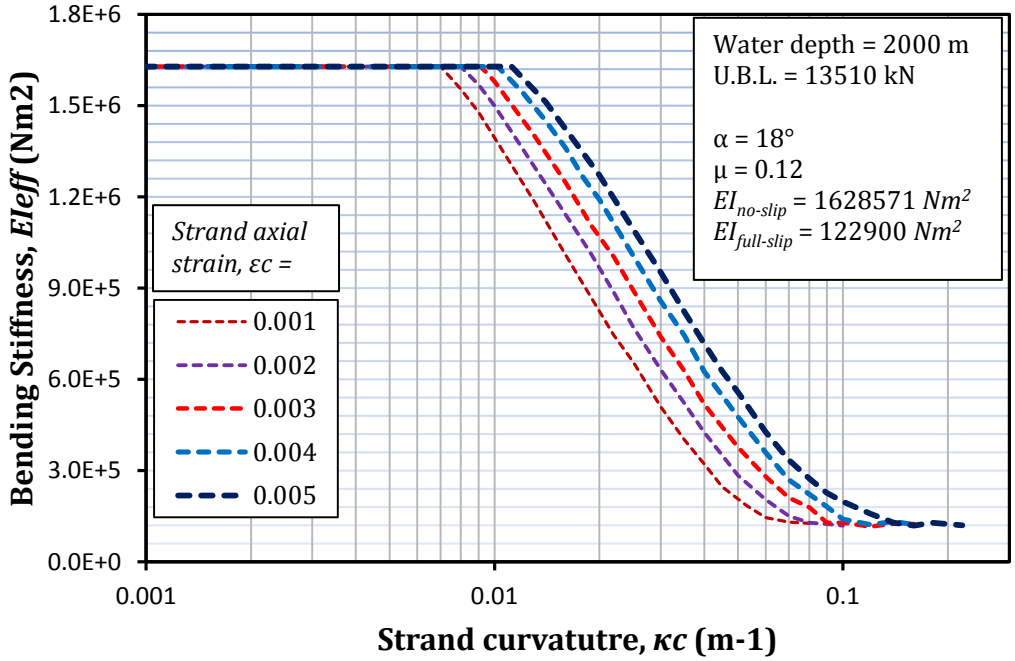

Figures 6.3 (g & h)- theoretical predictions of the variations in the flexural rigidity as a function of the bending curvature, for a 127 mm (α = 18°) outside diameter sheathed spiral strand subjected to an external hydrostatic pressure equivalent to water depth of (g) 1500 m; and (h) 2000 m.

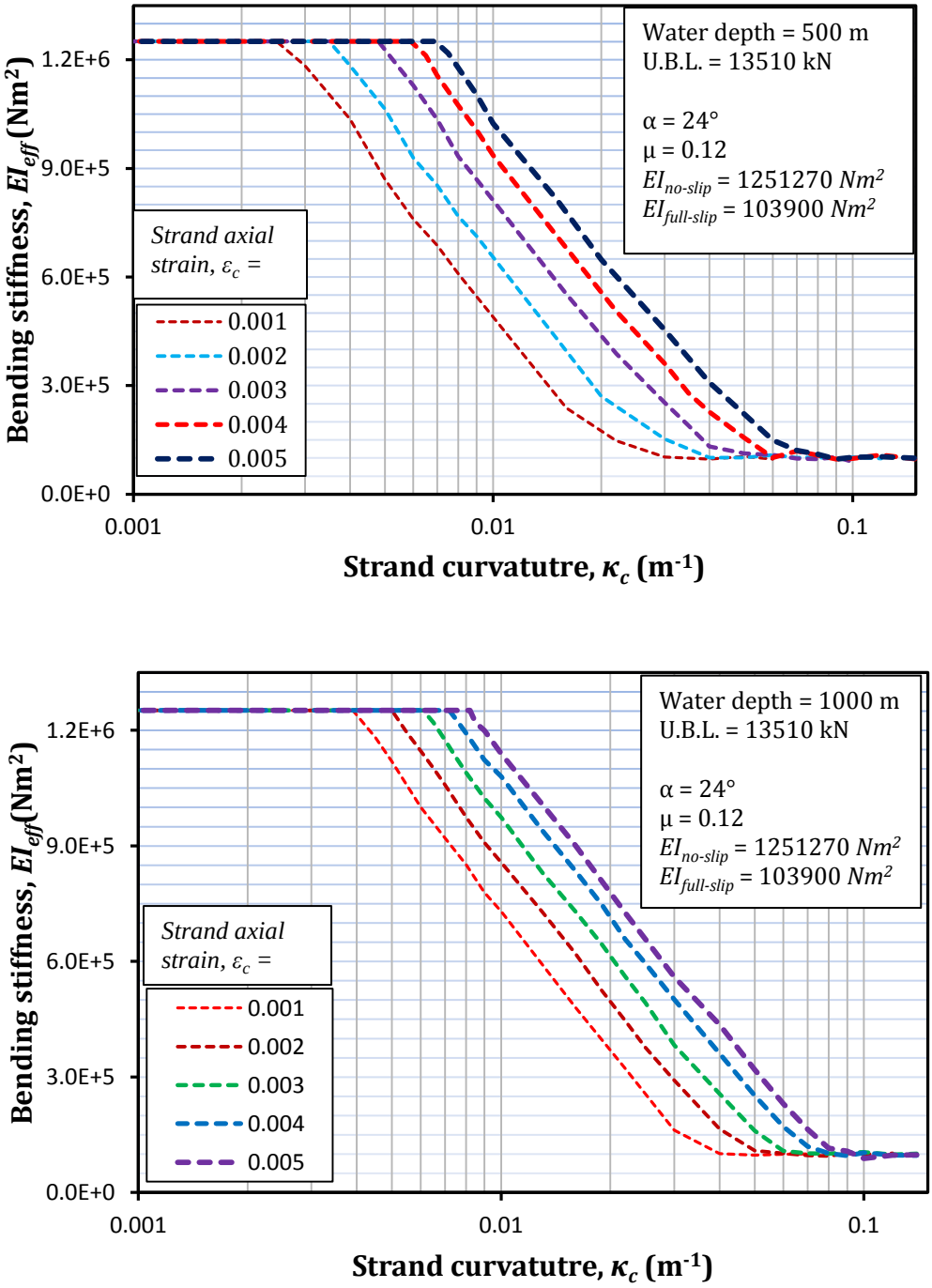

Figures 6.3 (i & j)- theoretical predictions of the variations in the flexural rigidity as a function of the bending curvature, for a 127 mm (α = 24°) outside diameter sheathed spiral strand subjected to an external hydrostatic pressure equivalent to water depth of (i) 500 m; and (j) 1000 m.

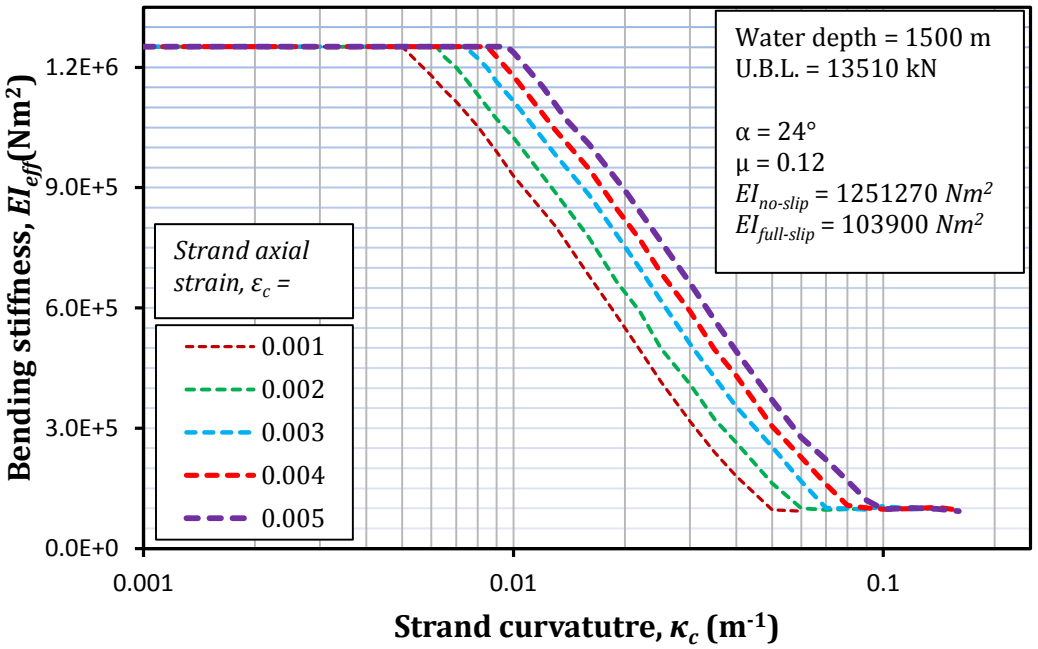

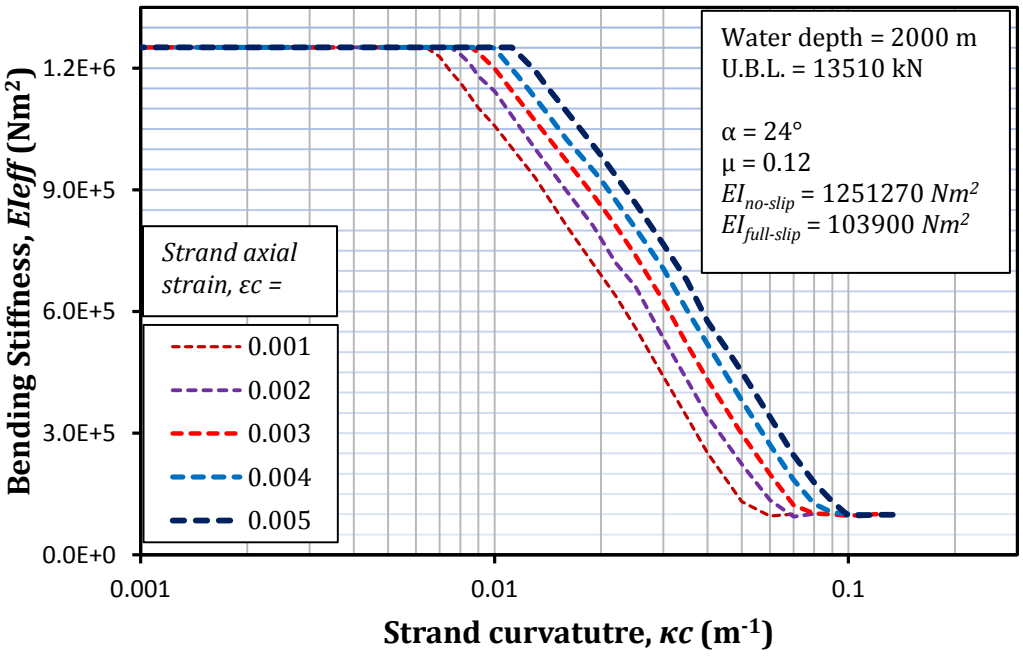

Figures 6.3 (*k* & *l*)- theoretical predictions of the variations in the flexural rigidity as a function of the bending curvature, for a 127 mm (α = 24°) outside diameter sheathed spiral strand subjected to an external hydrostatic pressure equivalent to water depth of (k) 1500 m; and (l) 2000 m; respectively

Figures 6.3 (a-d), (e-h) and (*i-l*) show the variation of the effective bending stiffness as a function of cable curvature for various water depths, for all the three different cable constructions of 127 mm diameter strands with lay angle of 12°, 18° and 24° respectively. For every strand four plots of the magnitude of this theoretically determined flexural rigidity are obtained when the sheathed strands are subjected to external hydrostatic pressures, equivalent to water depths of 500, 1000, 1500 and 2000 m respectively. The results clearly demonstrate that external pressures on sealed strands suppress the slippage of wires in the cable and, therefore bending stiffness of the strand remains at EI_{max} under large bending curvatures. Also, the no-slip and full-slip values of flexural rigidity are shown to be independent of the level of hydrostatic pressure. The no-slip (i.e. EI_{max}) bending stiffness values for above three strands are 2006667, 1620527 and 1254566 Nm^2 respectively. In the case of axial/torsional coupling the torsional rigidity of the sheath resists the unwinding of the cable and therefore the torsional stiffness of the cable increases. Unlike to the case of 0 m water depth (i.e. in atmospheric condition), the transition range of curvature between no-slip and full-slip states is found to be governed by the exact magnitude of the external hydrostatic pressure on the strand.

Based on the contact force distributions given Figures 6.4 (a-l), a careful examination of these plots reveals very interesting results. For water depths up to somewhere between 1000 m to 2000 m the overall bending stiffness for all the three strands starts degrading at approximately the same values of imposed curvature. This will lead the overall frictional energy dissipation the same for all the three strands. Furthermore, it is hoped that the knowledge of the magnitudes of bending stiffness and contact forces will be very useful in the fatigue life estimation of the cable. For increasing lay angle, as shown in Figures (a-l) the radial contact forces in the outer are greater than the inner layers, this will lead the fatigue life to the first outermost wire fractures to occur much earlier for larger lay angle.

Figures 6.4 (a-d) present simple plots for calculating the effective flexural stiffness for all the three sheathed strands subjected to water depths of 500 m, 1000 m, 1500 m and 2000 m respectively. After conducting a comprehensive theoretical parametric study, flexural rigidity of sheathed strands is found to be function of the axial load

perturbations and imposed bending curvature, for various levels of hydrostatic pressure on sheathed spiral strands in deep water applications. Thus in the present case of sheathed spiral strands, once again the reasonable estimate of the newly proposed parameter is sufficient for obtaining fairly accurate estimates of the effective flexural stiffness of the cable. As opposed to spiral strand in the air-conditions (i.e. 0 m water depth) for water depths up to 0-1000 m interwire slippage in the outer layers of all the three strands are found to start at approximately same bending curvature. For high levels of water depths (i.e. 1000 – 2000 m) wires in the outer layers of spiral strand with lay angle of 12° are found to stick together compared with the other two strands. Comparing the results in Figures 6.4 (a-d), the theoretical data is less scattered around the fitted curves when external hydrostatic pressure is considered, in contrast to the situation of 0 m water depth. For modest curvature, when all the wires in the cable are stuck together forming a solid rod, there is an upper bound limit of the new parameter given for these plots, i.e. 4. Beyond this value the simple plot developed is not applicable and if the value of the proposed parameter is greater than 4, the flexure rigidity of the cable will be at its maximum (i.e. EI_{max}).

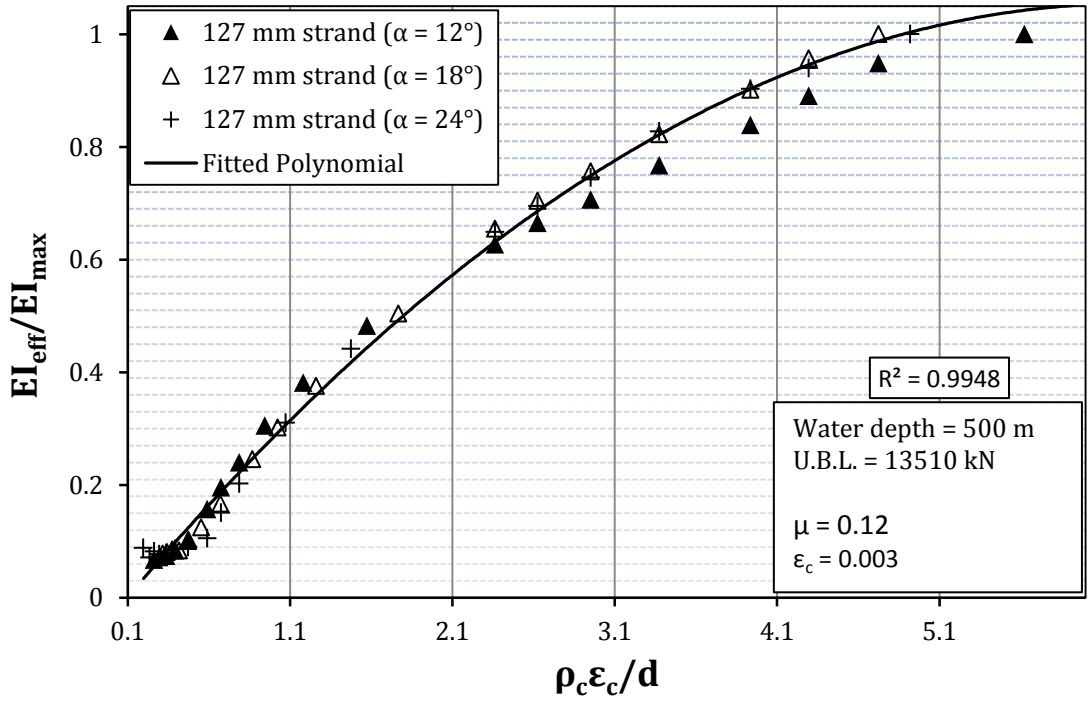

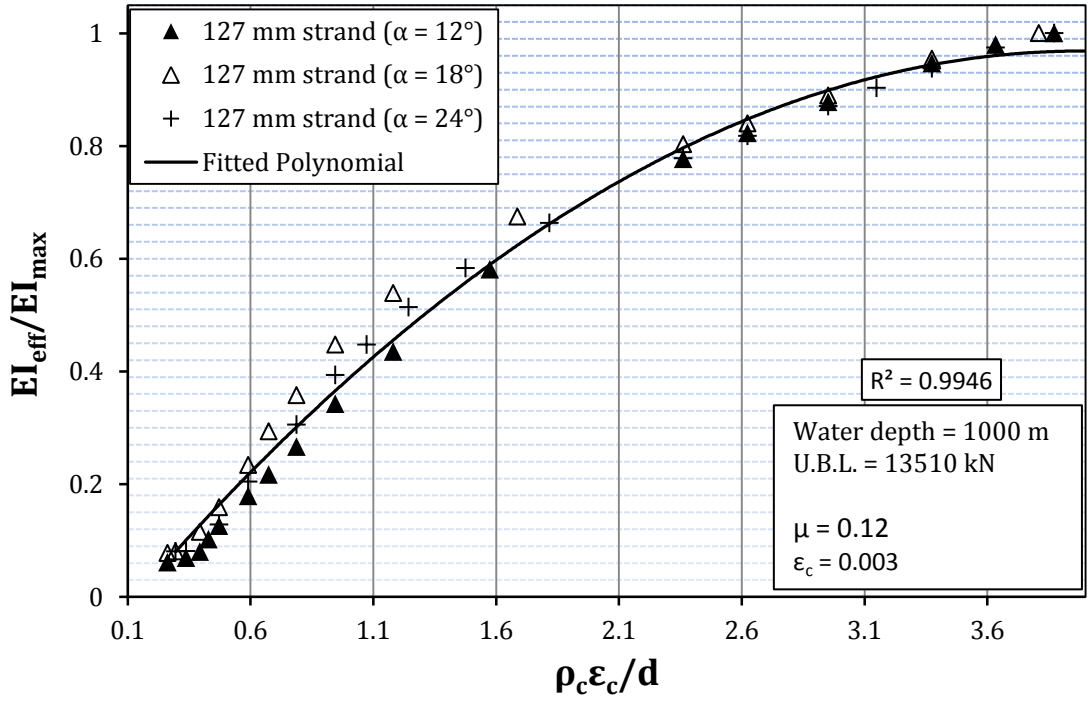

Figure 6-4 (a & b): Simple design curves for the estimation of the bending stiffness of the three 127 mm diameter strands having lay angles of 12, 18 and 24 respectively, subjected to an external hydrostatic pressure of (a) 500 m; (b) 1000m.

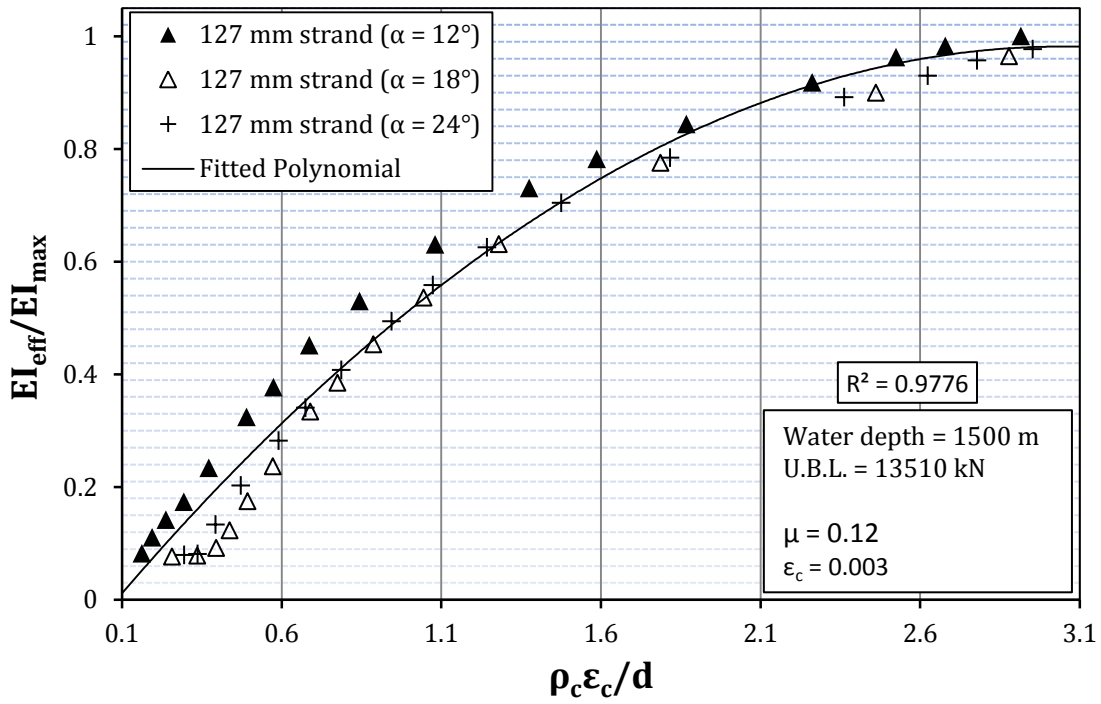

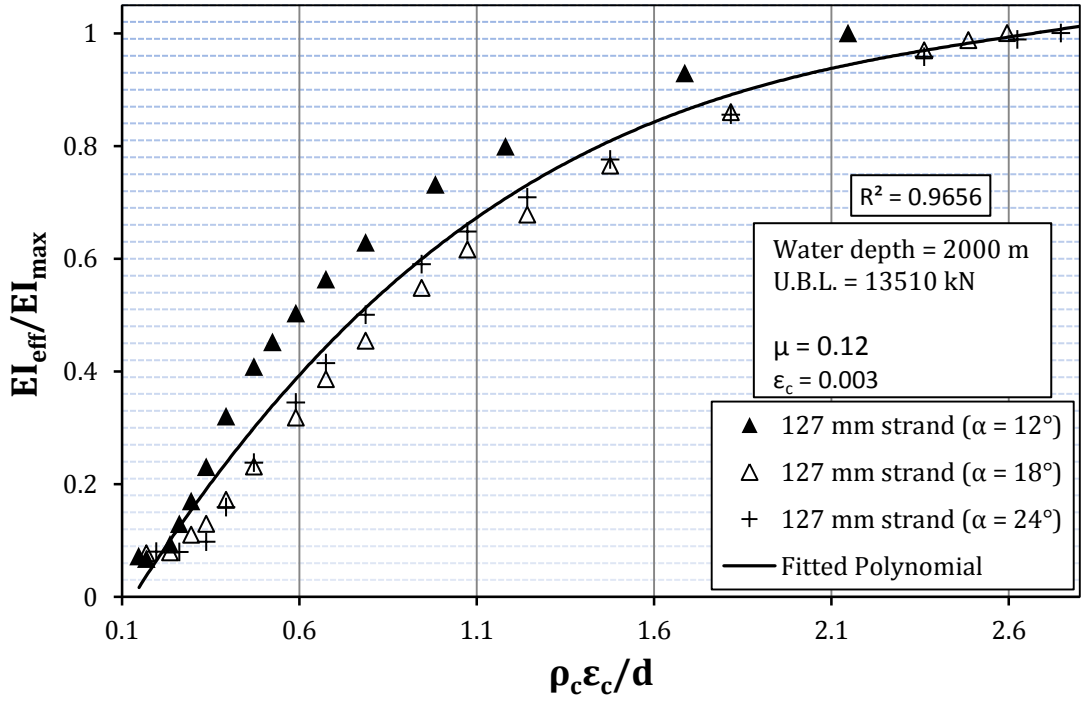

Figures 6.4 (c & d)-Simple design curves for the estimation of the bending stiffness of the three 127 mm diameter strands having lay angles of 12, 18 and 24 respectively, subjected to an external hydrostatic pressure of (c) 1500 m; (d) 2000m.

6.4 Simplified Routines for Calculating Flexural Rigidity of Sheathed Strand

As discussed in Chapter 5, the original formulations of the MHDS model for calculating bending stiffness of the cable are very complicated and unsuitable for everyday engineering applications. Therefore, a similar attempt as in Chapter 5 has been made to develop simplified routines for the analysis of sheathed spiral strands.

By carefully examining the numerical results, it is noticed that the effective bending stiffness of the cable is once again a non-linear function of the previously reported new parameter ($\rho_c\varepsilon_c/d$). As the external hydrostatic pressure increases, frictional forces between the wires increase, as a result wires start slipping at larger curvature in the presence of external pressures. This brings down the upper bound of the newly proposed dimensionless parameter for sheathed spiral strands from 10 (corresponding to 0 m water depth) to 4. After calculating this parameter, the so-obtained function for the bending stiffness of the cable may very nearly be expressed as a polynomial of the second degree of the general form:

$$\frac{EI_{eff}}{EI_{max}} = AX^2 + BX + C \tag{6.3}$$

where the constant coefficients A-C are given in Table 6.1 and each set of these coefficients correspond to the situations when the cables are subjected to different levels of water depths, 500 m $\leq$ h $\leq$ 2000 m. The correlation coefficients between the proposed polynomials and the calculated data are also given in Table 6.1, where the minimum correlation coefficient $R^2 = 0.9656$ is thought to be adequate for all practical purposes The fitted polynomials for Figures 6.4 (a-d) show that individual numerical results are almost independent of the level of hydrostatic pressure, for high levels of hydrostatic pressure (i.e. 1000 m and above) the values of the newly proposed parameter are slightly less than that for small hydrostatic pressure values (0 -1000 m).

Table 6-1: Values of the constant coefficients A-C in Eq. (6.3) for all the fitted curves in Figures 6.4 (a-d), along with correlation coefficients R^2.

Reference	Water depth (m)	A	B	C	R^2
Fig 6.4a	500	-0.0276	0.3465	-0.0331	0.9948
Fig 6.4b	1000	-0.0652	0.5198	-0.0672	0.9946
Fig 6.4c	1500	-0.1118	0.6809	-0.0555	0.9776
Fig 6.4d	2000	-0.184	0.8888	-0.0875	0.9656

Table 6-2a: Calculation routines of the newly proposed parameter and bending stiffness for an axial strain of 0.003 and external hydrostatic pressure equivalent to water depth, h = 500 m, using the Rigorous Method.

External Hydrostatic pressure on the srand equivalent to water depth, h = 500 m							
Strand outside diameter, d (m)	**Lay angle, α_i (°)**	**Strand axial strain, ε_c**	**Strand curvature, κ_c (m^{-1})**	**Radius of curvature, ρ_c (m)**	**$\rho_c\varepsilon_c/d$**	**Effective bending stiffness, EI_{eff} (Nm^2)**	**EI_{eff}/EI_{max}**
0.127	12	0.003	0.0042	238.10	5.6243	2000285	1
0.127	12	0.003	0.0055	181.82	4.2949	1782000	0.8909
0.127	12	0.003	0.007	142.86	3.3746	1535000	0.7674
0.127	12	0.003	0.009	111.11	2.6247	1330000	0.6649
0.127	12	0.003	0.015	66.67	1.5748	965800	0.4828
0.127	12	0.003	0.025	40.00	0.9449	611600	0.3058
0.127	12	0.003	0.035	28.57	0.6749	391200	0.1956
0.127	12	0.003	0.07	14.29	0.3375	149100	0.0745
127 mm diameter strand with lay angle, α_i = 18°							
0.127	18	0.003	0.005	200.00	4.7244	1628576	1
0.127	18	0.003	0.006	166.67	3.937	1468000	0.9014
0.127	18	0.003	0.008	125.00	2.9528	1232000	0.7565
0.127	18	0.003	0.01	100.00	2.3622	1065999	0.6546
0.127	18	0.003	0.02	50.00	1.1811	611833	0.3757
0.127	18	0.003	0.03	33.33	0.7874	400200	0.2457
0.127	18	0.003	0.05	20.00	0.4724	203200	0.1248
0.127	18	0.003	0.065	15.38	0.3634	127000	0.0780
127 mm diameter strand with lay angle, α_i = 24°							
0.127	24	0.003	0.0048	208.33	4.9213	1251200	1
0.127	24	0.003	0.006	166.67	3.937	1130000	0.9031
0.127	24	0.003	0.008	125.00	2.9528	933000	0.7457
0.127	24	0.003	0.01	100.00	2.3622	811999	0.6490
0.127	24	0.003	0.016	62.50	1.4764	553000	0.4420
0.127	24	0.003	0.03	33.33	0.7874	253200	0.2024
0.127	24	0.003	0.06	16.67	0.3937	101200	0.0809

Table 6.2b- Calculation routines of the newly proposed parameter and bending stiffness for an axial strain of 0.003 and external hydrostatic pressure equivalent to water depth, h = 1000 m, using the Rigorous Method.

External Hydrostatic pressure on the srand equivalent to water depth, h = 1000 m							
Strand outside diameter, d (m)	**Lay angle, α_i (°)**	**Strand axial strain, ε_c**	**Strand curvature, κ_c (m^{-1})**	**Radius of curvature, ρ_c (m)**	**$\rho_c\varepsilon_c/d$**	**Effective bending stiffness, EI_{eff} (Nm^2)**	**EI_{eff}/EI_{max}**
0.127	12	0.003	0.0061	163.93	3.872	2000666	1
0.127	12	0.003	0.009	111.11	2.625	1646000	0.8228
0.127	12	0.003	0.012	83.33	1.969	1383456	0.6915
0.127	12	0.003	0.015	66.67	1.575	1162400	0.5810
0.127	12	0.003	0.02	50.00	1.181	870000	0.4349
0.127	12	0.003	0.025	40.00	0.945	684800	0.3423
0.127	12	0.003	0.035	28.57	0.675	434200	0.2170
0.127	12	0.003	0.05	20.00	0.472	252000	0.1260
0.127	12	0.003	0.08	12.50	0.295	141100	0.0705
127 mm diameter strand with lay angle, α_i = 18°							
0.127	18	0.003	0.0062	161.29	3.810	1628576	1
0.127	18	0.003	0.008	125.00	2.953	1468000	0.9019
0.127	18	0.003	0.01	100.00	2.362	1308000	0.8036
0.127	18	0.003	0.014	71.43	1.687	1098250	0.6748
0.127	18	0.003	0.02	50.00	1.181	877333	0.5390
0.127	18	0.003	0.03	33.33	0.787	582600	0.3580
0.127	18	0.003	0.04	25.00	0.591	380400	0.2337
0.127	18	0.003	0.06	16.67	0.394	187700	0.1153
0.127	18	0.003	0.08	12.50	0.295	121100	0.0744
127 mm diameter strand with lay angle, α_i = 24°							
0.127	24	0.003	0.0061	163.93	3.872	1251794	1
0.127	24	0.003	0.008	125.00	2.953	1089999	0.8707
0.127	24	0.003	0.013	76.92	1.817	830000	0.6630
0.127	24	0.003	0.019	52.63	1.243	643333	0.5139
0.127	24	0.003	0.025	40.00	0.945	492666	0.3936
0.127	24	0.003	0.04	25.00	0.591	256000	0.2045
0.127	24	0.003	0.07	14.29	0.337	101700	0.0812

Table 6.2c- Calculation routines of the newly proposed parameter and bending stiffness for an axial strain of 0.003 and external hydrostatic pressure equivalent to water depth, h = 1500 m, using the Rigorous Method.

External Hydrostatic pressure on the srand equivalent to water depth, h = 1500 m							
Strand outside diameter, d (m)	**Lay angle, α_i (°)**	**Strand axial strain, ε_c**	**Strand curvature, κ_c (m^{-1})**	**Radius of curvature, ρ_c (m)**	**$\rho_c\varepsilon_c/d$**	**Effective bending stiffness, EI_{eff} (Nm^2)**	**EI_{eff}/EI_{max}**
0.127	12	0.003	0.0081	123.46	2.9163	2000666	1
0.127	12	0.003	0.012	83.33	1.9685	1646000	0.8227
0.127	12	0.003	0.02	50.00	1.1811	1261500	0.6305
0.127	12	0.003	0.03	33.33	0.7874	903000	0.4513
0.127	12	0.003	0.04	25.00	0.5906	649000	0.3244
0.127	12	0.003	0.06	16.67	0.3937	347600	0.1737
0.127	12	0.003	0.1	10.00	0.2362	146800	0.0734
127 mm diameter strand with lay angle, α_i = 18°							
0.127	18	0.003	0.0078	128.21	3.0285	1628571	1
0.127	18	0.003	0.014	71.43	1.6873	1262000	0.7749
0.127	18	0.003	0.025	40.00	0.9449	873000	0.5361
0.127	18	0.003	0.035	28.57	0.6749	626800	0.3849
0.127	18	0.003	0.05	20.00	0.4724	385500	0.2367
0.127	18	0.003	0.07	14.29	0.3375	200500	0.1231
0.127	18	0.003	0.09	11.11	0.2625	123500	0.0758
127 mm diameter strand with lay angle, α_i = 24°							
0.127	24	0.003	0.0074	135.14	3.1922	1252000	1
0.127	24	0.003	0.013	76.92	1.8171	981666	0.7841
0.127	24	0.003	0.019	52.63	1.2433	782666	0.6251
0.127	24	0.003	0.025	40.00	0.9449	618666	0.4941
0.127	24	0.003	0.035	28.57	0.6749	426600	0.3407
0.127	24	0.003	0.05	20.00	0.4724	253400	0.2024
0.127	24	0.003	0.08	12.50	0.2953	99500	0.0795

Table 6.2d- Calculation routines of the newly proposed parameter and bending stiffness for an axial strain of 0.003 and external hydrostatic pressure equivalent to water depth, h = 2000 m, using the Rigorous Method.

External Hydrostatic pressure on the srand equivalent to water depth, h = 2000 m							
Strand outside diameter, d (m)	**Lay angle, α_i (°)**	**Strand axial strain, ε_c**	**Strand curvature, κ_c (m^{-1})**	**Radius of curvature, ρ_c (m)**	**$\rho_c\varepsilon_c/d$**	**Effective bending stiffness, EI_{eff} (Nm^2)**	**EI_{eff}/EI_{max}**
0.127	12	0.003	0.011	90.91	2.147	2000470	1
0.127	12	0.003	0.02	50.00	1.181	1598833	0.7992
0.127	12	0.003	0.03	33.33	0.787	1258166	0.6289
0.127	12	0.003	0.04	25.00	0.591	1006500	0.5031
0.127	12	0.003	0.05	20.00	0.472	816200	0.4080
0.127	12	0.003	0.06	16.67	0.394	640300	0.3201
0.127	12	0.003	0.08	12.50	0.295	339200	0.1696
0.127	12	0.003	0.12	8.33	0.197	141700	0.0708
127 mm diameter strand with lay angle, α_i = 18°							
0.127	18	0.003	0.0091	109.89	2.596	1628571	1
0.127	18	0.003	0.013	76.92	1.817	1400333	0.8599
0.127	18	0.003	0.019	52.63	1.243	1104000	0.6779
0.127	18	0.003	0.025	40.00	0.945	892333	0.5479
0.127	18	0.003	0.035	28.57	0.675	628599	0.3860
0.127	18	0.003	0.05	20.00	0.472	376400	0.2311
0.127	18	0.003	0.07	14.29	0.337	210300	0.1291
0.127	18	0.003	0.1	10.00	0.236	128200	0.0787
127 mm diameter strand with lay angle, α_i = 24°							
0.127	24	0.003	0.0086	116.28	2.747	1251406	1
0.127	24	0.003	0.013	76.92	1.817	1070666	0.8556
0.127	24	0.003	0.019	52.63	1.243	887000	0.7088
0.127	24	0.003	0.03	33.33	0.787	626200	0.5004
0.127	24	0.003	0.04	25.00	0.591	431600	0.3449
0.127	24	0.003	0.06	16.67	0.394	198800	0.1589
0.127	24	0.003	0.09	11.11	0.262	99500	0.0795

Tables 6.2 (a-d) present a summary of the calculation routines of the newly proposed parameter for the simple method for all the three cable constructions. A summary of the final estimates of the flexural rigidity of the cable under varying cable curvature for water depths of 500 m, 1000 m, 1500 m and 2000 m are reported in these tables. This has been done using the original formulations as presented in chapter 4, catering for the effects of external hydrostatic pressures. The numerical results in these tables are used to develop a simple curve for the estimation of the bending stiffness of sheathed spiral strands. A comparison of the results based on simplified method and actual theory demonstrates the reasonable accuracy of the proposed simplified method for different levels of water depths and mean axial loads. Also, a careful examination these results suggest that under deep water applications slippage pattern for all the three strands are almost similar.

6.5 **Discussion**

The smooth transition of the bending stiffness of multi-layered sheathed spiral strands from no-slip to full-slip can be now calculated using simplified routines. Spiral strands used in deep water applications are subjected to relatively small load disturbances superimposed on a given strand tension force. A knowledge of the exact magnitude of the cable bending stiffness will also prove useful in the estimation of the natural frequencies of the structure supported by cables. The significant increase in the interwire/interlayer contact forces suggests that applying external hydrostatic pressure to sheathed spiral strands can result in a significant reduction in their axial fatigue life, which may have a significant effect on the estimated operational life span of the structures used in deep water applications. The newly proposed simple parameter may prove very useful as regards the dynamic response of an offshore platform or a cable stayed structure.

The calculated numerical results are found very close to the fitted polynomial for small levels of water depths up to 1000 m. For water depths above 1000 m the results showed slightly scatter around the fitted curves with a maximum scatter for 2000 m water depth. As opposed to the case of in air-condition (0 m water depth) the calculated bending stiffness values for cables with larger lay angles (i.e. 24°) are

noticed to be higher than the value predicted by simple method. Similarly, cables having small lay angles (i.e. 12°) are found to give lower value than the predicted value of the simple method. The overall scatter of the data around the fitted curves is noted to depend on the level of external hydrostatic pressure. For all the three strands subjected to different levels of external hydrostatic pressures, there appears to be a slight difference between the constant coefficients for the polynomial of general form given in Table 6.1.

6.6 Conclusion

By using an extensive series of theoretical parametric studies, simplified routines are proposed for obtaining the magnitudes of the effective flexural stiffness of sheathed spiral strand subjected to various levels of water depths. The sheathed strands in this study covers a wide range of strand construction details, levels of mean axial strains, and magnitudes of water depth. This has been done by extending the previously reported MHDS model, to cater for the effects of external hydrostatic pressure on sheathed spiral strands, which greatly influence the pattern of contact forces between wires in the strand. For a given mean axial strain, increasing the level of external hydrostatic pressure on sheathed spiral strand increases significantly the contact forces in the outer layers. It should be also pointed out that increasing the lay angle causes a reduction in the radial load transfer to the inner layers.

The results presented in this chapter should prove to be of great value in providing an insight into the bending behavior of sheathed spiral strands. Reliable estimates of the bending stiffness for use in connection with fatigue life estimation and hydrodynamic instability calculations. Meanwhile, the application of this idea need to be tested by more experiments and simulations.

Chapter 7

Predictions of the Bending Characteristics of Locked Coil Cables

7.1 Introduction.

The available strand constructions in the literature are normally made up exclusively of round wires and considerably less attention has been paid to the strands composed of shaped wires. Locked coil cables are cable constructions with one or more outer layers made up of of shaped (S and Z sections) wires which make it fully or partially lock. These types of configuration makes an important role in holding the cable together during bending cycle as well as improve its resistance to corrosion in deep water application. Furthermore, the smooth surfaces of locked coil cables enhanced the wearing properties compared to cables with round wires. The shaped wires in the outer layer have a genuine surface contact at the anchorages, as opposed to the point contact between intersecting wires in the case of round wire cables. However, there are few drawbacks associated with this type of cable construction: firstly it makes the visual inspection of the inner layers of the cable very difficult. Secondly, the strength to weight ratio and the flexibility of the cable is reduced significantly. For example for a wire of the same cross-sectional area Timiney et al., (1995) has shown small tensile grades of (1270-1370 N/mm^2) for fully locked wires compared with 1770-1860 N/mm^2 for round wires).

Both on the experimental and theoretical side, there is very little information available on locked coil cables. Although, locked coil cables are extensively used both by offshore and onshore industry; as hoisting ropes in mine shafts, stays for cable stayed bridges and guyed masts and tractive element in cable cars. Oplatka and Roth (1991) reported some experimental results on locked coil cables, investigating the bending fatigue characteristics at the end termination. Kopanakis (1992) and Gabriel (1993) also studied the bending fatigue phenomenon in the locked cables.

Fontanari (2009) studied the fire behaviour of the axially preloaded full locked coil ropes. The numerical and experimental results were obtained for two distinct full-locked coil ropes. Heat fluxes, temperature fields in the rope cross-section and fire endurance times were determined to establish how wires mechanical properties change with temperature. Subsequently, FE analysis were carried out to correctly model the mechanical behaviour of the rope at different temperatures and to predict the load redistribution during test among different layers.

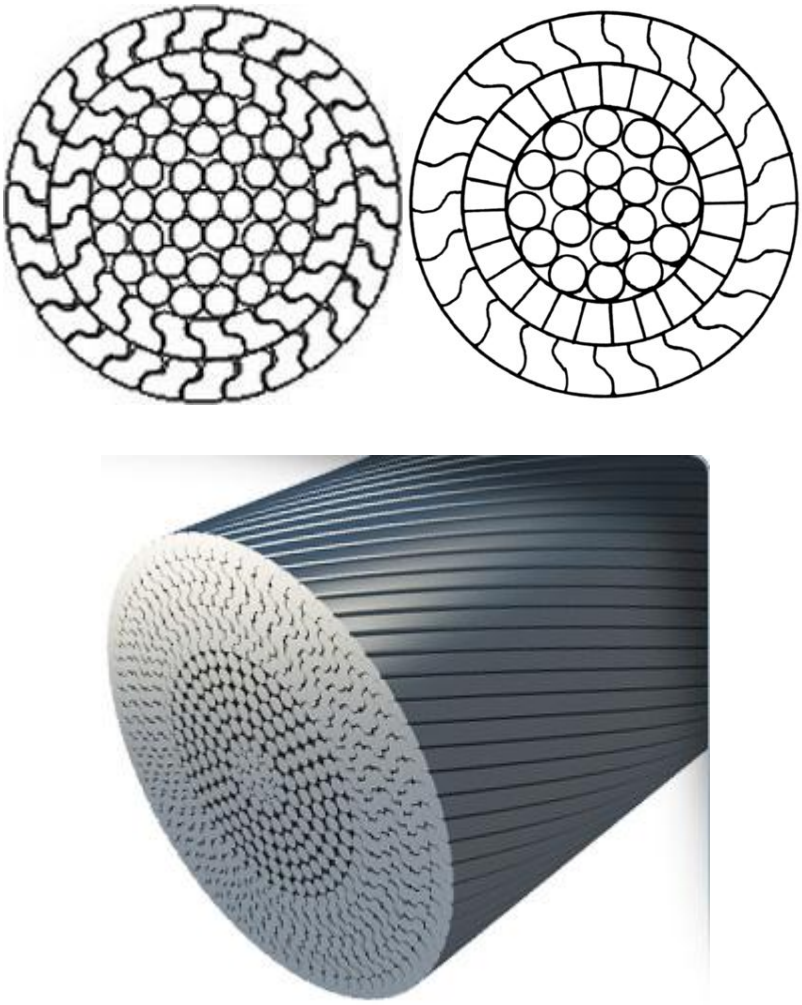

Figure 7-1: Typical locked coil cable constructions

7.2 Theory

As discussed earlier, the orthotropic sheet model is based on the assumption that each layer of wires in the strand can be represented by an equivalent orthotropic sheet in which the elastic properties in direction parallel and perpendicular to a wire axes are different. The approach is felt to be even more appropriate for modeling the layers of locked coil cables which very closely resembles the sheets of steel. In the case of round wire layers, the equivalent sheet stiffness in the direction perpendicular to the wire axes were estimated from the equations of contact mechanics. In the present case of locked coil cables, it is taken as equal to the value of Young's modulus of wire material. Thus the orthotropic sheet approach has been used to assess interwire contact forces and deformations in the locked coil cables. The mechanical characteristics of the locked coil cables subjected to tension and bending have been discussed in this chapter.

7.2.1 Cable Geometry

The nomenclature of the cable will remain the same as discussed in Chapter 3 for round wire cable, likewise a locked coil cable is considered as consisting of N layers and a core wire, with N_N being the outermost layer made up of shaped wires. Therefore, the formulations for the shaped wires in the outer layers will be changed accordingly. In the layers with shaped wires, the helix radius, r_i can be calculated as:

$$r_N = r_{N-1} + {}^{t_{N-1} + t_N}/_2 \tag{7.1}$$

where, the outermost layer is denoted by N with t_N and t_{N-1} being the thickness of the outermost and penultimate layers. The helix radii of the round wire in the inner layers are calculated as given in chapter 3, Eq. (3.31). The net steel area, A^S_{net} of a layer with shaped wires, is then given by:

$$A^S_{net,i} = 2\pi r_i t_i \qquad\qquad i = N, N-1 \tag{7.2}$$

In Eq. (7.2) r_i and t_i represents the helix radius and thickness of the layer respectively and the net steel area of a layer with round wires can be calculated by as:

$$A_{net,i}^{R} = n_i \frac{\pi D_i^2}{4 \cos \alpha_i} \tag{7.3}$$

Assuming that the core consists of a single wire of diameter, D_c, the net steel area of the locked coil cable, A_{net}can be estimated from:

$$A_{net} = \frac{\pi}{4} D_c^2 + \sum_{i=N-1}^{N} A_{net,i}^{S} + \sum_{i=1}^{N-1} A_{net,i}^{R} \tag{7.4}$$

7.2.2 Wire Kinematics and Contact Forces

In the orthotropic sheet model approach a strand consisting of a core and N layers of helical wires is mathematically represented by N concentric orthotropic cylinders, whose mechanical properties are averaged to as a continuum to match the behaviour of their corresponding layer of wires. As the kinematic relations of this approach are applicable for any shape wires, therefore the kinematics equations previously derived for round wires can be used for the layers with shaped wires. Therefore, the eight compatibility equations defining wire kinematics in spiral strands with round wires listed in Chapter 3 [Eq. (3.27), (3.30), (3.34)-(3.39)] can be used for locked coil cables.

However, the load transfer pattern from the outer layers to the inside is different. The radial force X_{RC_i}acting as a body force due to the tension force in the wires in *i*th layer, assuming that the wire axial strain ϵ_x is known Hruska's (1952):

$$X_{RC_i} = E \epsilon_x \frac{\sin^2 \alpha_i}{r_i \cos \alpha_i} \frac{2\pi r_i t_i}{n_i} \tag{7.5}$$

In Eq. (7.5), E is the Young modulus of the wire material, r_i and t_i are the helix radius and thickness of wires in the ith layer respectively and n_i is the number of wires in layer i. If however the locked coil cable is experiencing water pressure from outside, the magnitude of the radial load transfer force, X_{R_i} corresponding to the previously calculated radial loads can be given as:

$$X_{R_i} = \rho_w g h \frac{2\pi}{n_i} \left(r_i + \frac{t_i}{2} \right) \tag{7.6}$$

where, ρ_w is the density of water, g is the gravitational acceleration, h is the depth of water and n_i is the number of wires in ith layer. The radial force per unit length of shaped wires in an axially preloaded multi-layered assembly X_{MS_i}can be found then:

$$X_{MS_i} = X_{RC_i} + \rho_w g h \frac{2\pi}{n_i} \left(r_i + \frac{t_i}{2}\right) \tag{7.7}$$

If there is no external hydrostatic pressure acting on the cable and the cable is composed only a single layer of shaped wires as shown in Table 7.1 (a), then the radial load due to the tension force in the wires will transfer from the layer of the shaped wires according to Eq. (7.5) and the rest of the strand will be analyzed as discussed in Chapter 3.

The magnitude of the circumferential contact force, P_{RC_i} for the shaped wire layer is given by Raoof and Hobbs (1988b):

$$P_{RC_i} = E\epsilon_{yi}t_i \tag{7.8}$$

where, ϵ_{yi} is the normal strain between the centres of the two adjacent wires in line contact. The values of both ϵ_{xi} and ϵ_{yi} can be obtained by solving the set of the compatibility equations [Eq. (3.27), (3.30), (3.34)-(3.39)], for a chosen value of the strand axial strain, ε_c.

The axial and circumferential stresses σ'_x and σ'_y respectively, acting in the *i*th layer of a shaped wire strand under axial strain ε_c:

$$\sigma'_{xi} = E\epsilon_{xi}\cos\alpha_i \tag{7.9}$$

And $$\sigma'_{xi} = E\epsilon_{yi} \tag{7.10}$$

where, *i = N*, *N-1*, for the present strand constructions as given in Tables 7.1 (a & b) where the strand consists only the outer one or two layers are made up of shaped wires.

Using Eqs. [(7.5)-(7.7)], the radial and circumferential contact forces in the outer or the penultimate layer of the locked coil cables with outermost or penultimate layers

made up of shaped wires and inner layers made up of round wires. After the calculations of contact forces X_{RC_i} and P_{RC_i}, in the layers of shaped wires, the magnitude of the hoop direction force, P_{MS_i}, considering the effect of all outer layers taken into account, can be calculated from the knowledge of the corresponding radial force, X_{MS_i}. In the inner layers with round wires, the calculation of contact forces both in radial and hoop directions are calculated the same way as already presented in Chapter 3.

7.2.3 Orthotropic Sheet Compliances for Shaped Wire Layer

The equations defining the compliances for layers of round wires have already been given in Chapter 3, Eqs. [(3.50)-(3.53)]. In the present case of shaped wires, the compliances in the direction of wire axes ϵ_{11}, perpendicular ϵ_{22}, and coupled compliance, ϵ_{12} are the functions of the Young's modulus and Poisson's ratio of the wire material, whereas the tangential compliance ϵ_{33}, varies from no-slip to full-slip, when the interwire friction is being overcome with a full sliding taking place between the wires in line contact.

For a layer of shaped wires, the compliances in the directions parallel and perpendicular to the wire axes that are different from the layer of round wires [(3.50)-(3.53)] are given as:

$$\epsilon_{11} = \epsilon_{22} = \frac{1}{E} \tag{7.11}$$

$$\epsilon_{12} = -\upsilon\epsilon_{11} \tag{7.12}$$

In Eq. (7.11) and (7.12), E and υ is the Young modulus and Poisson's ratio of the wire material. As in the case of shaped wires, contact is achieved across the full width of the layer and unlike to the case of round wire layers, there is no accommodation made for the gaps between the wires in the layer while calculating the axial and normal compliances for the layer. The tangential compliance $\epsilon_{33} \rightarrow \infty$, as in the case of shaped wires, there is no gradual increases in the full-slip area and full sliding can be assumed to take place over the full width of the contact regions for the whole range of the tangential loads. The transformation of the orthotropic sheet compliances into the

direction of strand principal axes follows the same procedure as given in Chapter 3, Eqs. 3.48 (a-f).

7.3 Results and Discussion

Table 7-1a: Construction details of a locked coil cable of 31 mm outside diameter.

Layer No	Number of Wires (n)	Lay Direction	Size of Wires (mm)	Shape of Wires	Lay Angle α_i (°)	Helix Radius r_i (mm)	Net Steel Area A_n(mm^2)	Gross Steel Area A_n (mm^2)
1	28	RH	3.5 (= t)	Z	19.79	13.71	301.538	383.88
2	24	LH	2.65 (=D)	R	17.49	10.64	132.388	168.54
3	18	RH	2.65	R	16.1	7.93	99.291	126.41
4	12	LH	2.65	R	16.81	5.33	66.194	84.27
5	6	RH	2.65	R	18.55	2.76	33.097	42.14
King	1	-	3	R	-	-	7.070	-

Table 7-1b: Construction details of a locked coil cable of 62 mm outside diameter.

Layer No	Number of Wires (n)	Lay Direction	Size of Wires (mm)	Shape of Wires	Lay Angle α_i (°)	Helix Radius r_i (mm)	Net Steel Area A_n(mm^2)	Gross Steel Area A_n (mm^2)
1	39	RH	5.21 (= t)	Z	14	28.22	923.913	1176.210
2	17/17	LH	5.08x3.05/5 (=D)	half lock/round	14	23.77	541.000	688.733
3	10,4/14	RH	5.08x2.54 5.08x3.05/5 (=D)	half lock/round	14	18.49	425.000	541.057
4	18	LH	4.40 (=D)	R	14	13.75	273.731	348.480
5	12	RH	4.4	R	14	9.35	182.487	232.320
6	6	LH	4.4	R	14	4.95	91.244	116.160
King	1	-	5.5	R	-	-	23.761	-

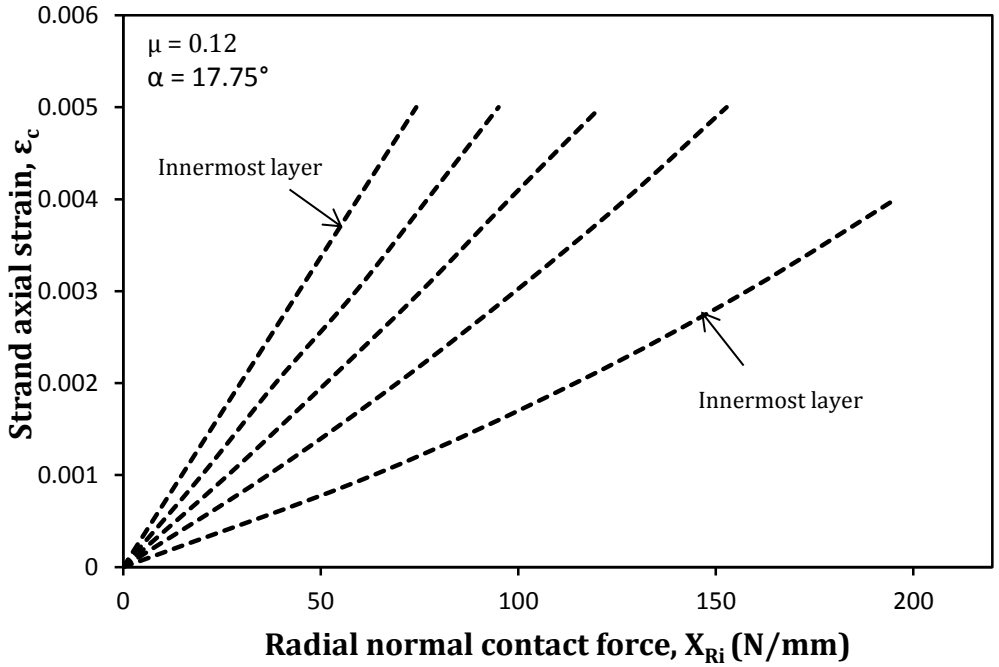

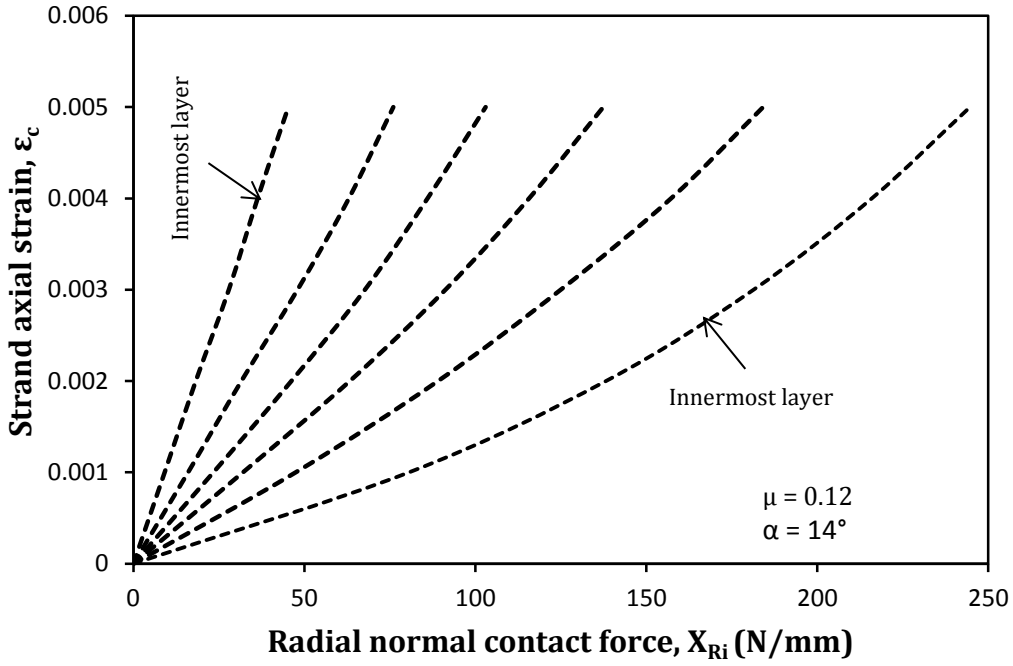

Figure 7-2 (a & b): Interlayer radial contact force in all the layers of two different locked coil cables of (a) 31 mm and; (b) 62 mm diameters.

The construction details of the two locked coil cables used in the present analysis are given in Tables 7.1 (a & b). These cables consist of several layers, having two external layers of shaped helical wires. The 31 mm locked coil cable consists of four layers of round wires and one outer layer of Z shaped wires, which was used by Oplatka and Roth (1991), in their restrained bending fatigue tests. Similarly, the 62 mm outer diameter cable composed of three layers of round wires, two layers with half lock/round wires and an outer layer of Z shaped wires. This cable was used in the axial and restrained bending fatigue tests of Transport Research Laboratories.

Figures 7.2 (a & b) present the interlayer radial contact force in all the layers of two different locked coil cable constructions of 31 and 62 mm diameter cable as a function of cable axial strain. The external helically interlocked wires not only resist the radially inward forces but also help in holding the cable together. In calculating the normal force acting on wires in the inner layers, an account has been made for the accumulation of normal forces from the wires in the outer layers (including shaped wire layer). For locked coil cables with its ends fixed against rotation, it is now possible to assess the distribution of the reaction to the contact forces between the hoop and radial components, and hence to calculate the bending stiffness of the cable as a function of these forces under increasing curvature. The results of the tension force in the wires are estimated by considering the deformations due to these contact forces and the Poisson's ratio effect of the material. These contact forces give rise to a friction force acting at the contact patches between any two wires.

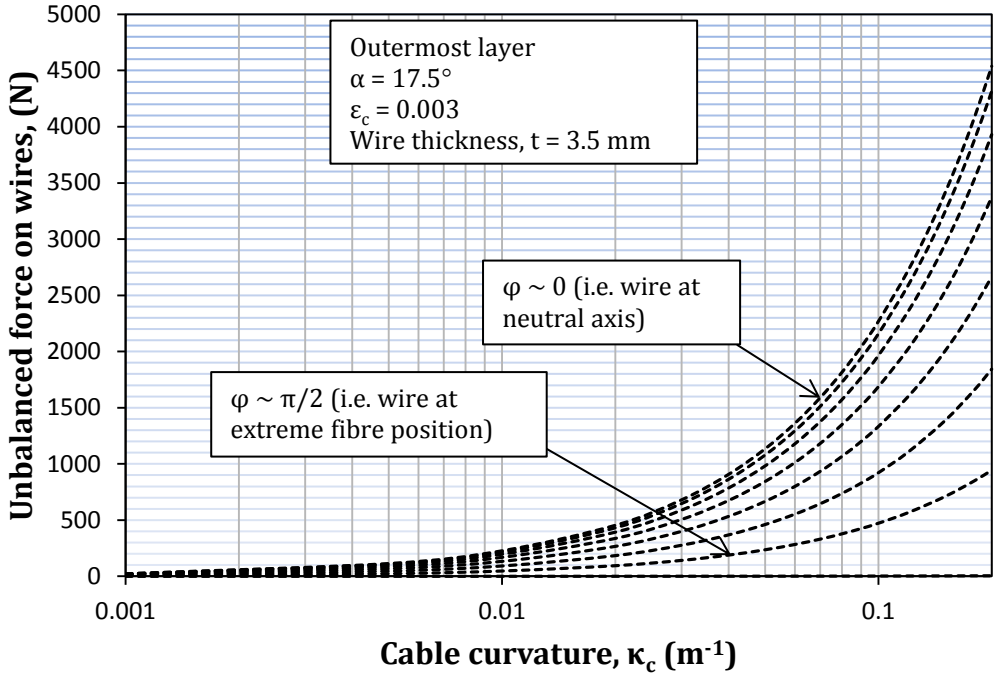

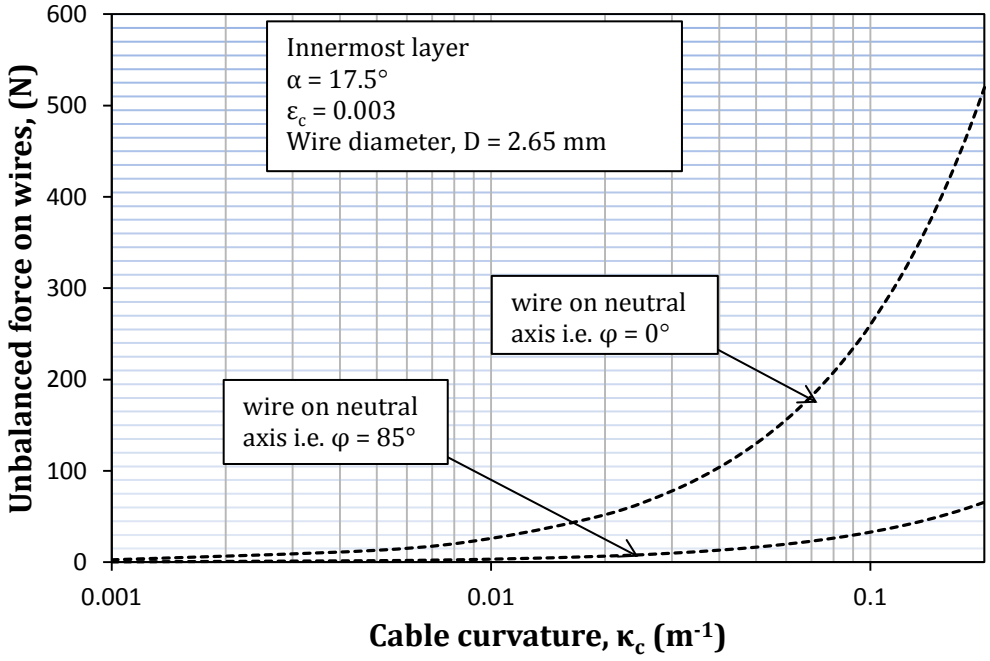

Figure 7-3 (a & b): Unbalanced force on individual wires of 31 mm diameter locked coil cable in (a) outermost layer and; (b) innermost layer respectively.

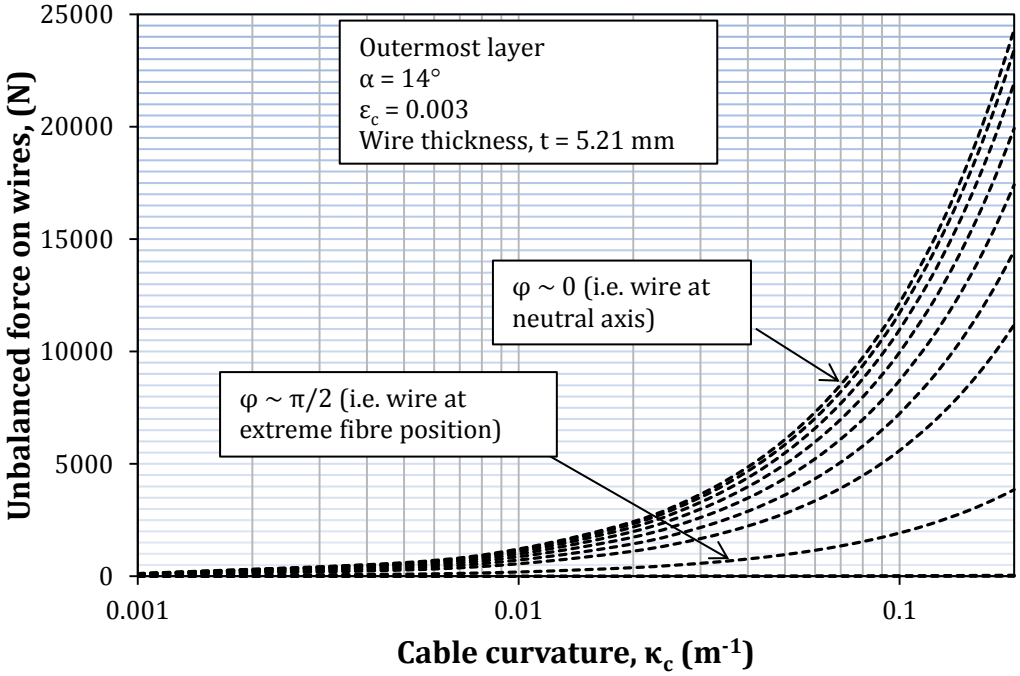

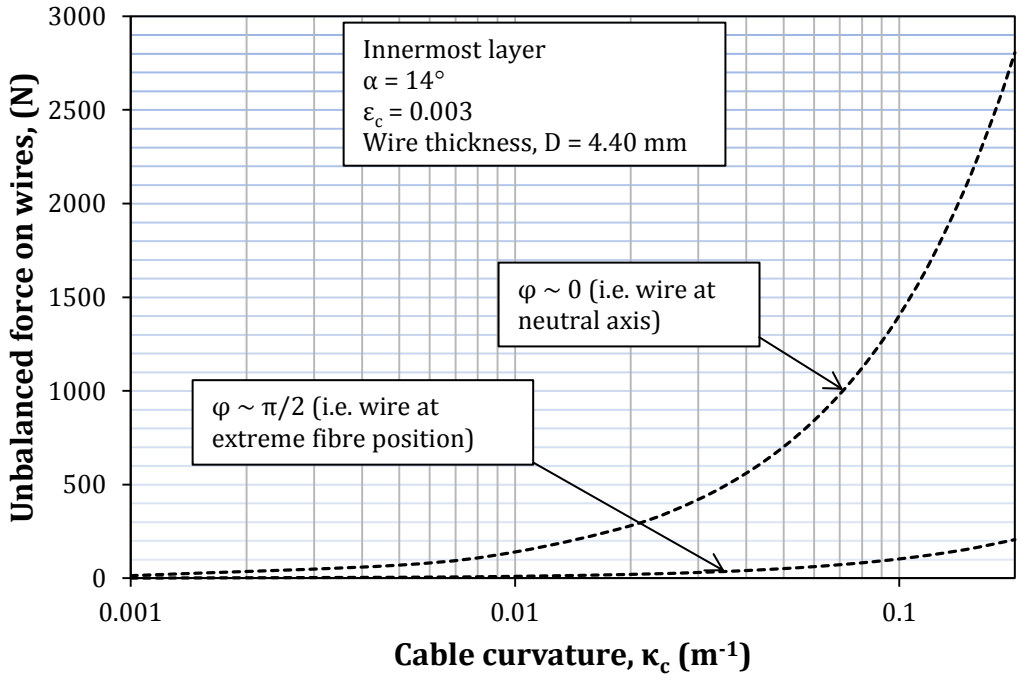

Figure 7.3 (c & d): Unbalanced force on individual wires of 62 mm diameter locked coil cable in (c) outermost layer and; (d) innermost layer respectively.

The mathematical model in this chapter is validated numerically, by producing results for two locked coil cables of 31 and 62 mm respectively. The upper bound of the cable curvature is approximated for these two cables, when the cable behaves as a solid bar. Figures 7.3 (a-d) show the plots for unbalanced force on wires in the outermost and innermost layers of 31 and 62 mm diameter locked coil cable subjected to an axial strain of $\varepsilon_c = 0.003$. Initially, when there is no load applied on the cable and the cable is in straight configuration (i.e. $\varepsilon_c = 0$, $\kappa_c = 0$); both the unbalanced forces and friction forces are zero. The wires in the cable are assumed to simply in contact with each other with no friction. Secondly, when the cable is subjected to tensile load only (i.e. $\varepsilon_c > 0$, $\kappa_c = 0$). In this case, the unbalanced force on wires is zero whereas friction forces exist because of the tension force in the cable. The flexural stiffness of the cable in this case remain at its maximum (EI_{max}) and the cable behaves fully composite behaviour. Finally, when the cable is subjected to tension and bending (i.e. $\varepsilon_c > 0$, $\kappa_c > 0$) with the assumed coefficient of friction $\mu = 0.12$, both unbalanced and frictional forces are acting on wires in all the layers of the cable .

As shown in Figures 7.3 (a-d), unbalanced force on wires in the outermost and innermost layers of the two cables is negligible at small values of bending curvature but, increase exponentially under increasing curvature. It is important to mention here that unbalanced force is symmetrical about flexural axis as opposed to frictional forces in the wires. The point at which unbalanced force acting on a wire in any layer exceeds the frictional force acting on it, the wire starts slippage until equilibrium is reached. It is clearly shown in Figures 7.3 (a-d) that the wires near the neutral axis experience largest unbalanced force as compared with the wires at the extreme fibre position (both in the lower and upper halves of the cable). For example, unbalanced force on wires in the outermost layer of 62 mm locked coil cable, is 4537 N and 30 N for a wire at neutral axis and extreme fibre position respectively. Similarly, the magnitude of unbalanced force on wire decreases for inner layers of the cable, because of the decreasing radial distance from the centre of the cable. A wire on the neutral axis in the outermost layer of 62 mm locked coil cable experiences an unbalanced force of 4537 N as opposed to 519 N for a wire on the neutral axis in the innermost layer.

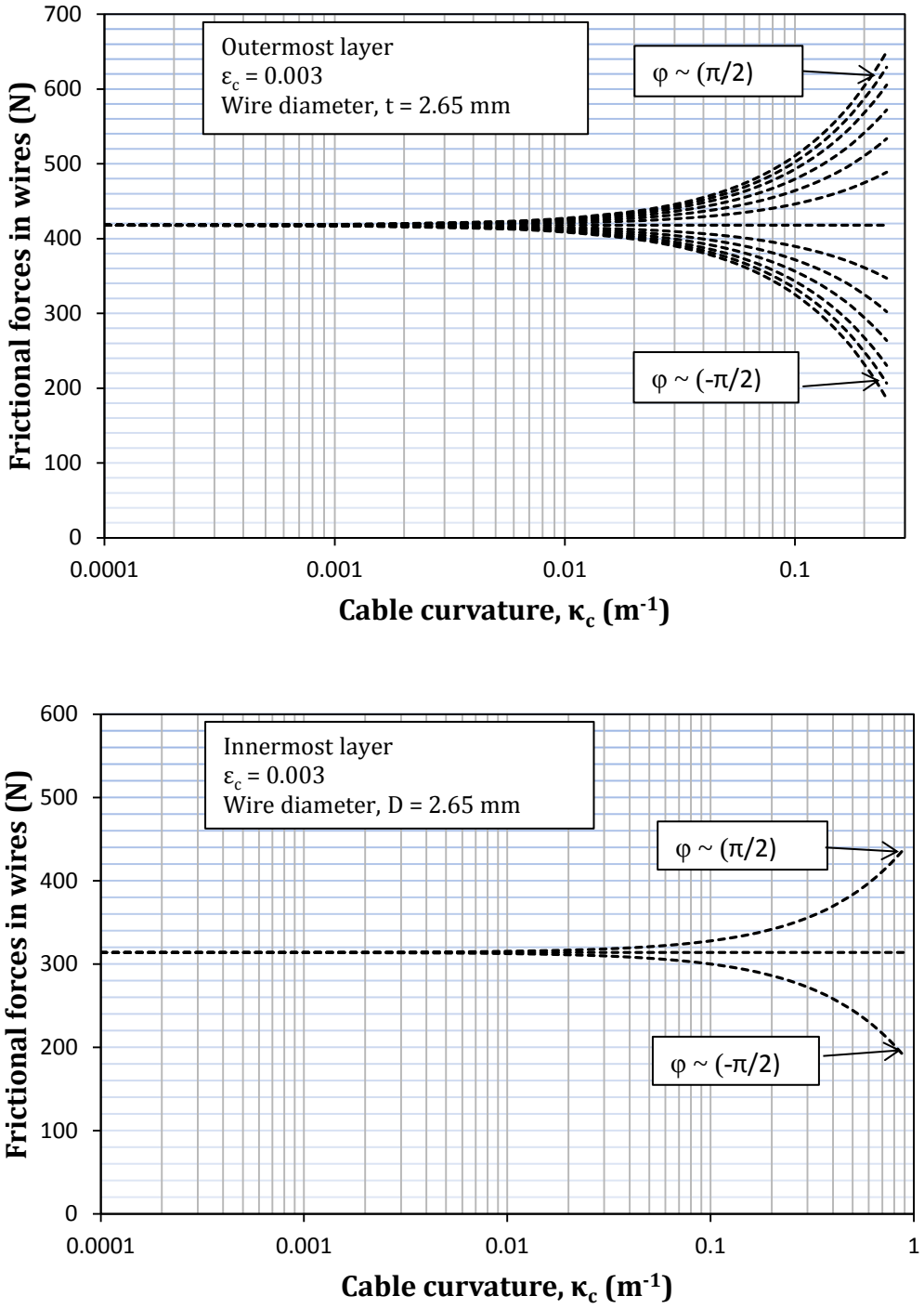

Figure 7-4 (a & b): Friction forces on individual wires of 31 mm diameter locked coil cable in (a) outermost layer and; (b) innermost layer respectively.

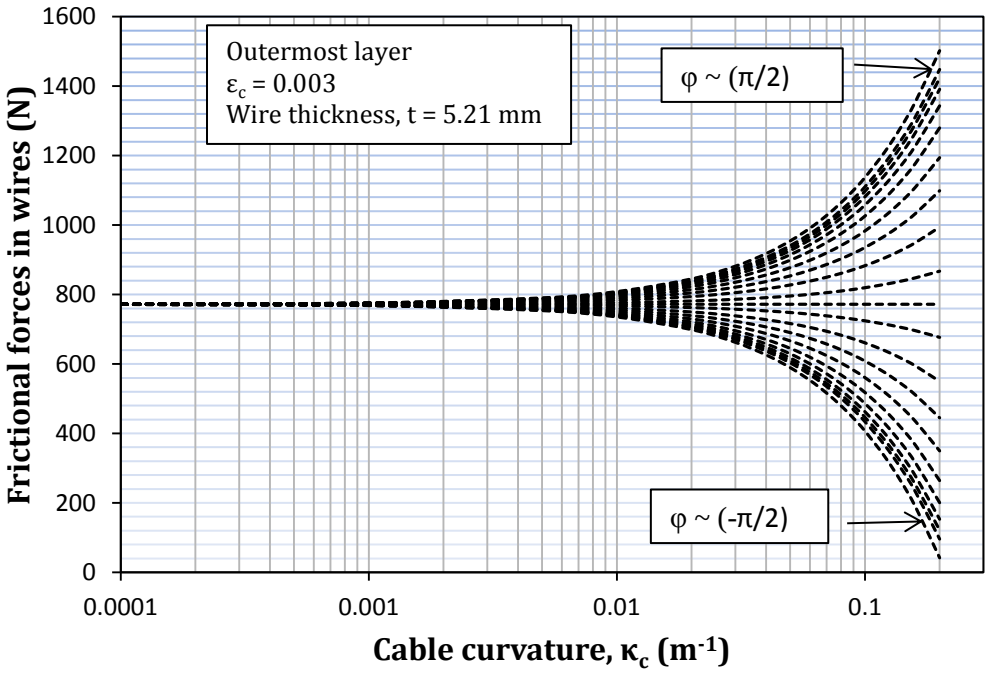

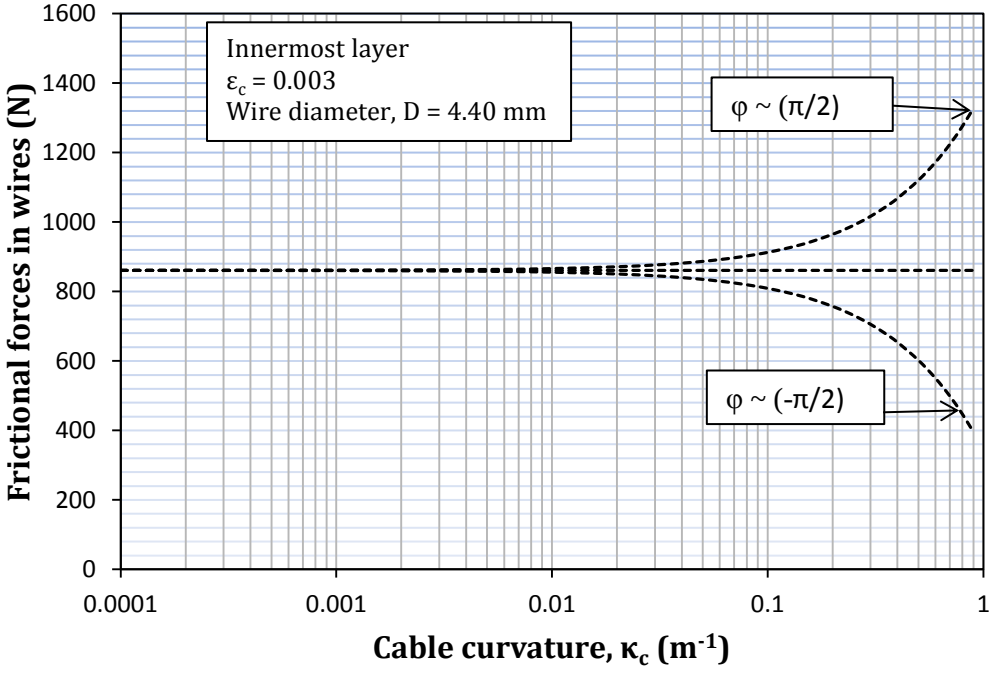

Figure 7.4 (c & d): Friction forces on individual wires of 62 mm diameter locked coil cable in (c) outermost layer and; (d) innermost layer respectively.

Figures 7.4 (a-d) show the frictional forces on wires in the outermost and innermost layers of the above two locked coil cables for a selective axial strain of $\varepsilon_c = 0.003$. The frictional forces of the wires in the upper half (i.e. convex side) of the cable are higher than those in the lower half (i.e. concave side) of the cable. This is because the positive curvature is assumed to cause maximum stress at the extreme fibre position in bending term. Thus, frictional forces on wires in different layers are shown to increase or decrease rapidly under increasing curvature. Frictional forces in the cable are non zero even for the cable in the straight configuration (i.e. $\kappa_c = 0$). Under larger values of imposed curvature, frictional forces in the wires decrease with tremendous increase in the unbalanced force on them, causing the entire lower half of the cable to be in slip state. The approximate upper bound of the cable curvature, for which the BEN kinematic beam assumption is valid to evaluate the stresses in the wires near end termination, have been shown for both the cables. Unlike a straight beam, there is no constant neutral axis along the cable length, and the location of the so called neutral axis rotated between the two extreme positions.

As predicted by the theory, due to minimal frictional force and high unbalanced force, wires near the neutral axis in the outermost layer start slippage and spread inward towards the centre of the cable. Figures 7.5 (a & b) show the values of the critical curvatures at which interwire slippage initiated at the neutral axis for all the three layers of two locked coil cable of 31 and 62 mm diameters respectively. As tension force in the cable increases, wires stick together under larger curvature, and the upper bound of the cable curvature, for which BEN beam assumption is valid increased. The locked cable in the present analysis was subjected to a wide range ($0.001 \leq \varepsilon_c \leq 0.005$) of mean axial load. It has been shown previously that unbalanced force on wires grows linearly with the increasing diameter of the strand, therefore, wires in the outermost layer of 62 mm cable slides much earlier than the outer wires in 31 mm cable. For example for a given axial strain of 0.001, the wires at the neutral axis of 31 mm cable slide at a curvature value of $\kappa_c = 0.0062\ m^{-1}$, whereas for 62 mm cable this occurs at $\kappa_c = 0.0022\ m^{-1}$. It is also demonstrated that the differences in the behaviour of the two sections are due to the helical nature of the wires and therefore, bending curvature has no influence on the core tension force and friction force. Also, this difference in the

behaviour of two sections will vanish when the lay angle tends to zero (i.e. parallel wire cable).

It is worth to mention, that the layers of the shaped wires in locked coil cable experience gross sliding throughout the cable for different load perturbations and bending curvatures. In gross sliding regime, the contact forces between the wires in line and point contact were determined by the previously summarized method in Chapter 3. As opposed to round wire cable, the outer layer of shaped wires hold the cable together and prevent kinking and bird caging, when the loads are compressive or there is a sudden drop in tension. As impact loads cause tensile and torsional wave through the cable and helical wires can separate from inner layers, Conway and Costello (1990).

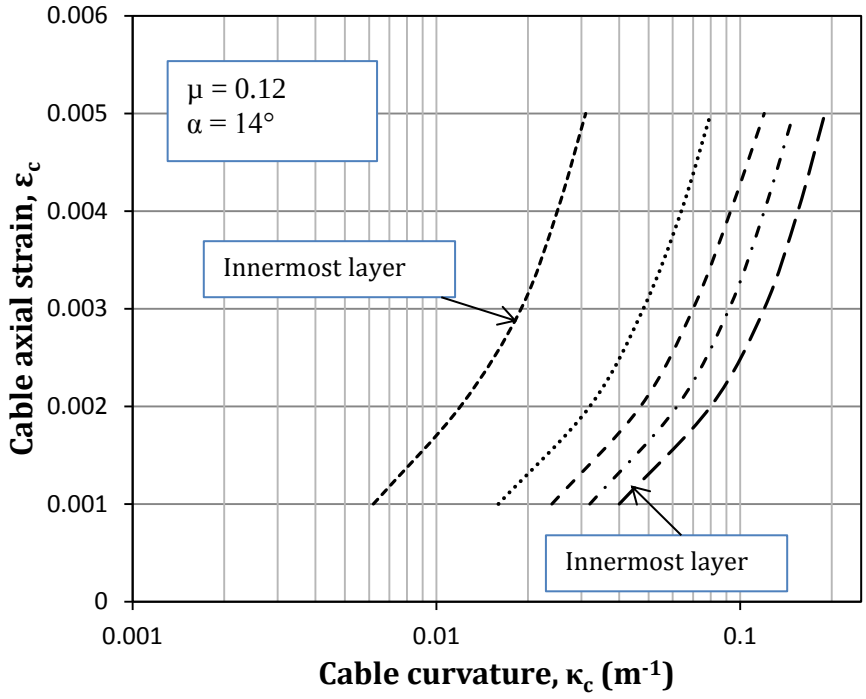

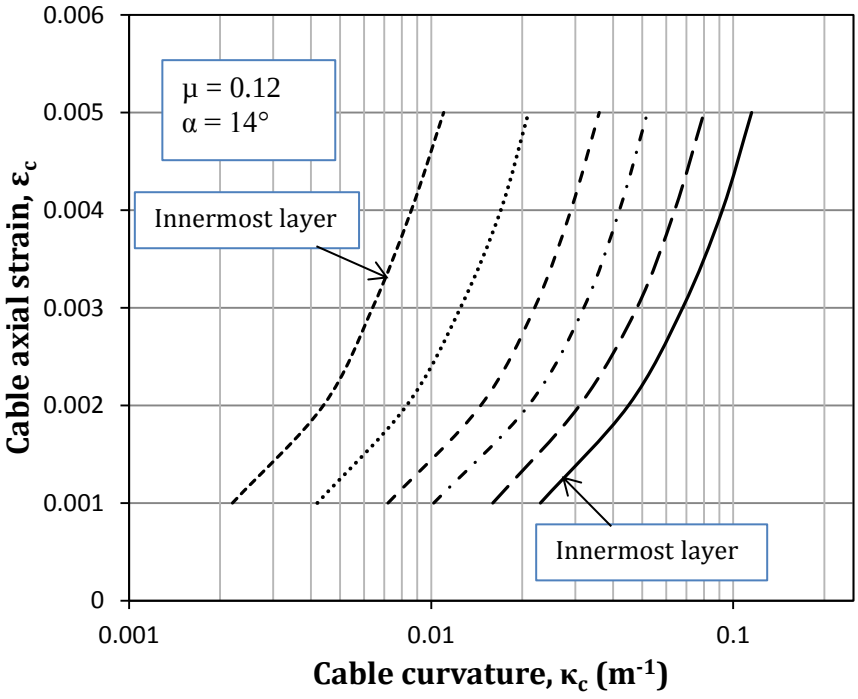

Figure 7-5 (a & b): Plots of the critical curvature at which interwire slippage initiated for all the layers two locked coil cables of (a) 31 mm; (b) 62 mm outside diameter respectively.

Figures 7.6 (a & b) present the effective bending stiffness for the above two locked coil cable for a wide range ($0.001 \varepsilon_c \leq 0.005$) of axial strains. The effective bending stiffness in the present analysis is shown to have a gradual transition from no-slip to full slip. The explicit formulation of slip initiation and progression in the helical layers of both shaped and round wires of the cable demonstrates the bending behaviour of cable to be modelled in the transition range. The strain distribution in the wires depends on the imposing curvature range. In line with the previous analysis, three distinct stages are evidenced in the bending behaviour of the cable. Initially, the cable behaves linearly when all the wires are in stick state, and the bending stiffness of the cable is maximum at this stage. In the second stage, the wires in the cable start slipping against each other, some parts in the cable are slipped and others did not. When, the slippage in the cable progressed from neutral axis to the extreme fibre position, all the wires in the cable are slipped, and the effective bending stiffness of the cable dropped down to a constant minimum value, depending on the friction coefficient. It is important to mention here that if the bending moment in the cable is reduced, the wires will tend to slip back; but the unbalanced force will oppose this slip. As a result the wires lockup and the cable return back to its fully stick state. A further reduction in the bending moment will cause slippage in the reverse direction. In line with the previous results, the behaviour of the locked coil cable under cyclic bending moment is analogous to the behaviour of an elastic-plastic material with hardening.

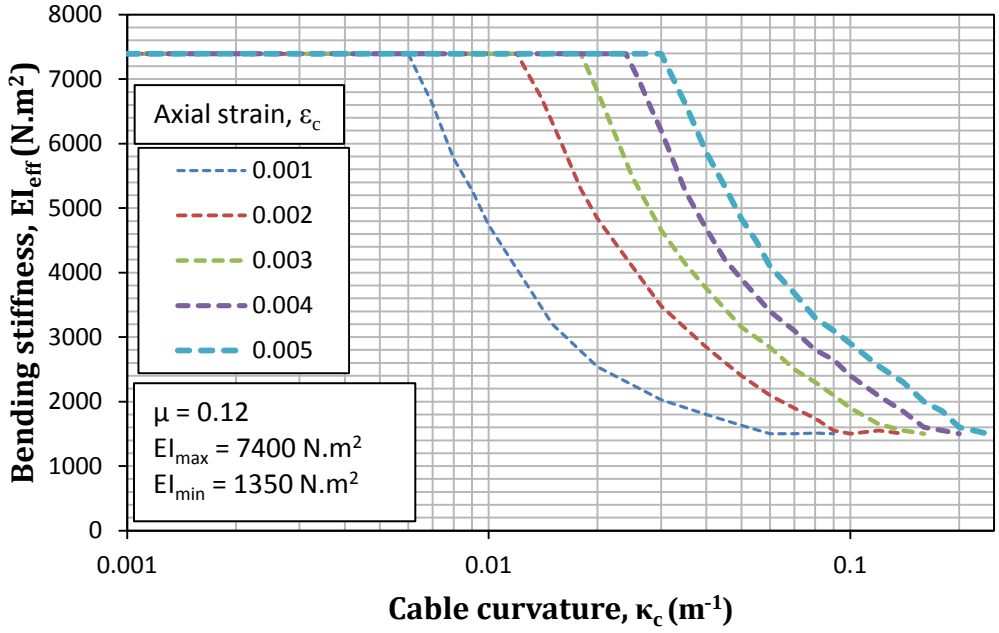

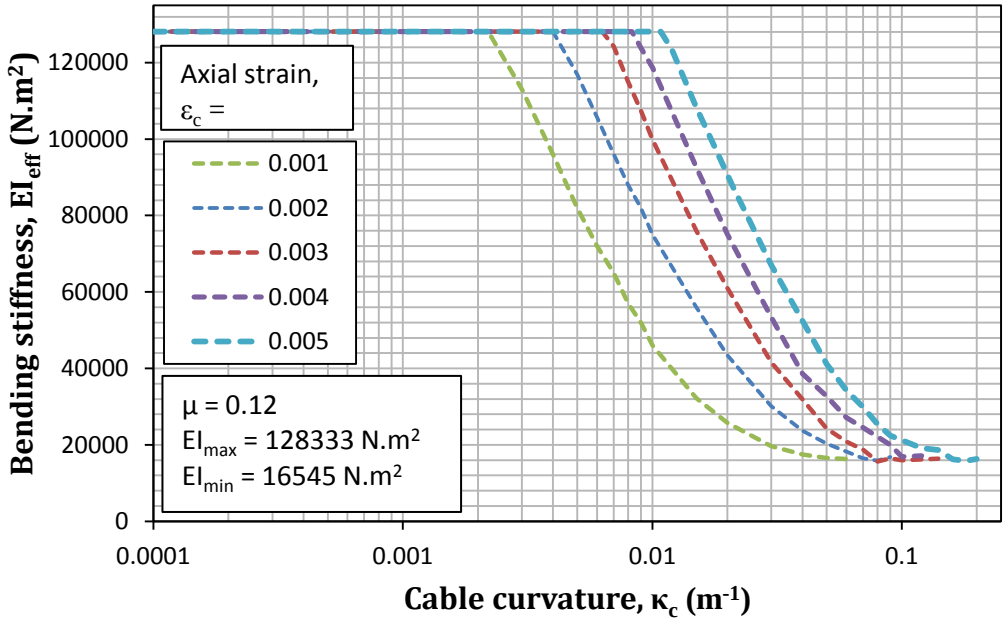

Figure 7-6 (a & b): Effective bending stiffness of two different locked coil cables of (a) 31 mm and; (b) 62 mm diameter.

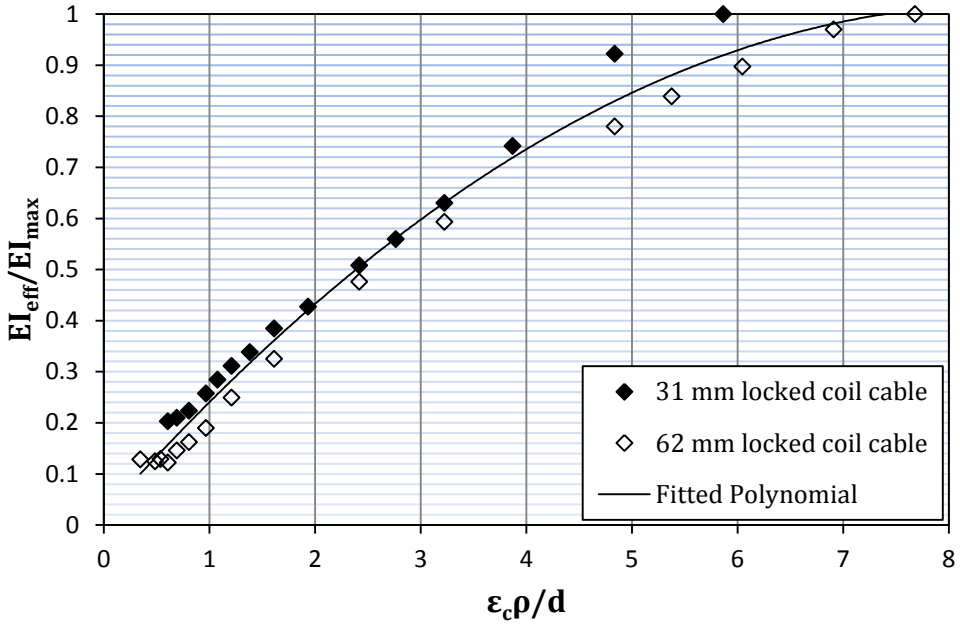

Figure 7-7: Simple design curve for the determination of bending stiffness of the given two locked coil cables.

7.4 Simple Method for Calculating Bending Stiffness

From the theoretically obtained results of bending stiffness for the two locked coil cable a simple curve has been developed as shown in Figure 7.7. This enables one to obtain the effective bending stiffness for the above two locked coil cables, as a function of the newly proposed dimensionless parameter. The data showed very small scatter around the fitted polynomial of a second degree. Therefore, fairly accurate values of the bending stiffness can be obtained by means of this simple method. The general form of the fitted line can be given as follows:

$$\frac{EI_{eff}}{EI_{max}} = AX^2 + BX + C \tag{6.3}$$

where X = $\rho\varepsilon_c/d$ is the dimensionless parameter, and A-C are the constant coefficients which are; A = -0.0136, B = 0.2329 and C = 0.0214 for the present case of locked coil cable.

As mentioned previously, the theoretical model developed in this chapter has already been verified and numerical results are obtained for the above two locked coil cables.

Tables 7.2 (a & b) demonstrate the calculation routines of the numerical results for the given two locked coil cables of 31 and 62 mm diameter respectively. The simple method developed for locked coil cables is based on these results. The significant effect of the shaped wires in the outer layers has already been demonstrated in this chapter. This has been done using the original formulations as presented in this chapter for locked coil cables. The numerical results obtained for two locked coil cable suggest that the wires in the outer layers of shaped wires slip at larger curvature as compared to the round wire cable, resulting bending stiffness of the cable to remain at EI_{max}. On the other the bending stiffness values predicted by the simple method closely resemble to the values given in Tables 7.2 (a & b) and show very small scatter around the fitted polynomial. Therefore, the simple two degree polynomial can be used reliably to estimate the overall effective bending stiffness of these locked coil cables.

Table 7-2 (a & b): Calculation routines and numerical results for two locked coil cables of (a) 31 mm; and (b) 62 mm diameter respectively.

Cable outside diameter, d (m)	Lay angle, α_i (°)	Cable axial strain, ε_c	Cable curvature, κ_c (m^{-1})	Radius of curvature, ρ_c (m)	$\rho_c\varepsilon_c/d$	Effective bending stiffness, EI_{eff} (Nm^2)	EI_{eff}/EI_{max}
0.062	14	0.003	0.0063	158.73	7.68	128095	1
0.062	14	0.003	0.007	142.86	6.91	124228	0.97
0.062	14	0.003	0.008	125.00	6.05	114940	0.90
0.062	14	0.003	0.009	111.11	5.38	107400	0.84
0.062	14	0.003	0.01	100.00	4.84	99899	0.78
0.062	14	0.003	0.015	66.67	3.23	76000	0.59
0.062	14	0.003	0.02	50.00	2.42	61000	0.48
0.062	14	0.003	0.03	33.33	1.61	41600	0.32
0.062	14	0.003	0.04	25.00	1.21	31900	0.25
0.062	14	0.003	0.05	20.00	0.97	24300	0.19
0.062	14	0.003	0.06	16.67	0.81	20800	0.16
0.062	14	0.003	0.07	14.29	0.69	18700	0.15
0.062	14	0.003	0.08	12.50	0.60	15600	0.12
0.062	14	0.003	0.09	11.11	0.54	16478	0.13
0.062	14	0.003	0.1	10.00	0.48	15987	0.12
0.062	14	0.003	0.14	7.14	0.35	16423	0.13

Cable outside diameter, d (m)	Lay angle, α_i (°)	Cable axial strain, ε_c	Cable curvature, κ_c (m^{-1})	Radius of curvature, ρ_c (m)	$\rho_c\varepsilon_c/d$	Effective bending stiffness, EI_{eff} (Nm^2)	EI_{eff}/EI_{max}
0.031	17.7	0.003	0.0165	60.61	5.87	7392	1
0.031	17.7	0.003	0.02	50.00	4.84	6814	0.92
0.031	17.7	0.003	0.025	40.00	3.87	5480	0.74
0.031	17.7	0.003	0.03	33.33	3.23	4660	0.63
0.031	17.7	0.003	0.035	28.57	2.76	4133	0.56
0.031	17.7	0.003	0.04	25.00	2.42	3756	0.51
0.031	17.7	0.003	0.05	20.00	1.94	3157	0.43
0.031	17.7	0.003	0.06	16.67	1.61	2843	0.38
0.031	17.7	0.003	0.07	14.29	1.38	2500	0.34
0.031	17.7	0.003	0.08	12.50	1.21	2300	0.31
0.031	17.7	0.003	0.09	11.11	1.08	2100	0.28
0.031	17.7	0.003	0.1	10.00	0.97	1900	0.26
0.031	17.7	0.003	0.12	8.33	0.81	1650	0.22
0.031	17.7	0.003	0.14	7.14	0.69	1550	0.21
0.031	17.7	0.003	0.16	6.25	0.60	1500	0.20

7.5 Conclusions

A theoretical model is proposed for estimating wire kinematics, pattern of interwire contact forces and effective bending stiffness of the axially preloaded locked coil cables. The model is the extension of the formulation proposed in Chapter 4, and fully takes into account interwire normal contact forces both in radial and hoop directions. Numerical results have been obtained for two different locked coil cables of 31 and 62 mm respectively, suggesting that the outer layers with the shaped wires play an important role in the pattern of contact force distribution and slip initiation. The overall frictional forces for the shaped wires are found to be higher than round wire cables of the same diameter. This delays the initiation of wire slippage in the outer layers and therefore bending stiffness of the cable keeps the maximum value at EI_{max} for larger values of bending curvatures. The plots for the variable bending stiffness for the two cables have been obtained and discussed.

Chapter 8

Conclusions and Future Work

8.1 Introduction

The aim of this work was to investigate the bending behaviour of helically wound steel cables of various types (i.e. spiral strands, sheathed spiral strands and locked coil cables) in presence of friction, and to propose theoretical models for their analysis. Bending of such cables may induce slippage between individual wires, which is mainly governed by interwire frictional forces acting at the contact patches between them. The phenomenon is particularly difficult to model mathematically, also because the friction forces are difficult to determine experimentally, and strongly depend on the manufacturing process.

In this work, the local bending behaviour of various types of helically wounded large diameter multi-layered cable has been examined. Relatively straightforward formulations have been developed for the determination of bending moment versus curvature relationships. This enables one to estimate the bending stiffness of the cable as a function of imposed cable curvature. The proposed formulations give an insight into the inner state of the cable, regarding relative displacements of individual wires and the stress distribution. The model fully takes into account the non-linearity of cable caused by sliding individual helical wires in the cable. The effect of interwire/ineterlayer contact forces, both in radial and hoop directions are taken into account. The model parameters have been identified from experimental data, and numerical analysis has been performed on a variety of cable constructions. Guided by previously reported experimental results, the theoretical analysis demonstrates that, similar to the simple case of the shear stress in a solid homogenous beam in bending, unbalanced force on wires is maximum at the neutral axis of the cable cross section and minimum at the extreme fire positions. Thus initially interwire slippage initiates at neutral axis and spread almost symmetrically towards the lower and upper halves of the cable.

The proposed model has been used to obtain a large body of numerical results for a variety of cable constructions, covering a wide range of geometrical and material parameters using the proposed model. Effective bending stiffness of the cable is shown to be a function of bending curvature, interlayer friction coefficients and interlayer normal contact forces. It is further shown that the effective bending stiffness of the cable vary between two extremes, corresponding to no-slip and full-slip cases. Initially the cable behaves as a solid bar when all the wires are in stick state and therefore, bending stiffness of the cable is at its maximum. The theoretical results of the model are compared with the previously available experimental results for two different cable constructions of 39 and 41 mm diameters and were found in good correlation. Regarding the magnitude of the bending stiffness, the theoretical predictions of the theory are compared with experimentally determined values of 164 mm diameter strand.

The model is further extended to cater for the effects of external hydrostatic pressure in deep water applications, which greatly influence the pattern of interwire contact forces and wire slippage. A theoretical model is also proposed for estimating wire kinematics, pattern of interwire contact forces and effective bending stiffness of the axially preloaded locked coil cables

Finally, a dimensionless parameter has been proposed, by means of which the effective bending stiffness of large diameter multi-layered cables may be estimated with an acceptable accuracy under any loading condition and applied bending.

8.2 Main Findings

A large body of available literature on wire ropes and spiral strands has been critically examined, and the gaps in previously reported models have been highlighted. Keeping in mind the growing demand for increasingly large diameter cables, the impression is gained that both on experimental and theoretical sides, too much attention has been paid to small diameter (seven wires) strands. It is also noted that most of the earlier researchers ignored the effect of interwire friction and contact deformations in their analysis. It is argued that predicting various characteristics of large diameter strands, based on the knowledge of the behaviour of small diameter cables, by extrapolation is

a very risky process. After the pioneering effort of Hruska, various other authors proposed different models of varying complexities and accuracy, to predict the response of wire ropes and spiral strands to various loading conditions. Accordingly, an effort has been made to assess contact forces and the associated relative displacements between wires, taking into account the friction between them.

Explicit formulations for the smooth transition of the flexural rigidity from no-slip to full-slip regimes of the cable as a function of bending curvature have been developed as part of the present study. Based on the newly proposed formulations, it is now possible to describe the cable sag at specific tension force and cable curvature along its axis. The relative displacement of the wires, the tensile, hoop and the bending stresses in the individual wires of the cable can be determined. Certain oversights in original HDS model (Hong et al., 2005) have been highlighted and subsequently improved. Normal contact forces in the hoop direction have shown to have a significant effect on the values of interlayer radial contact forces over the trellis contact patches and hence the interlayer slippage for the given value of mean axial strain and imposed curvature.

An extensive parametric study has been carried out on a variety of spiral strand constructions covering a wide range of geometrical parameters using the modified model. Effective bending stiffness of the cable is shown to be a function of bending curvature, interlayer friction coefficients and interlayer normal contact forces. It is argued that the small curvature assumption of the cable may be valid in parts away from termination, but the possible development of a large curvature at the bearings and end terminations cannot be ignored nor avoided. The effective bending stiffness of the cable is shown to vary between two extremes, corresponding to no-slip and full-slip cases. Initially the cable behaves as a solid bar when all the wires are in stick state and therefore, bending stiffness of the cable is maximum. Under increasing bending the slippage initiates at neutral axis and the effective bending stiffness of the cable decreases and eventually reaches a constant value. All the wires in slip state are shown to behave as an independent helical springs bending about their own axis in the presence of friction. The theoretical results of the model have been compared with the previously available experimental results for two different cable constructions of 39 and 41 mm diameters respectively and are found in good correlation.

A simple method for obtaining the effective bending stiffness of large diameter multi-layered cables has been developed. A sound understanding of the fundamental parameters influencing steel cable characteristics is obtained from the numerical results presented in Chapter 4. The simplified method is shown to have nominally very close values of the bending stiffness as the original formulations of MHDS model. This method can be used to hand calculations (using a pocket calculator).

The modified MHDS model in Chapter 4 has further extended, to cater for the effects of external hydrostatic pressure on sheathed spiral strands, which greatly influence the pattern of contact forces between wires in the strand. Numerical results have been obtained for three different 127 mm strands with lay angles of 12°, 18° and 24° experiencing a wide range of external hydrostatic pressures of 0 to 2000 m. Under such external pressures, the contact forces caused by the hydrostatic water pressure have been shown to become more significant compared with contact forces inside the cable by the tension force in the cable. The significant increase in normal contact forces between wires is shown to suppress the slippage of wires in the cable. Under such conditions, interwire fretting actions are believed to accompany with high levels of localized heating. Consequently, the axial and restrained bending fatigue life of the cable can be reduced in long term applications.

The no-slip and full-slip values of flexural rigidity of sheathed spiral strands are shown to be independent of the level of hydrostatic pressure. The practical importance of the bending stiffness for use in connection with fatigue life estimation and hydrodynamic instability calculations is demonstrated. It is argued that knowledge of the exact magnitude of the cable bending stiffness will also prove useful in the estimation of the natural frequencies of the structure supported by cables. Finally, simplified routines are proposed for obtaining the magnitudes of the effective flexural stiffness of sheathed spiral strand subjected to various levels of water depths.

Finally, a theoretical model is proposed for estimating wire kinematics, pattern of interwire contact forces and effective bending stiffness of the axially preloaded locked coil cables. The model is the extension of the proposed formulations in Chapter 4, and fully takes into account interwire normal contact forces both in radial and hoop directions. The proposed model has been applied to two different locked coil cables of

31 and 62 mm respectively. Numerical results suggest that the outer layers with the shaped wires play an important role in the pattern of contact force distribution and slip initiation. The overall frictional forces for the shaped wires are found higher than round wire cables of the same diameter. This delayed the initiation of wire slippage in the outer layers and therefore, bending stiffness of the cable remained at EI_{max} for large values of bending curvatures. In addition to this, the outer shaped wires layer resists the unwinding of the strand during bending.

Wherever possible, the theoretical results have been compared with experimental results from the available literature and very good correlations have been found.

8.3 Future Work

The study in this thesis can be extended further to investigate the following issues:

1. **Fatigue life estimation of the cable**

The work reported here may be regarded as an important step towards the fatigue life estimation of the cable. The study in this thesis throws some light on whether the traditional method of assuming a constant effective bending stiffness for predicting the minimum radii of curvature, at the fixed terminations to spiral strand, is a reasonable approach. It has been shown that for large diameter multi-layered strands, the difference between no-slip and full slip stiffnesses is unacceptably large, and therefore the fatigue life estimation based a constant bending stiffness value could be misleading. The results of the interwire contact forces and variable bending stiffness can be used in the future as an input to develop new bending fatigue design curves, e.g. following Raoof (1993b) method.

2. **Hysteresis during combined tension and bending of the cable**

A further important subject for future investigation is the hysteresis during bending of the cable. The axial and torsional hysteresis of cables and electrical conductors is of prime importance in the analysis of certain aero-hydrodynamic problems. The nonlinear properties of the cables are mostly caused by internal damping. Two main sources of internal losses are identified by Hobbs and Raoof (1984) for a vibrating

cable, these are; (i) dry friction between the wires; and (ii) viscous damping of the material of the wires. The combination of these two mechanisms of losses results in the hysteresis loop of the structure. The response of light and flexible structures to such dynamic forces (aero-or hydrodynamic and traffic load) are central to understand and for sufficiently large vibrations the effect of viscous damping of the material become negligible.

There are two types of interwire friction at play within a cable: (1) line contact between wires in the same layer; (2) trellis contact between two wires from different layers. When the wires in the cable start sliding with respect to each other, the normal force and friction coefficient result in a friction force directed opposite to the sliding direction. For each interwire slippage within a layer, energy dissipation can be determined by taking the surface area enclosed by the hysteresis loop. Where the overall energy dissipation during the bending cycle is mainly governed by interwire contact forces, and friction coefficient between wires. The results of the contact forces and slippage for the assumed friction coefficient can be used in future to calculate energy dissipation in these cables during bending.

3. An attempt to extend and implement the proposed formulation for wire rope (i.e. double helix wires)

The proposed model has been successfully implemented to various types spiral strand constructions (i.e. wire in the cable follows a single helical path around the core). The behaviour of the strand is perhaps best understood, because the single level (cf. ropes, double level) of twist in a given wire has made it possible to develop a strong body of analytical work (supported by experimental studies). It can be applied again the same way for determining the mechanical properties of wire ropes for double helices (i.e. wire in the cable following a double helical path around the core). In the case of wire ropes, due to the double helical configuration of wire around the core, the response of a wire rope is totally different than spiral strands. The parametric equations describing the double helix of a wire in the cable need to be derived. The radial component of the curvature can be used the same way for helical strand in the wire rope to determine the contact deformations.

REFERENCES

Argatov, I. (2011), "Response of a Wire Rope Strand to Axial and Torsional Loads: Asymptotic modeling of the Effect of Interwire Contact Deformations." *International Journal of Solids and Structures*" Vol. 48, No. 10, pp. 1413-1423.

Blouin, F., and **Cardou, A.** (1989), " A Study of Helically Reinforced Cylinders Under Axially Symmetric Loads and Application to Strand Mathematical Modelling", *Internatinal Journal of Solids and Structures*, Vol. 25, No. 2, pp. 189-200

Cardou, H., and **Joulicoeur, C.** (1997), "Mechanical Models of Helical Strands", *Applied Mech. Review, ASME*, Vol. 50, No. 1, January, pp. 1-14

Chi, M. (1971), "Analysis of Multi-Wire Strands in Tension and d Tension and Torsion", *Catholic University of America, Technical Report* 71-9, Washington D.C.

Chi, M. (1972), "Analysis of Operating Characteristics of Strands in Tension Allowing End Rotation", *Ocean Technology Division Meeting*, No. 73 -WA/Oct-19, ASME, New York, November, pp. 372-398.

Chiang, Young J. (1996), "Characterizing Simple-Stranded Wire Cables under Axial Loading", *Finite elements in Analysis and Design* Vol. 24, No. 2, pp. 49-66.

Conway, T. A. and **Costello, G. A.** (1990), "Bird-Caging in Wire Rope", *Journal of Engineering Mechanics*, Vol. 116, No. 4, pp. 822-831.

Costello, G.A. (1977), "Large Deflections of Helical Springs due to Bending", *Journal of Engineering Mechanics Division, ASCE*, Vol. 103, No. EM3, May, pp. 481-487.

Costello, G.A. (1978), "Analytical Investigations of Wire Rope", *Applied Mechanics Review*, Vol. 31, No. 7, July, pp. 897-900.

Costello, G.A. (1983), "Stresses in Multi-Layered Cables", *Journal of Energy Resources Technology, ASCE*, Vol. 105, pp. 337-340.

Costello, G.A. (1997), "Theory of Wire Rope", *Mechanical Engineering Series,* Springer Verlag, New york, Inc.

Costello, G. A., and **Butson, G. J.** (1982), "Simplified Bending Theory for Wire Rope", *Journal of the Engineering Mechanics Division, ASCE*, Vol. 108, No. EM2, pp. 219-227.

Costello, G. A., and **Miller, R. E.** (1979), "Simplified Lay Effects of Wire Rope", *Journal of the Engineering Mechanics Division, ASCE*, Vol. 105, No. EM4, August, pp. 597-608.

Costello, G. A., and **Phillips, J. W.** (1974), "Simplified A More Exact Theory for Twisted Wire Cables", *Journal of the Engineering Mechanics Division, ASCE*, Vol. 102, No. EM1, February, pp. 171-181.

Costello, G. A., and **Miller, R. E.** (1976), "Effective Modulus of Twisted Wire Cables", *Journal of the Engineering Mechanics Division, ASCE*, Vol. 105, No. EM4, August, pp. 597-608.

Costello, G. A., and **Sinha, S. K.** (1977a), "Static Behaviour of Wire Rope", *Journal of the Engineering Mechanics Division, ASCE*, Vol. 103, No. EM6, December, pp. 1011-1022.

Costello, G. A., and **Sinha, S. K.** (1977b), "Torsional Stiffness of Twisted Wire Cables", *Journal of the Engineering Mechanics Division, ASCE*, Vol. 103, No. EM4, August, pp. 766-770.

Davies, T. J. (2001), "Static, Dynamic and Fatigue Characteristics of Helical Cables", Thesis Presented to *Loughborough University* in Partial Fulfilment of the Requirements for the Degree of Doctor of Philosophy, February 2001.

Durelli, A. J. (1973), "Response of Epoxy Oversized Models of Strands to Axial and Torsional Loads", *Experimental Mechanics*, Vol. 13, August, pp. 313-321.

Durelli, A. J., **Machida, S.**, and **Parks, V. J.** (1972), "Strains and Displacements on a Steel Wire Strand", *Navel Engineers Journal*, Vol. 84, No. 6, December, pp. 85-93.

Elata, D., Eshkenazy, R., and Weiss, M. (2004), "The Mechanical Behaviour of a Wire Rope with an Independent Wire Rope Core", *International Journal of Solids and Structures,* Vol. 41, No. 5, pp. 1157-1172.

Erdonmez, C. and **Imrak, C. E.,** (2011), "A Finite Element Model for Independent Wire Rope Core with Double Helical Geometry Subjected to Axial Loads," Sadhana, *Indian Academy of Sciences*, Vol. 36, No. 6, pp. 995-1008.

Erik, R. (2011), "Behaviour of Steel Wire Ropes Subjected to Severely Oscillating Tensile Loads Alternating Between Taut and Slack", Pieter Schelte Jacket Lift System, Research Report Submitted to Delft University, The Netherland, September.

Fontanari, V., Monelli, B., and Degasperi, F., (2009), "Experimental and Numerical Analysis of Full-Locked Coil Ropes Fire Behaviour" Proceedings of SEM 2009 Annual Conference & Exposition on Experimental & Applied Mechanics, Bethel, CT: SEM *Society for Experimental mechanics*.

Gecha, E. Ya. (1989), "Stress and Strains in Cables Under the Actions of Tensile Forces And External Hydrostatic Pressures", *Soviet Machine Science*, No. 1, pp. 30-36.

Ghoreishi S.R., Cartraud P., Davies P., and Messager, T. (2007a), "Analytical Modeling of Synthetic Fibre Ropes Subjected to Axial Loads, Part I: A New Continuum Model for Multilayered Fibrous Structures", *International Journal of Solids and Structures*, Vol. 44, No. 9, pp. 2924-2942.

Ghoreishi S.R., Davies, P., Cartraud, P., and Messager, T., (2007b), "Analytical Modeling of Synthetic Fibre Ropes, Part II: A Linear Elastic Model for 1+ 6 Fibrous Structures", *International Journal of Solids and Structures,* Vol. 44, No. 9, pp. 2943-2960.

Ghoreishi, S.R., Messager, T., Cartraud, P., and Davies, P. (2004), Assessment of Cable Models for Synthetic Mooring Lines, *International Offshore and Polar Engineering Conference*, Toulon, France.

Giglio, M., and **Manes, A.,** (2003), "Bending Fatigue Tests on a Metallic Wire Rope for Aircraft Rescue Hoists," *Engineering Failure Analysis*, Vol. 10, No. 2, pp. 223-235.

Giglio, M. and **Manes, A.,** (2005), "Life Prediction of a Wire Rope Subjected to Axial and Bending Loads", *Engineering Failure Analysis*, Vol. 12, No. 4, pp. 549-568.

Grimes, J. J. (1965), Locked Coil Cable and Method of Making Same, *Google Patents*.

Hall, H. M. (1951), "Stresses in Small Wire Ropes", *Wire and Wire Rope Products*, Vol. 26, March, pp. 228 and 257-259.

Harris, S. T., Waterhouse, R. B., and **McColl, I. R.** (1993), "Fretting Damage in Locked Coil Steel Ropes", *Wear,* Vol. 170, No. 1, pp. 63-70.

Hobbs, R. E., and Ghavani, K. (1982) "The Fatigue of Structural Wire Strands", *International Journal of Fatigue,* Vol. 4, No. 2, pp. 69-72.

Hobbs, R. E., and **Nabijou, S.** (1995), "Changes in Wire Curvature as a Rope is Bent Over a Sheave", *Journal of Strain Analysis*, Vol. 30, No. 4, pp. 271-281.

Hobbs, R. E., and **Raoof, M.** (1982), "Interwire Slippage and Fatigue Prediction in Stranded Cables for TLP Tethers" in 'Behaviour of Offshore Structures', Chryssostomidid, C. And Conner, J. J.(eds.) Hemisphere Publishing/McGraw- Hill, New York, Vol. 2, pp. 77-99. (*Proceedings, 3rd International Conference on Behaviour of Offshore Structures*), 1982, M.I.T., Cambridge, MA, U.S.A.

Hobbs, R. E., and **Raoof, M.** (1984), "Hysteresis in Bridge Strand", *Proceedings of the Institution of Civil Engineers*, Part-II, Vol. 77, December, 1984, pp. 445-464.

Hobbs, R. E., and **Raoof, M.** (1986) "The Behaviour of Large Spiral Strands", *Proceedings of the 5th International Offshore Mechanics and Arctic Engineering Symposium, ASME*, Tokyo, Japan, Vol. 3, pp. 543-549.

Hong, K. J., Der Kiureghian A., and Sackman, J.L. (2005), "Bending Behaviour of Helically Wrapped Cables", *Journal of Engineering Mechanics,* Vol. 131, No. 5, pp. 500-511.

Hong, K. J., Yi C., and **Lee, Y. K.,** (2012), "Geometry and Friction of Helically Wrapped Wires in a Cable Subjected to Tension and Bending." *International Journal of Steel Structures,* Vol. 12, No. 2, pp. 233-242.

Hruska, F. H. (1951), "Calculation of Stresses in Wire Ropes", *Wire and Wire Products*, Vol. 26, September, pp. 766-767 and 799-801.

Hruska, F. H. (1952), "Radial Forces in Wire Ropes", *Wire and Wire Products*, Vol. 27, May, pp. 459-463.

Hruska, F. H. (1951), "Tangential Forces in Wire Ropes", *Wire and Wire Products*, Vol. 28, May, pp. 455-460.

Huang, N. C. (1978), "Finite Element Extension of an Elastic Strand with a Central Core", *Journal of Applied Mechanics, ASME*, Vol. 45, December, pp. 852-858.

Huang, Y. P. (1993), "Predictions of Static and Dynamic Performance of Multi-Layered Spiral Strands Under Various Loading Conditions", Thesis Presented to *South Bank University* in Partial Fulfilment of the Requirements for the Degree of Doctor of Philosophy, February.

Impollonia, N., Ricciardi, G., and Saitta F. (2009), "Dynamic behavior of stay cables with rotational dampers." *Journal of Engineering Mechanics "*, Vol. 136, No. 6, pp. 697-709.

Jiang, W. (1995), "A General Formulation of the Theory of Wire Ropes", *Journal of Applied Mechanics, ASME*, Vol. 62, September, pp. 747-755.

Jiang, W. G., and **Henshall, J. L**. (1999), "The Analysis of Termination Effects in Wire Strand Using the Finite Element Method", *Journal of Strain Analysis*, Vol. 34, No. 1, pp. 31-38.

Jiang, W. G. (2011). "A Concise Finite Element Model for Pure Bending Analysis of Simple Wire Strand", *International Journal of Mechanical Sciences*.

Jiang, W. G., Warby, M. K., and Henshall, J. L. (2008), "Statically Indeterminate Contacts in Axially Loaded Wire Strand", *European Journal of Mechanics-A/Solids,* Vol. 27, No. 1, pp. 69-78.

Jolicoeur, C. (1996), "Discussion: A General Formulation of the Theory of Wire Ropes", *Journal of Applied Mechanics, ASME*, Vol. 63, December, pp.1053.

Jolicoeur, C. (1997),"Comparative Study of Two Semi-continuous Models for Wire Strand Analysis", *Journal of Engineering Mechanics, ASCE*, Vol. 123, No. 8, pp.792-799.

Jolicoeur, C., and **Cardou, A.** (1994), "A Numerical Comparison of Current Mathematical Models of Twisted Wire Cables Under Axisymmetric Loads", *Journal of Energy Resources Technology, ASME*, Vol. 113, December, pp.241-249.

Jolicoeur, C., and **Cardou, A.** (1994), "Analytical Solution for Bending of Coaxial Orthotropic Cylinders", *Journal of Engineering Mechanics, ASCE*, Vol. 120, No. 12, December, pp.2556-2574.

Jolicoeur, C., and **Cardou, A.** (1996), "Semicontinuous Mathematical Model for Bending of Multi-Layered Wire Strands", *Journal of Engineering Mechanics, ASCE*, Vol. 122, No. 7, July, pp.643-650.

Judge, R., Yang, Z., Jones, S. and Beattie, G. (2012), "Full 3D Finite Element Modelling of Spiral Strand Cables," *Construction and Building Materials*, Vol. 35, No. 1, pp. 452-459.

Khan, S. W., and **Raoof, M. (2013),** "Restrained Bending Fatigue Design of Bridge Cables", Proceedings of the 6th Congress on Forensic Engineering, San Francisco, USA, pp. 113-122.

Knapp, R. H. (1975), "Non-Linear Analysis of a Helically Armoured Cable with Non-uniform Mechanical Properties in Tension and Torsion", *Proceedings, IEEE/MTS Conference: Engineering in the Ocean Environment*, San Diego, California, pp. 155-164.

Knapp, R. H. (1979), "Derivation of a New Stiffness Matrix for Helically Armoured Cables Considering Tension and Torsion", *International Journal for Numerical Methods in Engineering*, Vol. 14, pp. 515-529.

Knapp, R. H. (1988), "Helical Wire Stresses in Bent Cables", *Journal of Offshore Mechanics and Arctic Engineering, ASME*, Vol. 110, pp. 55-61.

Knapp, R. H. (1989), "Axial Fatigue Model for Wire Rope Strand", *Proceedings of the ACSE Structures Congress, Materials and Material Behaviour*, Orlando, FLA, U.S.A., pp. 347-359.

Kraincanic, I. (1995), “Analysis of Coupled Axial/Torsional Behaviour of Spiral Strands, Wire Ropes and Locked Coil Cables”, Thesis Presented to *South Bank University* in Partial Fulfillment of the Requirements for the Degree of Doctor of Philosophy, October 1995.

Kraincanic, I., and **E. Kebadze** (2001), "Slip initiation and progression in helical armouring layers of unbonded flexible pipes and its effect on pipe bending behaviour," *The Journal of Strain Analysis for Engineering Design*, Vol. 36, No. 3, pp. 265-275.

Kumar, K., and **Cochran, J. E.** (1987), “Closed-Form Analysis for Elastic Deformations of Multi-Layered Strands”, *Journal of Applied Mechanics, ASME*, Vol. 54, December, pp. 898-903.

Kumar, K., and **Cochran, J. E.** (1990), “Analytical Estimation for Static Deformation of Wire Ropes with Fibrous Core”, *Journal of Applied Mechanics, ASME*, Vol. 57, December, pp. 1000-1003.

LeClair R.A., (1989), “Upper Bound to Mechanical Power Transmission Losses in Wire Rope”, *Journal of Engineering Mechanics, ASCE,* Vol. 115 No. 9 pp. 2011-2019.

LeClair, R. A., and **Costello, G. A**. (1988), “Axial, Bending and Torsional Loading of a Strand with Friction”, *Journal of Offshore Mechanics and Arctic Engineering, ASME*, Vol. 110, February, pp. 38-42.

Lee, W. K. (1991), "An Insight into Wire Rope Geometry", *International Journal of Solids and Structures,* Vol. 28, No. 4 pp. 471-490.

Leissa, A. W. (1959), “Contact Stresses in Wire Ropes”, *Wire and Wire Products*, Vol. 34, March, pp. 372-374.

Love, A. E. H. (1944), “A Treatise on the Mathematical Theory of Elasticity”, Dover Publications, Newyork.

Lutchansky, M. (1969), “Axial Stresses in Armour Wires of Bent Submarine Cables”, *Journal of Engineering for Industry, ASME*, Vol. 91, August, pp. 687-693.

Machida, S., and **Durelli, A. J.** (1973), "Response of a Strand to Axial and Torsional Displacements", *Journal of Mechanical Engineering Science*, Vol. 15, No. 4, pp. 241-251.

Malinosky, V. A. (1993), "Bending Stiffness of Steel Wire Ropes", O.I.P.E.E.C Round Table Conference, Delft, The Netherland, pp. II35-II49.

Nabijou, S., and **Hobbs, R. E.** (1995a), "Frictional Performance of Wire and Fibre Ropes Bent Over Sheaves", *Journal of Strain Analysis*, Vol. 30, No. 1, pp. 45-57.

Nabijou, S., and **Hobbs, R. E.** (1995b), "Relative Movements within Wire Ropes Bent Over Sheaves", *Journal of Strain Analysis*, Vol. 30, No. 2, pp. 155-165.

Nawrocki, A., and **Labrosse, M.,** (2000), "A Finite Element Model for Simple Straight Wire Rope Strands", *Computers & Structures* Vol. 77, No. 4, pp. 345-359.

Papailiou, K. O. (1997), "On the Bending Stiffness of Transmission Line Conductors." Power Delivery, *IEEE Transactions on* 12(4): 1576-1588.

Papailiou, K. O. (1995), "Bending of Helically Twisted Cables Under Variable Bending Stiffness Due to Internal Friction, Tensile Force and Cable Curvature", Thesis presented to, *ETH Zürich*, Switzerland in Partial Fulfillment of the Requirements for the Degree of Doctor of Philosophy.

Phillips, J. W., and **Costello, G. A.** (1973), "Contact Stresses in Twisted Wire Cables", *Journal of Engineering Mechanics Division, ASCE*, Vol. 99, No. EM2, April, pp. 331-341.

Phillips, J. W., and **Costello, G. A.** (1977), "Axial Impact of Twisted Wire Cables", *Journal of Engineering Mechanics Division, ASCE*, Vol. 44, March, pp. 127-131.

Poffenberger, J. C., and **Swart, R. L.** (1965), "Differential Displacement and Dynamic Conductor Strains" IEEE Trans., *Power Apparatus and Systems*, PAS-84, 281–289.

Poser, M. (2001), "Full-scale Bending Fatigue Tests on Stay Cables", Thesis presented to the *University of Texas at Austin* in Partial Fulfilment of the Requirements for the Degree of Master of Science in Engineering, December.

Rawlins, C. B. (2009), "Flexural Self-Damping in Overhead Electrical Transmission Conductors", *Journal of Sound and Vibration,* Vol. 323, No. 1, pp. 232-256.

Ramsey, H. (1990), "Analysis of Interwire Friction in Multi-Layered Cable Under Uniform Extension and Twisting", *International Journal of Mechanical Sciences*, Vol. 32, No. 8, pp. 709-716.

Raoof, M. (1983), "Interwire Contact Forces and Static, Hysteretic and Fatigue Properties of Multi-Layered Structural Strands", Thesis Presented to the *University of London* in Partial Fulfillment of the Requirements for the Degree of Doctor of Philosophy, September.

Raoof, M. (1989) "Free Bending Tests on Large Spiral Strands", In ICE Proceedings, ICE Virtual Library, Vol. 87, pp. 605-626.

Raoof, M. (1990a), "Comparison Between the Performance of Newly Manufactured and Well-used Spiral Strands", *Proceedings of the Institution of Civil Engineers, Part-II*, Vol. 89, March, pp. 103-120.

Raoof, M. (1990b), "Free Bending of Spiral Strands*", Journal of Engineering Mechanics, ASCE*, Vol. 116, No. 3, pp. 512-530.

Raoof, M. (1990c), "Effect of Hydrostatic Pressure on Strand Behaviour", *Journal of Strain Analysis*, Vol. 25, No. 2, pp. 75-84.

Raoof, M. (1990d), "Axial Fatigue of Multi-Layered Strands", *Journal of Engineering Mechanics, ASCE*, Vol. 116, No. 10, pp. 2083-2099.

Raoof, M. (1990e), "Cable Behaviour Under Various Loading Conditions", *Structural Engineering Review*, Vol. 3, No. 2, pp. 89-99.

Raoof, M. (1991a), "Axial Fatigue Life Prediction of Structural Cables from First Principles", *Proceedings of the Institution of Civil Engineers, Part II*, Vol. 91, March, pp. 19-38.

Raoof M. (1992a), "Free Bending Fatigue of Axially Pre-Loaded Spiral Strands", *The Journal of Strain Analysis for Engineering Design*, Vol. 27, No. 3, pp. 127-136.

Raoof M. (1992b), “Free Bending Fatigue Life Estimation of Cables at Points of Fixity”, *Journal of Engineering Mechanics,* Vol. 118, No. 9, pp. 1747-1764.

Raoof, M. (1992c), “Design Recommendations for Steel Cables”, *Structural Engineering Review*, Vol. 4, No. 3, pp. 223-233.

Raoof M. (1993a), “Design of Sheathed Spiral Strands Against Free Bending Fatigue at Terminations”, *The Journal of Strain Analysis for Engineering Design,* Vol. 28, No. 3, pp. 163-174.

Raoof, M. (1993b), "Design of Steel Cables against Free-Bending Fatigue at Terminations”, *The Structural Engineer*, Vol. 71 No. 10, May, pp. 171-71.

Raoof, M. (1995), "Characteristics of Locked Coil Strands under Free Bending", *International Journal of Offshore and Polar Engineering* Vol. 5, No. 2, June, pp. 153-160.

Raoof, M. and **Davies, T. J.** (2004). "Determination of the Bending Stiffness for a Spiral Strand." *The Journal of Strain Analysis for Engineering Design,* Vol. 39, No. 1, pp. 1-13.

Raoof, M., and **Davies, T. J.** (2005), "End Fixity to Spiral Strands Undergoing Cyclic Bending." *The Journal of Strain Analysis for Engineering Design*, Vol. 40, No. 2, pp. 129-137.

Raoof, M., and **Davies, T. J.** (2006), “Simple Determination of the Maximum Axial and Torsional Energy Dissipation in large diameter spiral strands”, *Computer and Structures*, Vol. 84, pp. 676-689.

Raoof, M., and **Hobbs, R. E.** (1984), "The Bending of Spiral Strand and Armored Cables Close to Terminations", *Journal of Energy Resourses Technology, ASME*, Vol. 106, No. 3, pp. 349-355.

Raoof, M., and **Hobbs R. E.** (1988a) "Torsion Tests on Large Spiral Strands", The Journal of Strain Analysis for Engineering Design Vol. 23, No. 2, pp. 97-104.

Raoof, M., and **Hobbs R. E**. (1988b) “Analysis of Multi-Layered Structural Strands” *Journal of Engineering Mechanics*, *ASCE*, Vol. 114, July, pp. 1166-1182.

Raoof, M., and **Huang, Y. P.** (1993), "Upper Bound Prediction of Cable Damping Under Cyclic Bending", *Journal of Engineering Mechanics, ASCE*, Vol. 117 No. 12, December, pp. 2729-2747.

Raoof, M., and **Kraincanic, I.** (1993), "Recovery Length in Sheathed Spiral Strands in Deep-Water Platform Applications", *International Journal of Fatigue*, Vol.15, No. 6, pp. 485-492.

Raoof, M., and **Kraincanic, I.** (1994), "Axial/Torsional Coupling of Sheathed Spiral Strands in Deep Water Applications." *Proceedings of the ICE-Structures and Buildings*, Vol. 104, No. 4, pp. 377-390.

Raoof, M., and **Kraincanic, I.** (1995a), "Simple Derivation of the Stiffness Matrix for Axial/Torsional Coupling of Spiral Strands", *Computer and Structures*, Vol. 55, No. 4, pp. 589-600.

Raoof, M., and **Kraincanic, I.** (1995b), "Analysis of Large Diameter Steel Ropes", *Journal of Engineering Mechanics, ASCE*, Vol. 121, No. 6, June, pp. 667-675.

Raoof, M., and **Kraincanic, I.** (1995c), "Recovery Length in Multi-Layered Spiral Strands in Deep-Water Platform Applications*", Journal of Engineering Mechanics, ASCE*, Vol. 121, No. 7, July, pp. 795-800.

Ray A., Dhua, S., Mishra, K. and Jha S. (2003), "Microstructural Manifestations of Fractured Z-profile Steel Wires on the Outer Layer of a Failed Locked Coil Wire Rope", *Journal of Failure Analysis and Prevention*, Vol. 3, No. 4, pp. 51-55.

Sathikh, S., **Moorthy, M. B. K**., and **Krishnan, M**. (1996), "A Symmetric Linear Elastic Model for Helical Wire Strands Under Axisymmetric Loads", *Journal of Strain Analysis*, Vol. 31, No. 5, pp. 389-399.

Stanova E., Fedorko, G., Fabian, M., and Kmet, S. (2011). "Computer modelling of wire strands and ropes part II: Finite element-based applications." *Advances in Engineering Software*, Vol. 42, No. 6, pp. 322-331.

Tabatabai, H., Ciolko, A. T., and **Dickson, T. J.** (1995), "Implications of Test Results From Full-Scale Fatigue Tests of Stay Cables Composed of Seven-Wire Prestressing Strand", Proceedings of the Fourth International Bridge Engineering Conference, San Francisco, Published by *Transportation Research Board*, pp. 266-277.

Utting, W. S. (1988), "Wire Loading Near Rope Terminations", *Wire Industry*, March, pp. 251-257.

Utting, W. S. (1994a), "Survey of Literature on the Behaviour of Steel Wire Ropes-Part I", *Wire Industry*, September, Vol. 61, No. 729, pp. 633-635.

Utting, W. S. (1994b), "Survey of Literature on the Behaviour of Steel Wire Ropes-Part II", *Wire Industry*, November, Vol. 61, No. 731, pp. 746-748.

Utting, W. S. (1995), "Survey of Literature on the Behaviour of Steel Wire Ropes-Part III", *Wire Industry*, May, Vol. 62, No. 737, pp. 269-270.

Utting, W. S., and **Jones, N.** (1984), "A Survey of the Literature on the Behaviour of Wire Ropes", *Wire Industry*, Vol. 51, September, pp. 623-629.

Utting, W. S., and **Jones, N.** (1985),"Tensile Testing of a Wire Rope Strand", *Journal of Strain Analysis*, Vol. 20, No. 3, February, pp. 151-164.

Utting, W. S., and **Jones, N.** (1987a), "The Response of Wire Rope Strands to Axial Tensile Loads-Part I. Experimental Results and Theoretical Predictions", *International Journal of Mechanical Science*, Vol. 29, No. 9, pp. 605-619.

Utting, W. S., and **Jones, N.** (1987b), "The Response of Wire Rope Strands to Axial Tensile Loads-Part II. Experimental Results and Theoretical Predictions", *International Journal of Mechanical Science*, Vol. 29, No. 9, pp. 621-636

Utting, W. S., and **Jones, N.** (1987c), "Wire Tensions and Bending Moments in Axially Loaded Seven Wire Strand", *Journal of Strain Analysis and Design*, Vol. 23, August, pp. 109-116.

Utting, W. S., and **Jones, N.** (1988), "Axial-Torsional Interactions and Wire Deformations in 19-Wire Spiral Strand", *Journal of Strain Analysis and Design*, Vol. 23, No.2, pp. 79-86.

Velinsky, S. A. (1985) "General Nonlinear Theory for Complex Wire Rope", *International Journal of Mechanical Sciences,* Vol. 27, No. 7, pp. 497-507.

Vinogradov, O. G., and **Atatekin, I. S.** (1986), "Internal Friction due to Wire Twist in Bent Cables", *Journal of Engineering Mechanics, ASCE*, Vol. 112, No.9, September, pp. 859-873.

Wang, D., Zhang, D., Wang, S., and Ge, S. (2012), "Finite Element Analysis of Hoisting Rope and Fretting Wear Evolution and Fatigue Life Estimation of Steel Wires", *Engineering Failure Analysis,* Vol. 27, No.1, pp. 173-193.

Wood, S. L., and **Frank, K. H.** (2009), "Experimental Investigation of Bending Fatigue Response of Grouted Stay Cables", *Journal of Bridge Engineering*, Vol. 15, No. 2, pp. 123-130.

Wu Y. H., Sun, J. and **Zhang, K.** (2013), "Analysis of Stress-Strain Distribution for Wire Rope of Traction Hoister." *Applied Mechanics and Materials* Vol. 268, 1198-1202.

Yen, J. Y., and **Chen, C. H.** (2006), "Theoretical Approach to the Solutions of Axially Loaded Complex Ropes", *Journal of the Chinese Institute of Engineers,* Vol. 29, No. 4, pp. 725-731.

Zhu, Z., and **Meguid, S.** (2007), "Nonlinear Finite Element-Based Investigation of Flexural Damping of Slacking Wire Cables", *International Journal of Solids and Structures* Vol. 44, No. 16, pp. 5122-5132.